8-2020

Applications with Discrete and Continuous Models: Harvesting and Contact Tracing

Danielle L. Burton
University of Tennessee, Knoxville, dburton3@vols.utk.edu

To the Graduate Council:

I am submitting herewith a dissertation written by Danielle L. Burton entitled "Applications with Discrete and Continuous Models: Harvesting and Contact Tracing." I have examined the final electronic copy of this dissertation for form and content and recommend that it be accepted in partial fulfillment of the requirements for the degree of Doctor of Philosophy, with a major in Mathematics.

Suzanne Lenhart, Major Professor

We have read this dissertation and recommend its acceptance:

Louis Gross, Judy Day, Christopher Strickland

Accepted for the Council:

Dixie L. Thompson

Vice Provost and Dean of the Graduate School

(Original signatures are on file with official student records.)

Applications with Discrete and Continuous Models: Harvesting and Contact Tracing

A Dissertation Presented for the

Doctor of Philosophy

Degree

The University of Tennessee, Knoxville

Danielle Liane Burton

August 2020

To Mary Christian, Vienna Cornish, Johanna Kim, and Aren LaBianca. As promised.

Acknowledgments

I would like to thank my advisor Suzanne Lenhart, without whom I would never have made it. Shandelle Henson, without whom I wouldn't have gotten here to begin with. Nina Fefferman, Anne Ho, Maggie Wieczorek, and Mia Romano for your unwavering support of my mental health and going so many extra miles. Cassie Putman Micucci, Jimmy Scott, Khoa Dinh, and Kylie Berry for being the best office mates a person could desire. Nina's lab, current and past, for being awesome, eclectic, and welcoming. Joe Daws Jr. for always bringing such positive energy. Alex Lacy for always having the best earrings and the best attitude. Tyler Poppenwimer and Rebecca Pettit, my seminar buddies and fellow civilization players. (Tyler always got to the root of the issue.) Christina Edholm, the best roommate to have when working long days and terribly jetlagged.

Gabe Dusing, Bonnie Johnson, the Commission for LGBT People, and the Pride Center for your tireless work on behalf of the LGBT community.

Pam Armentrout for being a superhero. Kevin Sukanek, Joan Lind, Bob Guest, and Marie Jameson for your mentorship in teaching. PEER, Gladys Alexandre, Sekeenia Haynes, the PEER mentors, and my fellow PEER scholars for helping me develop as a scientist and for being such a great community. Earnest Brothers for your mentorship and your mentorship in mentorship. NIMBioS as an organization and as a group of people. Mike Frazier, Michael Wise, and Delong Li for deepening my understanding of PDEs. Tricia Phillips for your support, positivity, and help with my code. Hannah Thompson, Cara Sulyok, Cameron Cook, Ibrahim Aslan, Mahir Demir, Nate Pollesch, and the other math biology students who shared some of my time here. Ben Levy for checking my codes and my reasoning. Judy Day, Christopher Strickland, and Lou Gross for serving on my committee and for your mentorship.

Masamu organizers and participants, an excellent program full of excellent people. Southern African Mathematical Sciences Association for being so welcoming and active.

Daniel Franco and Frank Hilker, I hope we get to continue collaborating on research.

Thank you all for the time you invested in me, for making me smile, and for helping me keep going.

Abstract

Harvest plays an important role in management decisions, from fisheries to pest control. Discrete models enable us to explore the importance of timing of management decisions including the order of events of particular actions. We derive novel mechanistic models featuring explicit within season harvest timing and level. Our models feature explicit discrete density independent birth pulses, continuous density dependent mortality, and density independent harvest level at a within season harvest time. We explore optimization of within-season harvest level and timing through optimal control of these population models. With a fixed harvest level, harvest timing is taken as the control. Then with fixed timing, the harvest level is implemented as the control. Finally, both harvest timing and level are used as controls. We maximize an objective functional which includes management goals of maximizing yield, maximizing stock, and minimizing costs associated with both harvest intensity and harvest timing.

The 2014-2016 West African outbreak of Ebola Virus Disease (EVD) was the largest and most deadly to date. Contact tracing, following up those who may have been infected through contact with an infected individual to prevent secondary spread, plays a vital role in controlling such outbreaks. However, there were many complications and challenges to contact tracing efforts during the 2014-2016 outbreak. We present a system of ordinary differential equations to model contact tracing in Sierra Leone during the outbreak. Using data on cumulative cases and deaths we estimate most of the parameters in our model. We include the novel features of counting the total number of people being traced and tying this directly to the number of tracers doing this work. We explore the role contact tracing played in eventually ending the outbreak and examine the potential impact of improved contact tracing on the death toll.

Table of Contents

List of Tables

List of Figures

Chapter 1

Introduction

Discrete and continuous models have been used successfully to represent a variety of biological systems. In this dissertation, we explore two types of applications: harvesting actions in a population model and contact tracing in an epidemiological model. In the discrete context we explore the theoretical question of when during a season is the best time to harvest. In the continuous context we develop a model of contact tracing in Sierra Leone during the 2014-2016 Ebola epidemic.

In discrete models, the order of events is important [9]. As a simple example, suppose we have two events in a population model: growth and harvest. Suppose the population is growing at 10% each time step and there is a harvest removing 10 individuals each time step. The current population plus the growth may be represented by the equation

$$G(x) = x + 0.1x, \tag{1.1}$$

and the harvest may be represented by

$$H(x) = x - 10. \tag{1.2}$$

We begin with a population of 100 individuals.

We represent the population at time t as N_t. If growth occurs before harvest then the equation for the population size at the next census will be

$$N_{t+1} = H(G(N_t)) = 1.1N_t - 10. \tag{1.3}$$

With an initial population of $N_0 = 100$, the number of individuals after growth will be 110, 10 individuals will be harvested, and the population size at the next census will be $N_1 = 100$. Indeed the population will remain at 100 for as many time steps as these conditions hold.

If harvest occurs before growth then the equation for the population size at the next generation will be

$$N_{t+1} = G(H(N_t)) = 1.1(N_t - 10). \tag{1.4}$$

With an initial condition of $N_0 = 100$, then 10 individuals will be harvested and then growth will occur as $1.1 * 90 = 99$. The population size at the next census will be 99 individuals. Indeed, the population will continue to decrease with each additional time step.

In the growth-then-harvest case, a harvest of 10 individuals each time step is sustainable. But in the harvest-then-growth case a harvest of 10 individuals will eventually deplete the stock. The order of events is also important in the optimal control of discrete models for a variety of applications [9].

1.1 Summary of our investigation of two models

Harvest timing is an important management decision. A poorly timed harvest could result in stock depletion, pest resurgence, or population destabilization due to a population's age structure, or the order of other events such as birth. For many populations, the most appropriate models are discrete in time. In this dissertation we will develop two discrete mechanistic models of harvest timing. These models are built with hybrid freatures, discrete time expressions in the census time steps and continuous time dynamics within the seasons. Hybrid models may occur when some events happen quickly in time (like a discrete effect) and others happen over time. Both of our models will include density independent birth and density independent harvest, but they will differ in the exact nature of density dependent

mortality included. In both models the order of events will be continuous mortality for a portion of the season, then instantaneous harvest, then continuous mortality for the remainder of the season, and finally a birth pulse immediately before the census at the end of the season. If harvest timing occurs at the beginning of the season the order of events will be harvest, then continuous mortality for the entirety of the season, and finally the birth pulse. Our first model will have continuous per-capita mortality proportional to population size. This will give rise to a Beverton-Holt-like model [7]. Our second model will have continuous per-capita mortality proportional to the initial population size. This will give rise to a Ricker-type model [66]. After this careful derivation, we will examine the equilibria and stability of our models assuming fixed harvest timing and fixed harvest intensity. Then we will compare them with a model of harvest timing from the literature [74]. Finally, we will perform optimal control of harvest timing and harvest intensity in order to discover what conditions might give rise to a mid-season harvest and what conditions might give rise to a harvest at the beginning of the season. For our first model we will explore control of harvest timing with fixed harvest intensity, then control of harvest intensity with fixed harvest timing, and finally control of both harvest intensity and harvest timing. For our second model we will explore only control of both harvest intensity and harvest timing. For both models we will optimize an objective functional which includes maximizing stock, maximizing yield, and minimizing costs. These investigations are done numerically with optimization tools discussed in section 1.2.

Next we turn to a continuous model, using a system of ordinary differential equations (ODEs) to represent contact tracing in a novel way. In this system of ODEs the order of events does not matter since all events (such as transmission, transitions to other compartments, recovery, and deaths) occur simultaneously. The 2014-2016 West African Ebola outbreak was the deadliest in history. One of the important interventions which led to the ending of the epidemic was contact tracing. Contact tracing involves following people who have come into contact with a person infected with Ebola. If a contact develops symptoms, they are then isolated and tested. The goal is to prevent secondary transmission. We will develop a novel model of contact tracing during this outbreak, based on data for Sierra Leone. For our model of contact tracing, we will build upon an SEIR (Susceptible,

Exposed, Infectious, Recovered) model. We will add compartments for traced individuals, hospitalized individuals, and dead bodies that are unsafely buried. The novel features of our model are: keeping track of all individuals traced (not just those who eventually develop symptoms) and keeping track of the number of tracers doing contact tracing work. We will perform stability analysis of our model. Then we will parameterize our model against data from the Sierra Leone Ministry of Health [1, 2] that is publicly available. Finally, we will explore how contact tracing impacted the course of the epidemic, how much worse the epidemic might have been in the absence of contact tracing, and how contact tracing might lead to more rapid containment of future epidemics.

1.2 Numerical methods

For our optimization scheme to find the maximum of our objective functional with respect to the control of harvest timing and harvest intensity, we use MATLAB functions fmincon and multistart. Our objective functional includes terms with the goals of maintaining stock, maximizing yield, and minimizing costs. Because fmincon is a local minimizer, we use multistart to search our parameter space for the global minimum. The function multistart picks a given number of start points and then runs the chosen optimizer (in this case fmincon) from each of those start points. Then multistart organizes the outputs (from fmincon) according to size order of the value each returns from the objective functional one is optimizing. Thus multistart in conjunction with a local optimizer can provide better coverage of parameter space and make it more likely that one will find the global optimum rather than just a local optimum.

When we parameterize our Ebola model, we use MATLAB functions fmincon, multistart, and ode45. The function ode45 is a nonstiff, medium order solver, and there was no evidence in this work for the need of a stiff solver. We will use data from the Sierra Leone Ministry of Health detailing the cumulative confirmed cases and cumulative confirmed deaths over the course of the epidemic to parameterize our model [1, 2]. We will be estimating the following parameters:

- β_1: the rate of infection from contact between Susceptibles and Infecteds

- β_2: the rate of infection from contact between Susceptibles and Dead bodies
- γ: the rate of hospitalization for Infecteds
- κ_1: the number of contacts per hospitalized infected individual
- κ_2: the number of contacts per funeral
- r: the rate of hospitalization for traced individuals
- p: the proportion of tracing effort not devoted to hospitalization
- ν: the death rate for untreated individuals
- μ: the death rate for treated individuals
- ϕ_1: the recovery rate for untreated individuals
- ϕ_2: the recovery rate for treated individuals
- $F(0)$: the initial number of Susceptibles being traced
- $E(0)$: the initial number of Exposed individuals
- $E_F(0)$: the initial number of Exposed being traced
- $I(0)$: the initial number of Infectious individuals
- $D(0)$: the initial number of Dead bodies.

Other parameters take on values from the data and from the literature. We minimize the quantity

$$J = \sum_{i=77}^{504} \frac{(\text{Cases}_{Estimated}(i) - \text{Cases}_{Data}(i))^2}{(\text{Cases}_{Data}(i))^2} + \frac{(\text{Deaths}_{Estimated}(i) - \text{Deaths}_{Data}(i))^2}{(\text{Deaths}_{Data}(i))^2}, \quad (1.5)$$

where the time frame for our data is 77 to 504 days from the beginning of the outbreak. In addition to using this fitting technique and to better match the data, we allowed some parameters to change values later in the outbreak due to changes in behavior and treatment.

After parameterizing our model, we explore the impact of contact tracing by examining cumulative cases and cumulative deaths projections for different numbers of contact tracer workers and and by looking at how total deaths depend on parameters κ_1 and κ_2.

Chapter 2

Optimal control of harvest timing in a discrete model

2.1 Background

In discrete population models, the effect of the timing of harvest is important for management. To investigate harvest timing, we give the background on two classic discrete time models before we present our two mechanistic models.

2.1.1 Beverton-Holt model

The classic Beverton-Holt model [7] was developed by Beverton and Holt as they studied fisheries. They benefited from data collected during and immediately after WWII, data which contradicted many existing theories about fisheries and revealed new and unexpected properties. In their book they consider many different fish life cycles and explore how these different species' biologies might impact fishing. For example, do the young fish occupy a different location than the mature fish or not? Though Beverton and Holt wrote about age-dependent mortality in the same book, their simplest model has no age classes. They also consider "exploited" populations of fish in this book, that is to say populations undergoing

harvest. Of the many models in their book, the model of interest here may be written as

$$x_{t+1} = \frac{bx_t}{1 + \beta x_t} \tag{2.1}$$

where x_t is the number of individuals in the population at time t and b, β are positive constants. The parameter b can be interpreted as a per-capita birth rate and β as a per-capita death rate. To understand β as the per-capita death rate see [28]. We are interested in non-negative solutions x_t for (2.1) because only those solutions could represent time series for a population. The right-hand-side bears a resemblance to a Holling Type II functional form [40, 41], such as the Michaelis-Menten equation [60]. Holling Type II functional response indicates that at low densities the population will have a faster growth rate and at higher densities the population will have a slower growth rate. We will review the equilibria and stability of model (2.1).

First let's solve the equilibrium equation. If this were an ordinary differential equation (ODE), we'd set the right-hand-side equal to zero and solve for x. This would mean we assumed the change in x with respect to time is equal to zero. For a difference equation such as (2.1), assuming the state variable x doesn't change over time means that we set $x_{t+1} = x_t = x^*$ where x^* denotes an equilibrium state. Assuming $1 + \beta x^* \neq 0$ the equilibrium equation for (2.1) is

$$x^* = \frac{bx^*}{1 + \beta x^*}$$

$$x^* + \beta (x^*)^2 = bx^*$$

$$\beta (x^*)^2 + (1 - b)x^* = 0$$

$$x^* \left(\beta x^* + 1 - b\right) = 0.$$

Therefore the equilibria are

$$x_0^* = 0 \tag{2.2}$$

and

$$x_1^* = \frac{b - 1}{\beta}. \tag{2.3}$$

For $b \leq 1$, we have $x_1^* \leq 0$. We use equation (2.1) to model a population size and population values below zero are not biologically relevant. For $0 < b \leq 1$ the only equilibrium that is not negative is the extinction equilibrium x_0^*. But for $b > 1$ we have two distinct equilibria, x_0^* and x_1^*.

Next we need to determine the stability of the two equilibria we've found. First some definitions.

Definition 2.1 (Stable Equilibrium)**.** *We say that an equilibrium x^* is Lyapunov stable if for any $C_1 > 0$ there is $\delta > 0$ and a $t_0 > 0$ such that if $|x_0 - x^*| < \delta$ then $|x_t - x^*| < C_1$ for all $t > t_0$.*

Definition 2.2 (Asymptotically Stable Equilibrium)**.** *We say that the equilibrium x^* is locally asymptotically stable if it is stable and there exists some $\rho > 0$ such that if $|x_0 - x^*| < \rho$ then $\lim_{t\to\infty} |x_t - x^*| = 0$.*

We use the following theorem from [48].

Theorem 2.3 (Stability Criteria)**.** *Suppose the difference equation $x_{t+1} = f(x_t)$ has an equilibrium x^* and that f is continuously differentiable. Then x^* is asymptotically stable if $|f'(x^*)| < 1$ and unstable if $|f'(x^*)| > 1$.*

In our case, with $f(x) = \frac{bx}{1+\beta x}$,

$$\begin{aligned} f'(x) =& \frac{b\left(1+\beta x\right) - bx\left(\beta\right)}{\left(1+\beta x\right)^2} \\ =& \frac{b + b\beta x - b\beta x}{\left(1+\beta x\right)^2} \\ =& \frac{b}{\left(1+\beta x\right)^2}. \end{aligned}$$

At the trivial equilibrium x_0^* we have $f'(x_0^*) = b$. Therefore x_0^* is asymptotically stable if $b < 1$. And x_0^* is unstable if $b > 1$. The stability of x_1^* is determined by

$$
\begin{aligned}
f'(x_1^*) &= \frac{b}{\left(1+\beta\frac{b-1}{\beta}\right)^2} \\
&= \frac{b}{(1+b-1)^2} \\
&= \frac{1}{b}.
\end{aligned}
$$

Therefore x_1^* is asymptotically stable if $b > 1$. And x_0^* is unstable if $b < 1$. This bifurcation that occurs at $b = 1$ is called a transcritical bifurcation. Biologically we interpret this to mean that if $b < 1$ the population will go extinct as seen in Figure 2.1, but if $b > 1$, the population will persist and will asymptotically approach a stable level of population size, $\frac{b-1}{\beta}$. If $b > 1$ and the population begins below the positive equilibrium, it will monotonically increase toward the equilibrium because $f' > 0$. If $b > 1$ and the population begins above the positive equilibrium, the population will monotonically decrease toward the equilibrium. Figure 2.2 illustrates the two cases of monotonically increasing and monotonically decreasing to the equilibrium. In this case the parameters were $b = 5$ and $\beta = 4$, which yields an equilibrium of $x_1^* = 1$. The blue cobweb shows the case for an initial condition of $x_0 = 1.5$ and the black cobweb shows an initial condition of $x_0 = 0.5$. For the lower initial condition, the states monotonically increase to 1 and for the higher initial condition the states monotonically decrease to 1.

2.1.2 Ricker model

Another classic difference equation model was developed by Ricker [66]. Ricker's work, like that of Beverton and Holt, was strongly influenced by fisheries data. In particular, Ricker was interested in damped oscillations in stock and how removal of adult fish might paradoxically increase reproductive rates. The Ricker model is

$$
x_{t+1} = x_t e^{r(1-\frac{x_t}{k})} \tag{2.4}
$$

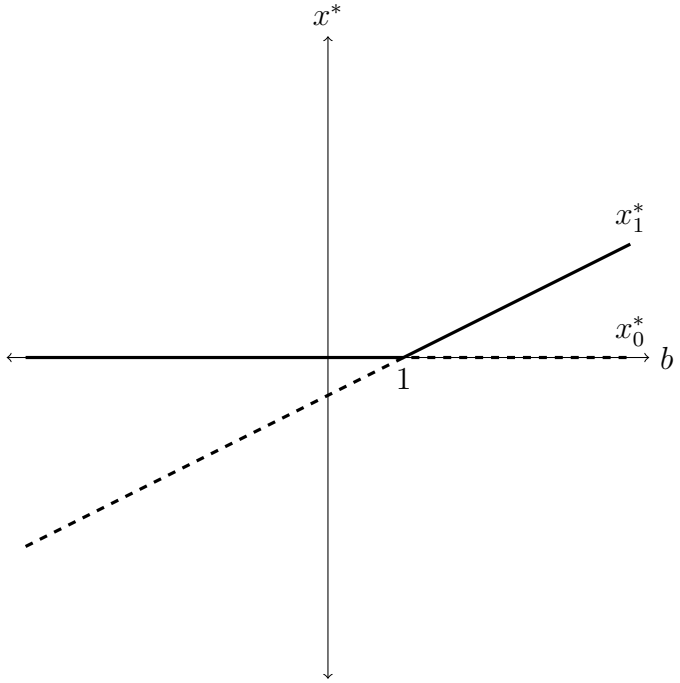

Figure 2.1: The transcritical bifurcation for the Beverton-Holt model is graphed above. The dashed lines indicate unstable equilibria and the solid lines indicate asymptotically stable equilibria.

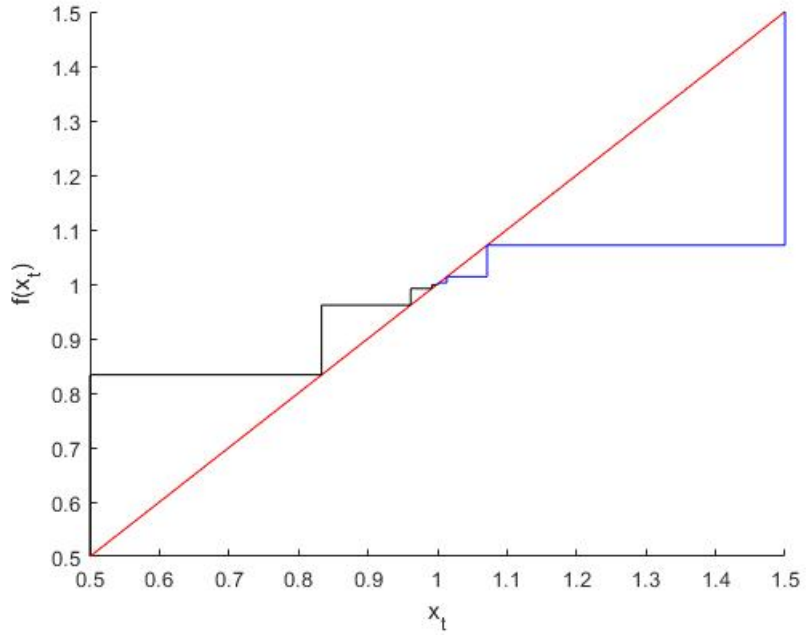

Figure 2.2: A cobweb diagram of the Beverton-Holt model for $b = 1$, $\beta = 4$ with $x_0 = 0.5$ in black and $x_0 = 1.5$ in blue.

where r, k are constants and $k > 0$. The parameter r is the birth parameter. If $r > 0$ then the population is increasing in size and if $r < 0$ then the population is decreasing in size. The parameter k is called the carrying capacity because it sets the maximum equilibrium population size as we will see in the exploration of equilibria and their stability below. The right hand side of this equation is $f(x_t) = x_t e^{r(1-\frac{x_t}{k})}$. To find expressions for the equilibria we set $f(x) = x$.

$$\begin{aligned} x =& xe^{r(1-\frac{x}{k})} \\ 0 =& x(e^{r(1-\frac{x}{k})} - 1). \end{aligned}$$

So one equilibrium is

$$x_0^* = 0.$$

The other equilibrium is given by the expression

$$\begin{aligned} 0 =& e^{r(1-\frac{x}{k})} - 1 \\ 1 =& e^{r(1-\frac{x}{k})} \\ 0 =& r(1 - \frac{x}{k}) \\ \frac{x}{k} =& 1 \\ x_1^* =& k. \end{aligned}$$

To examine stability, we need to find $f'(x)$,

$$\begin{aligned} f'(x) =& e^{r(1-\frac{x}{k})} - \frac{r}{k} x e^{r(1-\frac{x}{k})} \\ =& e^{r(1-\frac{x}{k})}(1 - \frac{rx}{k}). \end{aligned}$$

Hence

$$f'(x_0^*) = e^r$$

and x_0^* is asymptotically stable for

$$r < 0.$$

Further, x_0^* is unstable for

$$r > 0.$$

Now let's examine the stability condition for $x_1^* = k$,

$$f'(x_1^*) = 1 - r.$$

Therefore $x_1^* = k$ is asymptotically stable for

$$0 < r < 2$$

and unstable otherwise. Figure 2.3 shows a bifurcation diagram of the Ricker model for $k = 1$. At $r = 2$ the Ricker model undergoes a period doubling bifurcation which gives rise to stable 2-cycles. As r continues to grow the Ricker model undergoes further period doubling bifurcations, giving rise to 4-cycles, then 8-cycles and eventually exhibiting chaos. For some larger values of r, the Ricker model again exhibits periodicity, but for others it exhibits chaos [59]. Unlike with the Beverton-Holt model above, the Ricker model does not always monotonically approach the positive equilibrium from every initial condition when $0 < r < 2$. Figure 2.4 illustrates an example where the state overshoots the equilibrium and then has damped oscillations toward the equilibrium.

2.1.3 Order of events

In difference equation models the order of events can greatly affect outcomes. The importance of order of events to the model design process will be illustrated in this section.

Suppose we are studying a population that has two primary events: growth and harvest. Let's take the Beverton-Holt model (2.1) as our growth function:

$$G(x) = \frac{bx}{1 + \beta x}. \tag{2.5}$$

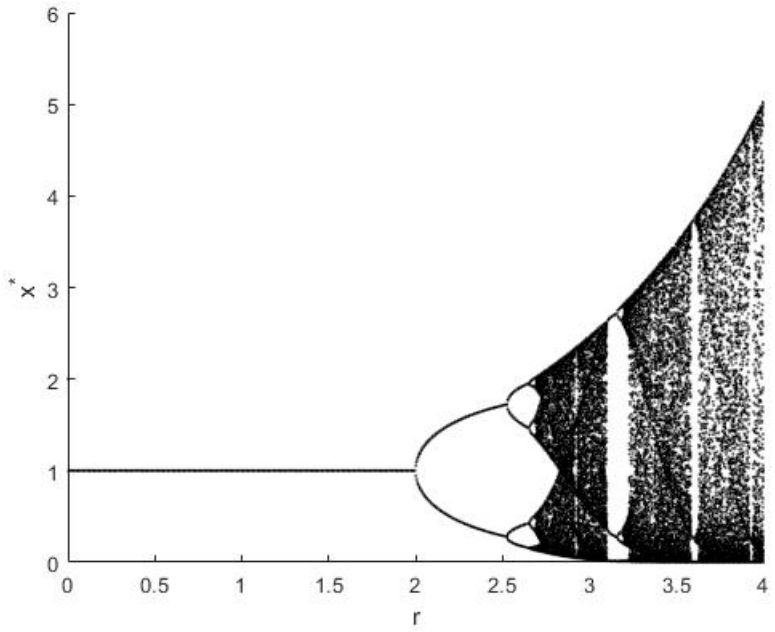

Figure 2.3: A bifurcation diagram for the Ricker model with $k = 1$.

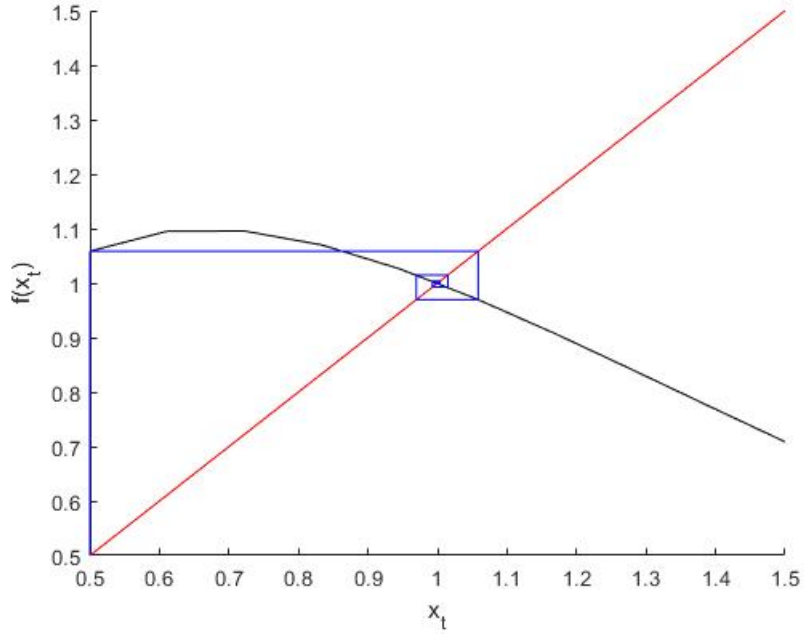

Figure 2.4: A cobweb diagram of the Ricker model for $r = 1.5$, $k = 1$ with $x_0 = 0.5$ in blue and $f(x)$ in black.

And let's use a linear harvest equation, representing proportional harvest of a population:

$$H(x) = (1-\gamma)x \tag{2.6}$$

with $0 < \gamma < 1$. The yield for this harvest equation is

$$Y(x) = \gamma x.$$

Case 1:

If growth occurs before harvest, then the population equation will be

$$N_{t+1} = H(G(N_t)) = (1-\gamma)\frac{bN_t}{1+\beta N_t}. \tag{2.7}$$

Here the yield will be

$$Y_t = \gamma\frac{bN_t}{1+\beta N_t}. \tag{2.8}$$

The equilibrium equation for model (2.7) is

$$\begin{aligned} N &= H(G(N)) \\ N &= (1-\gamma)\frac{bN}{1+\beta N} \\ N + \beta N^2 &= (1-\gamma)bN \\ \beta N^2 + (1-(1-\gamma)b)N &= 0 \\ N(\beta N + 1 - (1-\gamma)b) &= 0. \end{aligned}$$

The two equilibria then are

$$N_0^* = 0$$

and

$$N_1^* = \frac{(1-\gamma)b - 1}{\beta},$$

which is biologically feasible for $(1-\gamma)b > 1$. To determine stability conditions for these equilibria, we compute

$$\begin{aligned}\frac{d}{dN}H(G(N)) =& \frac{(1-\gamma)b(1+\beta)N - (1-\gamma)bN\beta}{(1+\beta N)^2} \\ =& \frac{(1-\gamma)b + (1-\gamma)b\beta N - (1-\gamma)b\beta N}{(1+\beta N)^2} \\ =& \frac{(1-\gamma)b}{(1+\beta N)^2}.\end{aligned}$$

Therefore $N_0^* = 0$ will be asymptotically stable if

$$(1-\gamma)b < 1$$

and unstable if

$$(1-\gamma)b > 1.$$

Similar to the Beverton-Holt equation (2.1), the extinction equilibrium will be unstable if birth is sufficiently large. However in this case b must be larger than for model (2.1) in order to overcome the drain of harvesting. The equilibrium $N_1^* = \frac{(1-\gamma)b-1}{\beta}$ will be asymptotically stable if

$$\begin{aligned}\frac{(1-\gamma)b}{(1+\beta\frac{(1-\gamma)b-1}{\beta})^2} <& 1 \\ \frac{(1-\gamma)b}{(1+(1-\gamma)b-1)^2} <& 1 \\ \frac{(1-\gamma)b}{((1-\gamma)b)^2} <& 1 \\ \frac{1}{(1-\gamma)b} <& 1 \\ 1 <& (1-\gamma)b \\ (1-\gamma)b >& 1\end{aligned}$$

and unstable if

$$(1-\gamma)b < 1$$

but in that case, N_1 is not biologically feasible. Therefore if birth is large enough to overcome the burden of harvest, the population will have an asymptotically stable positive equilibrium.

Case 2:

If harvest occurs before growth, then the population equation will be

$$N_{t+1} = G(H(N_t)) = \frac{b(1-\gamma)N_t}{1+\beta(1-\gamma)N_t}. \tag{2.9}$$

In this case, the yield will be

$$Y_t = \gamma N_t. \tag{2.10}$$

The equilibrium equation for this order of events is

$$\begin{aligned} N = G(H(N)) =& \frac{b(1-\gamma)N}{1+\beta(1-\gamma)N} \\ N + \beta(1-\gamma)N^2 =& b(1-\gamma)N \\ (1-b(1-\gamma))N + \beta(1-\gamma)N^2 =& 0 \\ N(1-b(1-\gamma) + \beta(1-\gamma)N) =& 0 \end{aligned}$$

Yielding two equilibria:

$$N_0^* = 0$$

and

$$N_1^* = \frac{b(1-\gamma)-1}{\beta(1-\gamma)}$$

for $b(1-\gamma) > 1$. Note that this N_1^* is different from that for the other order of events.

To determine the stability conditions for these equilibria we compute

$$\begin{aligned} \frac{d}{dN}G(H(N)) =& \frac{b(1-\gamma)(1+\beta(1-\gamma)N) - b(1-\gamma)N\beta(1-\gamma)}{(1+\beta(1-\gamma)N)^2} \\ =& \frac{b(1-\gamma) + b(1-\gamma)^2\beta N - b(1-\gamma)^2\beta N}{(1+\beta(1-\gamma)N)^2} \\ =& \frac{b(1-\gamma)}{(1+\beta(1-\gamma)N)^2}. \end{aligned}$$

The equilibrium $N_0^* = 0$ then is asymptotically stable when

$$b(1-\gamma) < 1$$

and unstable when

$$b(1-\gamma) > 1.$$

These conditions are identical as for the other order of events case. The positive equilibrium $N_1^* = \frac{b(1-\gamma)-1}{\beta(1-\gamma)}$ will be asymptotically stable when

$$\begin{aligned}
\frac{b(1-\gamma)}{(1+\beta(1-\gamma)\frac{b(1-\gamma)-1}{\beta(1-\gamma)})^2} &< 1 \\
\frac{b(1-\gamma)}{(1+b(1-\gamma)-1)^2} &< 1 \\
\frac{b(1-\gamma)}{(b(1-\gamma))^2} &< 1 \\
\frac{1}{b(1-\gamma)} &< 1 \\
b(1-\gamma) &> 1
\end{aligned}$$

and unstable when

$$b(1-\gamma) < 1$$

which is not biologically feasible.

For both cases of the order of events, stability hinges on the quantity $b(1-\gamma)$, and N_0^*, the extinction equilibrium, is asymptotically stable when this quantity is smaller than 1 and unstable when this quantity is larger than 1. For both cases, when $b(1-\gamma) > 1$ the positive equilibrium is asymptotically stable and when $b(1-\gamma) < 1$ the positive equilibrium is unstable. However, the positive equilibrium in each case has a different expression. For further details on these issues see [32].

Intuitively, the yield where growth has occurred first ought to be larger than the yield where growth occurred after harvest. Let's examine the conditions under which this holds.

$$\begin{aligned}
\gamma\frac{bN_t}{1+\beta N_t} &> \gamma N_t \\
\frac{bN_t}{1+\beta N_t} &> N_t \\
bN_t &> N_t + \beta N_t^2 \\
(b-1)N_t - \beta N_t^2 &> 0 \\
N_t(b-1-\beta N_t) &> 0.
\end{aligned}$$

In order to harvest at all we must have $N_t > 0$, so this leaves

$$\begin{aligned}
b-1-\beta N_t &> 0 \\
b-1 &> \beta N_t \\
\frac{b-1}{\beta} &> N_t.
\end{aligned}$$

Here we see there is some playoff between the birth parameter b and the mortality parameter β. Note that b must be sufficiently large relative to the size of β and the population size N_t for the order of events harvesting-after-growth to produce the larger yield.

Suppose $b(1-\gamma) > 1$ and therefore the positive equilibrium for each order of events case is asymptotically stable. For Case 1 this means $N_1^* = \frac{b(1-\gamma)-1}{\beta}$ is asymptotically stable, giving a yield of

$$\begin{aligned}
Y =& \frac{\gamma b\frac{b(1-\gamma)-1}{\beta}}{1+\beta\frac{b(1-\gamma)-1}{\beta}} \\
=& \frac{\gamma b\frac{b(1-\gamma)-1}{\beta}}{1+b(1-\gamma)-1} \\
=& \frac{\gamma b\frac{b(1-\gamma)-1}{\beta}}{b(1-\gamma)} \\
=& \gamma b\frac{b(1-\gamma)-1}{\beta}\frac{1}{b(1-\gamma)}
\end{aligned}$$

$$
\begin{aligned}
&= \frac{b(1-\gamma)-1}{\beta} \frac{\gamma}{1-\gamma} \\
&= \frac{\gamma(b(1-\gamma)-1)}{\beta(1-\gamma)}.
\end{aligned}
$$

For Case 2 this means $N_1^* = \frac{b(1-\gamma)-1}{\beta(1-\gamma)}$ is asymptotically stable, giving a yield of

$$
Y = \gamma \frac{b(1-\gamma)-1}{\beta(1-\gamma)}
$$

which is identical to the equilibrium yield for Case 1 above. However, the equilibrium values will only be reached asymptotically. In general, for almost any population value N_t, the yields for Case 1 and for Case 2 will be different.

In this simple example, the two order of events cases produce different equilibrium population levels and different yields. Therefore it is important to take care with order of events when building a discrete model to describe a population. The order of events is important in a wide variety of situations [88].

2.2 Motivation

The timing of harvest is a crucial management decision whether harvesting for profit, pest control, or with some other goal in mind [54]. Timing of harvest may need to take into account seasonal variations in mortality, which could have a profound effect on population stability [49, 87]. Harvesting can be performed at a particular instant, or over a particular period of time, or continuously [12, 47]. Harvesting can be used to stabilize fluctuating populations, with the goal of either preventing extinction or resolving a pest outbreak [37, 71]. Or harvesting may destabilize populations [8, 18].

Some authors have explored the role that order of events plays in the decision of when to harvest [47, 58]. Depending on the order of events, extra mortality due to harvesting may be either additive or compensatory [45]. There may be hydra effects, where increased mortality due to harvest paradoxically increases the population size [39, 55]. An event may impact per capita vital rates during the next event [65]. One must be careful when developing a model, particularly with density-dependent mortality, to avoid underestimating mortality

Table 2.1: The two limit cases of Seno's model correspond to the two order-of-events options.

Order of events	Harvest time	Seno's model
Harvest Reproduction	$\theta_t = 0$	$N_{t+1} = g((1-\gamma)N_t)(1-\gamma)N_t$
Reproduction Harvest	$\theta_t = 1$	$N_{t+1} = (1-\gamma)g(N_t)N_t$

and overestimating sustainable yield [47]. Harvest timing may have spatial effects too [34, 56]. When modeling some populations it is important to consider multiple life stages, which can give rise to very different dynamics [68]. It may be best, for example, to harvest adults shortly after a yearly breeding cycle to maximize yield and give juveniles a higher chance of survival [80]. There are many important decisions to make when building a model of harvest timing on a population.

We are interested in the precise timing of a harvest within a season. The only discrete model explicitly describing harvest at some time $\theta \in [0, 1]$ within a season (that is between time t and $t + 1$) was given by Seno's model [74, 75]:

$$N_{t+1} = \theta(1-\gamma)N_t g\left(N_t\right) + (1-\theta)(1-\gamma)N_t g\left((1-\gamma)N_t\right). \tag{2.11}$$

Here $\gamma \in [0, 1]$ is the proportion of the population harvested and $g(x)$ the per-capita growth function for the population in absence of harvest. This heuristic model is a convex combination of the two order-of-events cases: harvest-then-reproduce and reproduce-then-harvest. The models for these two cases are given in Table 2.1. The Seno model makes the assumptions

1. Harvest is instantaneous (or very brief relative to length of the entire season)
2. A proportion γ of the population is harvested at time θ
3. The harvest time θ is constant
4. To apply the model in a specific case, the population must meet the assumptions for the chosen per-capita growth function $g(x)$.
5. The season has unit length (or is scaled to unit length).

Though the time of harvest and the proportion of harvest are known, the yield is unknown, a topic on which Seno makes no comment. We know what the population is at time t and time $t+1$, but the population at any intermediate time is unknown. One might speculate that the yield could be approximated by a convex combination of the yields for the two order of events cases given in Table 2.1. That is, the yield might be proportional to

$$\theta_t \gamma N_t g\left(N_t\right) + (1-\theta_t)\gamma N_t.$$

But this would only be an approximation. It is also unclear when reproduction occurs. One term assumes reproduction occurs before harvest, while the other describes reproduction occurring after harvest. To improve clarity on these processes we will formulate mechanistic models [28] with the advantages of explicit order of events and, vitally, known yield. Our method can be adapted to a specific population's dynamics and the nature of the available data.

In addition to deriving two new mechanistic models, we will also investigate the effect of controlling the time of harvest, denoted θ_t, to achieve a desired goal. Such management goals might include maximizing profit, maximizing population size for conservation, or minimizing population size of a pest. Techniques of optimal control theory and optimization for discrete models will be used [9, 14, 76]. Then we will investigate controlling harvest intensity γ_t, allowing γ to vary depending on time. Finally, we will investigate optimal control of both θ_t and γ_t. Control of harvest timing in discrete models is a novel application of optimal control. This work is in collaboration with Suzanne Lenhart (University of Tennessee), Daniel Franco (Universidad Nacional de Educación a Distancia, Spain), and Frank Hilker (Osnabrück University, Germany).

2.3 First mechanistic model

For our first mechanistic model, we consider a population with initial size N_0 for the times $t = 1, \ldots, T$. We assume the season has unit length. The population at each discrete time t is given by N_t. The effects of the biological mechanisms between time t and $t+1$ will be represented in our model. The population between t and $t+1$ is represented by $n(\tau)$ for

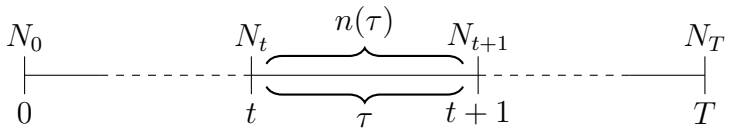

Figure 2.5: Timeline illustrating the variables N_t and $n(\tau)$.

Table 2.2: The population undergoes the above processes at the above times, where $\theta_t \in [0, 1]$.

Time	Process
$(t, t+\theta_t)$	continuous mortality
$t+\theta_t$	instantaneous harvest
$(t+\theta_t, t+1)$	continuous mortality
$t+1^-$	birth pulse
$t+1^+$	census

$\tau \in [0, 1]$. Figure 2.5 illustrates the relationships between N, n, t, and τ. The population undergoes three events: density-dependent mortality during the season, proportional harvest at the time θ_t within the season, and density-independent birth immediately before the census. We chose birth as the last event because we believe it is more logistically feasible to take a census immediately following a birth pulse than to take a census immediately before a birth pulse. Table 2.2 shows the time(s) at which each of the processes occur. By season we mean a time period which makes sense for a given population. For example, in studying deer it might be reasonable for a time step to take one year. However, in studying an organism with shorter generation time or longer generation time a time step might take two weeks or several years.

We assume per-capita within-season mortality is proportional to the population size. That is,

$$\frac{1}{n}\frac{dn}{d\tau} = -\beta n,$$

which gives

$$\frac{dn}{d\tau} = -\beta n^2 \tag{2.12}$$

$$n(0^+) = N_t \tag{2.13}$$

where $\beta > 0$. Let's solve (2.12) on a generic interval (a, τ) where a is the initial time, τ the current time, and $a < \tau$.

$$\begin{aligned}
\frac{-n'}{n^2} &= \beta \\
\int_a^\tau \frac{-n'(s)}{n^2(s)} ds &= \int_a^\tau \beta ds \\
\frac{1}{n(\tau)} - \frac{1}{n(a)} &= \beta\tau - \beta a \\
\frac{1}{n(\tau)} &= \frac{1}{n(a)} + \beta\tau - \beta a \\
\frac{1}{n(\tau)} &= \frac{1 + n(a)\left(\beta\tau - \beta a\right)}{n(a)} \\
n(\tau) &= \frac{n(a)}{1 + n(a)\beta\left(\tau - a\right)}
\end{aligned}$$

By setting $a = 0^+$, with the initial condition (2.13), the population for $\tau \in (0^+, \theta_t^-)$ is given by

$$n(\tau) = \frac{N_t}{1 + N_t\beta\tau}.$$

Therefore, the population just before harvest, at $\tau = \theta_t^-$, is

$$n(\theta_t^-) = \frac{N_t}{1 + N_t\beta\theta_t}.$$

Since a proportion γ of the population is harvested, the yield is

$$Y_t = \frac{\gamma N_t}{1 + N_t\beta\theta_t}. \tag{2.14}$$

After the instantaneous harvest, within-season mortality dynamics continue according to (2.12) with the new initial condition

$$n(\theta_t^+) = \frac{(1-\gamma)N_t}{1 + N_t\beta\theta_t}.$$

Using the solution to (2.12) with $a = \theta_t^+$ we find that the population size for $\tau \in (\theta_t^+, 1^-)$ is

$$\begin{aligned} n(\tau) &= \frac{\frac{(1-\gamma)N_t}{1+N_t\beta\theta_t}}{1+\left(\frac{(1-\gamma)N_t}{1+N_t\beta\theta_t}\right)\beta(\tau-\theta_t)} \\ &= \frac{(1-\gamma)N_t}{1+N_t\beta\theta_t+(1-\gamma)N_t\beta(\tau-\theta_t)} \\ &= \frac{(1-\gamma)N_t}{1+N_t\beta\left(\theta_t+(1-\gamma)(\tau-\theta_t)\right)} \\ &= \frac{(1-\gamma)N_t}{1+N_t\beta\left(\theta_t+\tau-\theta_t-\gamma\tau+\gamma\theta_t\right)} \\ &= \frac{(1-\gamma)N_t}{1+N_t\beta\left(\tau-\gamma(\tau-\theta_t)\right)}. \end{aligned}$$

The population just before the birth pulse, at $\tau = 1^-$, is

$$n(1^-) = \frac{(1-\gamma)N_t}{1+N_t\beta\left(1-\gamma(1-\theta_t)\right)}.$$

The birth pulse occurs at $\tau = 1^+$ and the population at the next census is

$$N_{t+1} = \frac{b(1-\gamma)N_t}{1+N_t\beta\left(1-\gamma(1-\theta_t)\right)} \tag{2.15}$$

where $b > \frac{1}{1-\gamma}$ is the per-capita growth rate. We must have $b > \frac{1}{1-\gamma}$ because otherwise the population would only be able to decrease from N_0 to extinction. This is an extension of the requirement for the Beverton-Holt model (2.1) that $b > 1$. Here the corresponding term is $b(1-\gamma)$, so we must have

$$\begin{aligned} b(1-\gamma) &> 1 \\ b &> \frac{1}{1-\gamma}. \end{aligned}$$

Note that

$$\begin{array}{ccccc} 0 & \leq & 1-\theta_t & \leq & 1 \\ 0 & \leq & \gamma(1-\theta_t) & \leq & 1 \\ 0 & \leq & 1-\gamma(1-\theta_t) & \leq & 1. \end{array}$$

Therefore, the denominator is positive.

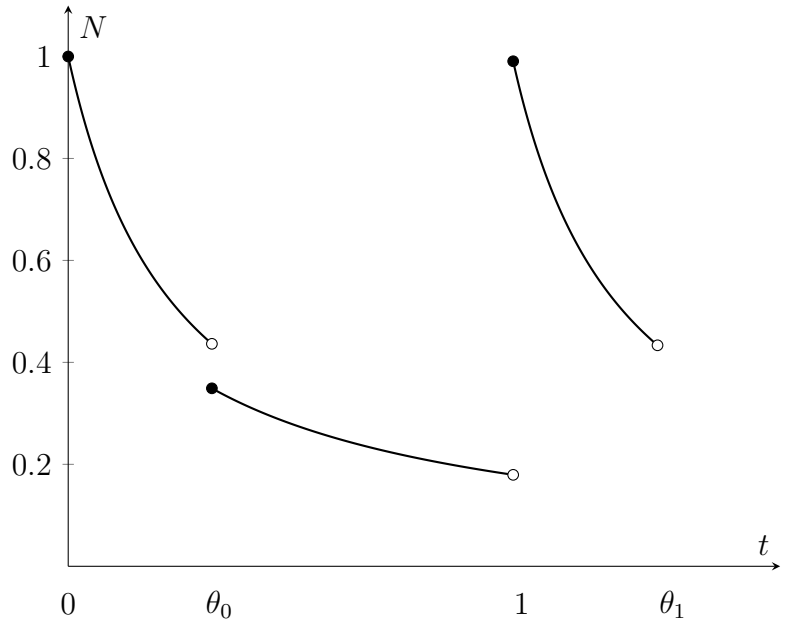

Figure 2.6: This figure illustrates the processes occurring between the discrete time steps of our model using the parameters $\beta = 4, b = 5, N_0 = 1, T = 5, \gamma = .02, C_1 = 0.1, A = 1, B = 1$.

Equation (2.15) represents the iterative formula for our mechanistic model. Though the underlying process of mortality is continuous, we can represent the population dynamics by the discrete expression given by equation (2.15). In modeling some populations such a discrete-continuous hybrid method is quite useful [38]. Figure 2.6 illustrates the processes that are occurring between each time step of the discrete model. This figure shows the population size at each instant between the initial population census ($t = 0$) and the next census ($t = 1$) and continues partway into the next time step until the second harvest, which occurs at time θ_1. Continuous density-dependent mortality causes the population to decrease between times 0 and θ_0. At time $\theta_0 = .3229$ the first harvest occurs and the population size drops discontinuously. From time θ_0 until time 1 the population undergoes continuous density-dependent mortality. At time 1 birth occurs, causing a discontinuous increase in population. Finally, between time 1 and $1 + \theta_1 = 1.3244$ the population once again undergoes continuous density-dependent mortality.

2.3.1 Some observations about our model

Our model makes the following assumptions:

1. The season has unit length.
2. The population undergoes continuous, density-dependent mortality.
3. Harvest is instantaneous.
4. Harvest is density-independent.
5. Birth is density-independent.
6. Census occurs immediately following birth.

To understand how the timing of harvest affects the population and yield, note that the next generation size of our model is a decreasing function of θ_t

$$\frac{\partial N_{t+1}}{\partial \theta_t} = \frac{-(1-\gamma)\gamma\beta b N_t^2}{(1+\beta(1-\gamma(1-\theta_t))N_t)^2}. \tag{2.16}$$

This means that harvesting at $\theta_t = 0$ will result in the highest next-generation size, while harvesting any time later in the season will result in a diminished next-generation size. Therefore, if we were to only consider the management goal of maximizing next-generation population size we would always harvest at $\theta_t = 0$.

The yield is also a decreasing function of harvest timing

$$\frac{\partial Y_t}{\partial \theta_t} = \frac{-\gamma\beta N_t^2}{(1+\beta\theta_t N_t)^2}. \tag{2.17}$$

Therefore, in order to maximize yield we would choose to harvest at the beginning of the season, $\theta_t = 0$. Any later season harvest would result in a lower yield. Oddly, this means that the two goals of maximizing next-generation population size and maximizing yield can both be achieved by harvesting at $\theta_t = 0$.

The limit cases of (2.15) are

$$N_{t+1} = \frac{(1-\gamma)bN_t}{1+\beta(1-\gamma)N_t} \tag{2.18}$$

for $\theta_t \equiv 0$ and

$$N_{t+1} = \frac{(1-\gamma)bN_t}{1+\beta N_t} \tag{2.19}$$

for $\theta_t \equiv 1$.

Equations (2.18) and (2.19) consist of three functions composed in a different order. The three functions are the mortality function

$$f_\beta(x) = \frac{x}{1+\beta x},$$

the harvest function

$$f_\gamma(x) = (1-\gamma)x,$$

and the birth function

$$f_b(x) = bx.$$

The order in which these functions are composed tells us the order of events for each equation. Equation (2.19) could be written as

$$f_b\left(f_\gamma\left(f_\beta\left(N_t\right)\right)\right)$$

or it could be written as

$$f_\gamma\left(f_b\left(f_\beta\left(N_t\right)\right)\right).$$

This means that equation (2.19) does not distinguish the order between the events of harvesting and birth, since they are both assumed to be density-independent and in this case occur one after the other. Birth may occur before harvest or harvest may occur before birth, and the expression would be the same. Mortality must have occurred first. Since the order of birth and harvest would affect yield, it is important that we remain consistent with our assumption that birth occurs last in the season during the remainder of our analysis. The order of events for expression (2.19), then, is mortality, then harvest, and then birth. We chose to have birth occur last, and therefore directly before the census, because we think it's more practical to observe births in the population and then perform the census rather than to attempt to census the population "immediately" before birth occurs.

Now consider the order of events in equation (2.18). This expression could be written as

$$f_b\left(f_\beta\left(f_\gamma\left(N_t\right)\right)\right).$$

The order of events is first harvest, then mortality, and finally birth.

Let's compare the limit cases of our model (that is with θ values at only 0 or only 1) with the model itself to gather further understanding of its dynamics. Observe that

$$\begin{array}{ccccc}
0 & \leq & \theta_t & \leq & 1 \\
-1 & \leq & -\theta_t & \leq & 0 \\
0 & \leq & 1-\theta_t & \leq & 1 \\
0 & \geq & -\gamma(1-\theta_t) & \geq & -\gamma \\
1 & \geq & 1-\gamma(1-\theta_t) & \geq & 1-\gamma \\
N_t & \geq & \left(1-\gamma(1-\theta_t)\right)N_t & \geq & (1-\gamma)N_t \\
\beta N_t & \geq & \beta\left(1-\gamma(1-\theta_t)\right)N_t & \geq & \beta(1-\gamma)N_t \\
1+\beta N_t & \geq & 1+\beta\left(1-\gamma(1-\theta_t)\right)N_t & \geq & 1+\beta(1-\gamma)N_t
\end{array}$$

$$\frac{1}{1+\beta N_t} \leq \frac{1}{1+\beta\left(1-\gamma(1-\theta_t)\right)N_t} \leq \frac{1}{1+\beta(1-\gamma)N_t} \tag{2.20}$$

$$\frac{(1-\gamma)bN_t}{1+\beta N_t} \leq \frac{(1-\gamma)bN_t}{1+\beta\left(1-\gamma(1-\theta_t)\right)N_t} \leq \frac{(1-\gamma)bN_t}{1+\beta(1-\gamma)N_t}. \tag{2.21}$$

In other words, $N_{t+1}(\theta_t \equiv 1) \leq N_{t+1}(0 < \theta_t < 1) \leq N_{t+1}(\theta_t \equiv 0)$. Therefore harvesting at $\theta_t = 1$ will result in the lowest next-generation size, harvesting at some intermediate value of $0 < \theta_t < 1$ will provide an intermediate next-generation size, and harvesting at $\theta_t = 0$ will generate the largest next-generation population size. This matches the conclusions we drew from the fact that $\frac{\partial N_{t+1}}{\partial \theta_t} < 0$. We can take convex combinations of these two limit case terms to form the corresponding Seno model, which we will examine in a later section.

If we set the harvest timing equal to a constant, we can find equilibria for our model. Let $\theta_t = \theta$, a constant, for all t. Let's call the right-hand side of equation (2.15)

$$f(x) = \frac{b(1-\gamma)x}{1+x\beta(1-\gamma(1-\theta))}.$$

The equilibrium equation for (2.15) then is

$$\begin{aligned} N =& f(N) \\ N =& \frac{b(1-\gamma)N}{1+N\beta(1-\gamma(1-\theta))} \\ N\left(1+N\beta(1-\gamma(1-\theta))\right) =& b(1-\gamma)N \\ N\Big(1-b(1-\gamma)+N\beta(1-\gamma(1-\theta))\Big) =& 0. \end{aligned}$$

One equilibrium is

$$N_0^* = 0 \tag{2.22}$$

and the other is

$$N_1^* = \frac{b(1-\gamma)-1}{\beta(1-\gamma(1-\theta))}. \tag{2.23}$$

Recall that this denominator is positive. This is similar to the classic Beverton-Holt model explored in section 2.1.1, where one equilibrium was $x_0^* = 0$ and the other was $x_1^* = \frac{b-1}{\beta}$. The second equilibrium, N_1^*, only exists when $b > \frac{1}{1-\gamma}$. Since $0 < \gamma < 1$, our birth rate b must be larger in order for this equilibrium to exist than for the equilibrium x_1^* to exist, which only requires $b > 1$.

To examine the stability of these equilibria we take the derivative of the right-hand side of (2.15):

$$N_{t+1} = f(N_t) = \frac{b(1-\gamma)N_t}{1+N_t\beta(1-\gamma(1-\theta_t))}.$$

This derivative is

$$f'(N_t) = \frac{b(1-\gamma)}{\left(1+\beta N_t(1-\gamma(1-\theta_t))\right)^2}. \tag{2.24}$$

Evaluating this equation at $N_t = N_0^* = 0$ yields

$$f'(0) = b(1-\gamma). \tag{2.25}$$

The equilibrium N_0^* is stable for

$$0 \leq b(1-\gamma) < 1 \tag{2.26}$$

and unstable for

$$b(1-\gamma) > 1. \tag{2.27}$$

We don't consider $b(1-\gamma) < 0$ because this case is not biologically relevant. Evaluating the derivative (2.24) at $N_t = N_1^*$ from equation (2.23) gives the expression

$$\begin{aligned} f'(N_1^*) =& \frac{b(1-\gamma)}{\left(1+\beta\left(\frac{b(1-\gamma)-1}{\beta(1-\gamma(1-\theta))}\right)(1-\gamma(1-\theta))\right)^2} \\ =& \frac{b(1-\gamma)}{(1+b(1-\gamma)-1)^2} \\ =& \frac{1}{b(1-\gamma)}. \end{aligned}$$

The equilibrium $N_1^* = \frac{b(1-\gamma)-1}{\beta(1-\gamma(1-\theta))}$ is asymptotically stable for

$$b(1-\gamma) > 1 \tag{2.28}$$

and unstable for

$$b(1-\gamma) < 1. \tag{2.29}$$

For $b(1-\gamma) = 1$, Theorem 2.3 does not apply. This is where $N_1^* = 0 = N_0^*$ and the exchange of stability occurs.

2.3.2 Order of events comparison

We decided to census immediately following the birth pulse because it seems more realistic to notice births and then census than to somehow census "immediately" before births occur. But what if we build our model with the other order of events? That order of events would be birth-mortality-harvest-mortality-census. Let's derive the model for this alternative order of events and compare it with our model.

The solution of the ODE in this case is still

$$n(\tau) = \frac{n(a)}{1+n(a)\beta(\tau-a)}$$

with initial condition $n(a)$ at some time $a < \tau$. If birth occurs first, then our initial condition is

$$n(0^+) = bN_t. \tag{2.30}$$

Using this initial condition we can solve to find the population size at time $\tau = \theta^-$, which is immediately before harvest. This population size is

$$n(\theta^-) = \frac{bN_t}{1 + bN_t\beta\theta}. \tag{2.31}$$

Since we harvest a proportion γ of the population, our yield will be

$$Y_t = \frac{\gamma bN_t}{1 + bN_t\beta\theta}, \tag{2.32}$$

and the remaining population is

$$n(\theta^+) = \frac{(1-\gamma)bN_t}{1 + bN_t\beta\theta}. \tag{2.33}$$

Using $n(\theta^+)$ as our new initial condition we can solve for the population size at census which occurs at time $\tau = 1$:

$$\begin{aligned} n(1) =& \frac{\frac{b(1-\gamma)N_t}{1+bN_t\beta\theta}}{1 + \frac{b(1-\gamma)N_t}{1+bN_t\beta\theta}\beta(1-\theta)} \\ =& \frac{b(1-\gamma)N_t}{1 + b\beta\theta N_t + b(1-\gamma)\beta(1-\theta)N_t} \\ =& \frac{b(1-\gamma)N_t}{1 + b\beta N_t(\theta + 1 - \theta - \gamma + \gamma\theta)}. \end{aligned}$$

Thus, the population at census is

$$N_{t+1} = \frac{(1-\gamma)bN_t}{1 + b\beta N_t(1 - \gamma(1-\theta))}. \tag{2.34}$$

Now let's compare the yield and next-generation population size for this order of events with our model.

$$\begin{aligned}
1 &< b \\
1 + bN_t\beta\theta &< b + bN_t\beta\theta \\
\frac{1}{1 + bN_t\beta\theta} &> \frac{1}{b + bN_t\beta\theta} \\
\frac{\gamma bN_t}{1 + bN_t\beta\theta} &> \frac{\gamma bN_t}{b + bN_t\beta\theta} \\
\frac{\gamma bN_t}{1 + bN_t\beta\theta} &> \frac{\gamma N_t}{1 + N_t\beta\theta}.
\end{aligned}$$

Therefore, the yield for birth first (equation (2.32)) would be greater than the yield for birth last (equation (2.14)). Next let's compare the next-generation population size.

$$\begin{aligned}
b &> 1 \\
b\beta N_t(1 - \gamma(1 - \theta)) &> \beta N_t(1 - \gamma(1 - \theta)) \\
1 + b\beta N_t(1 - \gamma(1 - \theta)) &> 1 + \beta N_t(1 - \gamma(1 - \theta)) \\
\frac{1}{1 + b\beta N_t(1 - \gamma(1 - \theta))} &< \frac{1}{1 + \beta N_t(1 - \gamma(1 - \theta))} \\
\frac{(1 - \gamma)bN_t}{1 + b\beta N_t(1 - \gamma(1 - \theta))} &< \frac{(1 - \gamma)bN_t}{1 + \beta N_t(1 - \gamma(1 - \theta))}.
\end{aligned}$$

Therefore, the next-generation population size for our model (2.15) is larger than the next-generation size for the alternative order of events model (2.34).

2.3.3 Comparison with the Seno model

Recall that the Seno model, given by equation (2.35), is a convex combination of harvesting at the beginning and at the end of the season using a without-harvest growth function. The Seno model which compares with our mechanistic model (2.15) has the without harvest per-capita growth function $g(x) = \frac{b}{1+\beta N_t}$. This yields the corresponding model:

$$N_{t+1} = \theta_t(1 - \gamma)N_t\frac{b}{1 + \beta N_t} + (1 - \theta_t)(1 - \gamma)N_t\frac{b}{1 + \beta(1 - \gamma)N_t}. \tag{2.35}$$

Note that equation (2.35) is equal to our model for $\theta_t = 0$ and for $\theta_t = 1$. To compare our mechanistic model (2.15) with (2.35), consider the function

$$f(x) = \frac{1}{1+\beta x}. \tag{2.36}$$

Its first derivative is

$$f'(x) = -\beta(1+\beta x)^{-2}$$

and its second derivative is

$$f''(x) = 2\beta^2(1+\beta x)^{-3} > 0.$$

The function f in (2.36) is convex. Thus we may apply Jensen's inequality [69] to get

$$\begin{aligned}
f(\theta_t N_t + (1-\theta_t)(1-\gamma)N_t) &\leq \theta_t f(N_t) + (1-\theta_t) f((1-\gamma)N_t) \\
\frac{1}{1+\beta\left(\theta_t N_t + (1-\theta_t)(1-\gamma)N_t\right)} &\leq \theta_t \frac{1}{1+\beta N_t} + (1-\theta_t)\frac{1}{1+\beta(1-\gamma)N_t} \\
\frac{1}{1+\beta N_t\left(\theta_t + 1 - \gamma - \theta_t + \gamma\theta_t\right)} &\leq \theta_t \frac{1}{1+\beta N_t} + (1-\theta_t)\frac{1}{1+\beta(1-\gamma)N_t} \\
\frac{1}{1+\beta N_t\left(1-\gamma(1-\theta_t)\right)} &\leq \theta_t \frac{1}{1+\beta N_t} + (1-\theta_t)\frac{1}{1+\beta(1-\gamma)N_t}.
\end{aligned}$$

Multiplying on both sides by the non-negative quantity $(1-\gamma)bN_t$ yields

$$\frac{(1-\gamma)bN_t}{1+\beta N_t\left(1-\gamma(1-\theta_t)\right)} \leq \theta_t \frac{(1-\gamma)bN_t}{1+\beta N_t} + (1-\theta_t)\frac{(1-\gamma)bN_t}{1+\beta(1-\gamma)N_t}. \tag{2.37}$$

Therefore the next generation size of our mechanistic model is less than or equal to the next generation size of the Seno model (2.35).

Numerical simulations indicate that for a reasonable range of parameters the values of N_t from our model, (2.15), do not much differ from Seno's model, (2.35). Appendix A contains estimates of the relative and absolute differences between the two models. Unfortunately, none of those estimates are insightful. We explored the relative difference between the two models numerically. We built an LHS matrix with 10,000 possible parameter sets. An LHS (Latin Hypercube Sampling) matrix divides the distribution of each parameter into, in this case 10,000, areas of equal probability. One sample is taken from each of these areas,

and they are randomly combined with samples of other variables to generate 10,000 possible parameter vectors. We chose the ranges $T \in [5, 15]$, $N_0 \in [0.5, 10]$, $\theta \in [10^{-4}, 1]$, $\gamma \in [10^{-4}, 1]$, $b \in [.01, 1000]$, and $\beta \in [.01, 1000]$. By θ here we mean a constant, that is, $\theta_t = \theta$ for each t. Whereas in our optimal control work, θ_t varies at each time step. We assumed each parameter was uniformly distributed on these ranges. To compare the time series outputs of the two models, we used

$$\sum_{t=1}^{T} \frac{(S_t - N_t)^2}{{S_t}^2} \tag{2.38}$$

to measure the differences, where S_t indicates a value in the time series given by Seno's model and N_t a value in the time series given by our model. The resulting 10,000 values we obtained from computing (2.38) for each set of parameters in the LHS matrix are shown as a histogram in Figure 2.7a. Notice that the relative differences for all of the parameter sets are very small, with the overwhelming majority of the values at the left end of the histogram (that is, virtually identical to zero). We conclude that though Seno's model (2.35) and our model (2.15) look like they would act on θ_t rather differently, in practice this doesn't seem to be the case. Both models are based on many of the same mechanistic assumptions. Indeed, Seno's model may be thought of as some sort of first order approximation of our model in terms of θ_t. Since the two models do not differ notably in output (even for much larger N_0 than the range above) but our model has an explicit yield and greater biological interpretability, we will perform optimal control analysis on our model alone.

2.4 Optimal control of harvest intensity and timing

For our model (2.15) we consider possible components which a management goal might have and some simple ways of incorporating them into our objective functional. We do not consider optimal control of the Seno model because yield is unknown and is often an important factor in management decisions. Since the two models give such similar outputs, we use our mechanistic model for optimal control and interpretation. For a specific application, the objective functional might be quite different from what we consider here.

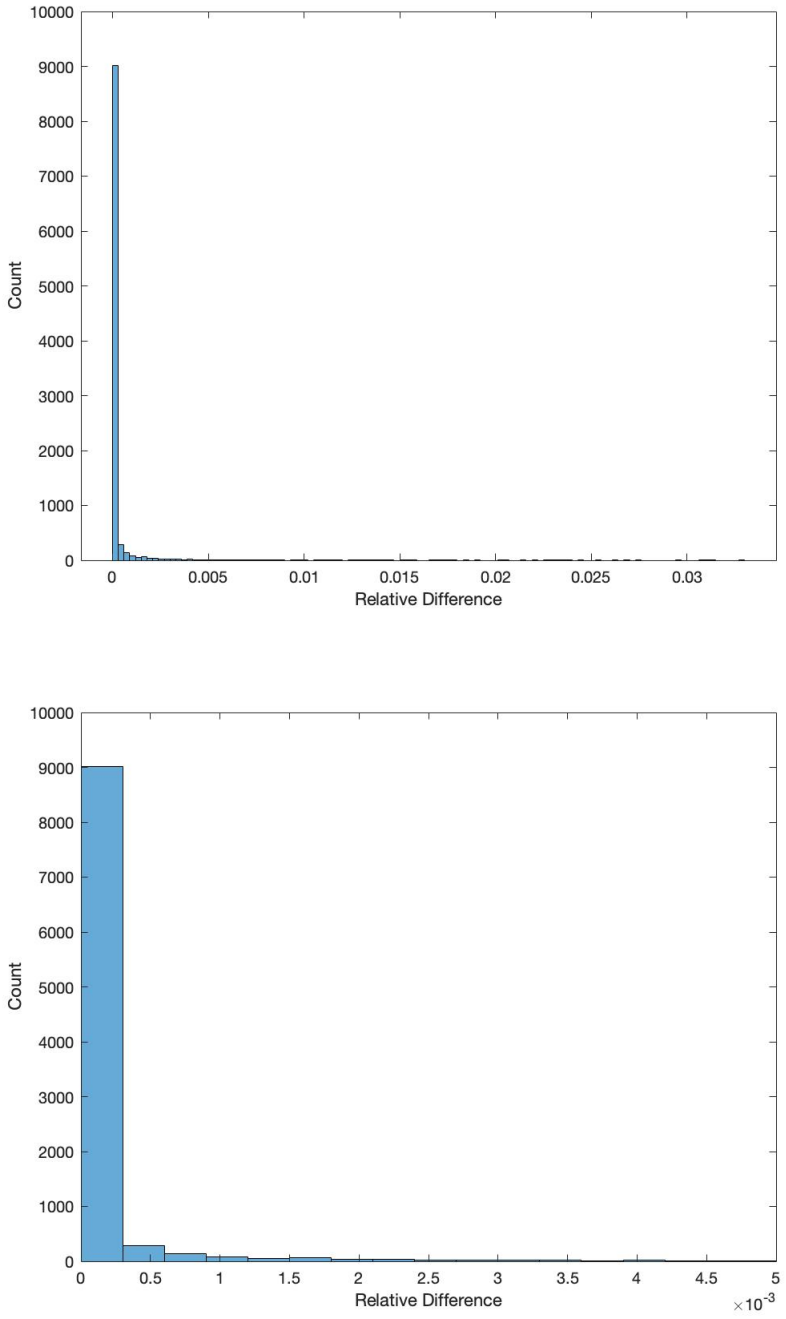

Figure 2.7: The upper graph shows the whole histogram of relative differences between our model and the Seno model. The lower graph zooms in on the left end of the histogram. The maximum value is 0.0328, the mean is $3.2179e-4$, and the variance is $3.1222e-6$.

We analyze (2.15) for our choices of objective functionals under various parameter choices and provide some numerical results.

Managers might try to maximize population size, either the weighted sum of population size at each time step,

$$\sum_{t=1}^{T} A_t N_t \tag{2.39}$$

where A_t are weights for $t < T$, while keeping A_T nonzero for conservation at the final time, where N_t is given by (2.15). In some applications (such as for fisheries), $A_t = 0$ for $t < T$. Note that we will use the notation A to mean the vector $(A_1, A_2, \ldots, A_T)$. Alternately managers may want to maximize yield, perhaps in order to maximize revenue,

$$\sum_{t=0}^{T-1} B_t Y_t \tag{2.40}$$

where B_t is revenue per unit and Y_t denotes the yield at time t. Note that Y_t is a function of N_t given by (2.14). We will see in our results some interplay between A_T and B. The population N_0 is given, but the yield between $t = 0$ and $t = 1$ is dependent on the control time θ_0, thus the indices on the sums in (2.39) and (2.40) start at different times. Managers may also want to minimize cost in some way. The objective functional we wish to maximize as a function of harvest timing is given by

$$J(\theta, \gamma) = A_T N_T + \sum_{t=0}^{T-1} \left(A_t N_t + B_t Y_t - C(\theta_t, \gamma_t) \right) \tag{2.41}$$

where T is the final time, $\theta = (\theta_0, \ldots, \theta_{T-1})$, $\gamma = (\gamma_0, \ldots, \gamma_{T-1})$, and $C(x, y)$ is a continuous cost function. We assume $A_t, B_t \geq 0$. There can be an interplay in balancing the three parts of this objective functional. Note that units of the A_t, B_t and C are adjusted so that the terms in J are in units of dollars. The cost of harvesting may vary depending on the time of the year, due to ease of harvest or labor seasonality.

Define the control set

$$U = \{(\theta, \gamma) = (\theta_0, \theta_1, \ldots, \theta_{T-1}, \gamma_0, \gamma_1, \ldots, \gamma_{T-1}) | \theta_t, \gamma_t \in [0, 1] \forall t \in \{0, 1, \ldots, T-1\}\}. \tag{2.42}$$

We seek to find $(\theta^*, \gamma^*) \in U$ such that

$$J(\theta^*, \gamma^*) = \sup_{(\theta,\gamma)\in U} J(\theta, \gamma). \tag{2.43}$$

Because C, N_{t+1}, and Y_t are continuous functions, J is a continuous real-valued function of θ and of γ, on the compact set $U = [0, 1]^{2T}$. Therefore J achieves a maximum in U. Call this maximum (θ^*, γ^*) and let (θ^n, γ^n) be a sequence in U converging to (θ^*, γ^*). Let N^n be a sequence of time series $\{N_0, N_1^n, \ldots, N_T^n\} \in X = [0, \infty)^{T+1}$ where each term is defined by the difference equation (2.15) evaluated at the corresponding (θ^n, γ^n). That is,

$$N_{t+1}^n = \frac{b(1-\gamma^n)N_t^n}{1 + \beta N_t^n(1 - \gamma^n(1-\theta_t^n))}.$$

Let f be the right-hand side of the above equation. We have f continuous in (θ^n, γ^n) and N^n. Now I will show that f is uniformly bounded. Equation (2.21) gives

$$\frac{(1-\gamma)bN_t^n}{1+\beta N_t^n} \leq f(N_t^n) \leq \frac{(1-\gamma)bN_t^n}{1+\beta(1-\gamma)N_t^n}.$$

Since the denominator on the right-hand side is greater than 1 we have

$$f(N_t^n) \leq (1-\gamma)bN_t^n.$$

Iteratively we have

$$\begin{aligned} f(N_t^n) \leq & (1-\gamma)b\left((1-\gamma)bN_{t-1}^n\right) \\ \leq & (1-\gamma)b\left((1-\gamma)b\left((1-\gamma)bN_{t-2}^n\right)\right) \\ & \vdots \\ \leq & (1-\gamma)^{t+1}b^{t+1}N_0. \end{aligned}$$

Thus N_t^n is uniformly bounded by $(1-\gamma)^T b^T N_0$. Therefore there exists a convergent subsequence of (θ^n, γ^n) and N^n so that

$$\begin{aligned} N_{t+1}^* =& f(N_t^*, \theta_t^*, \gamma^*) \\ =& \frac{b(1-\gamma^*)N_t^*}{1+\beta N_t^*(1-\gamma^*(1-\theta_t^*))}. \end{aligned}$$

We call N^* the optimal state corresponding to that optimal control (θ^*, γ^*). Therefore, we have the following theorem.

Theorem 2.4 (Existence of an optimal control)**.** *There exists an optimal control* $(\theta^*, \gamma^*) \in U$ *such that* $J(\theta^*, \gamma^*) = \sup_{(\theta,\gamma)\in U} J(\theta, \gamma)$.

2.4.1 Optimal control of harvest timing only

We will now present numerical results and explain the optimization technique for controlling the harvest timing only. Several baseline parameter scenarios and some variations will be illustrated with a range of dynamics. We will perform optimal control of θ and keep γ fixed. We consider the quadratic cost function for the cost of harvest to be

$$C(x) = C_1(\hat{x} - x)^2 \tag{2.44}$$

where $\hat{x} \in [0, 1]$ and $\hat{x}$ would correspond to the portion of the season when it is easiest or costs the least to harvest. This could be because of labor seasonality, because of target species behavior such as migration or seasonal aggregation, or other reasons. If $\hat{x} = 0$, it would be least costly to harvest at the beginning of the season and most costly to harvest at the end of the season. This cost, in this case, is monotonically increasing during the season. Or, if $\hat{x} = 1$ where it would be least costly to harvest at the end of the season, with cost decreasing throughout the season.

For our analysis we consider $\hat{x} = \frac{1}{2}$. This cost with $\hat{x} = \frac{1}{2}$ decreases during the first half of the season and increases during the second half of the season. Results for $\hat{x} \in (0, 1)$ not equal to $\frac{1}{2}$ are qualitatively similar.

Our objective functional for control of $\theta = (\theta_0, \ldots, \theta_{T-1})$ only, then, is

$$J_1(\theta) = A_T N_T + \sum_{t=0}^{T-1} \left(A_t N_t + B_t Y_t - C_1 \left(\frac{1}{2} - \theta_t \right)^2 \right). \tag{2.45}$$

We will illustrate here why we do not use optimal control theory for a discrete time system [76]. If we did, then equation (2.15) is our state equation, equation (2.45) is our objective functional, and we use them to form a Hamiltonian. In this case the Hamiltonian is

$$H_t = A_t N_t + B_t \frac{\gamma N_t}{1 + N_t \beta \theta_t} - C_1 (\hat{x} - \theta_t)^2 + \lambda_{t+1} \frac{b(1-\gamma) N_t}{1 + N_t \beta \left(1 - \gamma(1 - \theta_t)\right)} \tag{2.46}$$

which holds for $t = 0, \ldots, T-1$. The adjoints, λ_t, are defined by the solutions of the backwards difference equations

$$\lambda_t = \frac{\partial H_t}{\partial N_t} \tag{2.47}$$

$$\lambda_T = A_T. \tag{2.48}$$

For each time $t \in \{0, \ldots, T-1\}$ we maximize the Hamiltonian with respect to θ_t to produce an optimal control θ^*, λ_{t+1}, and N_t^* where N_t^* is the optimal state corresponding to that optimal control θ^*.

For this Hamiltonian the adjoint equations are

$$\lambda_t = \lambda_{t+1} \frac{(1-\gamma) b}{(1 + \beta N_t (1 - \gamma(1 - \theta_t)))^2} + A_t + B_t \frac{\gamma}{(1 + \beta \theta_t N_t)^2} \tag{2.49}$$

$$\lambda_T = A_T. \tag{2.50}$$

We assume that $A_T \geq 0$. Since every term on the RHS of (2.49) is positive except potentially λ_{t+1}, and $\lambda_T \geq 0$, we conclude that $\lambda_t > 0$ for all $t \in 1, \ldots, T-1$. λ_t are the marginal variations of J_1 with respect to the state, N_t. We have

$$\frac{\partial H_t}{\partial \theta_t} = -B_t \frac{\gamma \beta N_t^2}{(1 + \beta N_t \theta_t)^2} + 2C_1 (\hat{x} - \theta_t) - \lambda_{t+1} \frac{(1-\gamma)\gamma b \beta N_t^2}{(1 + \beta N_t (1 - \gamma(1 - \theta_t)))^2}$$

and

$$\frac{\partial^2 H_t}{\partial \theta_t^2} = 2B\frac{\gamma\beta^2 N_t^3}{(1+\beta N_t(1-\gamma(1-\theta_t)))^3} - 2C_1 + 2\lambda_{t+1}\frac{(1-\gamma)b\gamma^2\beta^2 N_t^3}{(1+\beta N_t(1-\gamma(1-\theta_t)))^3}. \tag{2.51}$$

The only term in the second derivative equation which isn't positive is $-2C_1$, since we've established that $\lambda_{t+1} \geq 0$. Therefore H_t will be concave only when C_1 is sufficiently large. However, an optimal control may still exist even when H_t is not concave.

In some cases one can solve for a characterization of the optimal control in terms of the states N_t, the adjoints λ_t by setting $\frac{\partial H_t}{\partial \theta_t} = 0$ and solving the resulting equation for θ_t [50, 76]. If we attempt this here, the resulting expression is

$$\begin{aligned}
\frac{\lambda_{t+1}(1-\gamma)\gamma b\beta N_t^2}{(1+\beta N_t(1-\gamma(1-\theta_t)))^2} =& 2C_1(\hat{x}-\theta_t) - B_t\frac{\gamma\beta N_t^2}{(1+\beta N_t\theta_t)^2} \\
\lambda_{t+1}(1-\gamma)\gamma b\beta N_t^2\left(1+\beta N_t\theta_t\right)^2 =& 2C_1(\hat{x}-\theta_t)\left(1+\beta N_t\theta_t\right)^2\left(1+\beta N_t(1-\gamma(1-\theta_t))\right)^2 \\
& - B_t\gamma\beta N_t^2\left(1+\beta N_t(1-\gamma(1-\theta_t))\right)^2.
\end{aligned}$$

This is quintic in θ_t (see the C_1 term). We can't solve for θ_t explicitly.

Since we can't solve for the characterization of the optimal control explicitly, we use the MATLAB function fmincon with multistart to optimize the objective functional (2.45) directly. To check our results we wrote a brute force approximation code. This code composes all vectors of length T made up of permutations with repetition from the set $\{0, 0.1, 0.2, 0.3, 0.4, 0.5, 0.6, 0.7, 0.8, 0.9, 1\}$. Each of these vectors represents a possible control vector θ. We take each vector and compute the associated state and yield, then use those to compute the associated value of the objective functional. We use a logic loop to select the θ vector which gives the maximum of the values obtained from the objective functional. This vector is not precisely an optimal control, but an approximation of that optimal control for the given parameters. We can then compare the θ vector chosen by the brute force method with that chosen as optimal control by the direct optimization program. The direct optimization performed well under this comparison test with the brute force method.

We consider maximization of the objective functional (2.45). The term $A_t N_t$ indicates a desire to conserve the stock from which we are harvesting. One can think of it as a

way of making sure the stock doesn't become depleted, perhaps a way of balancing profit with sustainability. Notice that the term $A_t N_t$ is maximized when $\theta_t = 0$ for all t because $\frac{\partial N_{t+1}}{\partial \theta_t} < 0$. The yield or profit term,

$$\frac{B_t \gamma N_t}{1 + \beta N_t \theta_t},$$

is also maximized at $\theta_t = 0$ because the derivative of the yield with respect to θ_t is negative as shown in equation (2.17). Therefore it is only the cost term $-C_1(\hat{x} - \theta_t)^2$ which might not be maximized at $\theta_t = 0$. The combination of these terms might have nonzero optimal θ_t as long as some terms are not maximized at $\theta_t = 0$. Our goal is to find some parameter sets which generate nonzero optimal controls. For this reason, we do not consider the parameter choice $\hat{x} = 0$. Instead we focus on $\hat{x} = 0.5$. Results for other choices of $\hat{x}$ away from 0 and 1 are qualitatively similar.

Now we are beginning to show some numerical results. We now describe our notation for the displayed results and for the comparisons with beginning- and end-of-season harvest. Each time series graph in the figures below shows the optimal control in black squares and the optimal state in blue circles. Each of the controls is graphed on the x-axis with its position on the x-axis marking the timing of the harvest. For example, if the harvest is set for $\theta \equiv 0$, then the controls will appear at $t = 0, 1, \ldots, T-1$ but if the controls are set for $\theta \equiv 0.5$ then the markers for the controls will appear at $t = 0.5, 1.5, \ldots, T-0.5$. The value for the objective functional at the optimal θ is given in the captions, labeled $J_1(\theta^*)$. For comparison, the values of the objective functional for $\theta \equiv 0$ and $\theta \equiv 1$ are also given, we have chosen the notation $J_1(0)$ and $J_1(1)$ where $0 = (0, \ldots, 0) \in \mathbb{R}^T$ and $1 = (1, \ldots, 1) \in \mathbb{R}^T$. All the results below are for the vectors $A = 1$ and $B = 1$. During these numerical results there was no evidence of nonuniqueness of optimal controls.

Table 2.3 contains the first set of baseline parameters for optimal control of θ only. Figure 2.8 shows the states and yields for the baseline parameters from Table 2.3 without optimal control. Table 2.4 records the variations on the baseline parameters from Table 2.3 that we explored. Other variations were also explored but did not produce interesting results and have been omitted.

Table 2.3: First set of baseline parameters for controlling harvest timing only.

Parameter	Value
T	5
C_1	0.1
γ	0.2
β	4
b	5
N_0	1
A	1
B	1

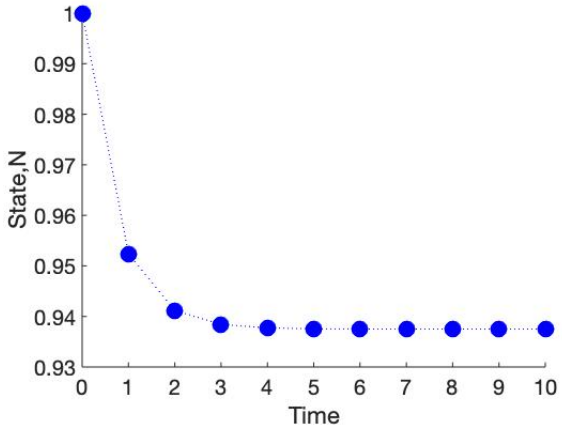

(a) State for $\theta \equiv 0$

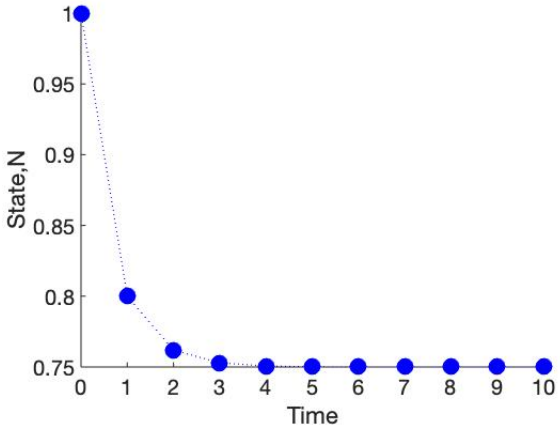

(b) State for $\theta \equiv 1$

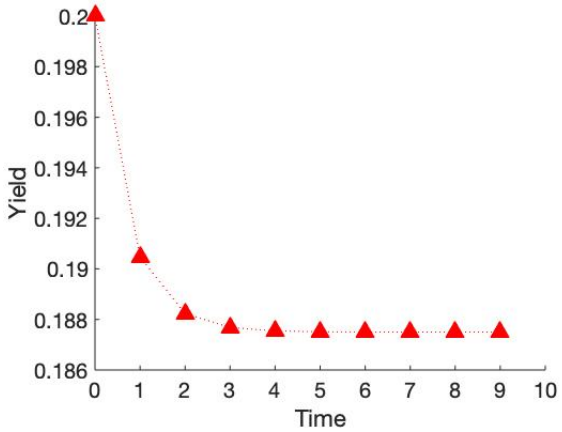

(c) Yield for $\theta \equiv 0$

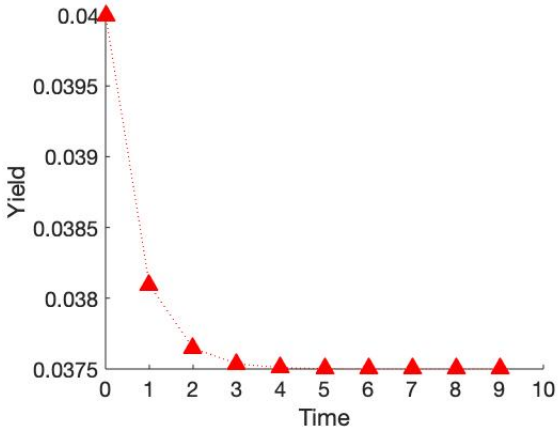

(d) Yield for $\theta \equiv 1$

Figure 2.8: Baseline states and yields under parameter choices from Table 2.3.

Table 2.4: Summary of optimal harvest timing results for variations on the baseline parameters from Table 2.3. The parameters column only lists those which differ from baseline.

Figure	Parameters	$J_1(\theta^*)$	$\frac{J_1(\theta^*)-J_1(0)}{J_1(\theta^*)}$
2.9	baseline	6.54	0
2.10a	$\gamma = 0.02$	5.97	0.004
2.10b	$\gamma = 0.9$	3.01	0.011
2.11	$C_1 = 1$	5.64	0.04
2.12	$C_1 = 1, A_T = 100, A_t = 0$ for $t < T$	93.56	0.001
2.13	$C_1 = 1, N_0 = 10$	16.75	0.008

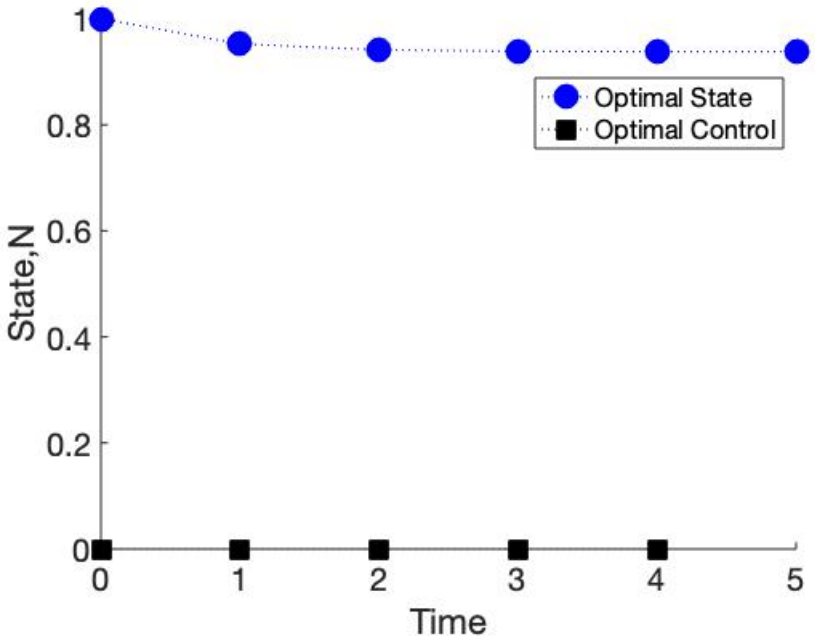

Figure 2.9: This graph was generated with the parameter choices in Table 2.3. The optimal control is $\theta^* = 0$. The values of the objective functional were $J_1(\theta^*) = 6.54 = J_1(0)$, while $J_1(1) = 4.88$.

As a baseline case we consider the parameter choices in Table 2.3. The optimal control under these conditions is shown in Figure 2.9. With these choices of b and β, the without-harvest positive equilibrium would be $N_1^* = 1$. This equilibrium would be asymptotically stable since $\frac{1}{b} = \frac{1}{5} < 1$. With harvest timing fixed at $\theta \equiv 0$ or $\theta \equiv 1$, population and yield would be as in Figure 2.8. For the parameter choices in Table 2.3, there is no reasonable value of C_1 or β which provides a nonzero θ^*.

Next we explored keeping the same parameters as in Table 2.3 except for changing $\gamma = 0.2$ to first a small value of γ (Figure 2.10a) and then a large value of γ (Figure 2.10b). Both of these values of γ offer nonzero optimal control results, though neither has values for $J_1(\theta^*)$ that differ substantially from $J_1(0)$. For the case of very low γ ($\gamma = 0.02$), the value for $J_1(1) = 5.78$ is also very close to the optimal value of $J_1(\theta^*) = 5.97$. These two values differ only by 3%, suggesting that it matters little when harvest occurs at such a low harvest effort. However for Figure 2.10b with a very high value of $\gamma = 0.9$ the value for $J_1(1) = 1.33$ is 56% smaller than $J_1(\theta^*) = 3.01$, so the choice of harvest timing matters more here. These results indicate that there may be some sort of playoff between θ and γ.

In Figure 2.10b there is a vicious cycle: the high value of γ puts increased pressure on the population, leading to lower population size. Then harvesting later increases the pressure on the population even more. In contrast, in Figure 2.10a there is very little pressure on the population because γ is very low. The population size doesn't change much at all. Therefore, harvesting midseason can increase the pressure on a population or it may not.

In Figure 2.11 the parameter choices are the same as those from Table 2.3 except for a value of $C_1 = 1$, an order of magnitude greater than the baseline value for C_1. Notice that this lowers the population size, because harvesting earliest is best for maintaining population size, and shifts the harvest time closer to the middle of the season. Since we have chosen $\hat{x} = 0.5$ the middle of the season is when harvest costs are minimized. The optimal harvest times with this high value for C_1 are slightly earlier than the middle of the season. The objective functional values are $J_1(\theta^*) = 5.64$, $J_1(0) = 5.41$, and $J_1(1) = 3.76$. $J_1(0)$ is only 4% smaller than $J_1(\theta^*)$, but $J_1(1)$ is 33% smaller than $J_1(\theta^*)$. This result shouldn't be surprising since the cost term is the only term pushing harvest later in the season. When the weight on that term increases, minimizing costs becomes relatively more important.

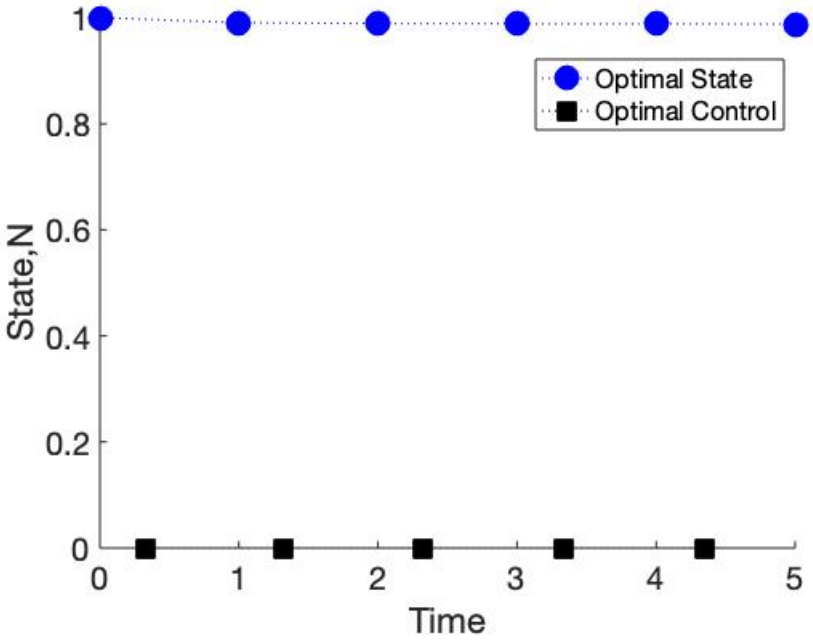

(a) $\gamma = .02$

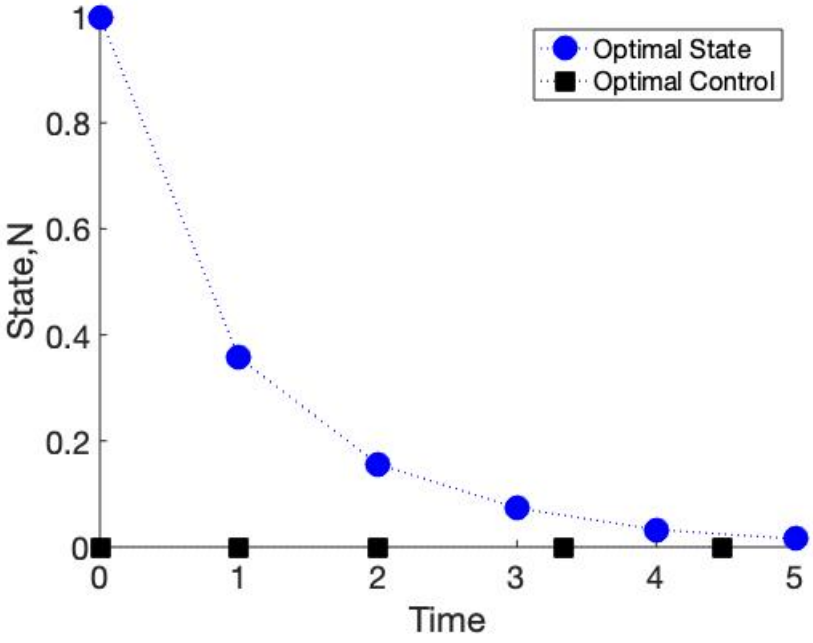

(b) $\gamma = 0.9$

Figure 2.10: The graphs above were generated with parameters the same as in Table 2.3 except for the given values of γ. The values of the objective functional for the top graph are $J_1(\theta^*) = 5.97$, $J_1(0) = 5.95$, and $J_1(1) = 5.78$. The values of the objective functional for the bottom graph are $J_1(\theta^*) = 3.01$, $J_1(0) = 2.98$, and $J_1(1) = 1.33$.

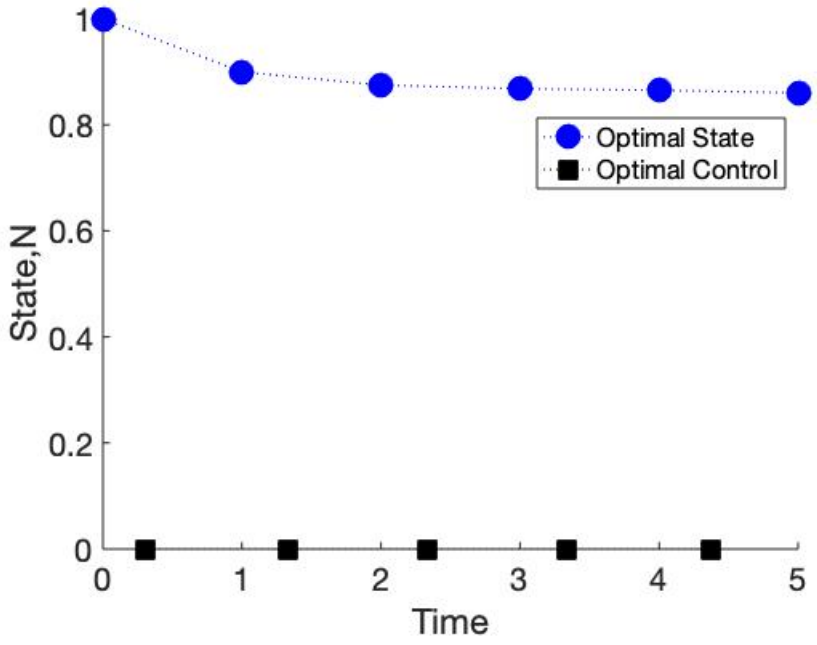

Figure 2.11: The graph above was generated with the same parameters as in Table 2.3 except for $C_1 = 1$. The values of the objective functional were $J_1(\theta^*) = 5.64$, $J_1(0) = 5.41$, and $J_1(1) = 3.76$.

In Figure 2.12 the parameter choices are the same as in Figure 2.11 but instead of $A_t = 1$ for all t, with $A_T = 100$ and $A_t = 0$ for $t < T$. In this case, the first two harvests are mid-season and the final three harvests are at the beginning of the season, allowing the final population to be as large as possible.

In Figure 2.13 the parameter choices from Table 2.3 are the same except for $N_0 = 10$ instead of $N_0 = 1$ and $C_1 = 1$ instead of $C_1 = 0.1$. Notice that initially it is best to harvest earliest in the season and take advantage of the population surplus. The initial population size of 10 is far above the without-harvest equilibrium value of 1. The population would decrease to 1 on its own within a few time steps in the absence of harvest. With harvest at $\theta \equiv 0$, as seen in Figure 2.8, the initial population of 10 is still much higher than the pseudo-equilibrium population of just below .94. After this aggressive initial harvesting, however, the population size drops down quickly and it becomes best to harvest closer to the middle of the season. This is because the smaller harvest reduces the benefits gained from yield and population maintenance and therefore the relative importance of minimizing costs

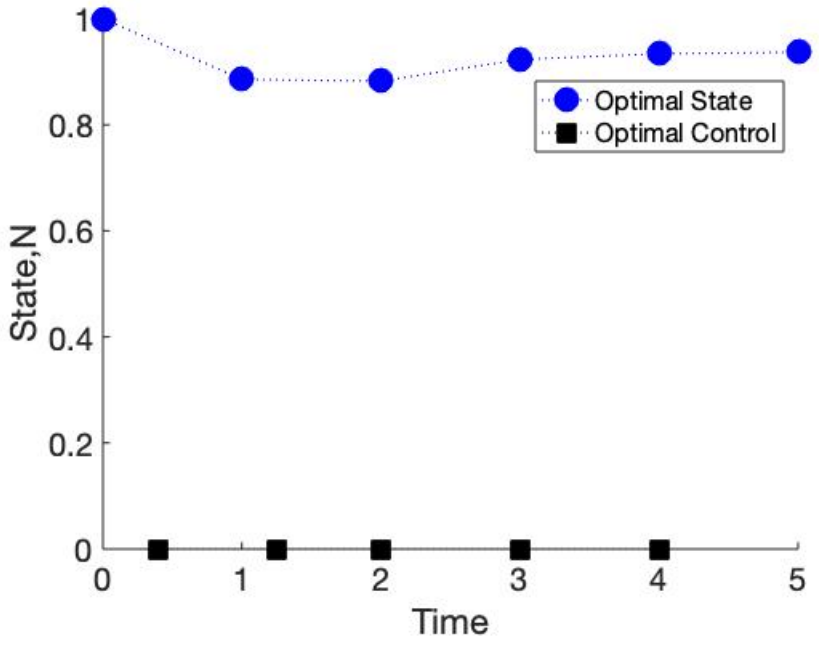

Figure 2.12: The graph above was generated with the same parameters as in Table 2.3 except for $C_1 = 1$ and $A_T = 100$. The values of the objective functional were $J_1(\theta^*) = 93.56$, $J_1(0) = 93.46$, and $J_1(1) = 73.96$.

increases. However, because the earlier contributions to the objective functional are large, there is only 0.8% difference between $J_1(\theta^*) = 16.75$ and $J_1(0) = 16.61$.

Figure 2.14 shows time series for the state and yield for the second baseline parameter choices from Table 2.5 with either $\theta \equiv 0$ or $\theta \equiv 1$. With these values for b and β the without-harvest equilibrium would be $N_1^* = 50$ and this equilibrium would be asymptotically stable since $\frac{1}{b} = \frac{1}{6} < 1$. Note that these second baseline parameters include lower density-dependent mortality and somewhat higher birth rate, so the equilibrium is larger than for the first baseline parameters and the population is faster-growing. Table 2.6 records the variations on baseline parameters from Table 2.5 that we explored. The highest numbers in the fourth column reflect the parameter combinations for which harvest timing not being equal to 0 was most important. The smallest numbers reflect cases where harvest timing of 0 was very close to optimal.

Figure 2.15, generated using the set of parameters in Table 2.5, illustrates a second baseline case. The initial condition is much smaller than 50, therefore even with harvest

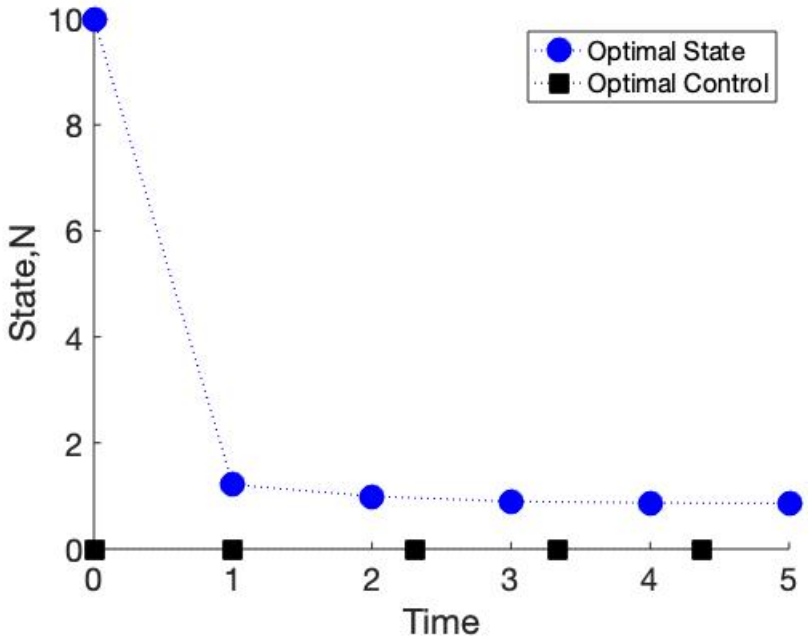

Figure 2.13: The graph above was generated with the same parameters as in Table 2.3 except for $C_1 = 1$ and $N_0 = 10$. The values of the objective functional were $J_1(\theta^*) = 16.75$, $J_1(0) = 16.61$, and $J_1(1) = 12.99$.

Table 2.5: Second set of baseline parameters for controlling harvest timing only.

Parameter	Value
T	10
C_1	0.1
γ	0.2
β	0.1
b	6
N_0	30
A	1
B	1

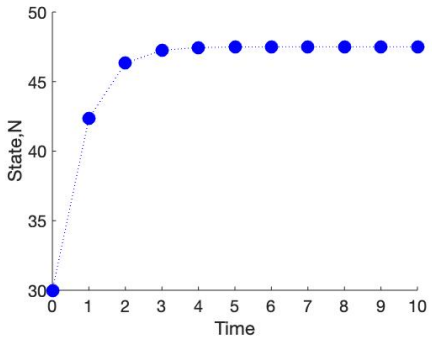

(a) State for $\theta \equiv 0$

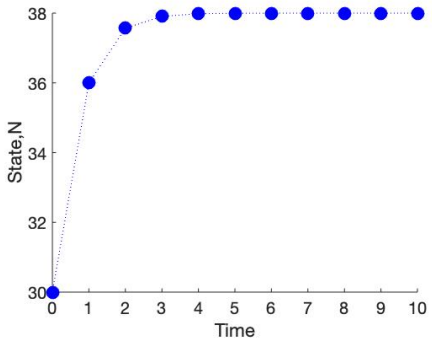

(b) State for $\theta \equiv 1$

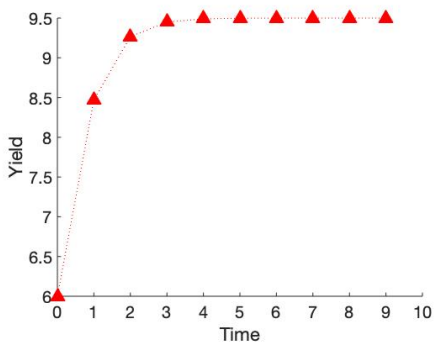

(c) Yield for $\theta \equiv 0$

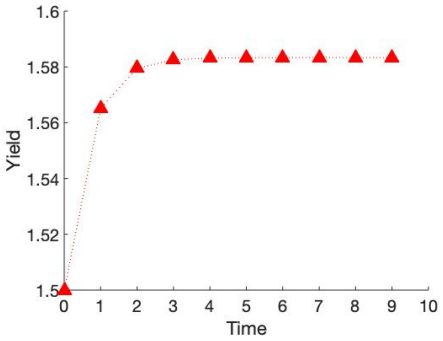

(d) Yield for $\theta \equiv 1$

Figure 2.14: Second baseline states and yields under parameter choices from Table 2.5.

Table 2.6: Summary of results for controlling harvest timing only with variations on the baseline parameters from Table 2.5. The parameters column only lists those which differ from baseline.

Figure	Parameters	$J_1(\theta^*)$	$\frac{J_1(\theta^*)-J_1(0)}{J_1(\theta^*)}$
2.15	second baseline	588.29	0
2.16a	$\gamma = 0.0001$	523.89	0.0004
2.16b	$\gamma = 0.9$	115.27	0.0004
2.17	$C_1 = 100$	479.14	0.29
2.18	$C_1 = 100, C_T = 100, C_t = 0$ for $t < T$	4719.8	0.03

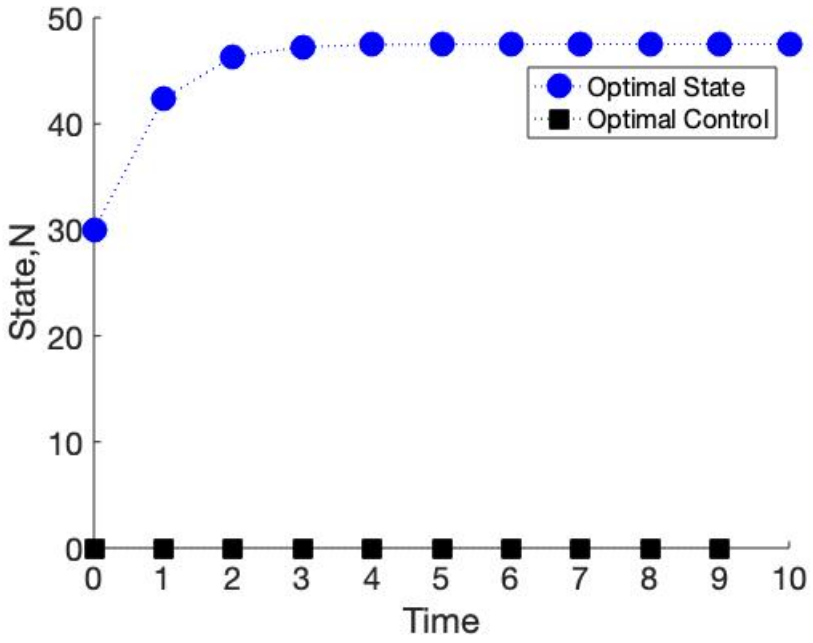

Figure 2.15: The graph above was generated using the set of parameters in Table 2.5 (note that with these choices of β and b, 50 is the without-harvest equilibrium). The values of the objective functional were $J_1(\theta^*) = 588.29 = J_1(0)$, while $J_1(1) = 422.93$.

the population increases. It appears to approach some sort of equilibrium. The value for $J_1(\theta^*) = 588.29$ is identical to that of $J_1(0)$ because $\theta^* \equiv 0$. $J_1(1) = 422.93$ is 28% smaller. Under moderate harvesting intensity, it remains best to harvest early. This strategy results in a reliably large harvest and allows the population size to remain relatively large (over 45, close to the without-harvest equilibrium).

In Figure 2.16a the parameters are the same as in Table 2.5 except for $\gamma = .0001$ much smaller the baseline value of $\gamma = 0.2$. This tiny rate of harvest produces such a small yield that controlling costs becomes relatively much more important. To minimize cost, optimal harvest time approaches the middle of the season. The objective functional values are $J_1(\theta^*) = 523.89$, $J_1(0) = 523.69$, and $J_1(1) = 523.61$. $J_1(0)$ is only .04% smaller than $J_1(\theta^*)$ and $J_1(1)$ is only .05% smaller than $J_1(\theta^*)$.

In Figure 2.16b the parameters are the same as in Figure 2.15 except for $\gamma = 0.9$, much larger than the baseline value of $\gamma = 0.2$. Under this immense harvest pressure, the population size drops rapidly. By time step 7 the population size is small enough that revenue becomes relatively less important than minimizing cost. In the last three time steps harvest timing drifts closer and closer to the middle of the season. At a value of $J_1(\theta^*) = 115.27$, $J_1(\theta*)$ is only .04% larger than $J_1(0) = 115.22$. However, $J_1(\theta^*)$ is 56% larger than $J_1(1) = 51.01$. This indicates that while harvest timing is important at high harvest intensity, for these parameters there is little to be gained by deviating from harvesting at the beginning of the season.

Figure 2.17 used the same parameters as Table 2.5 except for large $C_1 = 100$, increased from $C_1 = 0.1$. This high weight on the cost shifted importance away from maximizing revenue and conserving stock toward minimizing cost. As a result, optimal harvest timing was in the middle of the season. $J_1(0) = 338.54$ was 29% smaller than $J_1(\theta^*) = 479.14$. And $J_1(1) = 173.18$ was 64% smaller than $J_1(\theta^*)$. Under these conditions the cost saved by harvesting at the optimal time outweighs the revenue lost by not harvesting at the beginning of the season.

Figure 2.18 was generated with the same parameters as in Table 2.5 except for $C_1 = 100$ (increased from $C_1 = 0.1$), $A_T = 100$, and $A_t = 0$ for $t < T$ (changed from $A_t = 1$ for all t). Until about time step 6 both optimal control and optimal state are the same as in Figure

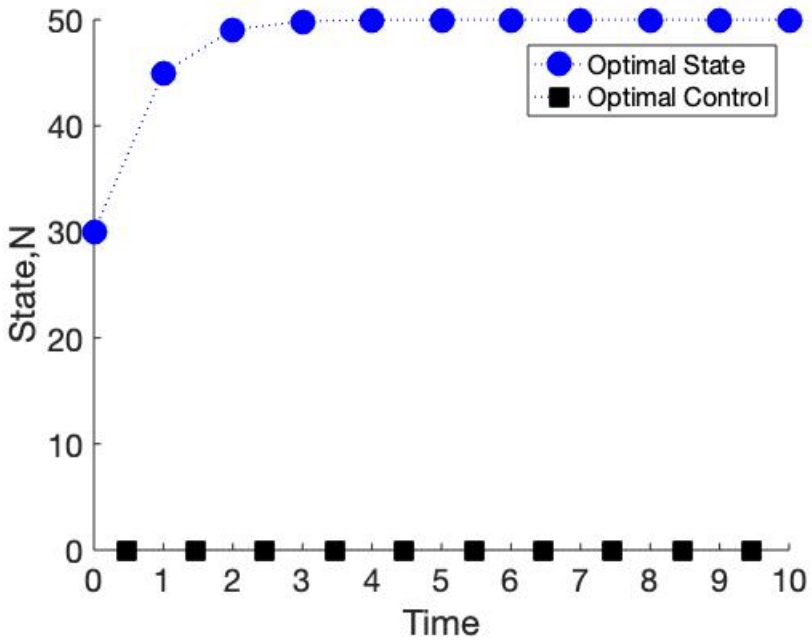

(a) $\gamma = .0001$

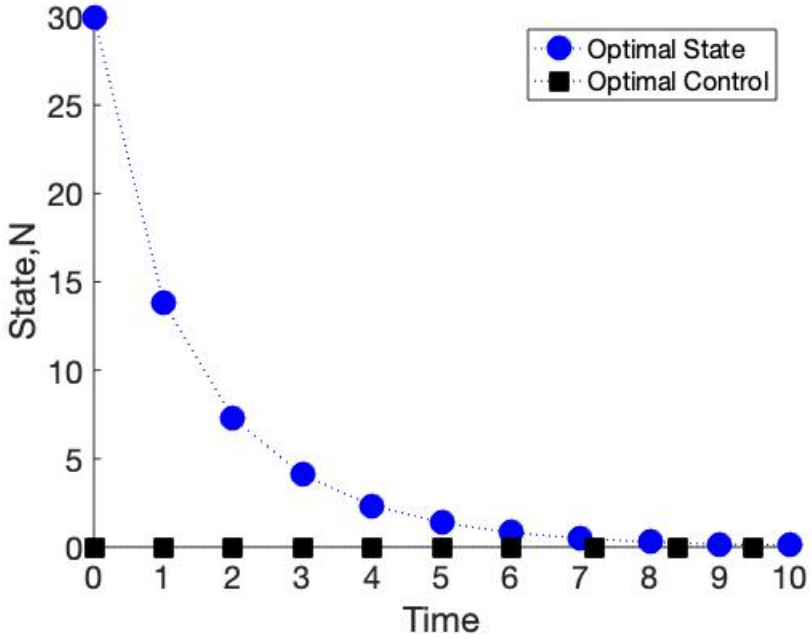

(b) $\gamma = 0.9$

Figure 2.16: The graphs above were generated with parameters the same as in Table 2.5 except for the two given values of γ. The values of the objective functional for the top graph are $J_1(\theta^*) = 523.89$, $J_1(0) = 523.69$, and $J_1(1) = 523.61$. The values of the objective functional for the bottom graph are $J_1(\theta^*) = 115.27$, $J_1(0) = 115.22$, and $J_1(1) = 51.01$. Compare the top with Figure 2.10a and the bottom with Figure 2.10b.

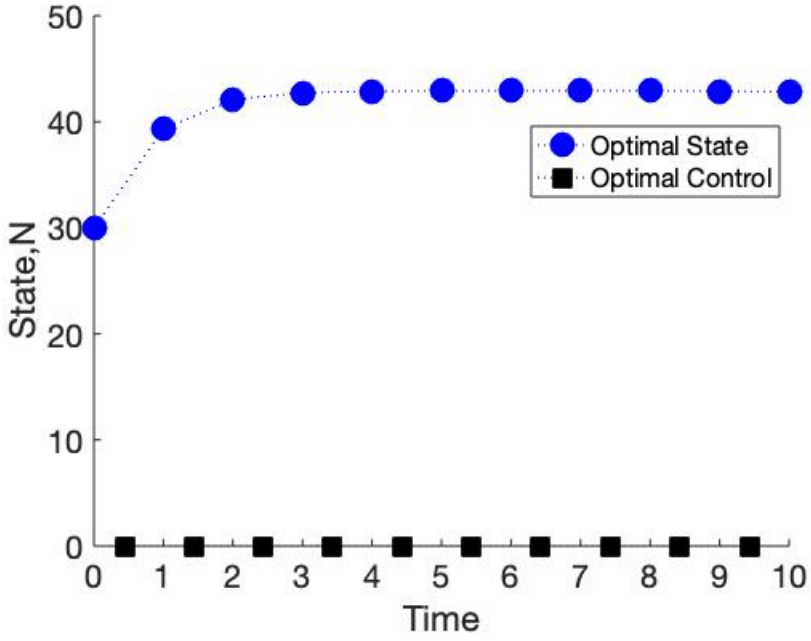

Figure 2.17: The graph above was generated with the same parameters as in Table 2.5 except for $C_1 = 100$. The values of the objective functional were $J_1(\theta^*) = 479.14$, $J_1(0) = 338.54$, and $J_1(1) = 173.18$. Compare with Figure 2.11.

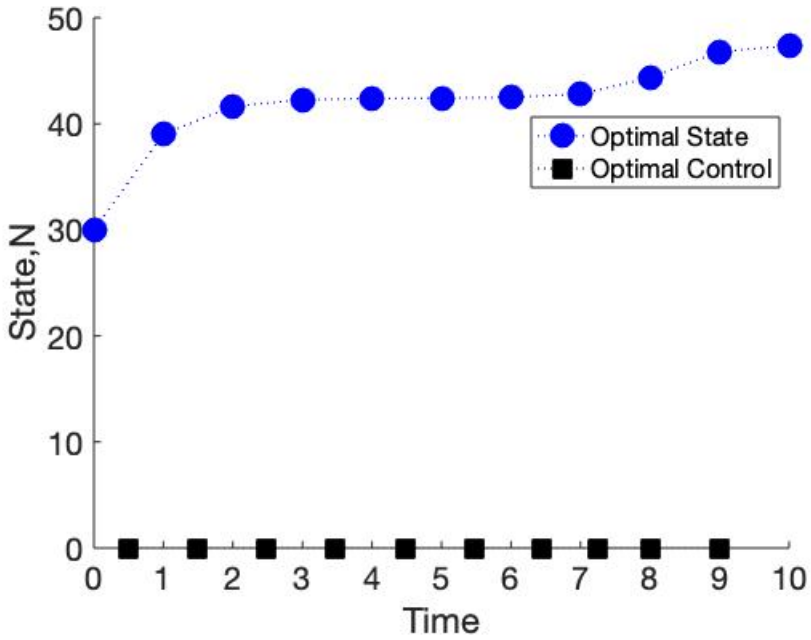

Figure 2.18: The graph above was generated with the same parameters as in Table 2.5 except for $C_1 = 100$ and $A_T = 100$. The values of the objective functional were $J_1(\theta^*) = 4719.8$, $J_1(0) = 4590.2$, and $J_1(1) = 3565.7$. Compare with Figure 2.17.

2.17. After that, harvest timing moves earlier, causing population to grow until the last step so that the final population will be as high as possible.

Let's compare the results for variations on the first set of baseline parameters from Table 2.3 with those for the second set of baseline parameters from Table 2.5. Compare Figure 2.15 with Figure 2.9 to note that though the population size is different, population values appear to be approaching an equilibrium and harvest timing remains 0. Compare Figure 2.16a with Figure 2.10a. For the larger population size, we have taken a smaller value of γ to illustrate the effect of small γ because of scaling. In both figures, though, low harvest intensity leads to mid-season harvest timing. Notice also that the larger population in Figure 2.16b means that it takes longer for the high harvest level to deplete the population to the point where harvest timing moves to the middle of the season than it does in Figure 2.10b. But in both cases once stock becomes depleted it is best to harvest mid-season. It takes a higher value of C_1 (that is a higher cost) in Figure 2.17 to move harvest times to midseason than it does in Figure 2.11, but in both cases high costs shift importance away from maximizing revenue toward minimizing costs. Therefore, results are qualitatively similar for the two baseline sets of parameters explored here. Indeed, results are qualitatively similar for much of parameter space. In general, it seems best to harvest early for most parameter combinations. However, when yield is low (due to low harvest intensity or low stock) or when costs related to harvest timing are high it is best to harvest mid-season.

Looking at the objective functional (2.41) term by term we see that only the cost term might not be optimized at a control of $\theta \equiv 0$. The terms $A_T N_T$ and $A_t N_t$ are maximized at $\theta \equiv 0$ because $\dfrac{\partial N_{t+1}}{\partial \theta_t} < 0$. The term $B_t Y_t$ is maximized at $\theta \equiv 0$ because $\dfrac{\partial Y_t}{\partial \theta_t} < 0$. If $\hat{x} \neq 0$ the cost term is the only term not optimized at $\theta \equiv 0$. It is odd that the goals of both conservation and maximal yield are optimized for the same value of θ. This does not match ecological intuitions. Our model describes very simple population dynamics. Perhaps for those species which fit the assumptions of our model, the two goals are not in conflict. One oddity of our model, for example, is that if $\theta \equiv 0$ then harvest happens immediately after birth. This would mean that the species must mature over a very short time relative to the length of the season, because otherwise we would be harvesting juveniles. And, if there were surviving adults from the previous season, the profit for harvesting a juvenile would

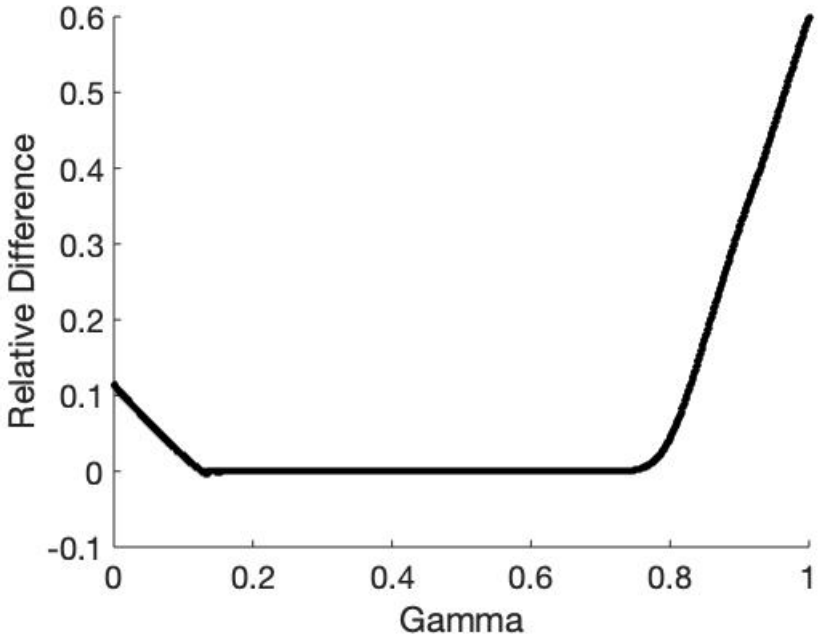

Figure 2.19: The y-axis displays $\frac{J(\theta^*)-J(0)}{J(\theta^*)}$ for each value of γ. Other parameters were as in Table 2.5.

be the same as the profit for harvesting an adult, since we do not differentiate between the two classes. These assumptions do not hold true for many species where harvest timing is an important consideration. We would not wish to harvest immature fish, for example. But there might be species where harvesting young individuals is more attractive, for example as a matter of taste. We will expand our consideration to more complicated models in future work. Next, though, we consider the case where ecological or economic constraints fix the harvest timing to a mid-season time.

To explore the playoff between γ and θ^*, we ran our direct optimization code on 1000 values of γ uniformly distributed on $[0, 1]$ with other parameters as in Table 2.5. Figure 2.19 shows the relative difference in the values of the optimal objective functional from that for $\theta \equiv 0$, that is $\frac{J(\theta^*)-J(0)}{J(\theta^*)}$. Figure 2.20 shows how the maximum value of the vector θ^* varies over the range of γ for these parameters. Figure 2.21 shows time on one axis, γ on another, and the height is determined by the components of the corresponding θ^*. In general, optimal θ_t values for earlier time steps are lower than those for later time steps. For small or large

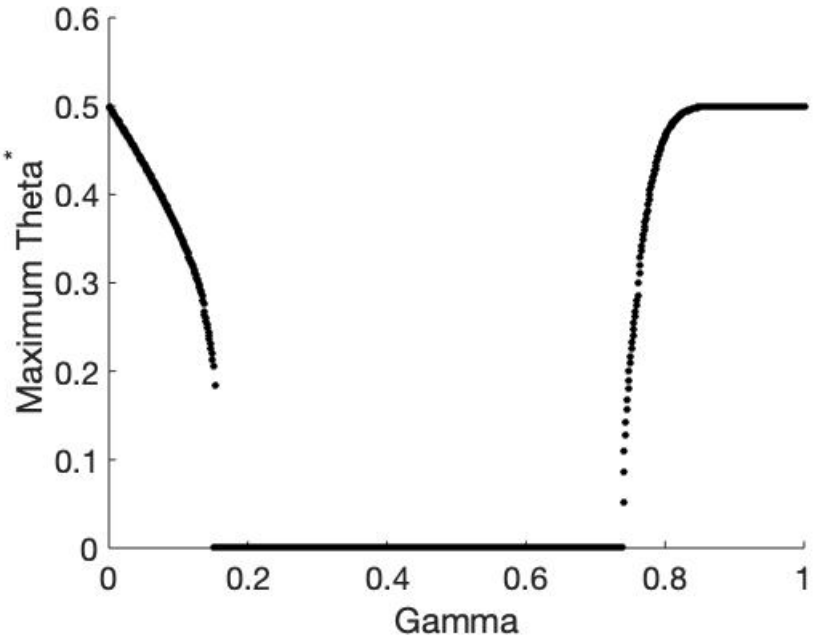

Figure 2.20: The largest component of each vector θ^* is displayed on the y-axis. Parameters other than γ were as in Table 2.5.

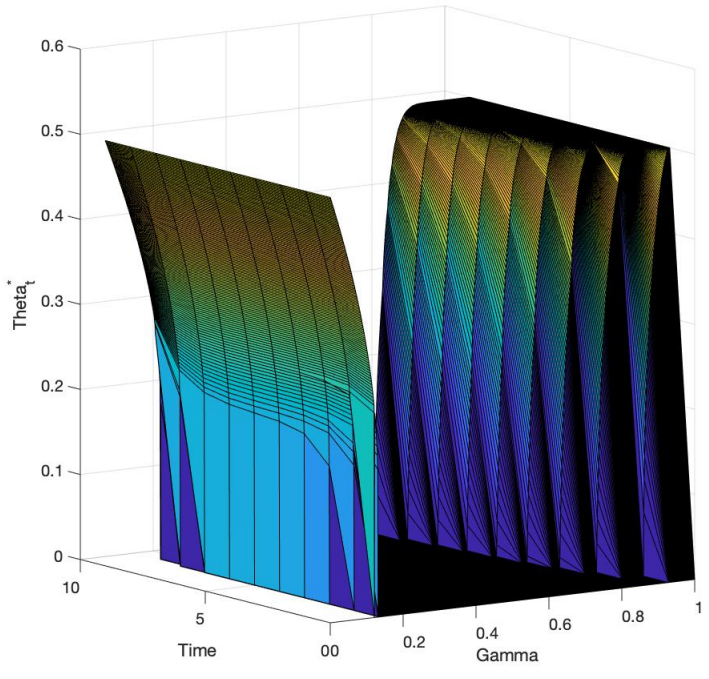

Figure 2.21: Parameters other than γ were as in Table 2.5.

values of γ, θ^* is nonzero. For intermediate values of γ, approximately from $\gamma = .15$ to $\gamma = .74$, $\theta^* \equiv 0$.

2.4.2 Optimal control of harvest intensity only

We now consider controlling harvest intensity γ instead of harvest timing θ. We will consider two cases for the timing of harvest: $\theta \equiv 0$ and $\theta \equiv 0.5$. In both cases we seek to maximize the objective functional

$$J_2(\gamma) = A_T N_T + \sum_{t=0}^{T-1} \left(A_t N_t + B_t Y_t - C_2 \gamma_t - C_3 \gamma_t^2 \right) \tag{2.52}$$

where $A_T N_T$ represents our desire to conserve the population,

$$B_t Y_t = \frac{B_t \gamma_t N_t}{1 + \beta N_t \theta_t}$$

corresponds with our goal of maximizing profit, and $C_2\gamma_t + C_3\gamma_t^2$ represents the nonlinear cost of harvesting. Note that in the yield,

$$\frac{N_t}{1 + \beta N_t \theta_t}$$

is the size of the population at θ_t, the time of harvest. With nonzero A_t for $t < T$ all parameter sets we triend resulted in $\gamma^* \equiv 0$, so we removed that term. Thus, our objective functional becomes

$$J_2(\gamma) = A_T N_T + \sum_{t=0}^{T-1} \left(B_t Y_t - C_2 \gamma_t - C_3 \gamma_t^2 \right). \tag{2.53}$$

As in section 2.4.1 we use a direct optimization of the objective functional using MATLAB functions fmincon and multistart.

For each of the figures below the top graph shows the optimal states and the bottom graph shows the optimal controls. For $\theta \equiv 0.5$ the state and control are in blue circles and for $\theta \equiv 0$ the state and optimal control are in green triangles. In the legends, by "Optimal State$_0$" we mean the state associated with the control $\theta \equiv 0$ and by "Optimal Gamma$_0$" we mean the optimal control γ^* associated with $\theta \equiv 0$. The optimal state and optimal control associated

Table 2.7: Baseline parameters for controlling harvest intensity only.

Parameter	Value
T	10
β	0.1
b	6
N_0	30
C_2	0.2
C_3	0.2
A	1
B	1

Table 2.8: Summary of results for optimal control of harvest intensity only. In the parameters column only variations from the baseline are listed.

Figure	Parameters	$J_2(\gamma^*)$, $\theta \equiv 0$	$J_2(\gamma^*)$, $\theta \equiv 0.5$	Relative Difference
2.22	baseline	191.9627	96.90	0.50
2.23	$A = 0$	169.7516	63.43	0.63
2.24	$N_0 = 10$	171.2708	91.68	0.46
2.25	$N_0 = 10, C_2 = C_3 = 5$	120.12	64.2132	0.47
2.26	$N_0 = 10, b = 1.2$	9.6661	7.19	0.26
2.27	$N_0 = 10, b = 20$	731.9510	277.68	0.62

with $\theta \equiv 0.5$ are listed in the legends as "Optimal State" and "Optimal Control." Each caption lists the objective functional value for $\theta \equiv 0$ and the objective functional value for $\theta \equiv 0.5$. The baseline parameter values for each of these figures is given in Table 2.7. For these parameters the without-harvest equilibrium is 50. Table 2.8 shows the variations on the baseline parameters that we explored.

Figure 2.22 was generated using the parameter values from Table 2.7. We see that the optimal controls and optimal states for $\theta \equiv 0.5$ and for $\theta \equiv 0$ have the same trends but different values. In Figure 2.22a population sizes for both the $\theta \equiv 0.5$ and $\theta \equiv 0$ drop down initially until settling at a relatively steady value for time steps 2 through 8. After step 8, population size grows rapidly until the final time, $T = 10$. In Figure 2.22b, the optimal control for both $\theta \equiv 0.5$ and for $\theta \equiv 0$ stays relatively steady for times $t = 0$ through $t = 7$. Then the optimal controls drop to much lower values for the last two time steps. The optimal

state for $\theta \equiv 0.5$ tends to be smaller and so does the optimal control. Because of the weight placed on population size at the final time, both populations are harvested more lightly as time draws to a close allowing the populations to rebound to a higher value. For $\theta \equiv 0.5$ the objective function value is $J_2(\gamma^*) = 96.90$ and for $\theta \equiv 0$ the objective function value is $J_2(\gamma^*) = 191.96$, a percent difference of 50%. With these parameter values there is great advantage to harvesting early. Note that for $\theta \equiv 0.5$ the values for N_t are lower than than those for $\theta \equiv 0$, as are the values of γ_t^*.

Figure 2.23 shows a case where all other parameters are held equal to Table 2.7 but the weight on final population size is $A = 0$ instead of $A = 1$. The values of the states and controls are similar to 2.22 with an early small decline in population and then a steady population and a steady level of harvest until near the end of the time interval. Since no weight is given to having a population conserved, harvest intensity rises and the populations crash. The values of the objective functional are $J_2(\gamma^*) = 169.75$ for $\theta \equiv 0$ and $J_2(\gamma^*) = 63.43$ for $\theta \equiv 0.5$, a percent difference of 63%. Again, harvesting early is highly advantageous.

Figure 2.24 has the same parameters as Table 2.7 except for $N_0 = 10$, decreased from the baseline value of $N_0 = 30$. Here the initial optimal controls are lower, allowing the population to reach a greater size before harvesting at intensities very close to those in figure 2.22. Like figure 2.22, they demonstrate a decrease in optimal harvest intensity at later times to allow for population rebound. The values of the objective functional are $J_2(\gamma^*) = 171.27$ for $\theta \equiv 0$ and $J_2(\gamma^*) = 91.68$ for $\theta \equiv 0.5$, a percent difference of 46%.

Figure 2.25 has the same values for all parameters as Table 2.7 except with higher $C_2 = C_3 = 5$ (changed from 0.2). These high costs cause a much greater decrease in harvest for $\theta \equiv 0$ than for $\theta \equiv 0.5$. Optimal states are higher under these higher harvest costs. The values of the objective functional are $J_2(\gamma^*) = 120.12$ for $\theta \equiv 0$ and $J_2(\gamma^*) = 64.21$ for $\theta \equiv 0.5$, a percent difference of 47%. Other cases of larger values for C_2 and C_3 are not shown here, but increasing to $C_2 = C_3 = 20$ causes harvest to become too costly to harvest at all, while increasing $C_2 = C_3 = 2$ is insufficient to show any change from the baseline case.

Figure 2.26 has the same parameter values as Table 2.7 except for $b = 1.2$ (decreased from $b = 6$) and $N_0 = 10$ (decreased from $N_0 = 30$). With these parameter values the

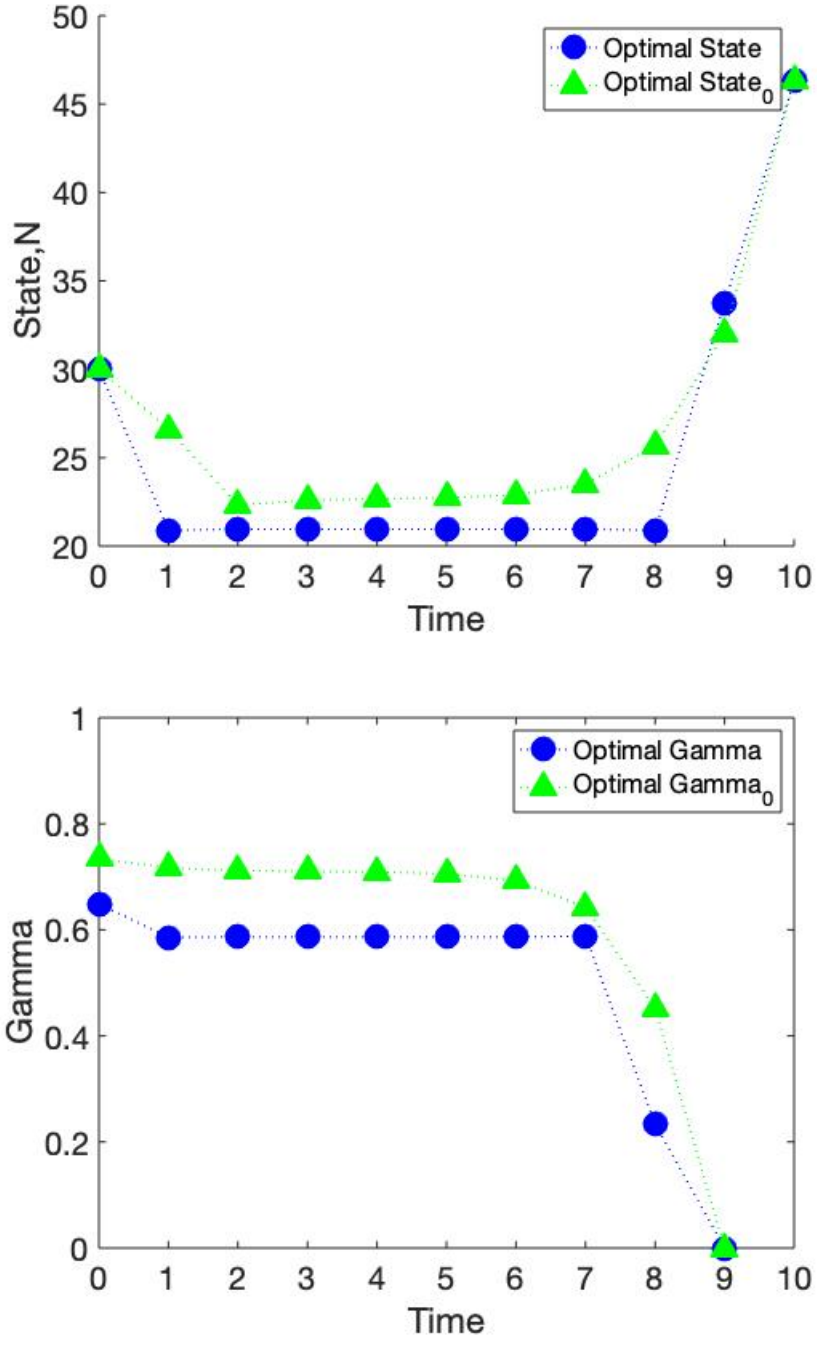

Figure 2.22: The graphs above were generated with parameters from Table 2.7. The labels without subscript refer to the case with $\theta \equiv 0.5$ and the labels with subscript 0 refer to the case with $\theta \equiv 0$. The values of the objective functional are $J_2(\gamma^*) = 191.96$ for $\theta \equiv 0$ and $J_2(\gamma^*) = 96.90$ for $\theta \equiv 0.5$. For these parameter values the without-harvest equilibrium would be 50.

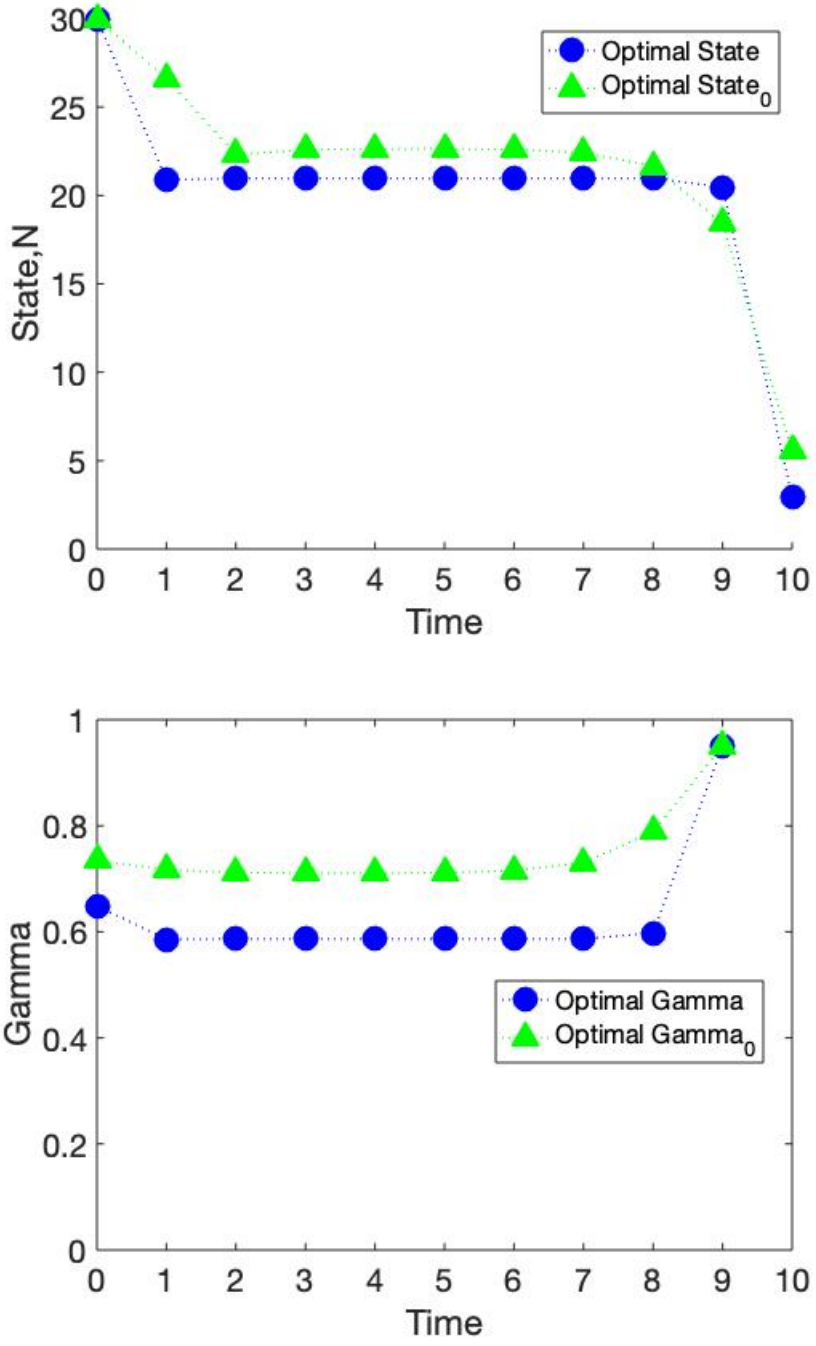

Figure 2.23: The graphs above were generated with parameters from Table 2.7 except for $A = 0$. The values of the objective functional are $J_2(\gamma^*) = 169.75$ for $\theta \equiv 0$ and $J_2(\gamma^*) = 63.43$ for $\theta \equiv 0.5$.

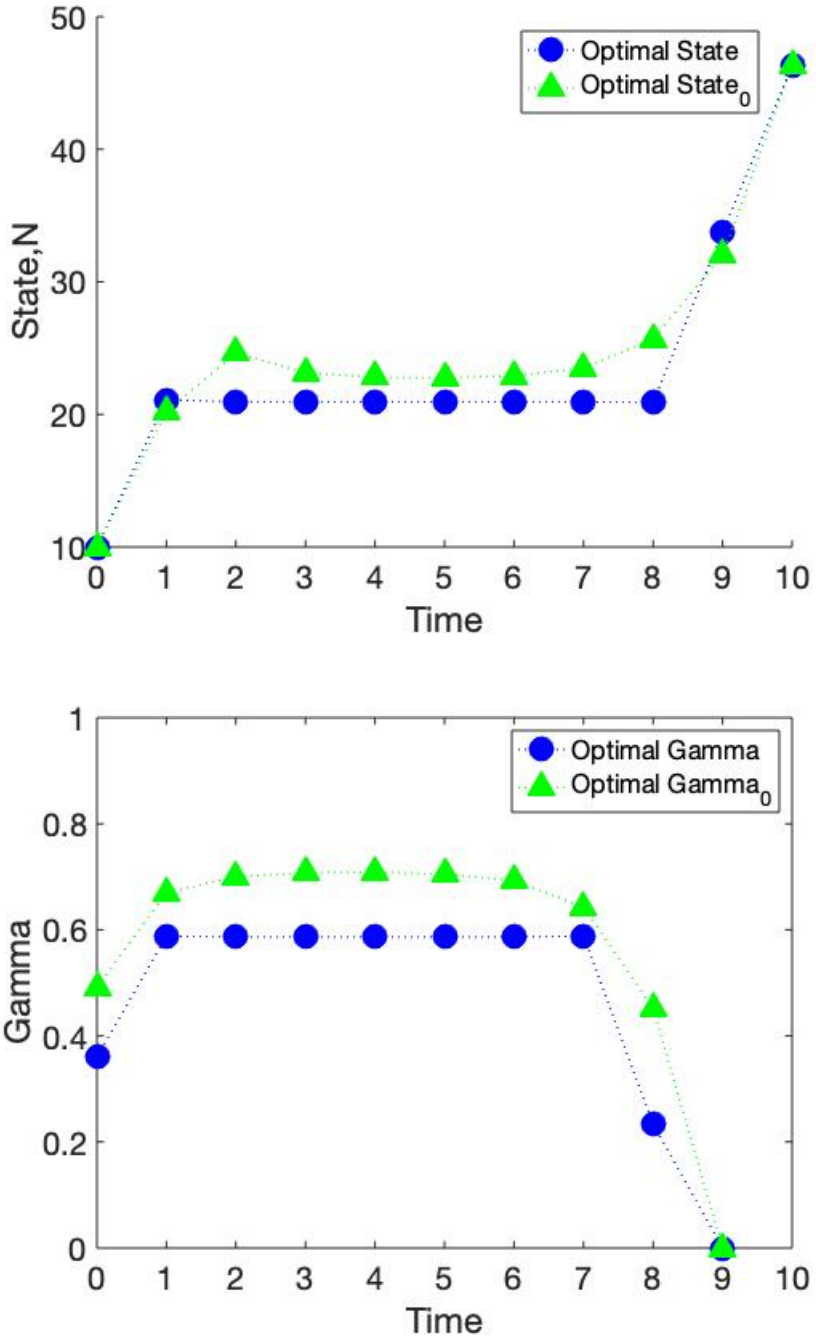

Figure 2.24: The graphs above were generated with parameters from Table 2.7 except for $N_0 = 10$. The values of the objective functional are $J_2(\gamma^*) = 171.27$ for $\theta \equiv 0$ and $J_2(\gamma^*) = 91.68$ for $\theta \equiv 0.5$.

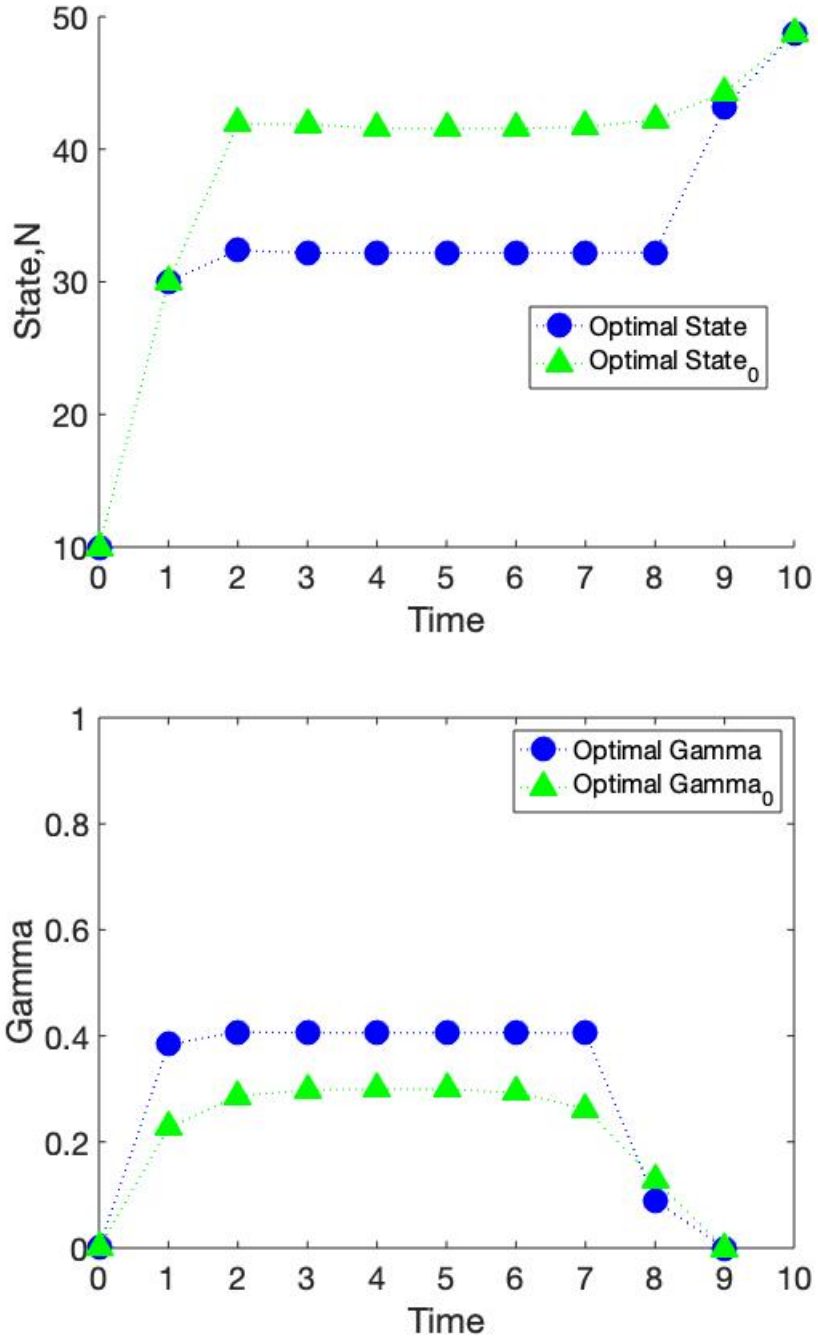

Figure 2.25: The graphs above were generated with parameters from Table 2.7 except for $N_0 = 10$ and $C_2 = C_3 = 5$. The values of the objective functional are $J_2(\gamma^*) = 120.12$ for $\theta \equiv 0$ and $J_2(\gamma^*) = 64.21$ for $\theta \equiv 0.5$.

without-harvest equilibrium is 2. Here the population has very little growth, and it is best to have high harvest effort early on. The population crashes because of the low growth and then it is best not to harvest at all. The values of the objective functional are $J_2(\gamma^*) = 9.67$ for $\theta \equiv 0$ and $J_2(\gamma^*) = 7.19$ for $\theta \equiv 0.5$, a percent difference of 26% (the lowest difference we observed). Increasing the death rate parameter, β, has a similar effect, causing high early harvest, a population crash, and then no harvest at all.

Figure 2.27 has the same parameter values as Table 2.7 except for $b = 20$ (increased from $b = 6$). With these parameter values the without-harvest equilibrium is 190. Here the population growth is very strong and harvesting intensity is higher. The values of the objective functional are $J_2(\gamma^*) = 731.95$ for $\theta \equiv 0$ and $J_2(\gamma^*) = 277.68$ for $\theta \equiv 0.5$, a percent difference of 62%. Decreasing the death rate parameter, β, has a similar effect.

For every parameter combination we tried, it was always better to harvest early rather than mid-season. In some cases harvest intensity was optimal at very high levels, and in some cases it was optimal at much lower levels, but the general trends in optimal state and in optimal harvest intensity were similar for $\theta \equiv 0$ and for $\theta \equiv 0.5$. In each case early harvest intensity was high or low to bring the population to a pseudo-equilibrium where harvest intensity could be maintained at a strong level for intermediate time steps. Then harvest intensity dropped low to allow the population to grow toward the final time if a positive weight was given to final population size. But with zero weight given to final population size, harvest intensity ramped up to increase the final yields.

2.4.3 Optimal control of harvest intensity and harvest timing

Let's investigate the control of both harvest timing θ and harvest intensity γ. We consider the objective functional to be maximized

$$J_3(\theta, \gamma) = A_T N_T + \sum_{t=0}^{T-1} \left(A_t N_t + B_t Y_t - C_1(\frac{1}{2} - \theta_t)^2 - C_2\gamma_t - C_3\gamma_t^2 \right) \tag{2.54}$$

where $C_2\gamma_t + C_3\gamma_t^2$ represents the nonlinear cost of harvest, and $C_1(\frac{1}{2} - \theta_t)^2$ represents the cost associated with the timing of the harvest. As in section 2.4.1 we wish to conserve the population ($A_t N_t$) and gain revenue from the yield ($B_t Y_t$). Once again we use direct

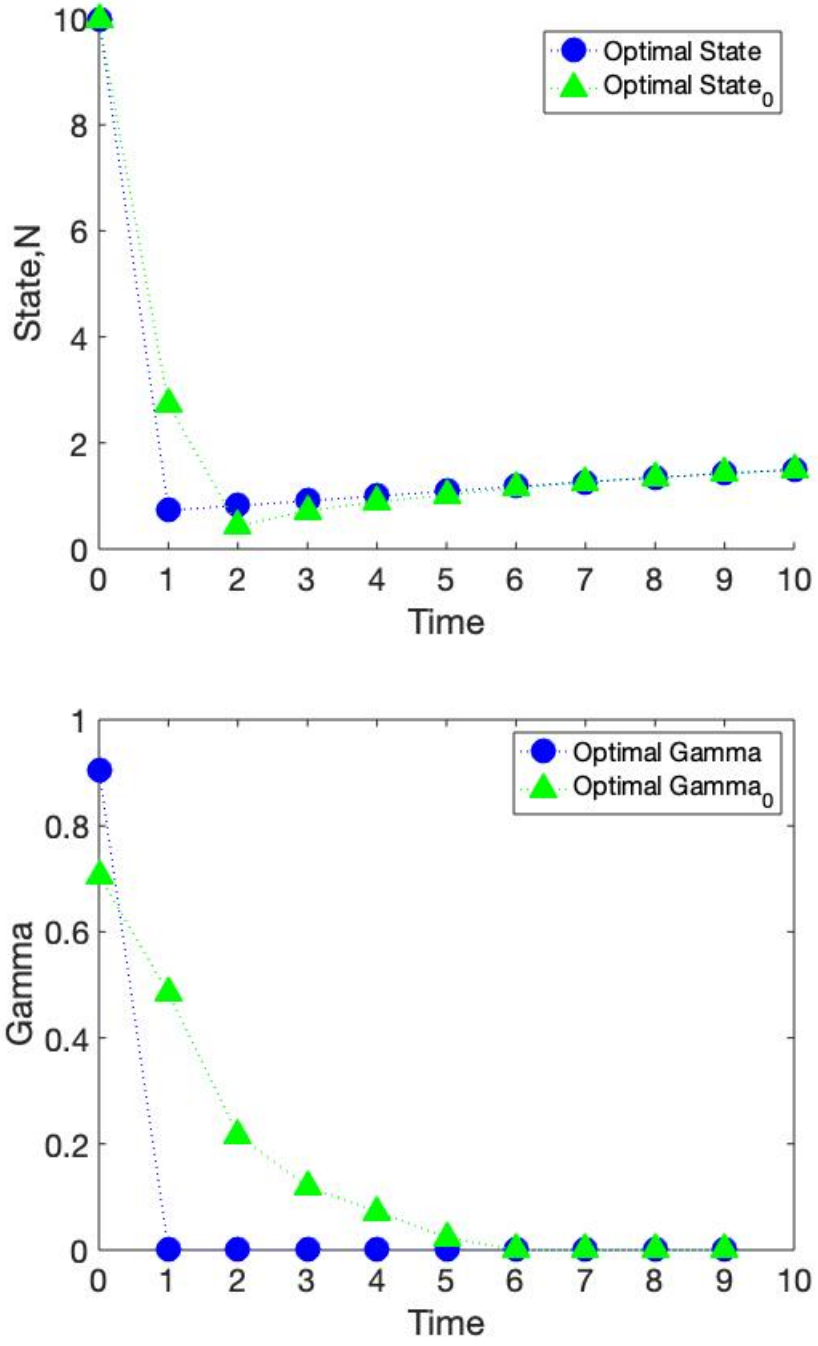

Figure 2.26: The graphs above were generated with parameters from Table 2.7 except for $b = 1.2$ and $N_0 = 10$. The values of the objective functional are $J_2(\gamma^*) = 9.67$ for $\theta \equiv 0$ and $J_2(\gamma^*) = 7.19$ for $\theta \equiv 0.5$.

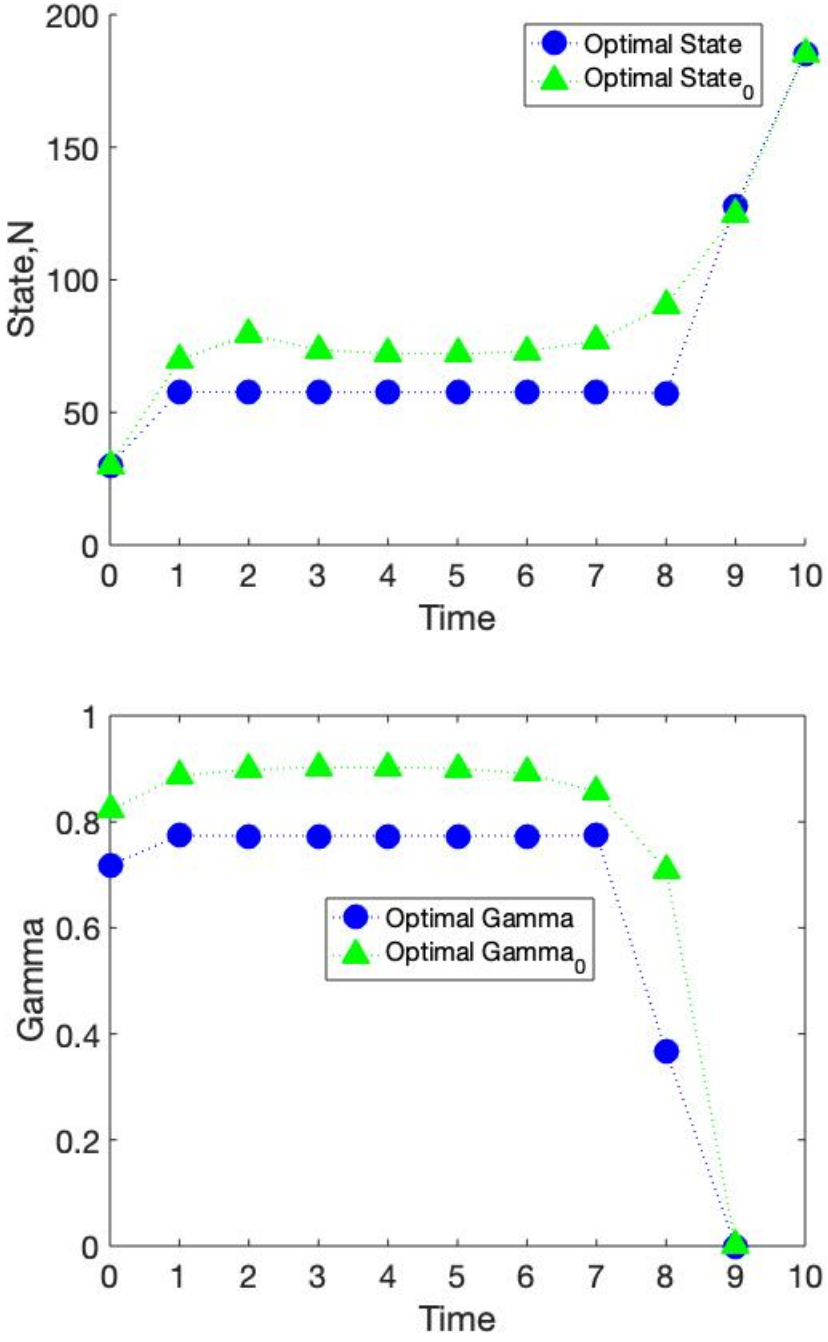

Figure 2.27: The graphs above were generated with parameters from Table 2.7 except for increasing b to 20 and setting $N_0 = 10$. The values of the objective functional are $J_2(\gamma^*) = 731.95$ for $\theta \equiv 0$ and $J_2(\gamma^*) = 277.68$ for $\theta \equiv 0.5$. Notice the ratio between the two values for $J_2(\gamma^*)$ is much larger in this case.

Table 2.9: Baseline parameters for controlling both harvest intensity and harvest timing. Note that many of these are the same as those from the second baseline case for control of harvest timing only. The only differences are the inclusion of values for C_2 and C_3, which were not part of the objective functional for control of harvest timing only.

Parameter	Value
T	10
β	0.1
b	6
N_0	30
C_1	0.1
C_2	0.2
C_3	0.2
A	1
B	1

Table 2.10: Summary of results for controlling both harvest intensity and harvest timing. The parameters column lists only those which differ from the baseline case, which is listed in Table 2.9.

Figures	Parameters	$J_3(\theta^*, \gamma^*)$	$\frac{J_3(\theta^*,\gamma^*)-J_3(0,\gamma^*)}{J_3(\theta^*,\gamma^*)}$
2.28	baseline	596.00	0
2.29	$b = 1.2$	53.03	0.004
2.30	$b = 2, C_1 = 1, A = 0$	42.00	0.024
2.31	$b = 2, C_1 = 1$	120.82	0.017
2.32	$C_1 = 50$	512.79	0.15

optimization of the objective functional (2.54). In each pair of graphs below the top graph shows the state in blue circles and the harvest timing in black squares while the bottom graph shows the harvest intensity, γ_t, in pink diamonds.

In addition to performing optimal control on the baseline set of parameters listed in Table 2.9, we will also try the variations on these baselines listed in Table 2.10.

Our set of baseline parameters for these simulations is listed in Table 2.9. With these parameter values the without-harvest equilibrium is 50. For this combination of parameters, used to generate Figure 2.28, it is best to harvest always at the beginning of the season, meaning $\theta^* \equiv 0$. Harvest intensity begins below 0.2 in the first step, allowing the population

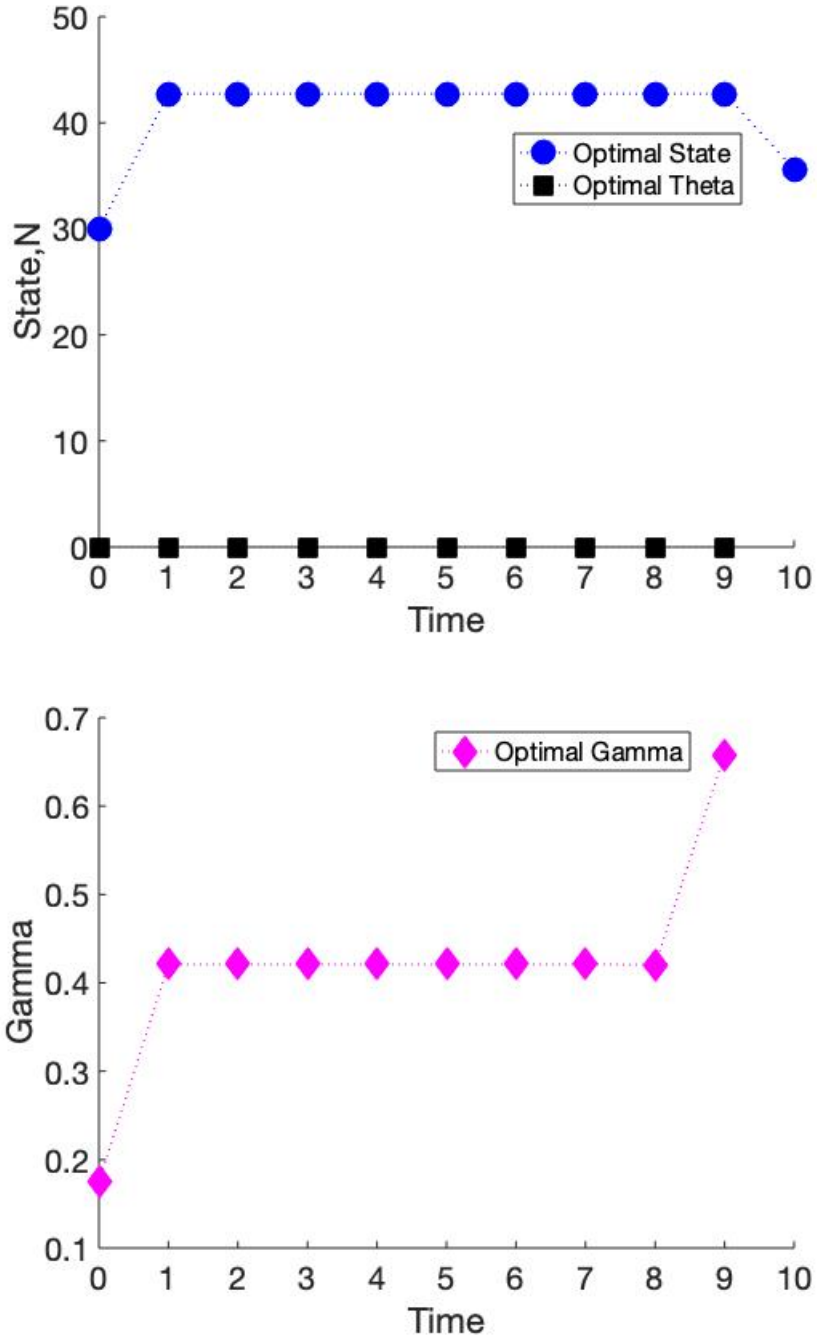

Figure 2.28: The graphs for optimal control of γ and θ above were generated with parameters from Table 2.9. The values of the objective functional are $J_3(\theta^*, \gamma^*) = 596.00 = J_3(0, \gamma^*)$ and $J_3(1, \gamma^*) = 282.31$.

to reach a higher level. Once the population reaches this level harvesting can be maintained at an intensity of above 0.4 without a drop in population. Harvest intensity is higher during the final harvest (above 0.6) because the final population size is not weighted higher than intermediate population sizes, so it is best to get a higher final yield. The values of the objective functional are $J_3(\theta^*, \gamma^*) = 596.00 = J_3(0, \gamma^*)$ and $J_3(1, \gamma^*) = 282.31$. Harvesting at the beginning of the season gives a 53% higher objective functional value than harvesting at the end of the season.

Figure 2.29 was generated with the same parameters as in Table 2.9 except for a smaller value of $b = 1.2$ (decreased from $b = 6$). With these parameter values the without-harvest equilibrium is 2. Under these circumstances harvest intensity starts high (above 0.7) because the initial population is well above what the environment can sustain, and this high harvest is taken at the beginning of the season. Then harvest intensity drops to near 0 and harvest timing shifts to midseason to keep the population level and minimize the cost of harvesting. The final harvest has a higher intensity again and the final harvest timing is at the beginning of the season, causing the final population size to drop lower. The values of the objective functional are $J_3(\theta^*, \gamma^*) = 53.03$, $J_3(0, \gamma^*) = 52.83$ and $J_3(1, \gamma^*) = 26.24$. $J_3(\theta^*, \gamma^*)$ differs from $J_3(0, \gamma^*)$ by only 0.4%. Qualitatively similar results occur for changing β to be larger instead of changing b to be smaller. That is, for a larger β, intensity is high in early time steps and the last time step with very low intensity in intermediate time steps. For the first few time steps and the last, harvest timing is at the beginning of the seasons and for intermediate time steps harvest timing is during the middle of the season.

In Figure 2.30 we keep the parameters from Table 2.9 except for $b = 2$ and $C_1 = 1$, meaning birth has decreased from baseline of $b = 6$ and cost associated with timing has increased from baseline of $C_1 = 0.1$. This produces cycles of harvest timing and harvest intensity combinations. Harvest intensity is very high (about 0.9 in the first cycle and about 0.5 in the remaining cycles) for one time step and then very low (close to 0) for one step. On the step with the high intensity, harvest timing is at the beginning of the season. Then for the low-harvest step harvest timing is at mid-season. This produces cycles in the population where the population drops low, then recovers over the low-harvest mid-season step and then drops low again. In this case, the cycle in harvest intensity seems to be the most crucial

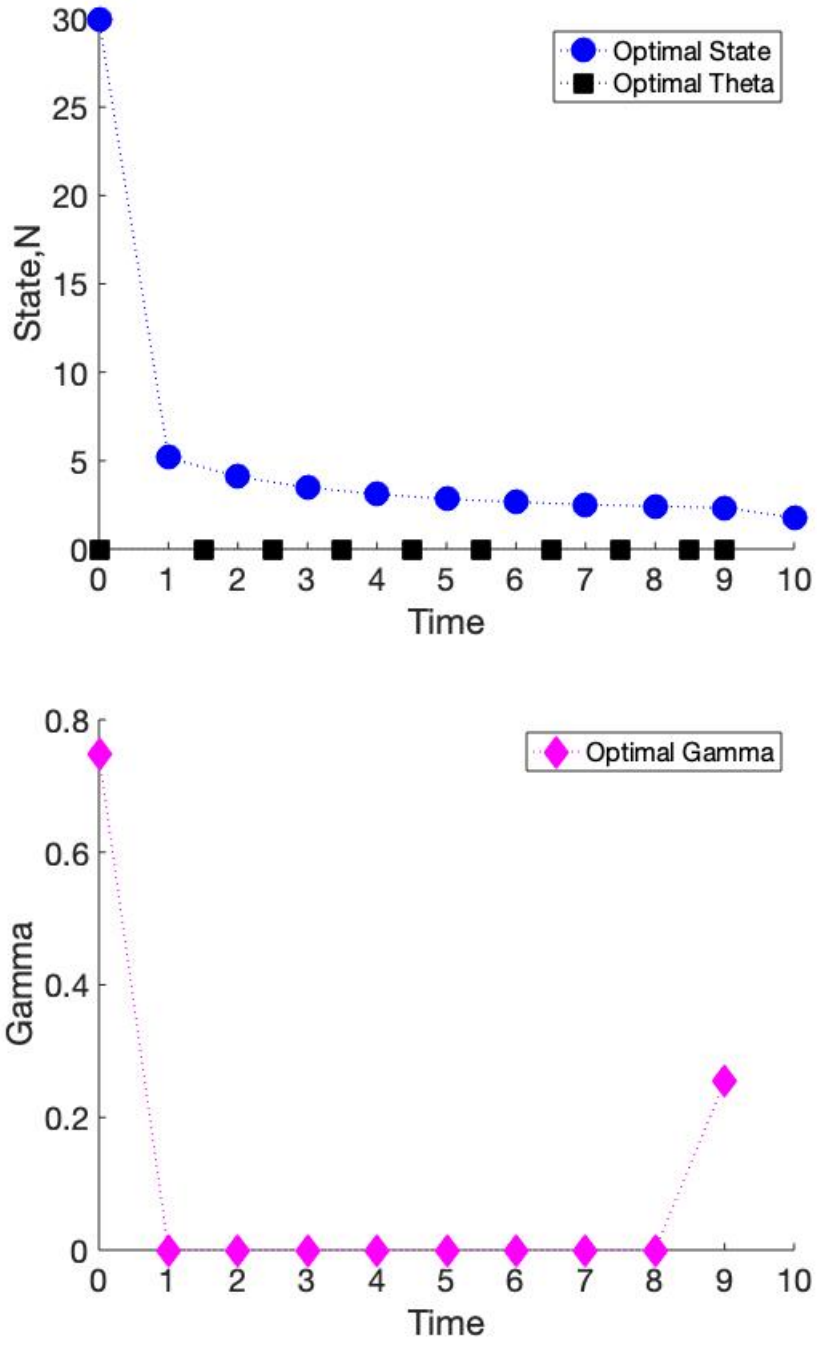

Figure 2.29: The graphs for optimal control of γ and θ above were generated with parameters from Table 2.9 except for $b = 1.2$. The values of the objective functional are $J_3(\theta^*, \gamma^*) = 53.03$, $J_3(0, \gamma^*) = 52.83$ and $J_3(1, \gamma^*) = 26.24$.

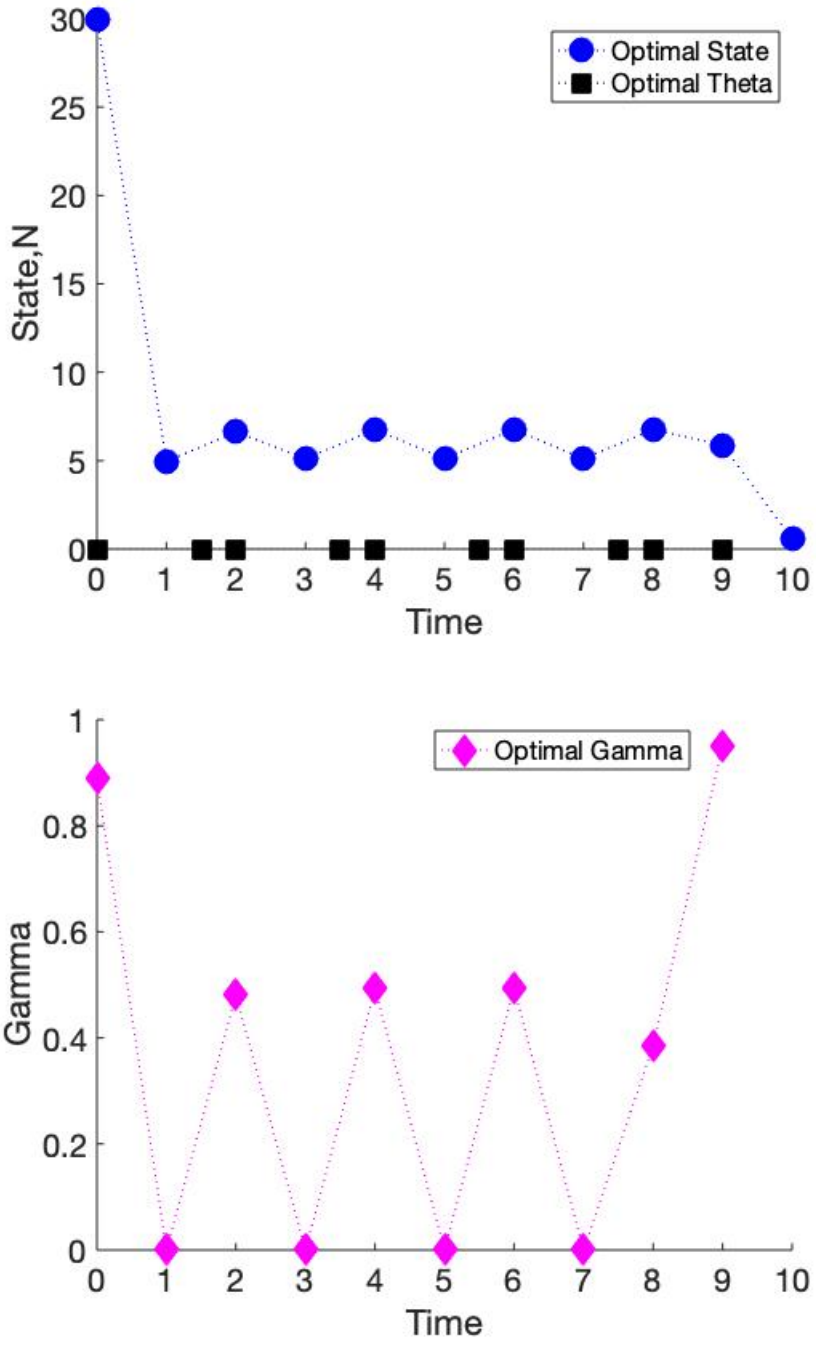

Figure 2.30: The graphs for optimal control of γ and θ above were generated with parameters from Table 2.9 except for $b = 2$, $C_1 = 1$ and $A = 0$. The values of the objective functional are $J_3(\theta^*, \gamma^*) = 42.00$, $J_3(0, \gamma^*) = 41.00$ and $J_3(1, \gamma^*) = 10.71$.

part of the maximization process. The objective functional values for combining exclusively beginning-of-season harvest timing with the same cycle of harvest intensity is similar to that for the cyclic harvest timing. In other words $J_3(\theta^*, \gamma^*)$ differs from $J_3(0, \gamma^*)$ by only 2.4%. The values of the objective functional are $J_3(\theta^*, \gamma^*) = 42.00$, $J_3(0, \gamma^*) = 41.00$ and $J_3(1, \gamma^*) = 10.71$.

Figure 2.31 shows the optimal control results for the same paramters as in Figure 2.30 except for $A = 1$ rather than $A = 0$. Figure 2.31 shows that without setting $A = 0$, we do not get cycles.

Figure 2.32 was generated with parameters from Table 2.9 except for $C_1 = 50$ (increased from $C_1 = 0.1$). For some seasons it is best to harvest hardly at all (intensity close to 0) with mid-season harvest while for other seasons it is best to harvest early in the season with high intensity (about 0.6).

Some of the conclusions from control of harvest timing only seem to also hold when both harvest timing and harvest intensity are controlled. For example, lower yield seems to go along with harvest timings closer to mid-season. However, we observe novel behavior as well. In particular, sometimes there are cycles of both harvest intensity and harvest timing. These cycles seem to occur when emphasis is taken away from population conservation and shifted toward revenue maximization and cost minimization.

2.5 Second mechanistic model

Many different mechanistic models could be derived using the same process with different assumptions about each process. Here we'll derive another mechanistic model using the same setup with a different nonlinearity in the mortality process. Instead of the ODE (2.12), for the within season dynamics we'll use

$$\frac{dn}{d\tau} = -\mu N_t n(\tau) \tag{2.55}$$

$$n(0^+) = N_t \tag{2.56}$$

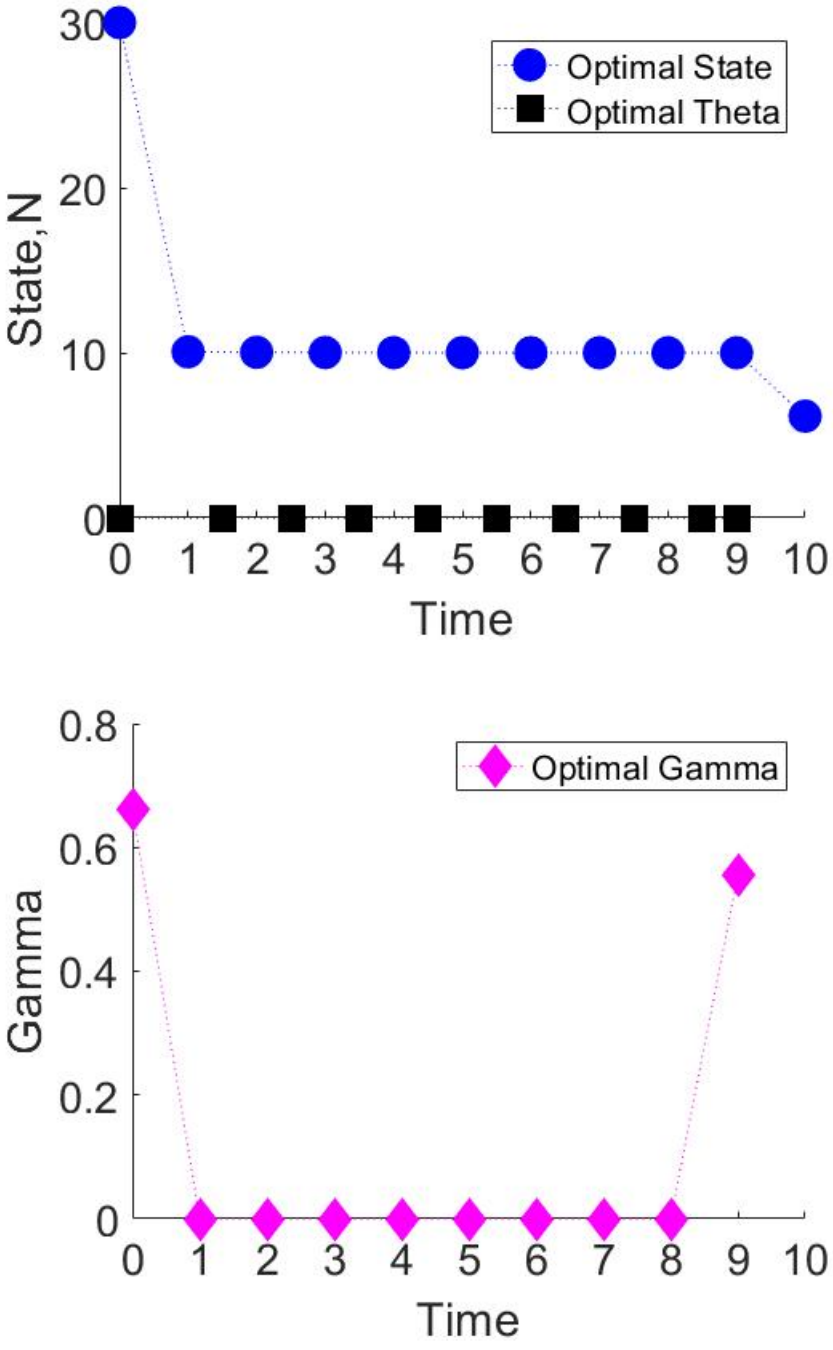

Figure 2.31: The graphs for optimal control of γ and θ in the first model above were generated with parameters from Table 2.9 except for $b = 2$ and $C_1 = 1$. The values of the objective functional are $J_3(\theta^*, \gamma^*) = 120.82$, $J_3(0, \gamma^*) = 118.82$ and $J_3(1, \gamma^*) = 86.88$.

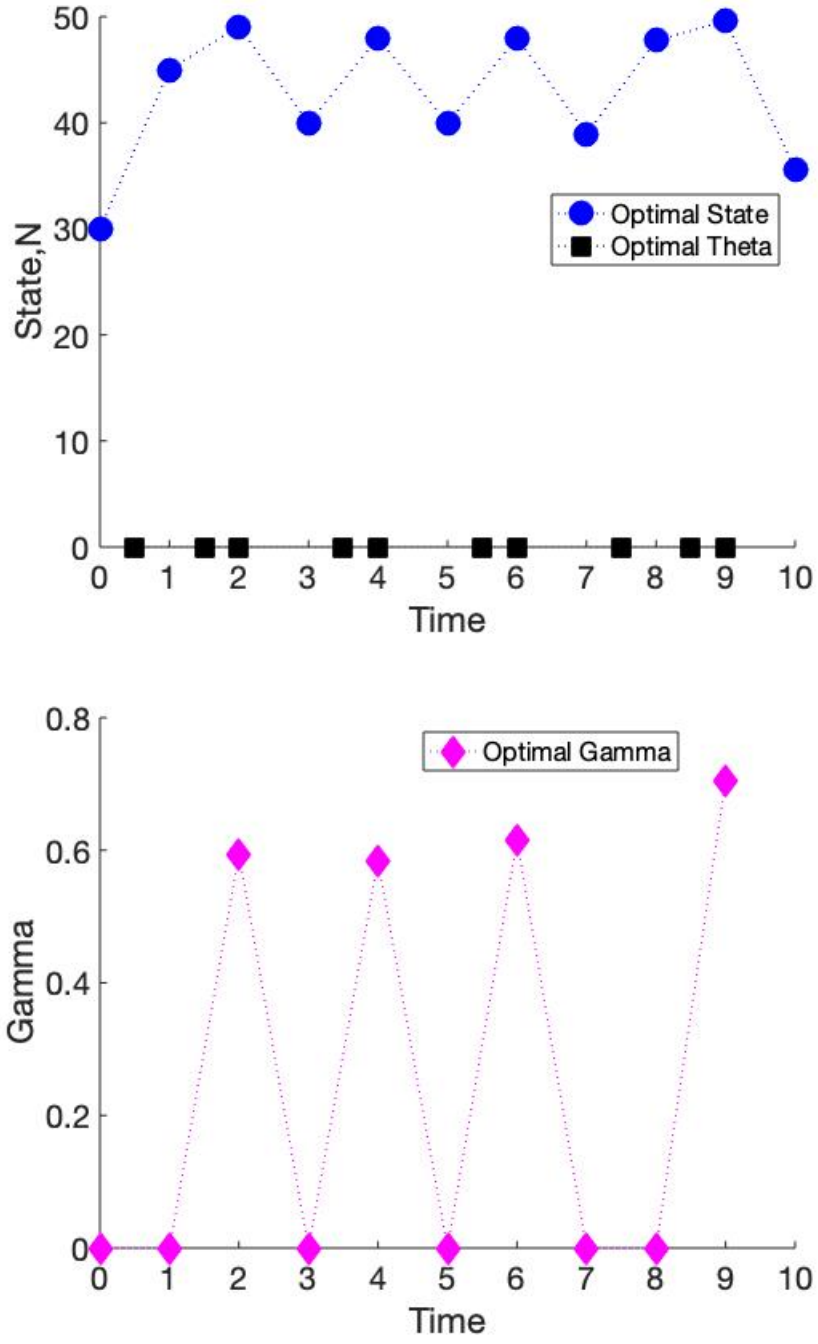

Figure 2.32: The graphs for optimal control of γ and θ in the first model above were generated with parameters from Table 2.9 except for $C_1 = 50$. The values of the objective functional are $J_3(\theta^*, \gamma^*) = 512.79$, $J_3(0, \gamma^*) = 437.79$ and $J_3(1, \gamma^*) = 228.76$.

where $\mu > 0$. See Kokko and Lindström for an biological explination of this mortality rate related to food reserves for overwintering [47]. Here the per capita death rate is proportional to the N_t, the population size at the beginning of the season, whereas in equation (2.12) the per capita death rate was proportional to the current population size $n(\tau)$. First we solve ODE (2.55) on the generic interval (a, τ) with constant $a < \tau$.

$$\begin{aligned} n' + \mu N_t n &= 0 \\ \int_a^\tau e^{\mu N_t s} \left(n'(s) + \mu N_t n(s)\right) ds &= 0 \\ e^{\mu N_t \tau} n(\tau) - e^{\mu N_t a} n(a) &= 0 \\ e^{\mu N_t \tau} n(\tau) &= e^{\mu N_t a} n(a) \\ n(\tau) &= n(a) e^{-\mu N_t (\tau - a)}, \end{aligned}$$

which we call the general solution of our within season mortality dynamics (2.55). Setting $a = 0^+$ using the initial condition (2.56) gives us the following expression for the population size on $(0^+, \tau)$ for $\tau \leq \theta_t^-$

$$n(\tau) = N_t e^{-\mu N_t \tau}.$$

The population size just before harvest, at $\tau = \theta_t^-$, is

$$n(\theta_t^-) = N_t e^{-\mu N_t \theta_t^-}.$$

The yield, then, is

$$Y_t = \gamma N_t e^{-\mu N_t \theta_t}. \tag{2.57}$$

The remaining population after harvest is the new initial condition for the rest of the within season dynamics:

$$n(\theta_t^+) = (1 - \gamma) N_t e^{-\mu N_t \theta_t}.$$

We again use ODE (2.55) and our general solution and letting $a = \theta_t^+$ gives us the population size on the interval (θ_t^+, τ) for $\tau \leq 1^-$

$$\begin{aligned} n(\tau) &= (1-\gamma)N_t e^{-\mu N_t \theta_t} e^{-\mu N_t(\tau-\theta_t)} \\ &= (1-\gamma)N_t e^{-\mu N_t(\tau-\theta_t+\theta_t)} \\ &= (1-\gamma)N_t e^{-\mu N_t \tau}. \end{aligned}$$

Therefore, the population just before birth is described by

$$n(1^-) = (1-\gamma)N_t e^{-\mu N_t}.$$

After birth the next census yields a population size of

$$N_{t+1} = b(1-\gamma)N_t e^{-\mu N_t} \tag{2.58}$$

with $b > 0$. Though yield (2.57) depends on the harvest timing θ_t, the population size (2.58) is independent of harvest timing.

2.5.1 Observations about our second model

The next generation size does not depend on harvest timing. This does not match ecological intuition. Yield decreases as a function of harvest timing:

$$\frac{\partial Y_t}{\partial \theta_t} = -\mu\gamma N_t^2 e^{-\mu N_t \theta_t}. \tag{2.59}$$

The order of events for this model is mortality, then harvest, and finally birth.

The equilibrium equation for this model (holding γ_t constant) is

$$\begin{aligned} N = f(N) &= b(1-\gamma)Ne^{-\mu N} \\ 0 &= (b(1-\gamma)-1)Ne^{-\mu N}, \end{aligned}$$

which gives only the trivial equilibrium

$$N_0^* = 0.$$

Its stability is determined by

$$\begin{aligned}\frac{d}{dN}f(N) =& b(1-\gamma)e^{-\mu N} - \mu b(1-\gamma)Ne^{-\mu N} \\ =& b(1-\gamma)(1-\mu N)e^{-\mu N}.\end{aligned}$$

So $N_0^* = 0$ is asymptotically stable for

$$b(1-\gamma) < 1$$

and unstable for

$$b(1-\gamma) > 1.$$

This is similar to the stability of the extinction equilibrium for the Ricker model, where the birth rate $r > 0$ makes extinction unstable. To compare to our birth rate, which is not in the exponent, notice that $r > 0$ is equivalent to $e^r > 1$. So we might express the stability for the extinction equilibrium for the Ricker model by x_0^* is asymptotically stable if $e^r < 1$ and unstable if $e^r > 1$. This parallels the stability conditions on N_0^*.

2.5.2 Alternative order of events comparison

As we did with our first model, let's compare our second model with the alternative order of events case birth-mortality-harvest-mortality-census. The solution of the ODE in this case is still

$$n(\tau) = n(a)e^{-\mu N_t(\tau - a)} \tag{2.60}$$

where $n(a)$ is the initial condition for some time $a < \tau$. Taking birth first, our initial condition is

$$n(0^+) = bN_t. \tag{2.61}$$

With this initial condition we can solve for the population size just before harvest, at time $\tau = \theta^-$. The population just before harvest is then

$$n(\theta^-) = bN_t e^{-\mu N_t \theta}. \tag{2.62}$$

We harvest a proportion γ of the population, so the yield is

$$Y_t = \gamma b N_t e^{-\mu N_t \theta}. \tag{2.63}$$

This yield is larger than for the other order of events because the other order of events didn't have the b in the yield and $b > 1$. The remaining population size is

$$n(\theta^+) = (1-\gamma) b N_t e^{-\mu N_t \theta}. \tag{2.64}$$

Taking this as our new initial condition, we can solve for the population size at census (time $\tau = 1$):

$$N_{t+1} = (1-\gamma) b N_t e^{-\mu N_t} \tag{2.65}$$

which is identical to the equation for the other order of events.

2.5.3 Comparison with the Seno model

The corresponding Seno model has per-capita growth function

$$g(x) = be^{-\mu x}.$$

This choice of growth function in the Seno model yields

$$N_{t+1} = \theta_t (1-\gamma) b N_t e^{-\mu N_t} + (1-\theta_t)(1-\gamma) b N_t e^{-(1-\gamma)\mu N_t} \tag{2.66}$$

which does depend on θ_t. However, as discussed above, we can only approximate the yield for any Seno equation. The limit case $\theta_t = 0$ for Seno model (2.66) is

$$N_{t+1} = (1-\gamma)bN_t e^{-(1-\gamma)\mu N_t}. \tag{2.67}$$

This doesn't match our mechanistic model (2.58). However, the limit case for Seno for $\theta_t = 1$ is

$$N_{t+1} = (1-\gamma)bN_t e^{-\mu N_t}, \tag{2.68}$$

which is identical to our model (2.58). Our model (2.58) matches one of the limit cases for Seno's corresponding model. We might conclude that this mechanistic model is actually less general than the corresponding Seno model. Or we might conclude that the Seno model for this case adds unnecessary complexity for the biological situation. For insights into this Seno model see [33].

As we did with our first mechanistic model, we compared this second model to the corresponding Seno model over a large area of parameter space. We built an LHS matrix with 10,000 possible parameter sets. We chose the ranges $T \in [5, 15]$, $N_0 \in [0.5, 10]$, $\theta \in [10^{-4}, 1]$, $\gamma \in [10^{-4}, 1]$, $b \in [.01, 10]$, and $\mu \in [.01, 10]$. The resulting histogram is shown in Figure 2.33a. Our second model differs more from the Seno-Ricker model than does our first model from the Seno-Beverton-Holt model. But for most of the parameter space explored the differences are still quite small.

2.5.4 Optimal control of harvest timing and harvest intensity in our second model

We perform optimal control of both γ and θ using an objective functional similar to (2.54) with our model (2.58) determining the state values and the corresponding yield (2.57). Our objective functional, then, is

$$J_4(\theta, \gamma) = AN_T + \sum_{t=0}^{T-1} \left(B_t \gamma N_t e^{-\mu N_t \theta_t} - C_1(\frac{1}{2} - \theta_t)^2 - C_2\gamma_t - C_3\gamma_t^2 \right). \tag{2.69}$$

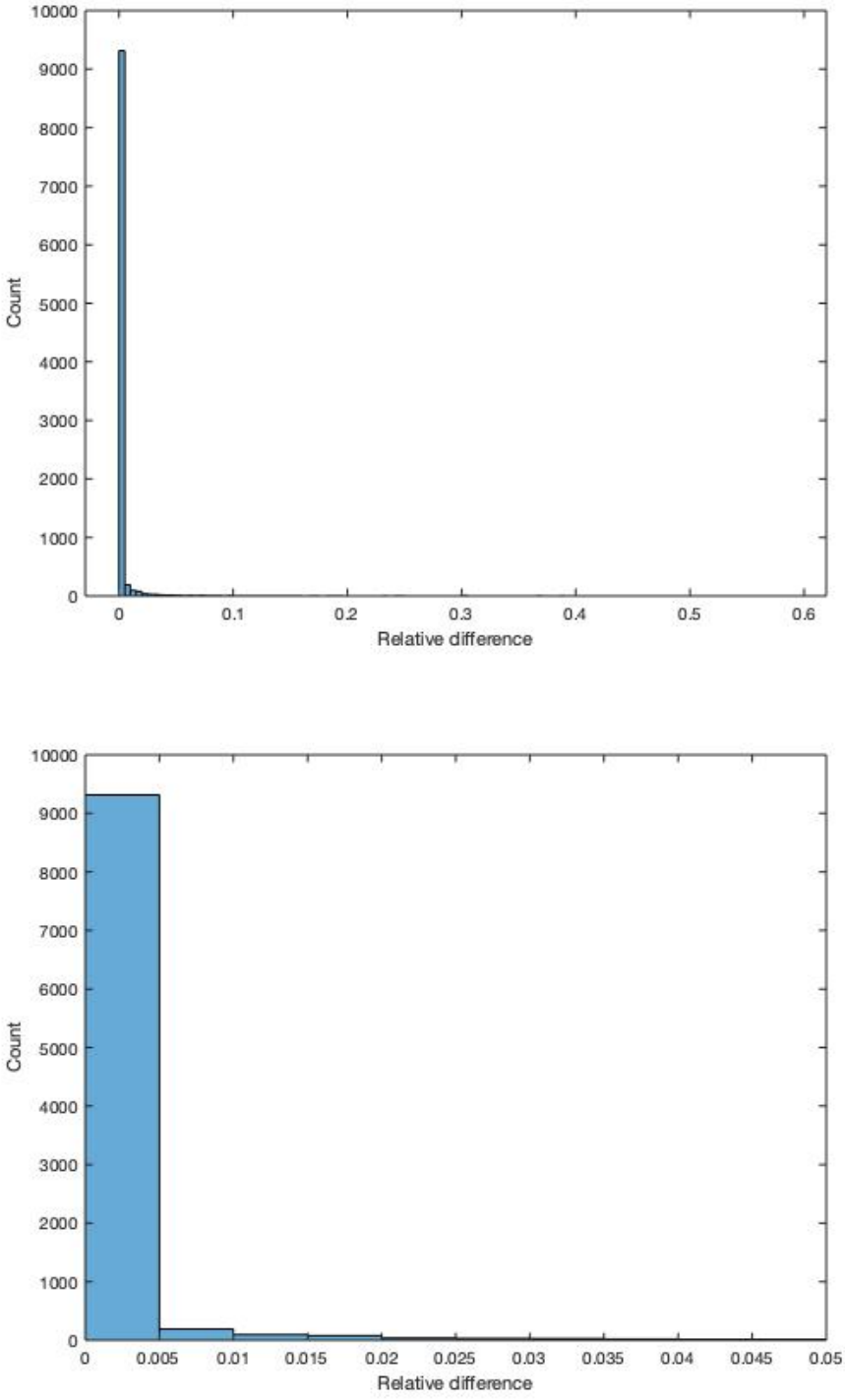

Figure 2.33: The upper graph shows the whole histogram of relative differences between our second model and the corresponding Seno model. The lower graph zooms in on the right end of the histogram. The maximum value is 0.5854, the mean is 0.0039, and the variance is $6.6552e-4$.

Table 2.11: First set of baseline parameters for optimal control of both harvest timing and harvest intensity of our second mechanistic model.

Parameter	Value
T	10
μ	0.1
b	6
N_0	30
C_1	0.1
C_2	0.2
C_3	0.2
A	1
B	1

We again use direct optimization of the objective functional with fmincon and multistart in MATLAB. The proof for existence of the optimal control is similar to that given in section 2.4.

Table 2.11 contains the first set of baseline parameters that we used for control of the second model. They are the same as the set of baseline parameters used in controlling both harvest timing and harvest intensity for our first model. Figure 2.34 shows states and yields for those parameters without optimal control. In Figure 2.34 notice that the states remain the same regardless of the change in θ from 0 to 1, but the yields vary dramatically. Table 2.12 shows the variations on baseline parameters that we explored. The last column shows the relative difference between the optimal-timing-optimal-intensity pair and pairing optimal intensity with beginning-of-season harvest instead. This illustrates the relative importance, or lack, of optimal timing.

Figure 2.35 was generated using the baseline parameters found in Table 2.11. The first harvest is early and heavy (about 0.7 intensity), followed by two mid-season harvests with intensity close to 0. After these initial harvests, the harvest timing-intensity pair settles into a cycle alternating high-intensity (above 0.4) early harvests with low intensity (close to 0) mid-season harvests. The final harvest has intensity close to 1 and the population is almost depleted by this last effort. The cycle in harvest intensity seems to be more important to maximizing the objective functional than does the cycle in harvest timing, because $J_4(\theta^*, \gamma^*) = 227.18$ only differs from $J_4(0, \gamma^*) = 227.06$ by 0.06%.

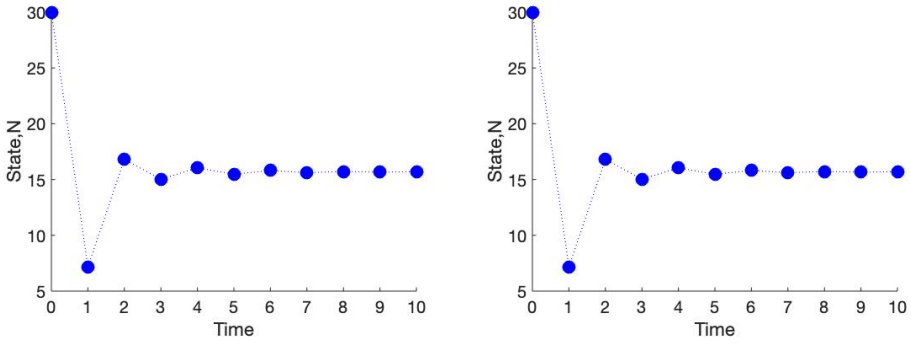

(a) State for $\theta \equiv 0$

(b) State for $\theta \equiv 1$

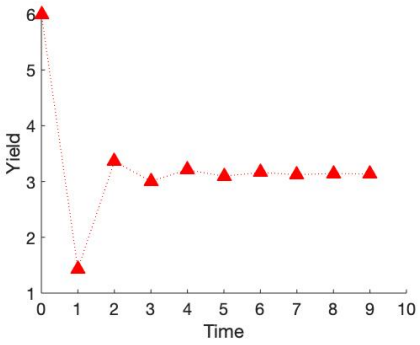

(c) Yield for $\theta \equiv 0$

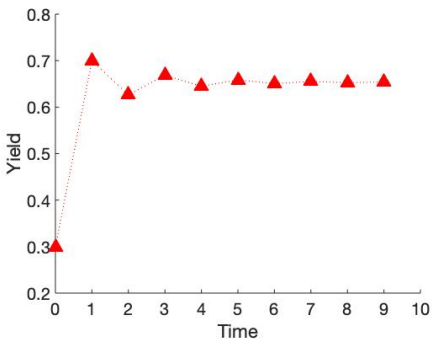

(d) Yield for $\theta \equiv 1$

Figure 2.34: Baseline states and yields using parameters from Table 2.11 with our second model.

Table 2.12: Summary of the results of optimal control of both harvest intensity and harvest timing in our second model for variations on the baseline parameters from Table 2.11. The parameters column lists only variations from the baseline.

Figures	Parameters	$J_4(\theta^*, \gamma^*)$	$\frac{J_4(\theta^*,\gamma^*)-J_4(0,\gamma^*)}{J_4(\theta^*,\gamma^*)}$
2.35	baseline	227.18	0.0006
2.36	$A_t = 0$ for $t < T$	105.75	0.0014
2.37	$N_0 = 10$	211.30	0.0006
2.38	$N_0 = 10, T = 11$	229.27	0.0007
2.39	$b = 1.2$	60.59	0.0037
2.40	$b = 2, C_1 = 1$	99.44	0.02
2.41	$A = 0$	83.79	0.0018
2.42	$A = 0, C_1 = 10$	73.89	0.20
2.43	$A = 0, N_0 = 10$	71.78	0.0017

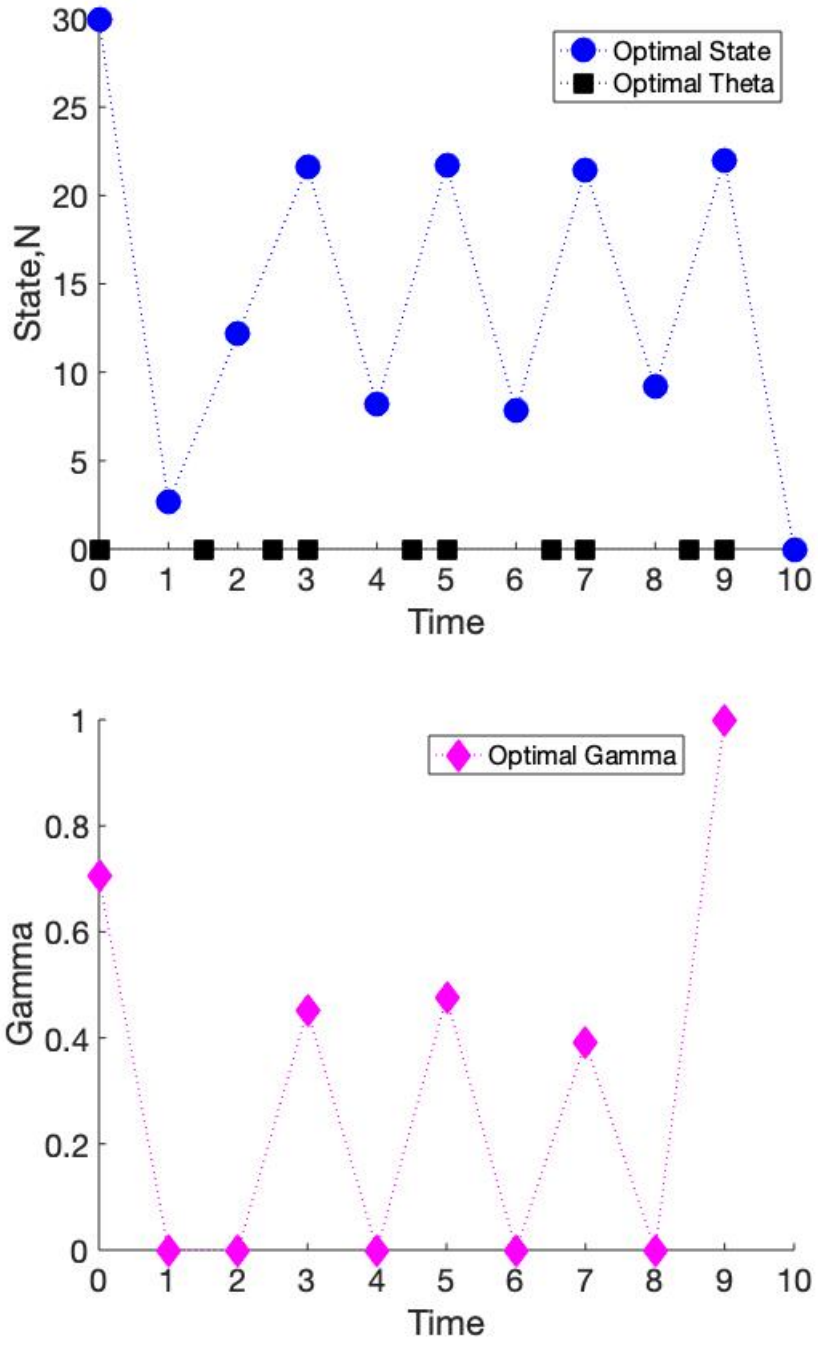

Figure 2.35: The graphs for optimal control in our second model of γ and θ above were generated with parameters as in Table 2.11. The values of the objective functional are $J_4(\theta^*, \gamma^*) = 227.18$, $J_4(0, \gamma^*) = 227.06$ and $J_4(1, \gamma^*) = 162.22$.

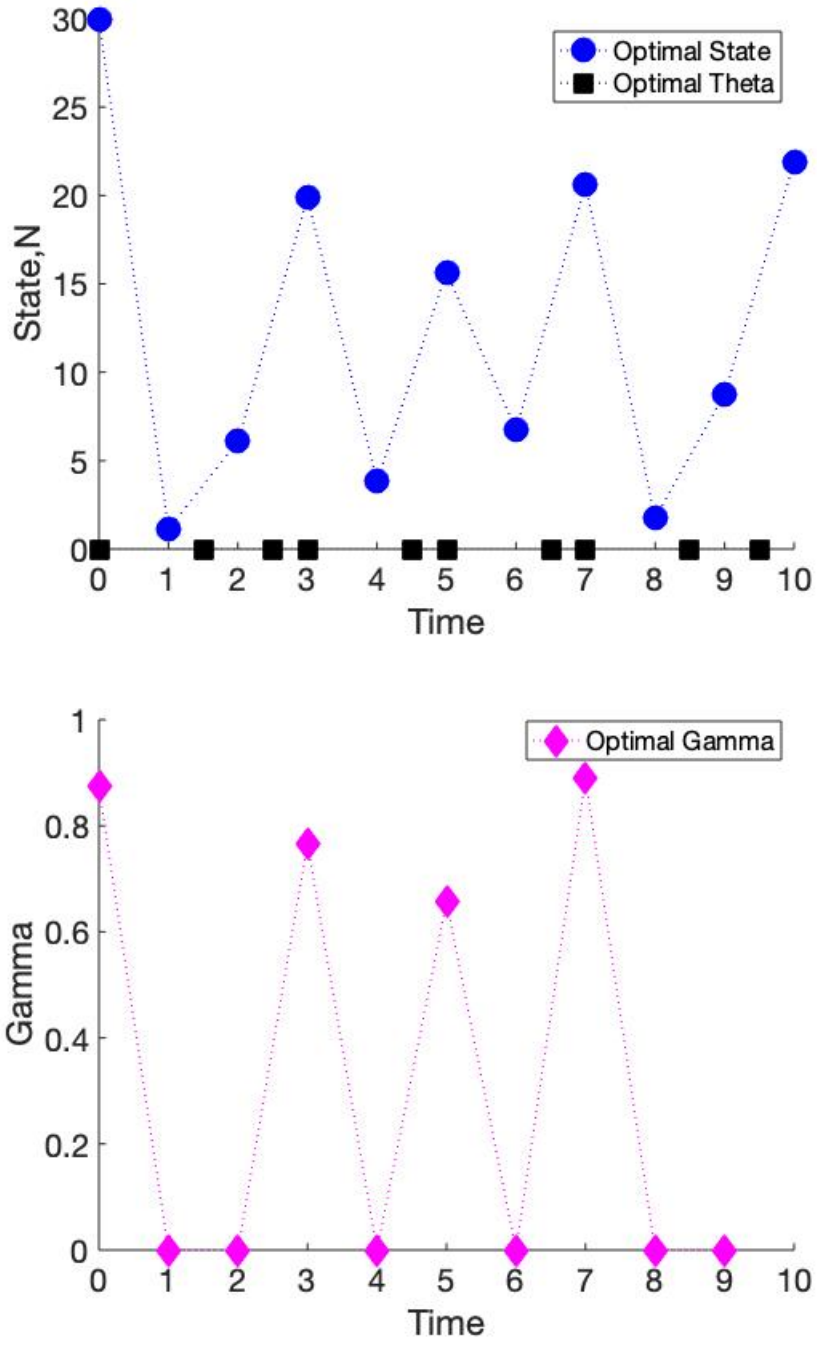

Figure 2.36: The graphs for optimal control in our second model of γ and θ above were generated with parameters as in Table 2.11 except for $A_t = 0$ for $t < T$. The values of the objective functional are $J_4(\theta^*, \gamma^*) = 105.75$, $J_4(0, \gamma^*) = 105.60$ and $J_4(1, \gamma^*) = 28.57$.

Figure 2.36 was generated with parameters as in Table 2.11 except for $A_t = 0$ for $t < T$ (altered from $A_t = 1$ for all t). This takes the emphasis off of intermediate population conservation but leaves importance on final population conservation. Under these conditions the initial harvest is high intensity (about 0.9) and early followed by two harvests near 0 intensity and mid-season. After this there are alternating high-intensity early-season harvests and very low intensity mid-season harvests. These cycles are not as steady as the cycles observed in Figure 2.35, but the high-intensity years have higher intensity. The second from last harvest is very high intensity (close to 0.9), followed by two very low intensity harvests (close to 0) allowing the population to recover from this particularly intense harvest in time for the final population to be high again. As with Figure 2.35, it is the pattern in intensity that matters more than the pattern in timing because $J_4(\theta^*, \gamma^*) = 105.75$ differs from $J_4(0, \gamma^*) = 105.60$ by only .14%.

Figure 2.37 was generated with parameters as in Table 2.11 except for $N_0 = 10$ (increased from $N_0 = 30$). Figure 2.38 was generated with these same parameter choices but with $T = 11$ lengthening the time period from $T = 10$. We wanted to see whether the cycle would continue, or whether it would break and result in a final high-intensity harvest. In both sets of figures there are cycles of low intensity (near 0) mid-season harvest followed by higher intensity (above 0.4) early-season harvest. However, they each end on a different part of the cycle. Figure 2.37 has a very high intensity (near 1) final harvest while Figure 2.38 has a very low intensity final harvest. As a result, in Figure 2.37a the final population is near extinction while the final population in Figure 2.38a is at the usual high point in the cycle. For Figure 2.37 the objective functional values are $J_4(\theta^*, \gamma^*) = 211.30$, $J_4(0, \gamma^*) = 211.18$ and $J_4(1, \gamma^*) = 157.43$. For Figure 2.38 the objective functional values are $J_4(\theta^*, \gamma^*) = 229.27$, $J_4(0, \gamma^*) = 229.12$ and $J_4(1, \gamma^*) = 185.46$. In both cases harvest intensity patterns again prove more important than harvest timing patterns with $J_4(\theta^*, \gamma^*)$ differing from $J_4(0, \gamma^*)$ by 0.06% and by 0.07% respectively.

Figure 2.39 was generated with parameters as in Table 2.11 except for $b = 1.2$ (decreased from $b = 6$). With this low of a birth rate, the initial population size is above what is sustainable. The first harvest is heavy (intensity above 0.8) and early, taking advantage of the surplus population. All other harvests are very low intensity (near 0) and mid-season.

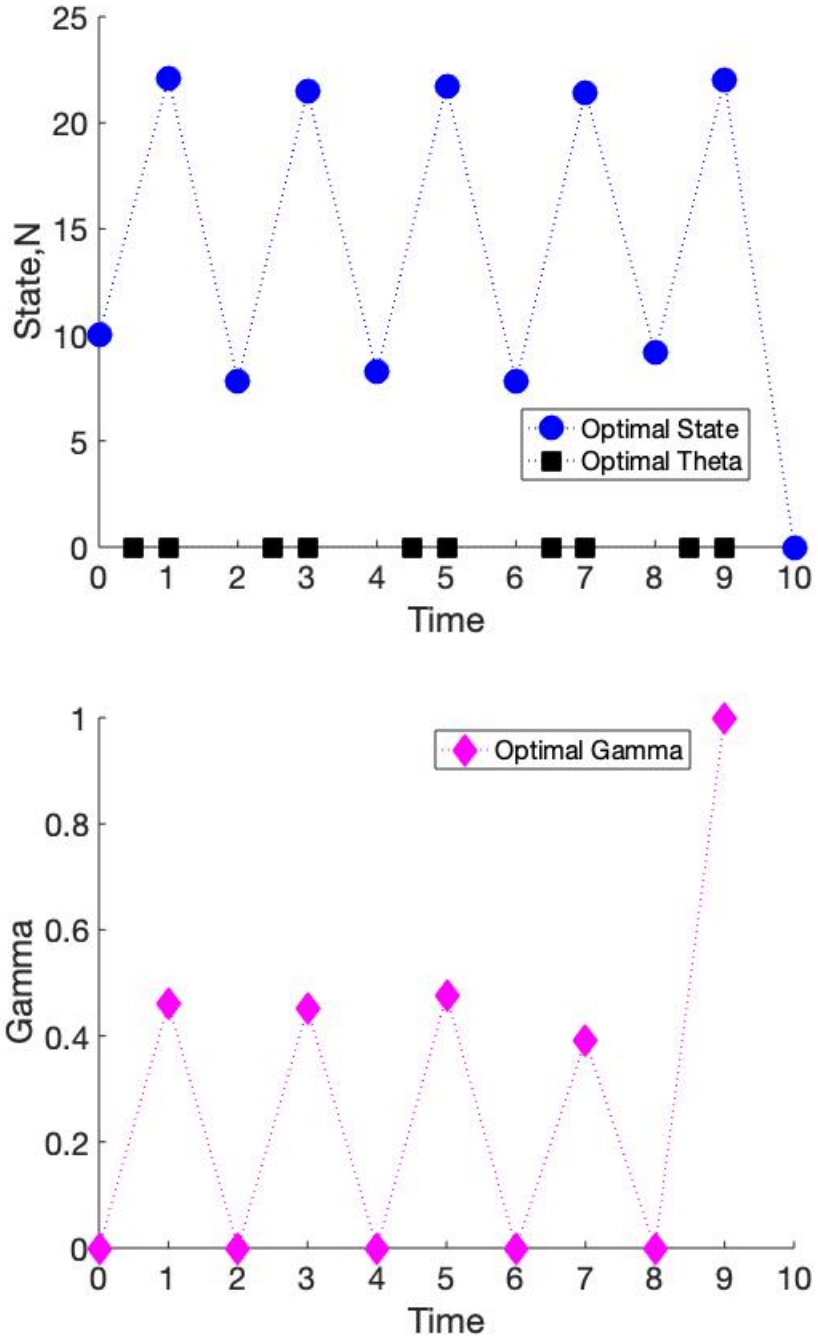

Figure 2.37: The graphs for optimal control in our second model of γ and θ above were generated with parameters as in Table 2.11 except for $N_0 = 10$. The values of the objective functional are $J_4(\theta^*, \gamma^*) = 211.30$, $J_4(0, \gamma^*) = 211.18$ and $J_4(1, \gamma^*) = 157.43$.

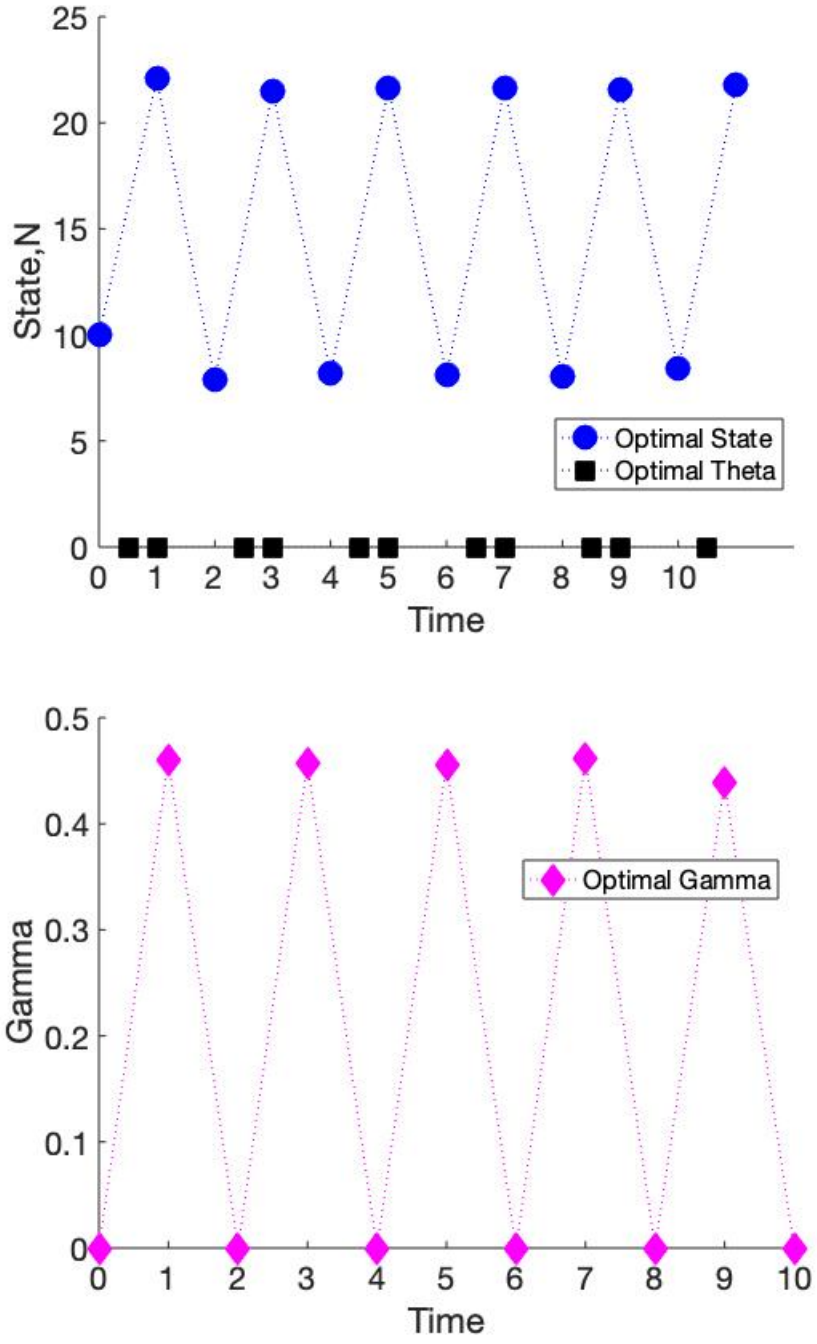

Figure 2.38: The graphs for optimal control in our second model of γ and θ above were generated with parameters as in Table 2.11 except for $N_0 = 10$ and $T = 11$. The values of the objective functional are $J_4(\theta^*, \gamma^*) = 229.27$, $J_4(0, \gamma^*) = 229.12$ and $J_4(1, \gamma^*) = 185.46$.

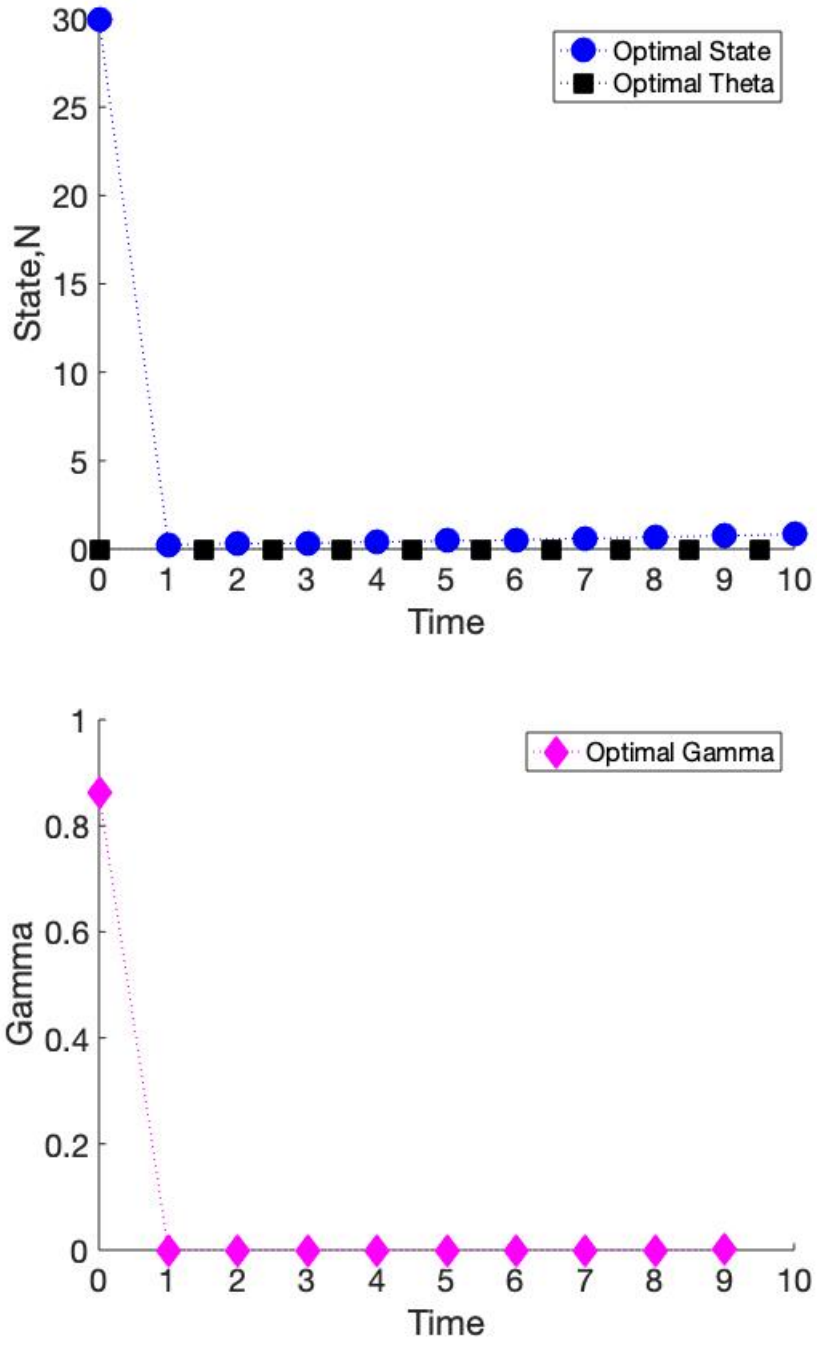

Figure 2.39: The graphs for optimal control in our second model of γ and θ above were generated with parameters as in Table 2.11 except for $b = 1.2$. The values of the objective functional are $J_4(\theta^*, \gamma^*) = 60.59$, $J_4(0, \gamma^*) = 60.37$ and $J_4(1, \gamma^*) = 35.82$.

The population exhibits some small recovery by the final time step, but is still far below its initial value. The objective functional values are $J_4(\theta^*, \gamma^*) = 60.59$, $J_4(0, \gamma^*) = 60.37$ and $J_4(1, \gamma^*) = 35.82$ with $J_4(\theta^*, \gamma^*)$ differing from $J_4(0, \gamma^*)$ by only 0.37%.

Figure 2.49 was generated with parameters as in Table 2.11 except for $b = 2$ (increased from $b = 6$) and increasing C_1 from 0.1 to 1. With the birth rate still low, the initial harvest is high intensity at above 0.6 but not as high intensity as the initial harvest in Figures 2.39a and 2.39b. As in Figure 2.39 the remaining harvests have intensity close to 0 and timing mid-season, but this time the population recovers much more than it did in Figure 2.39. The objective functional values are $J_4(\theta^*, \gamma^*) = 99.44$, $J_4(0, \gamma^*) = 97.19$ and $J_4(1, \gamma^*) = 78.33$. The difference between $J_4(\theta^*, \gamma^*)$ and $J_4(0, \gamma^*)$ is 2%, showing that harvest timing is more important here since the cost associated with harvesting away from mid-season is higher.

Figure 2.41 was generated with the parameters from Table 2.11 except for $A_t = 0$ for all t (changed from $A_t = 1$ for all t). In this case there is a cycle with one high intensity early season harvest followed by two very low intensity mid-season harvests. The high intensity harvests are all greater than 0.8, with the final harvest having intensity close to 1 causing the population to near extinction. The values for the objective functional are $J_4(\theta^*, \gamma^*) = 83.79$, $J_4(0, \gamma^*) = 83.64$ and $J_4(1, \gamma^*) = 6.60$, with $J_4(\theta^*, \gamma^*)$ and $J_4(0, \gamma^*)$ differing by 0.18%.

Figure 2.42 was generated with the same parameters as Figure 2.41, but with a higher cost associated with harvest timing increased from $C_1 = 0.1$ to $C_1 = 10$. They exhibit a very similar cycle to Figure 2.41, but in the final time step the harvest intensity is near 1 and the population crashes. The objective functional values are $J_4(\theta^*, \gamma^*) = 73.89$, $J_4(0, \gamma^*) = 58.89$ and $J_4(1, \gamma^*) = -18.15$, with a 20% difference between $J_4(\theta^*, \gamma^*)$ and $J_4(0, \gamma^*)$. The negative value for $J_3(1, \gamma^*)$ is due to relatively low yield and high cost of harvest timing.

Figure 2.43 was generated with parameters as in Table 2.11 except for $A = 0$ (instead of $A = 1$) and $N_0 = 10$ (instead of $N_0 = 30$). Under these conditions harvest intensity switches between high and very low and harvest timing switches between early and mid-season. The high intensity harvests vary from above 0.6 at the lowest to nearly 1 at the highest, which happens in the final harvest. The objective functional values are $J_4(\theta^*, \gamma^*) = 71.78$, $J_4(0, \gamma^*) = 71.66$ and $J_4(1, \gamma^*) = 9.29$, with $J_4(\theta^*, \gamma^*)$ differing from $J_4(0, \gamma^*)$ by only 0.17%.

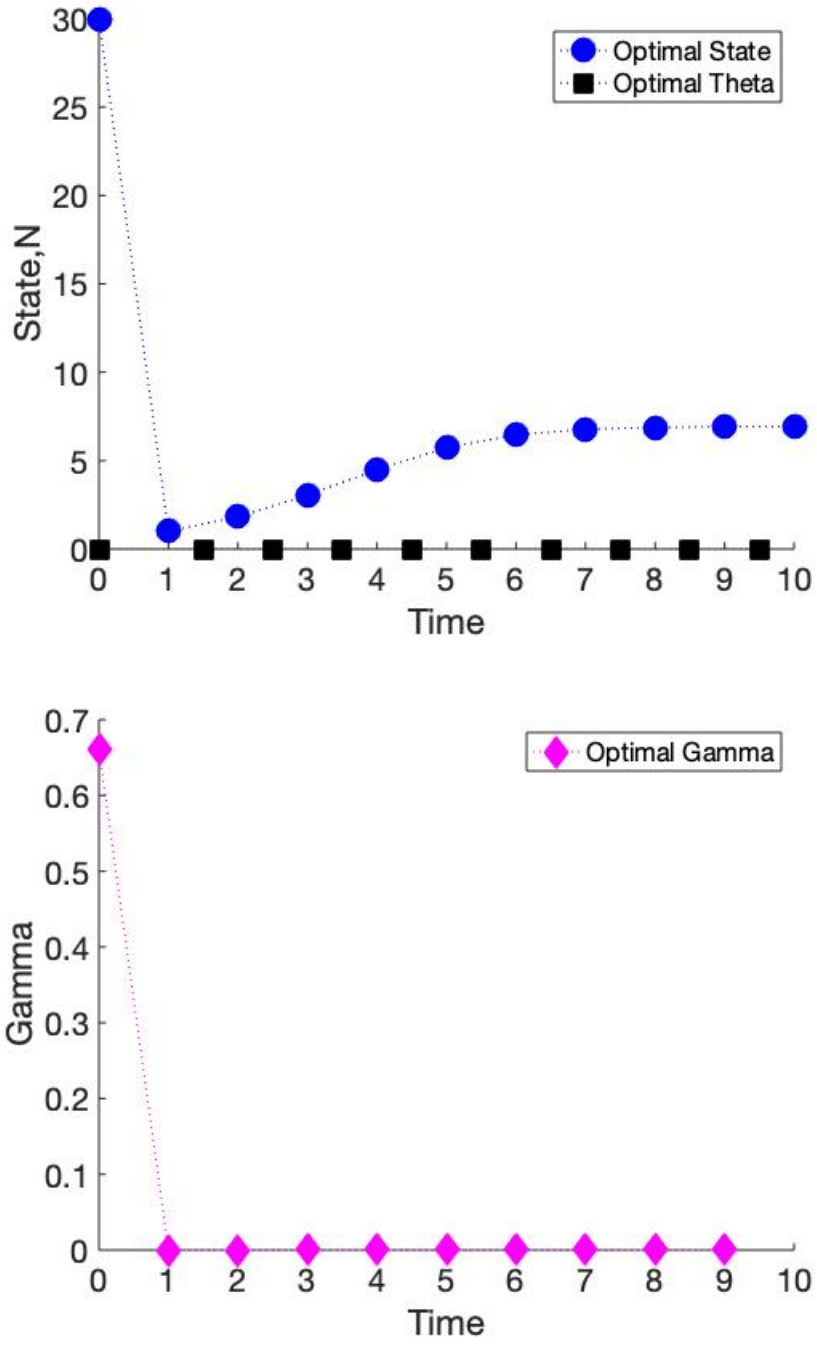

Figure 2.40: The graphs for optimal control in our second model of γ and θ above were generated with parameters as in Table 2.11 except for $b = 2$ and $C_1 = 1$. The values of the objective functional are $J_4(\theta^*, \gamma^*) = 99.44$, $J_4(0, \gamma^*) = 97.19$ and $J_4(1, \gamma^*) = 78.33$.

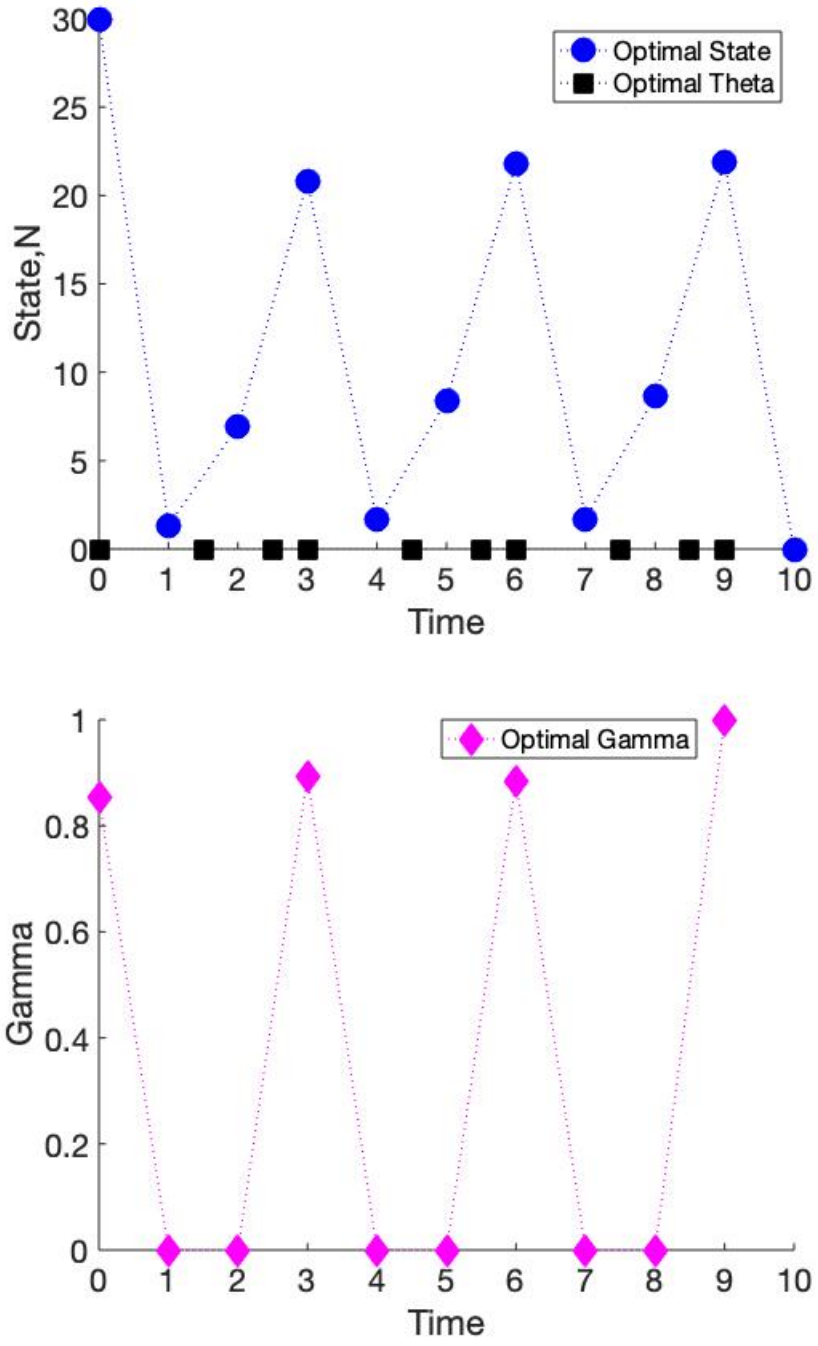

Figure 2.41: The graphs for optimal control in our second model of γ and θ above were generated with parameters as in Table 2.11 except for $A = 0$. The values of the objective functional are $J_4(\theta^*, \gamma^*) = 83.79$, $J_4(0, \gamma^*) = 83.64$ and $J_4(1, \gamma^*) = 6.60$.

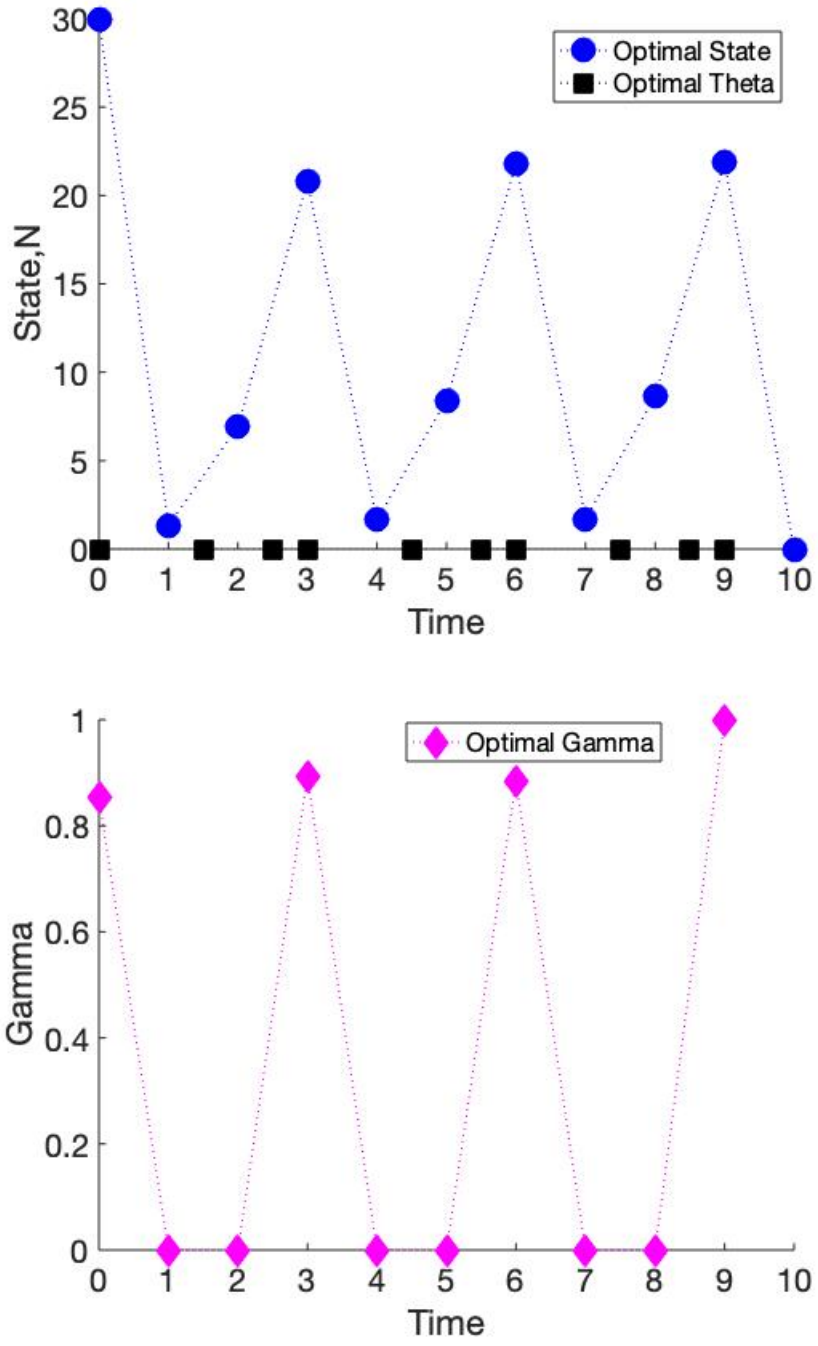

Figure 2.42: The graphs for optimal control in our second model of γ and θ above were generated with parameters as in Table 2.11 except for $A = 0$ and $C_1 = 10$. The values of the objective functional are $J_4(\theta^*, \gamma^*) = 73.89$, $J_4(0, \gamma^*) = 58.89$ and $J_4(1, \gamma^*) = -18.15$.

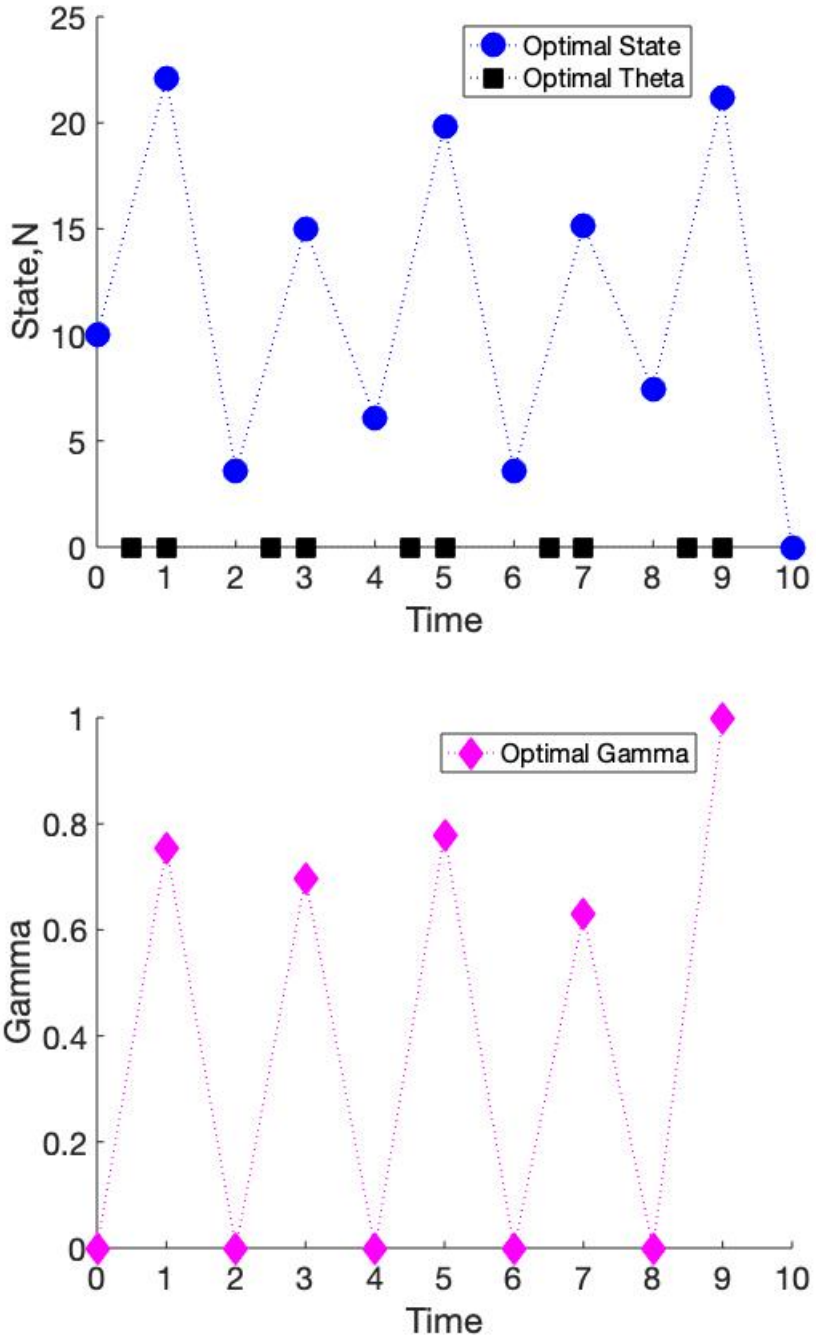

Figure 2.43: The graphs for optimal control in our second model of γ and θ above were generated with parameters as in Table 2.11 except for $A = 0$ and $N_0 = 10$. The values of the objective functional are $J_4(\theta^*, \gamma^*) = 71.78$, $J_4(0, \gamma^*) = 71.66$ and $J_4(1, \gamma^*) = 9.29$.

Table 2.13: Second set of baseline parameters for controlling harvest timing and intensity in our second model.

Parameter	Value
T	10
μ	1
b	5
N_0	1
C_1	0.1
C_2	0.2
C_3	0.2
A	1
B	1

With the parameters in Table 2.11 we see cycles in the population caused by cycles in harvest intensity and in harvest timing (though the patterns in harvest intensity seem to be more important than those in harvest timing). These cycles occur for parameter values where the population would not normally experience cycles, as seen in Figure 2.34. Several variations on parameters cause cycles as well, including in Figure 2.41a where the population appears to be in an approximate 3-cycle and in Figure 2.43a where the population appears to be in an approximate 4-cycle (though more time would be needed to establish this pattern for certain). These results emphasize the dramatic impacts which harvest can have on populations, including in some cases causing near extinction.

Table 2.13 lists the second set of baseline parameters when controlling both harvest intensity and harvest timing. These parameters have a higher baseline mortality rate, meaning that there will generally be less population available for harvest. Therefore, harvest timing will be more important. Figure 2.44 shows the states and yields for these baseline parameters without optimal control. Table 2.14 lists the variations on the baseline parameters that we explored.

Figure 2.45 was generated with parameters as in Table 2.13. During the first several seasons a cycle of high-intensity early season harvest followed by very low intensity mid-season harvest seems to develop. Then suddenly there are two very low intensity seasons in

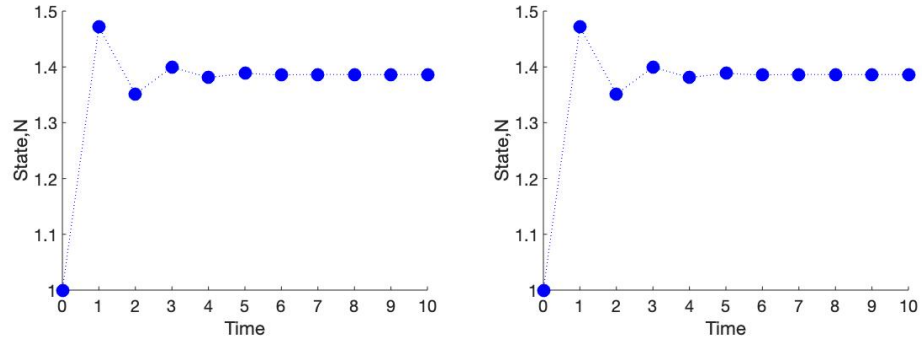

(a) State for $\theta \equiv 0$

(b) State for $\theta \equiv 1$

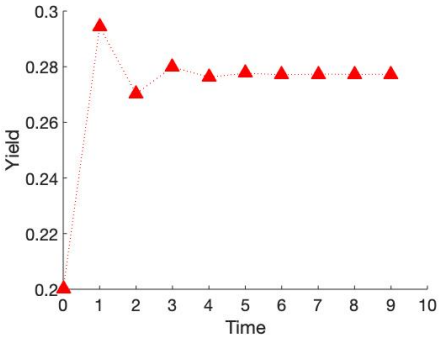

(c) Yield for $\theta \equiv 0$

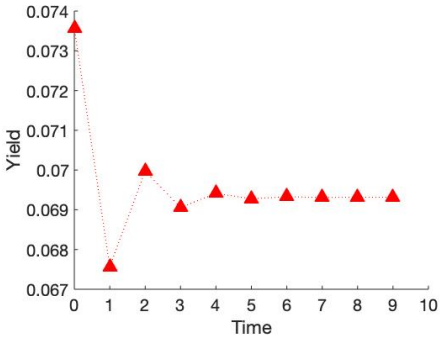

(d) Yield for $\theta \equiv 1$

Figure 2.44: Baseline states and yields for the parameters listed in Table 2.13 in our second model.

Table 2.14: Summary of objective functional results for varying parameters from the second set of baseline parameters in Table 2.13 for our second model. The parameters column lists only variations from the second baseline.

Figures	Parameters	$J_4(\theta^*, \gamma^*)$	$\frac{J_4(\theta^*,\gamma^*)-J_4(0,\gamma^*)}{J_4(\theta^*,\gamma^*)}$
2.45	second baseline	17.58	0.009
2.46	$A_t = 0$ for $t < T$	5.48	0.03
2.47	$N_0 = 0.5$	16.95	0.009
2.48	$N_0 = 0.5, T = 11$	18.60	0.008
??	$b = 1.2$	3.63	0.07
2.50	$b = 4$	14.93	0.015
2.51	$b = 10, C_1 = 1$	28.28	0.04
2.52	$A = 0$	4.58	0.04
2.53	$A = 0, C_1 = 10$	1.58	14.2757
2.54	$A = 0, N_0 = 0.5$	4.43	0.03

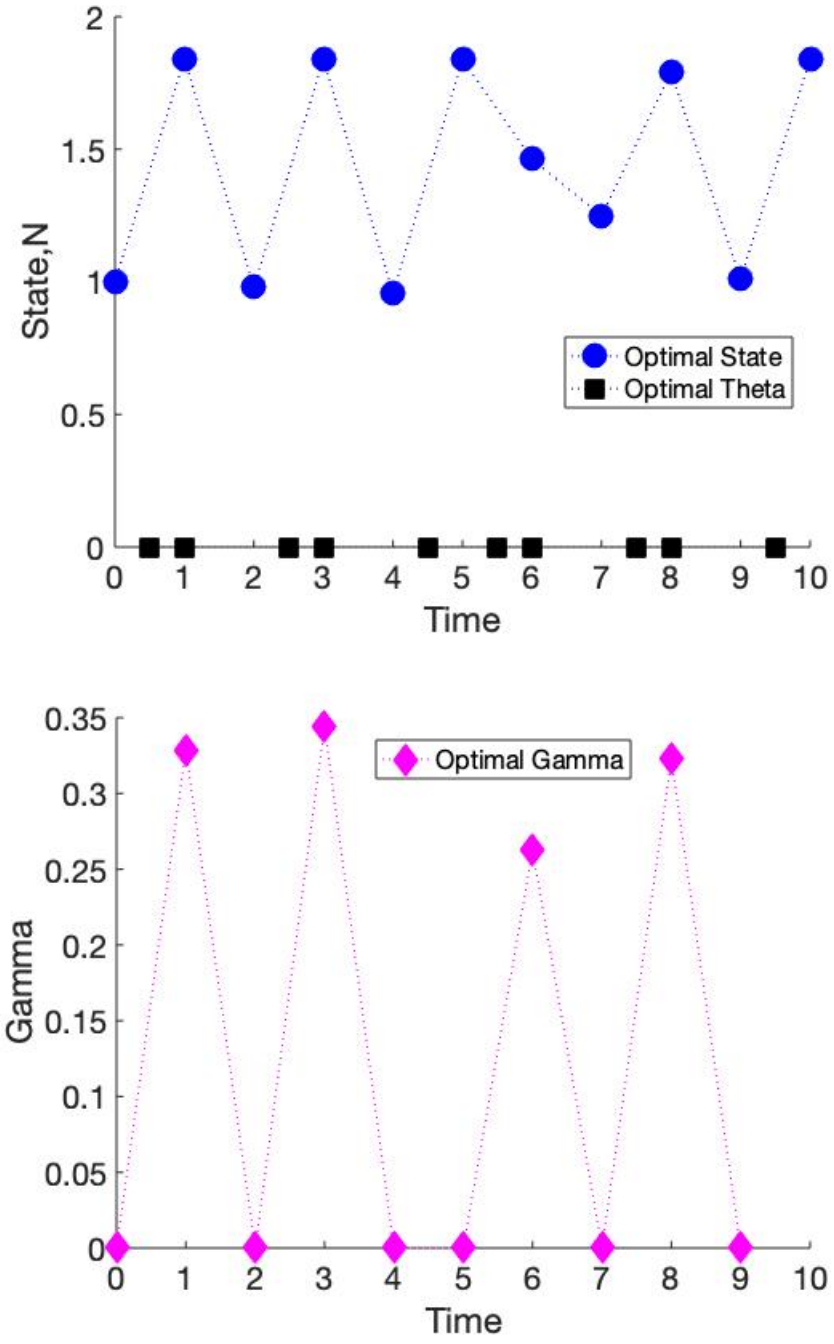

Figure 2.45: The graphs for optimal control in our second model of γ and θ above were generated with parameters as in Table 2.13. The values of the objective functional are $J_4(\theta^*, \gamma^*) = 17.58$, $J_4(0, \gamma^*) = 17.43$ and $J_4(1, \gamma^*) = 15.61$.

a row, which are followed by cycles again. The objective functional values are $J_4(\theta^*, \gamma^*) = 17.58$, $J_4(0, \gamma^*) = 17.43$ and $J_4(1, \gamma^*) = 15.61$, with $J_4(\theta^*, \gamma^*)$ differing from $J_4(0, \gamma^*)$ by only 0.9%.

Figure 2.46 was generated with parameters as in Table 2.13 except with $A_t = 0$ for $t < T$ (instead of $A_t = 1$ for all t). When we made a similar change to the first baseline parameters (generating Figure 2.36) we saw some disruption of the cycles from the baseline parameter scenario. Here the cycles are replaced by different cycles. One high-intensity (above 0.8) early season year is followed by two very low intensity mid-season years. The values of the objective functional are $J_4(\theta^*, \gamma^*) = 5.48$, $J_4(0, \gamma^*) = 5.30$ and $J_4(1, \gamma^*) = 1.37$. Again, $J_4(\theta^*, \gamma^*)$ and $J_4(0, \gamma^*)$ are very similar, this time with a difference of 3%

In Figure 2.47 we used the parameters from Table 2.13 except for $N_0 = 0.5$ (decreased from $N_0 = 1$). These results can be compared with those of Figure 2.37, where the initial condition was reduced from the first set of baseline parameters. In both cases there are cycles of high harvest intensity early in the season then very low harvest intensity mid-season. However, in this case there is a delay of one season before the cycles begin, which allows the population to grow above 1.5 before harvest begins. This is probably because our initial condition is even lower than before. The high-intensity numbers are above 0.3. Contrary to Figure 2.37, our final harvest is not of high intensity and does not bring the population close to extinction. The reason for this is unclear. The objective functional values are $J_4(\theta^*, \gamma^*) = 16.95$, $J_4(0, \gamma^*) = 16.80$ and $J_4(1, \gamma^*) = 14.87$, with $J_4(\theta^*, \gamma^*)$ and $J_4(0, \gamma^*)$ differing by 0.9%.

Figure 2.48 investigated whether adding a time step to those allotted in Figure 2.47 would cause a final very high intensity harvest bringing the population to extinction. We wanted to explore whether the cycle would continue its trajectory, or whether the cycle would break and the final harvest would be of unexpected intensity. They were generated using the parameters in Table 2.13 except for $N_0 = 0.5$ and $T = 11$. These parameters produced a cycle as expected, with similar intensities to Figure 2.47, but the final harvest was very low intensity (close to 0) rather than very high intensity. We can compare these results to those of Figure 2.38, where the final time was also extended to 11. In both cases the final

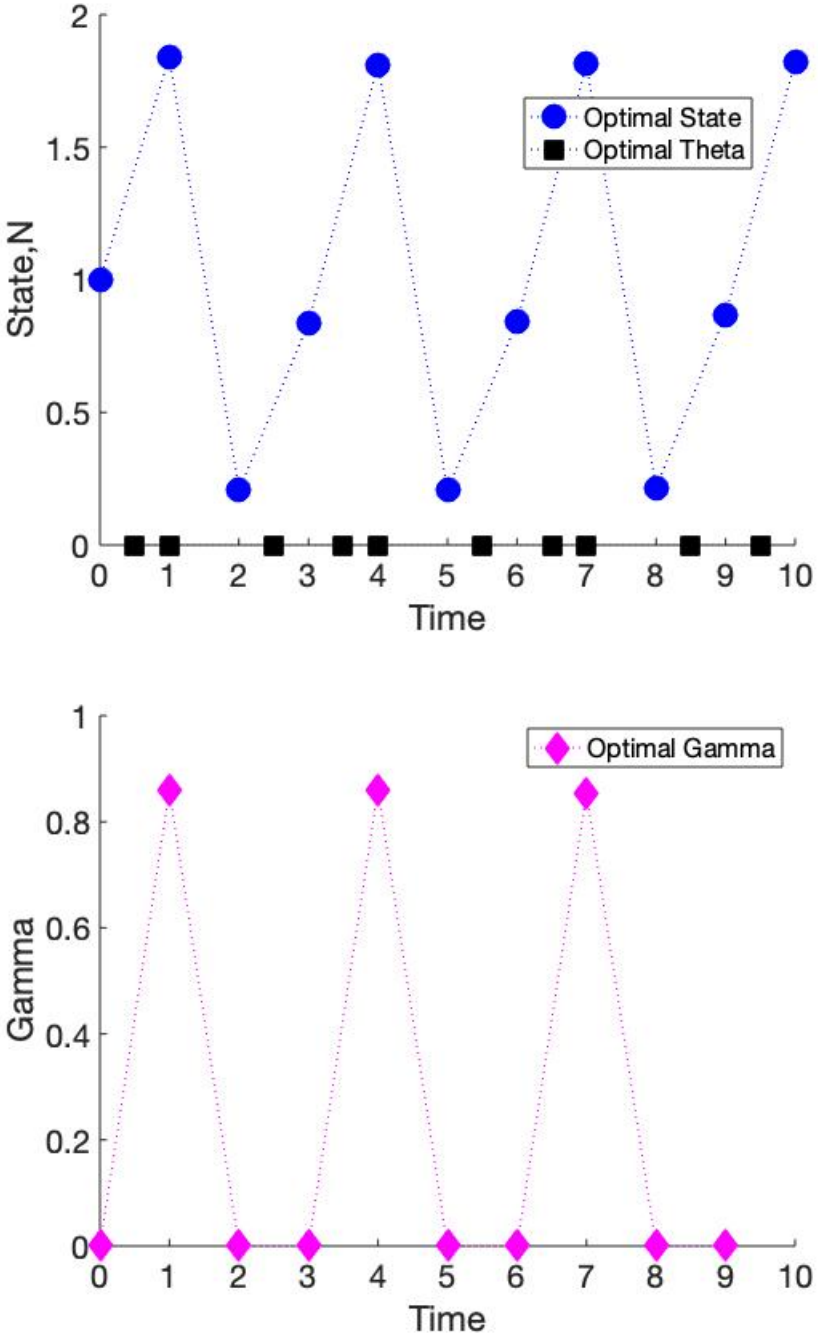

Figure 2.46: The graphs for optimal control in our second model of γ and θ above were generated with parameters as in Table 2.13 except with $A_t = 0$ for $t < T$. The values of the objective functional are $J_4(\theta^*, \gamma^*) = 5.48$, $J_4(0, \gamma^*) = 5.30$ and $J_4(1, \gamma^*) = 1.37$.

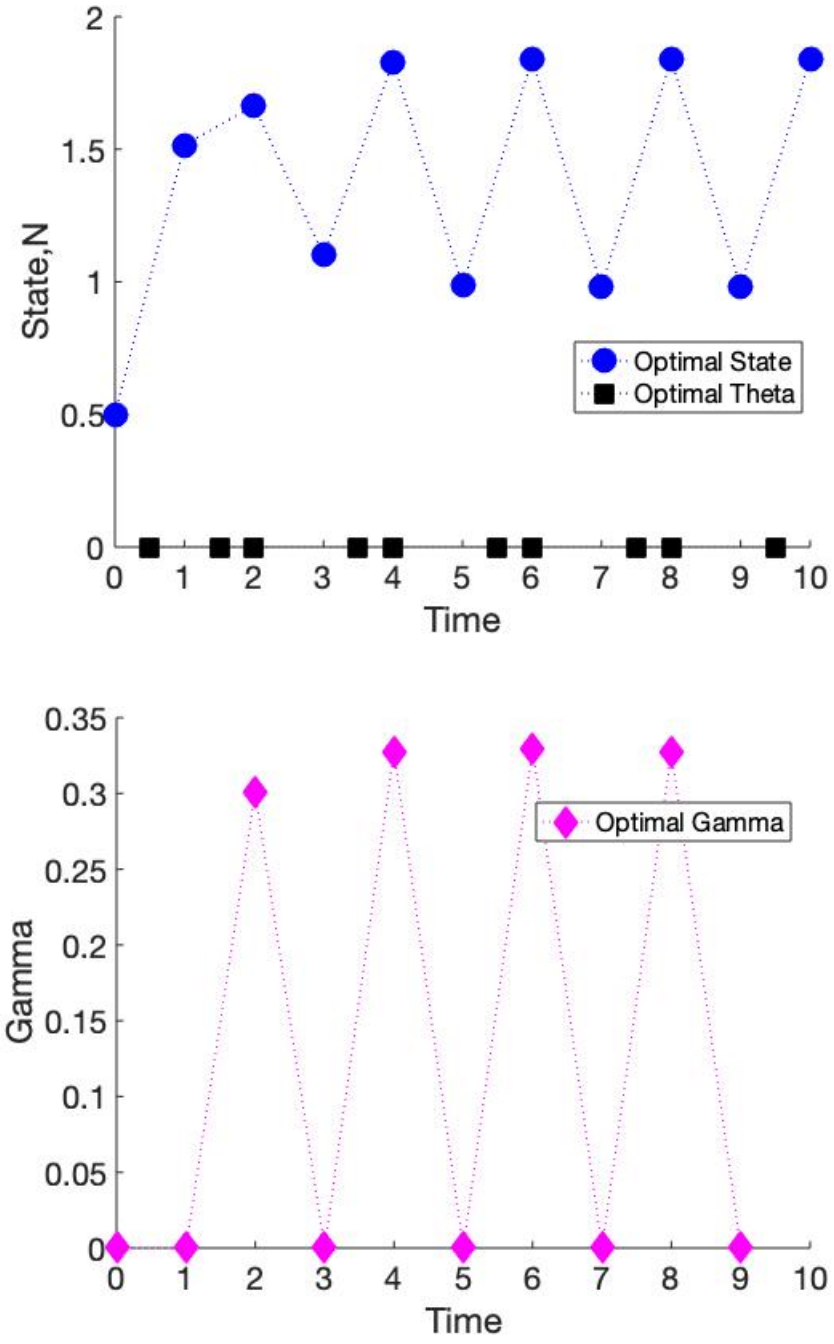

Figure 2.47: The graphs for optimal control in our second model of γ and θ above were generated with parameters as in Table 2.13 except for $N_0 = 0.5$. The values of the objective functional are $J_4(\theta^*, \gamma^*) = 16.95$, $J_4(0, \gamma^*) = 16.80$ and $J_4(1, \gamma^*) = 14.87$.

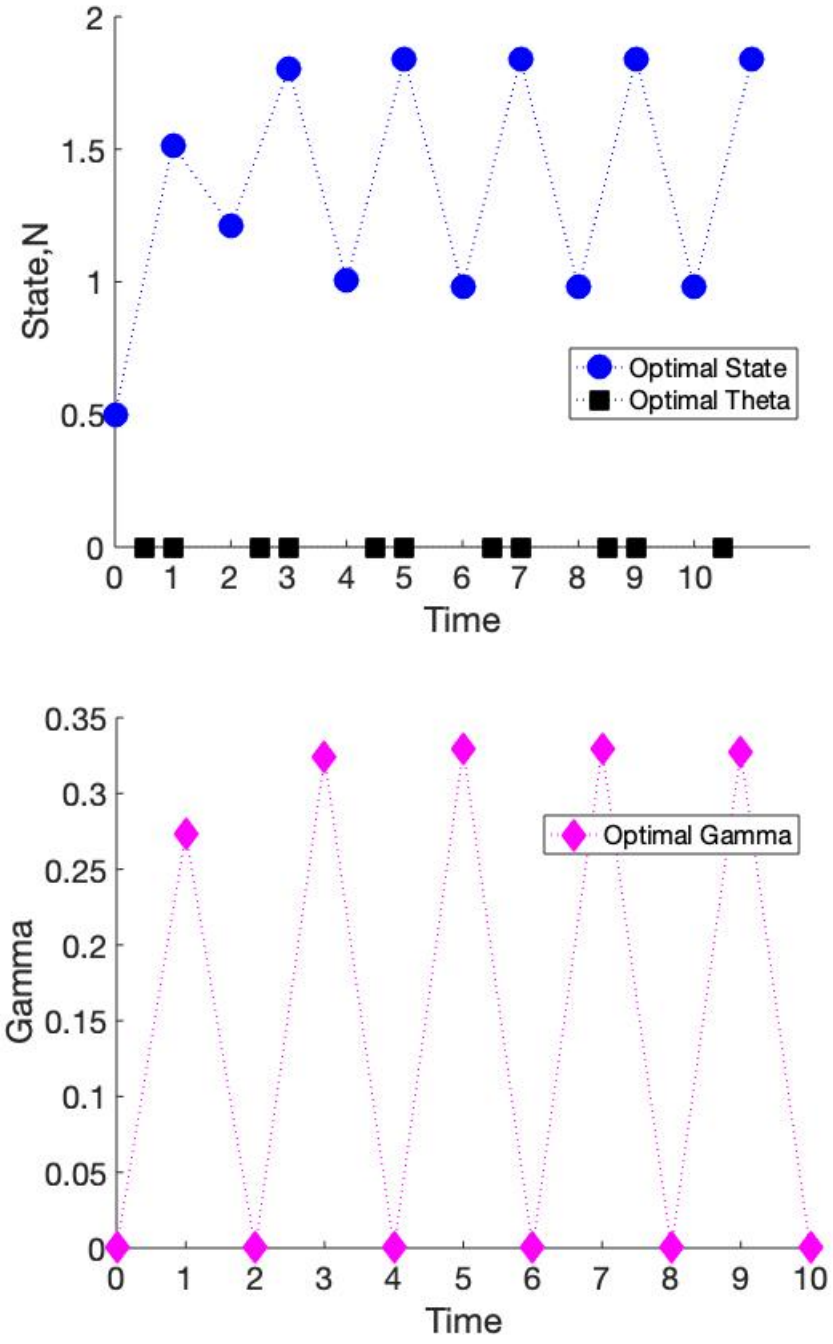

Figure 2.48: The graphs for optimal control in our second model of γ and θ above were generated with parameters as in Table 2.13 except for $N_0 = 0.5$ and $T = 11$. The values of the objective functional are $J_4(\theta^*, \gamma^*) = 18.60$, $J_4(0, \gamma^*) = 18.45$ and $J_4(1, \gamma^*) = 16.12$.

harvest was very low intensity. Here the objective functional values were $J_4(\theta^*, \gamma^*) = 18.60$, $J_4(0, \gamma^*) = 18.45$ and $J_4(1, \gamma^*) = 16.12$ with $J_4(\theta^*, \gamma^*)$ and $J_4(0, \gamma^*)$ differing by only 0.8%.

Figure **??** was generated with parameters as in Table 2.13 except for $b = 1.2$ (decreased from $b = 5$). They can be compared to Figure 2.39 which also had such a low birth rate. However in this case it is best not to harvest at all, as all harvest intensities are on the order of 10^{-8}. Whereas in Figure 2.39 it was best to harvest heavily during the first time step and then have very low harvest intensity. The difference between these two cases is the higher mortality rate in the second set of baseline parameters as compared with the mortality rate from the first set of baseline parameters. With such low harvest intensities, the harvest timings are all mid-season. The objective functional values were $J_4(\theta^*, \gamma^*) = 3.63$, $J_4(0, \gamma^*) = 3.38$ and $J_4(1, \gamma^*) = 3.38$ with $J_4(\theta^*, \gamma^*)$ and $J_4(0, \gamma^*)$ differing by 7%.

Other values of b lower than $b = 5$ from Table 2.13 generated similarly small harvest intensities until we took b to be as large as 4 in Figure 2.50. There seems to be some threshold below which birth is too low to allow for harvesting the population. Once we are above this threshold, we do not immediately see cycles but instead only one harvest of moderate intensity with all other harvests very close to 0 intensity. In this case it is the next-to-last harvest which exhibits intensity away from 0, but this intensity is only about 0.17, nothing near as high as the initial intensity seen in Figures 2.39a and 2.39b. Here the objective functional values were $J_4(\theta^*, \gamma^*) = 14.93$, $J_4(0, \gamma^*) = 14.70$ and $J_4(1, \gamma^*) = 14.53$, with $J_4(\theta^*, \gamma^*)$ and $J_4(0, \gamma^*)$ differing by 1.5%.

We may raise birth even higher, as in Figure 2.51 which was generated with parameters as in Table 2.13 except for $b = 10$ (increased from $b = 5$) and increased C_1 from 0.1 to 1. Here we see cycles similar to those we saw with our first model when cost due to harvest timing was high. While the controls seem to exhibit the by now familiar cycle of alternating high intensity (above 0.5) early harvest with very low intensity mid-season harvest, this appears to cause the state to enter something resembling a 4-cycle. The final harvest is close to 1, causing the population to crash toward extinction. The objective functional values are $J_4(\theta^*, \gamma^*) = 28.28$, $J_4(0, \gamma^*) = 27.03$ and $J_4(1, \gamma^*) = 17.07$, with $J_4(\theta^*, \gamma^*)$ and $J_4(0, \gamma^*)$ differing by 4%.

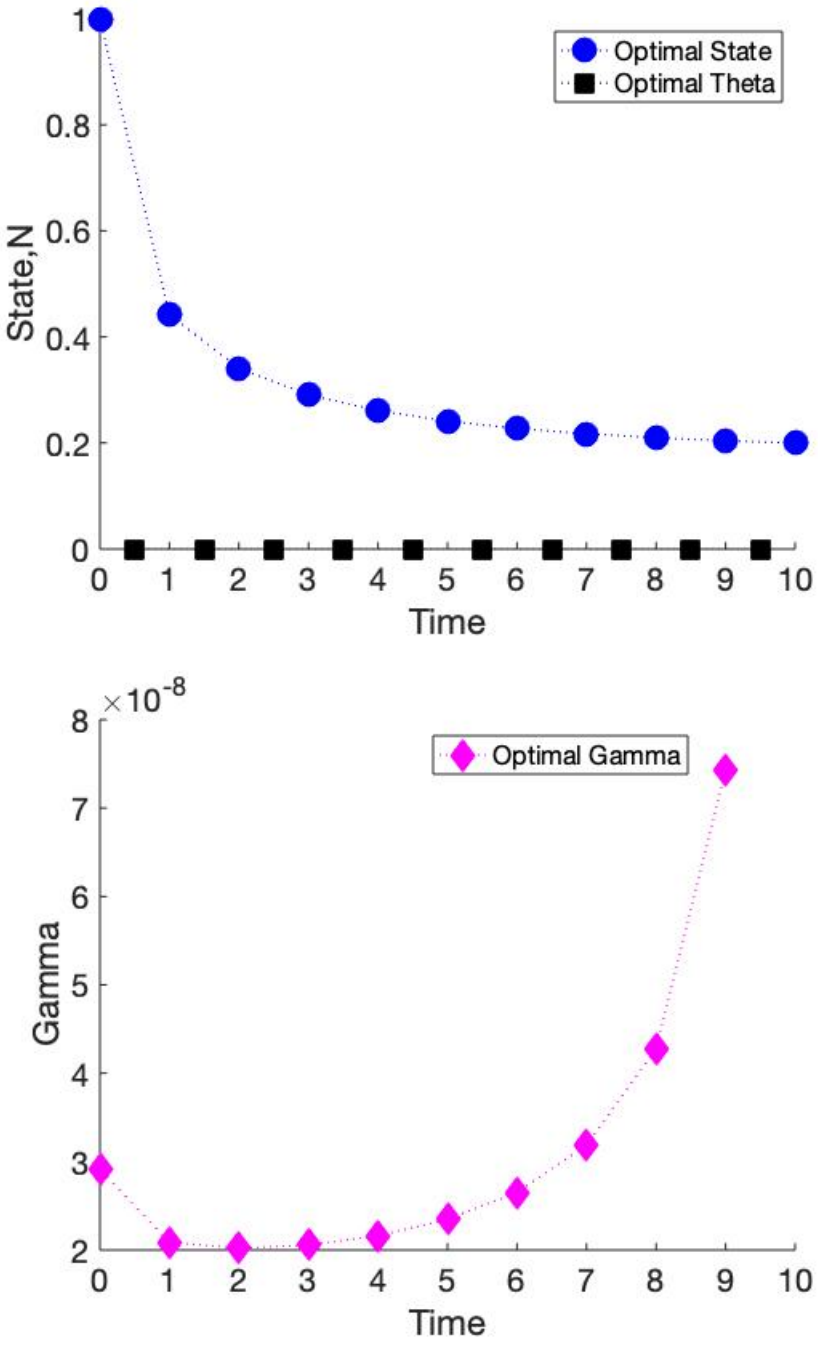

Figure 2.49: The graphs for optimal control in our second model of γ and θ above were generated with parameters as in Table 2.13 except for $b = 1.2$. The values of the objective functional are $J_4(\theta^*, \gamma^*) = 3.63$, $J_4(0, \gamma^*) = 3.38$ and $J_4(1, \gamma^*) = 3.38$.

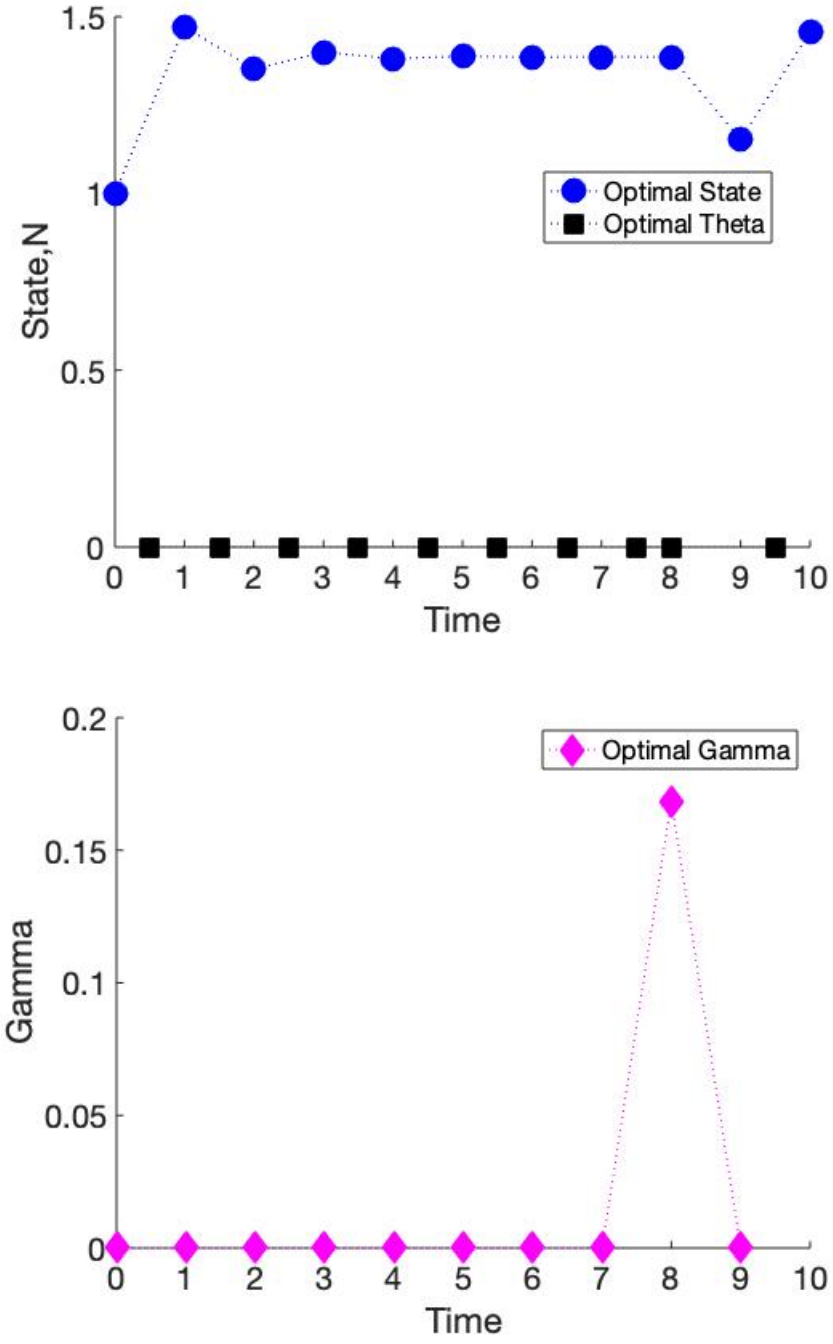

Figure 2.50: The graphs for optimal control in our second model of γ and θ above were generated with parameters as in Table 2.13 except for $b = 4$. The values of the objective functional are $J_4(\theta^*, \gamma^*) = 14.93$, $J_4(0, \gamma^*) = 14.70$ and $J_4(1, \gamma^*) = 14.53$.

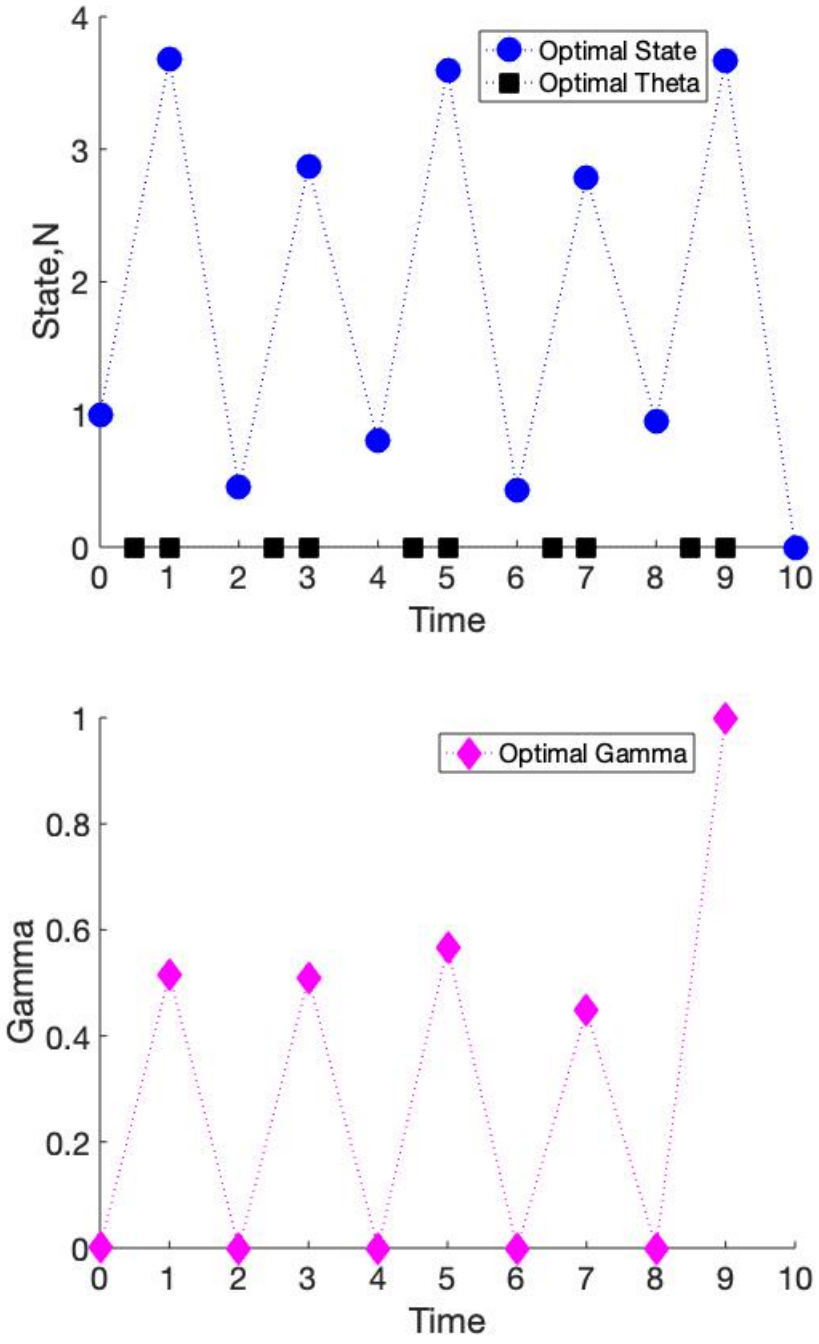

Figure 2.51: The graphs for optimal control in our second model of γ and θ above were generated with parameters as in Table 2.13 except for $b = 10$ and $C_1 = 1$. The values of the objective functional are $J_4(\theta^*, \gamma^*) = 28.28$, $J_4(0, \gamma^*) = 27.03$ and $J_4(1, \gamma^*) = 17.07$.

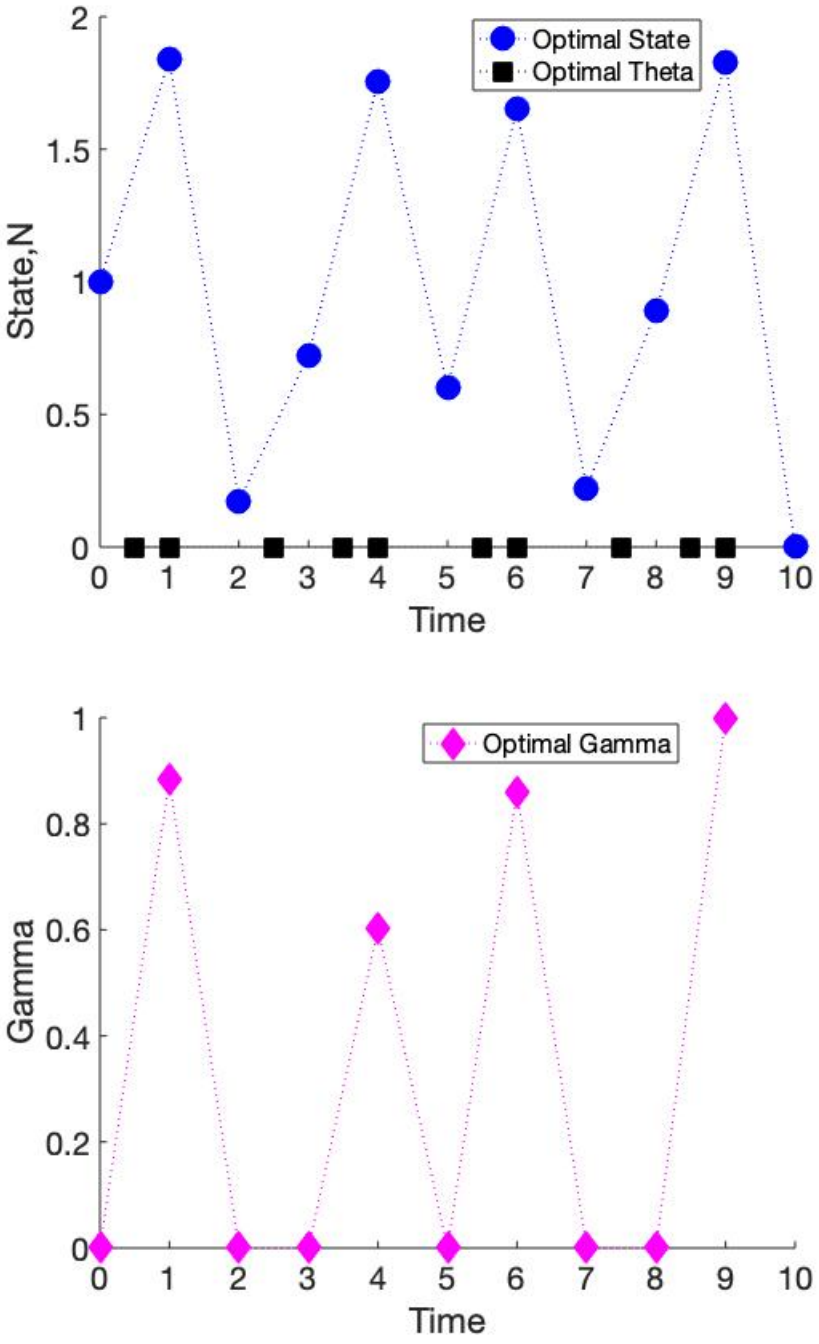

Figure 2.52: The graphs for optimal control in our second model of γ and θ above were generated with parameters as in Table 2.13 except with $A = 0$. The values of the objective functional are $J_4(\theta^*, \gamma^*) = 4.58$, $J_4(0, \gamma^*) = 4.43$ and $J_4(1, \gamma^*) = -0.49$.

Figure 2.52 was generated with parameters as in Table 2.13 except with $A = 0$ (instead of $A = 1$) and can be compared with Figure 2.41. Here, however, no cycle establishes itself. The high intensity harvests vary from about 0.6 to close to 1. As in Figure 2.41, the final harvest nearly wipes out the population. The objective functional values are $J_4(\theta^*, \gamma^*) = 4.58$, $J_4(0, \gamma^*) = 4.43$ and $J_4(1, \gamma^*) = -0.49$, with $J_4(\theta^*, \gamma^*)$ and $J_4(0, \gamma^*)$ differing by 4%.

Figure 2.53 was generated with the same parameters as Figure 2.52 except for a high cost associated with harvest timing $C_1 = 10$ (increased from the baseline of $C_1 = 0.1$). In this case there are growing oscillations in harvest intensity and harvest timing is strictly mid-season. The objective functional values here are $J_4(\theta^*, \gamma^*) = 1.58$, $J_4(0, \gamma^*) = -21.04$ and $J_4(1, \gamma^*) = -24.79$, with a 1428% difference between $J_4(\theta^*, \gamma^*)$ and $J_4(0, \gamma^*)$.

Figure 2.54 was generated with parameters as in Table 2.13 except with $A = 0$ (instead of $A = 1$) and $N_0 = 0.5$ (instead of $N_0 = 1$) and can be compared with Figure 2.43. In both cases the final harvest has intensity of about 1 leading to a population crash. However here, as with Figure 2.52, no cycle seems to be best and the harvest intensity has non-cyclic alternating behavior. The objective functional values are $J_4(\theta^*, \gamma^*) = 4.43$, $J_4(0, \gamma^*) = 4.28$ and $J_4(1, \gamma^*) = -0.47$ with $J_4(\theta^*, \gamma^*)$ and $J_4(0, \gamma^*)$ differing by 3%.

Next, we considered what would happen if we ran optimal control of harvest timing and intensity on our second model for longer time periods. For many combinations of parameters, larger values of T produced the same patterns as $T = 10$. However, this was not always the case.

The graphs on the bottom of Figure 2.55 were generated with the same set of parameters as those on the top except for longer $T = 20$. Oddly, the increase in time shifts the optimal controls from a rough 3-cycle to a rough 2-cycle. The cycles in the longer time period have lower peaks than those in the shorter time period. The objective functional values for the figures on the right were $J_4(\theta^*, \gamma^*) = 147.70$, $J_4(0, \gamma^*) = 147.45$ and $J_4(1, \gamma^*) = 17.84$ with $J_4(\theta^*, \gamma^*)$ and $J_4(0, \gamma^*)$ differing by 0.17%.

In Figure 2.56, the controls on the top with shorter time exhibit a rough 2-cycle while the controls on the bottom with longer time $T = 20$ exhibit a rough 3-cycle for most of the time period. The controls on the bottom have a break in this cycle at time steps 7 through

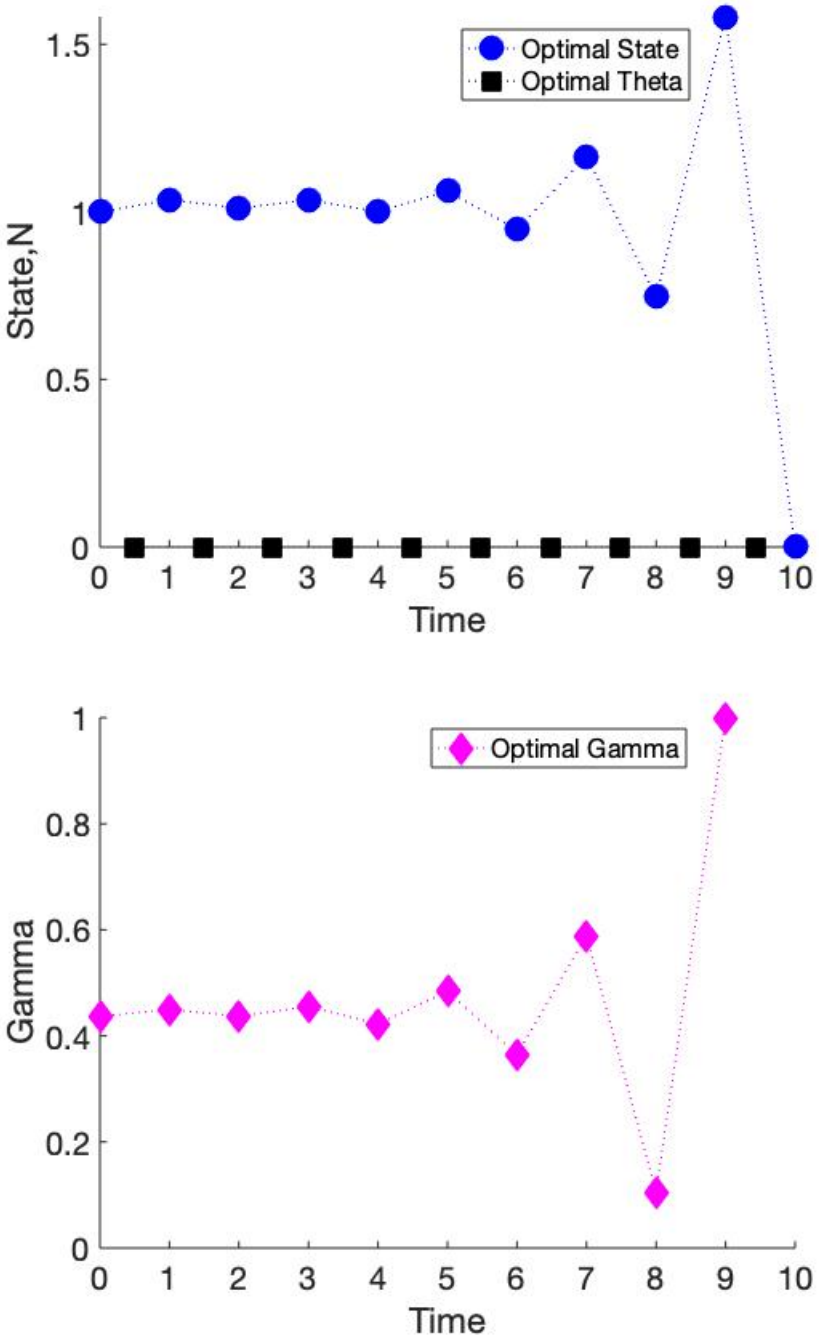

Figure 2.53: The graphs for optimal control in our second model of γ and θ above were generated with parameters as in Table 2.13 except with $A = 0$ and $C_1 = 10$. The values of the objective functional are $J_4(\theta^*, \gamma^*) = 1.58$, $J_4(0, \gamma^*) = -21.04$ and $J_4(1, \gamma^*) = -24.79$.

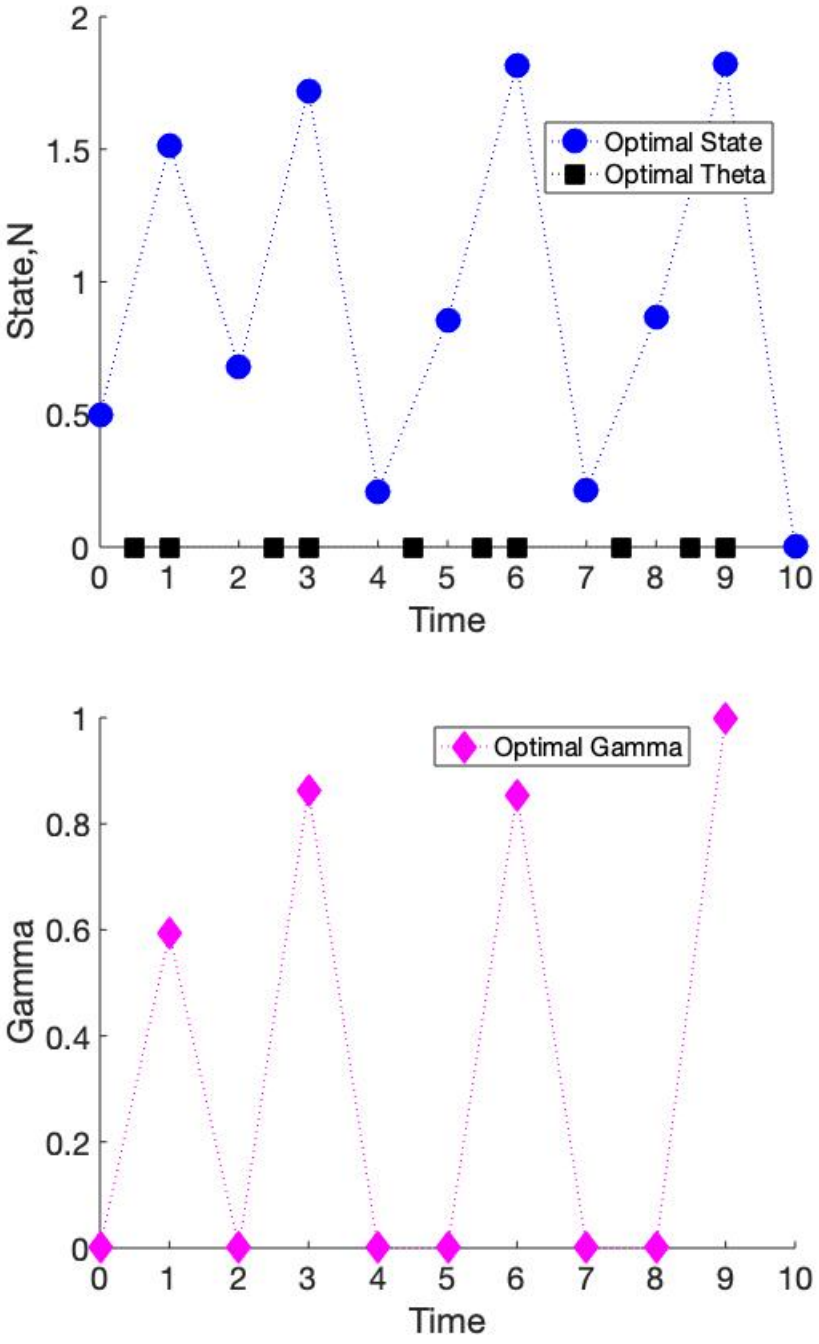

Figure 2.54: The graphs for optimal control in our second model of γ and θ above were generated with parameters as in Table 2.13 except with $A = 0$ and $N_0 = 0.5$. The values of the objective functional are $J_4(\theta^*, \gamma^*) = 4.43$, $J_4(0, \gamma^*) = 4.28$ and $J_4(1, \gamma^*) = -0.47$.

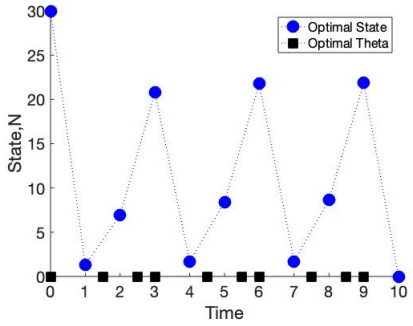

(a) $T = 10$

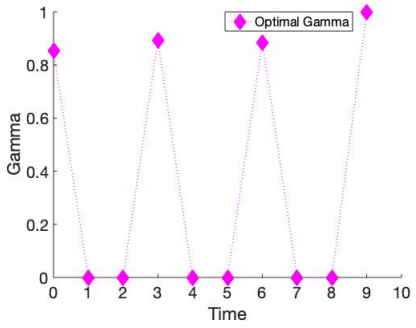

(b) $T = 10$

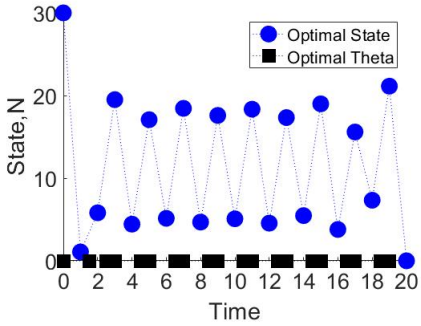

(c) $T = 20$

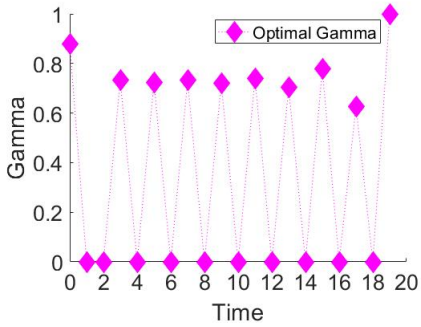

(d) $T = 20$

Figure 2.55: The parameters that generated the figures above were from Table 2.11 except for $A_t = 0$ for all t. The figures on the top are the same as Figure 2.41 for our second model. The objective functional values for the figures on the bottom with $T = 20$ were $J_4(\theta^*, \gamma^*) = 147.70$, $J_4(0, \gamma^*) = 147.45$ and $J_4(1, \gamma^*) = 17.84$.

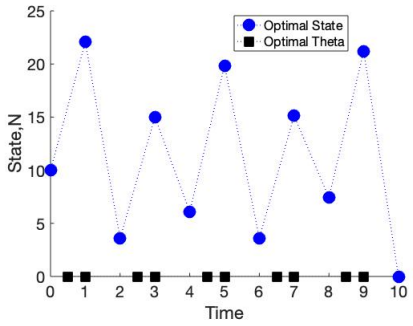

(a) $T = 10$

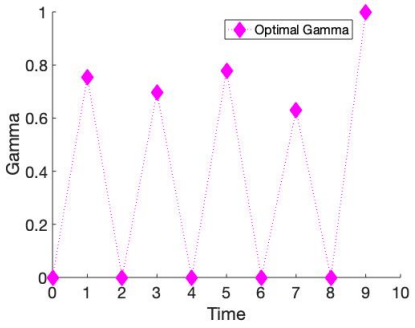

(b) $T = 10$

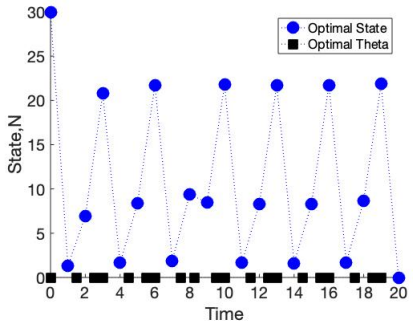

(c) $T = 20$

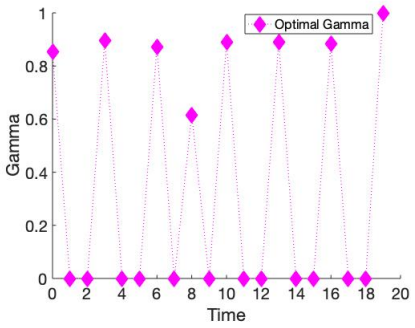

(d) $T = 20$

Figure 2.56: The parameters that generated the figures above were from Table 2.11 except for $A_t = 0$ for all t and $C_1 = 10$. The figures on the left are the same as Figure 2.43 for our second model. The objective functional values for the figures on the right with $T = 20$ were $J_4(\theta^*, \gamma^*) = 127.06$, $J_4(0, \gamma^*) = 97.06$ and $J_4(1, \gamma^*) = -35.63$.

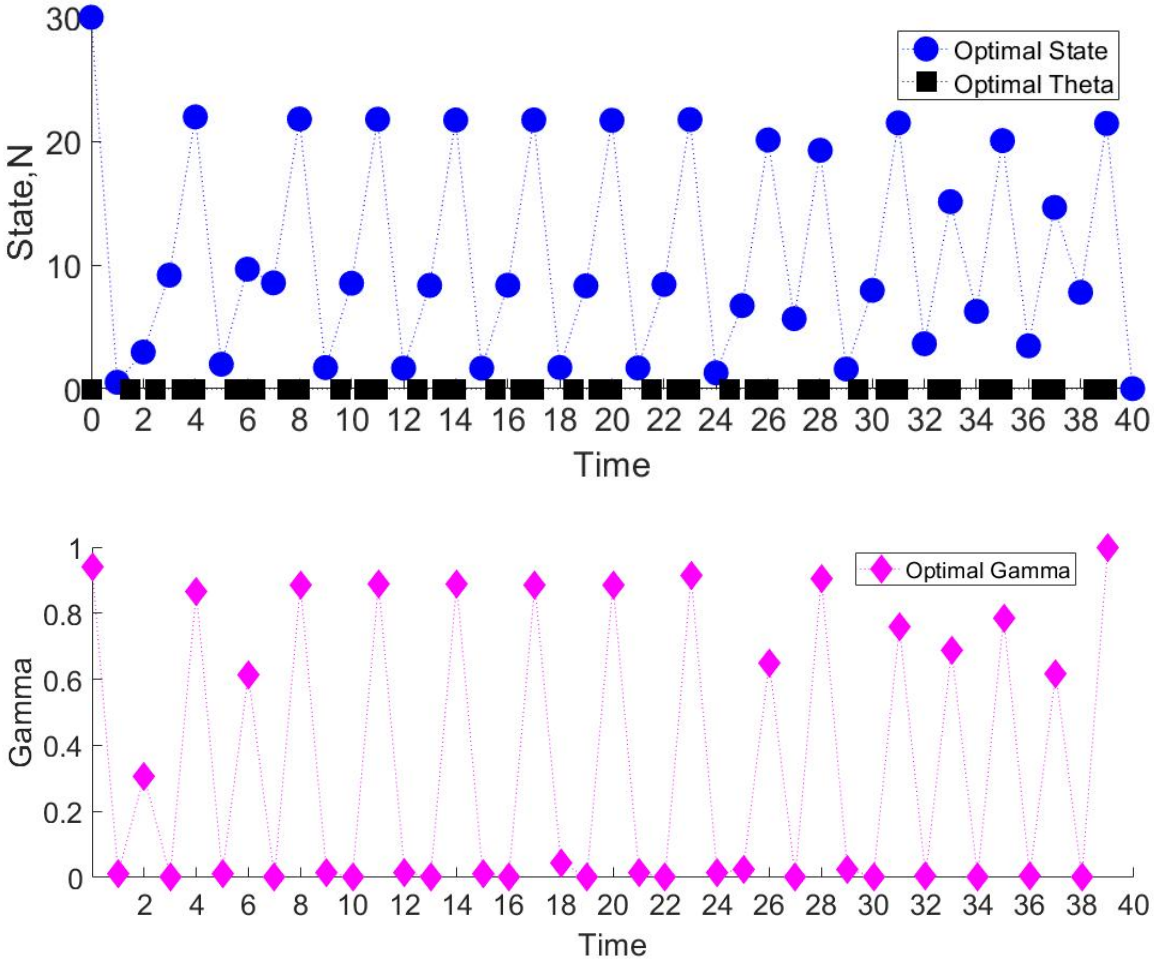

Figure 2.57: The graphs for optimal control in our second model of γ and θ above were generated with parameters as in Table 2.11 except for $A_t = 0$ for all t, $C_1 = 10$, and $T = 40$. The values of the objective functional are $J_4(\theta^*, \gamma^*) = 229.08$, $J_4(0, \gamma^*) = 169.13$ and $J_4(1, \gamma^*) = -69.71$.

9. The objective functional values for the figures on the bottom were $J_4(\theta^*, \gamma^*) = 127.06$, $J_4(0, \gamma^*) = 97.06$ and $J_4(1, \gamma^*) = -35.63$ with $J_4(\theta^*, \gamma^*)$ and $J_4(0, \gamma^*)$ differing by 24%.

Figure 2.57 shows the dynamics for the same parameters as in Figure 2.56 except with longer $T = 40$. The optimal control in Figure 2.57b does not exhibit an unbroken pattern, but rather exhibits more breaks from pattern than those seen in Figure 2.56.

Figure 2.58 has roughly the same optimal controls for the first 9 time steps. However, in the longer time graphs on the bottom we see that by step 15 the pattern breaks down. In this case rather than a different pattern for the whole time, as in the two previous figures,

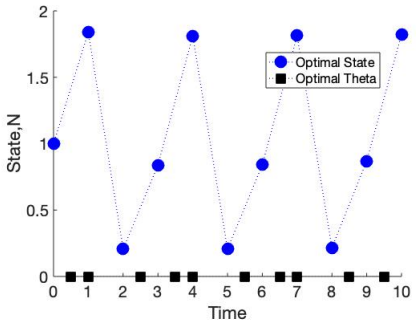

(a) $T = 10$

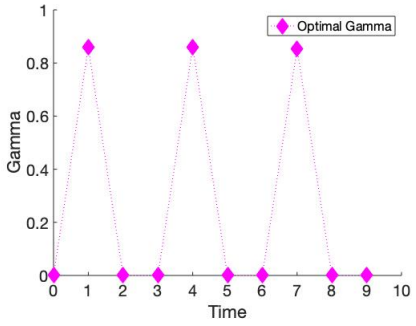

(b) $T = 10$

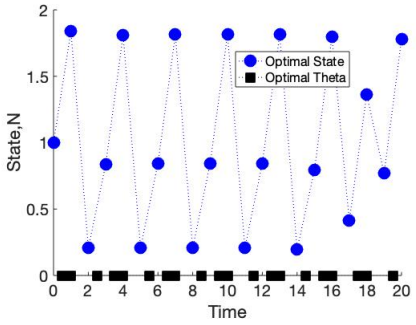

(c) $T = 20$

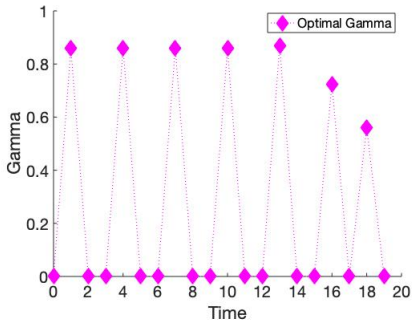

(d) $T = 20$

Figure 2.58: The parameters that generated the figures above were from Table 2.13 except for $A_t = 0$ for all $t < T$. The figures on the top are the same as Figure 2.46 for our second model. The objective functional values for the figures on the bottom with $T = 20$ were $J_4(\theta^*, \gamma^*) = 9.46$, $J_4(0, \gamma^*) = 9.16$ and $J_4(1, \gamma^*) = 1.10$.

there was instead a different pattern later in time. The objective functional values for the figures on the bottom were $J_4(\theta^*, \gamma^*) = 9.46$, $J_4(0, \gamma^*) = 9.16$ and $J_4(1, \gamma^*) = 1.10$ with $J_4(\theta^*, \gamma^*)$ and $J_4(0, \gamma^*)$ differing by 3%.

In Figure 2.59, the controls in the top graphs do not appear to establish any pattern. But the controls in the bottom graphs with longer time establish a rough 3-cycle. The objective functional values for the figures on the bottom with $T = 20$ were $J_4(\theta^*, \gamma^*) = 8.64$, $J_4(0, \gamma^*) = 8.34$ and $J_4(1, \gamma^*) = -0.88$ with $J_4(\theta^*, \gamma^*)$ and $J_4(0, \gamma^*)$ differing by 3%.

Figure 2.60 again has controls on the top that don't seem to establish a pattern. But on the bottom with time increased, in this case to $T = 30$, a pattern establishes for about the first half of the time steps. Then the pattern gradually breaks down, until the final harvest when a high-intensity early-season harvest crashes the population. The objective functional values for the figures on the bottom were $J_4(\theta^*, \gamma^*) = 12.47$, $J_4(0, \gamma^*) = 12.07$ and $J_4(1, \gamma^*) = -1.02$ with $J_4(\theta^*, \gamma^*)$ and $J_4(0, \gamma^*)$ differing by 3%.

From these examples we see with longer T that a pattern may continue or may not. The lengthening of T may have unexpected effects.

2.6 Optimal control of harvest intensity and timing in both models with discount factor

Suppose we take a new objective functional

$$J_5(\theta, \gamma) = A_T N_T + \sum_{t=0}^{T-1} \left(\delta^t \left(A_t N_t + B_t Y_t - C_1 (\frac{1}{2} - \theta_t)^2 - C_2 \gamma_t - C_3 \gamma_t^2 \right) \right) \tag{2.70}$$

where δ is a discount factor, N_t and Y_t refer to the state and yield for either the first or second mechanistic model. A discount factor ensures that funds obtained earlier are worth more due to being able to invest them.

Figure 2.61 shows optimal control of the first model and was generated with the same parameters as Figure 2.31 except with the discount factor of $\delta = 0.95$. Note that the high-intensity final harvest seen in Figure 2.31 is absent here because of the discount factor. The objective functional values for $J_5(\theta^*, \gamma^*) = 99.81$ and $J_5(0, \gamma^*) = 98.05$ differ by only 1.8%.

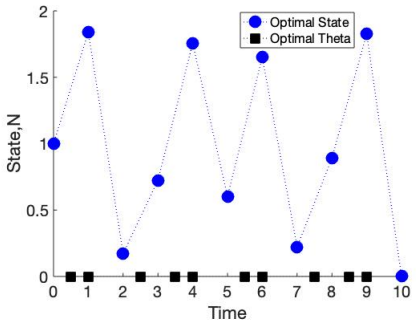

(a) $T = 10$

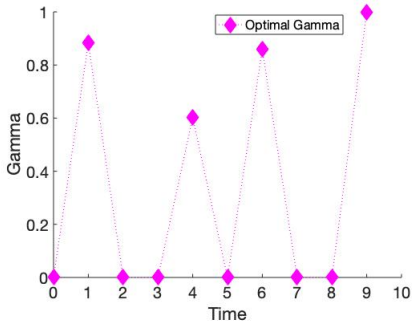

(b) $T = 10$

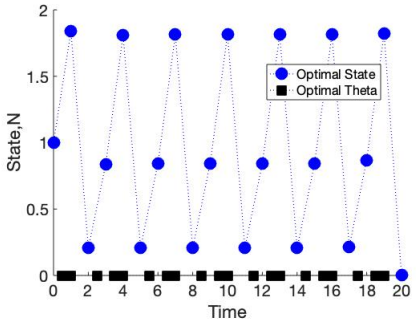

(c) $T = 20$

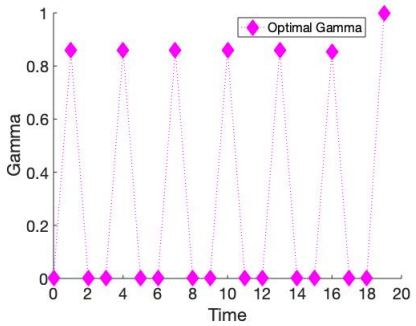

(d) $T = 20$

Figure 2.59: The parameters that generated the figures above were from Table 2.13 except for $A_t = 0$ for all t. The figures on the top are the same as Figure 2.52 for our second model. The objective functional values for the figures on the bottom with $T = 20$ were $J_4(\theta^*, \gamma^*) = 8.64$, $J_4(0, \gamma^*) = 8.34$ and $J_4(1, \gamma^*) = -0.88$.

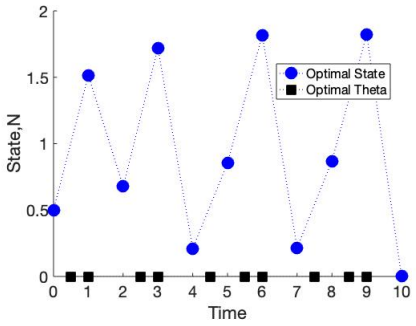

(a) $T = 10$

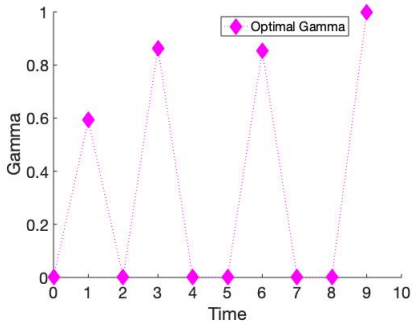

(b) $T = 10$

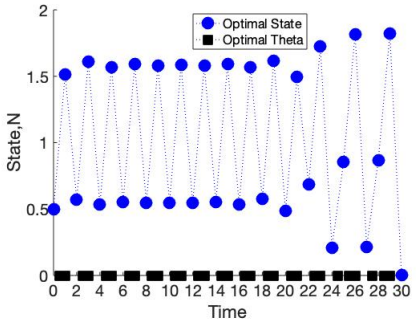

(c) $T = 30$

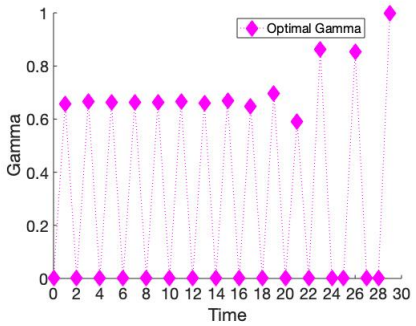

(d) $T = 30$

Figure 2.60: The parameters that generated the figures above were from Table 2.13 except for $A_t = 0$ for all t and $N_0 = 0.5$. The figures on the top are the same as Figure 2.54 for our second model. The objective functional values for the figures on the bottom with $T = 30$ were $J_4(\theta^*, \gamma^*) = 12.47$, $J_4(0, \gamma^*) = 12.07$ and $J_4(1, \gamma^*) = -1.02$.

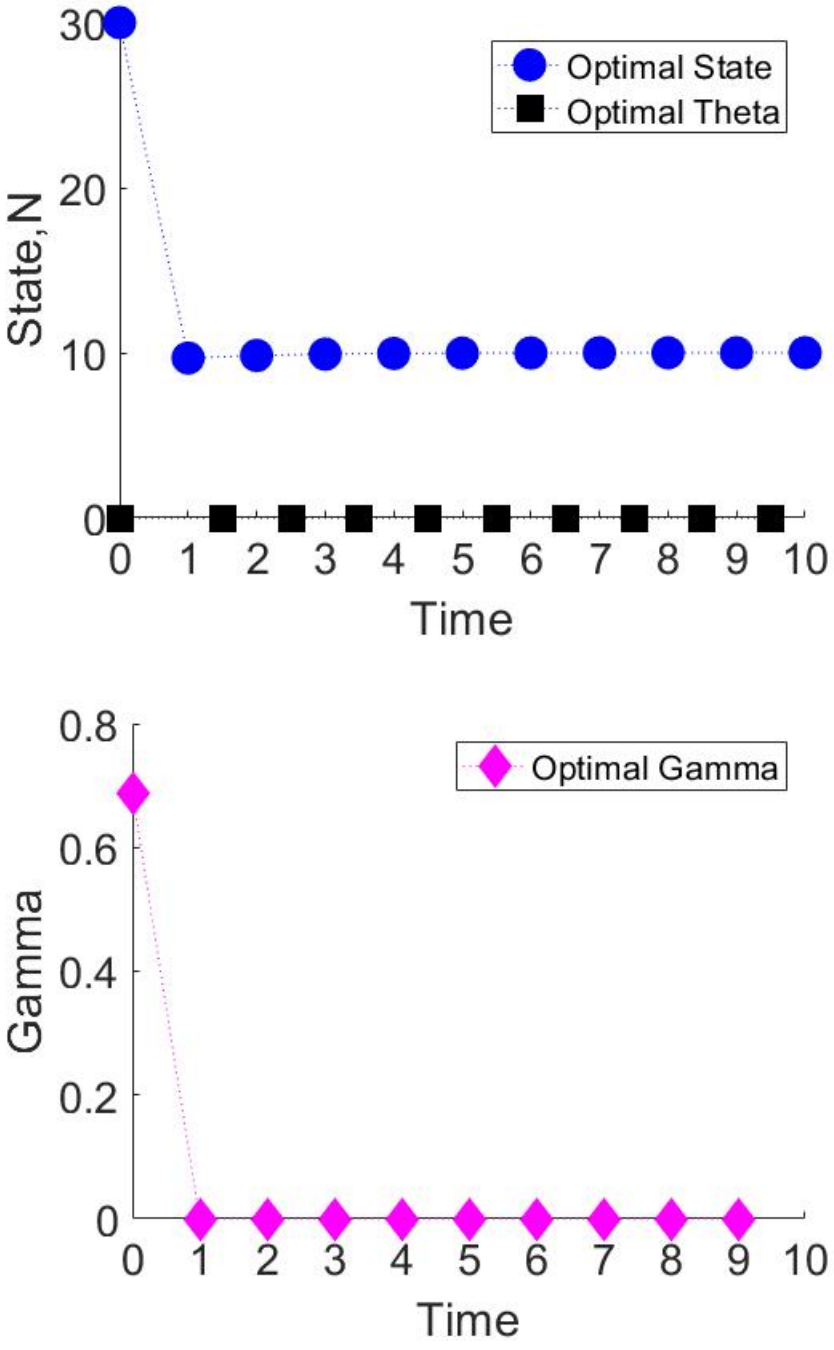

Figure 2.61: The graphs for optimal control and discounting in our first model of γ and θ above were generated with parameters as in Table 2.9 except for $b = 2$, $C_1 = 1$ and $\delta = 0.95$. The values of the objective functional are $J_5(\theta^*, \gamma^*) = 99.81$, $J_5(0, \gamma^*) = 98.05$ and $J_5(1, \gamma^*) = 70.96$.

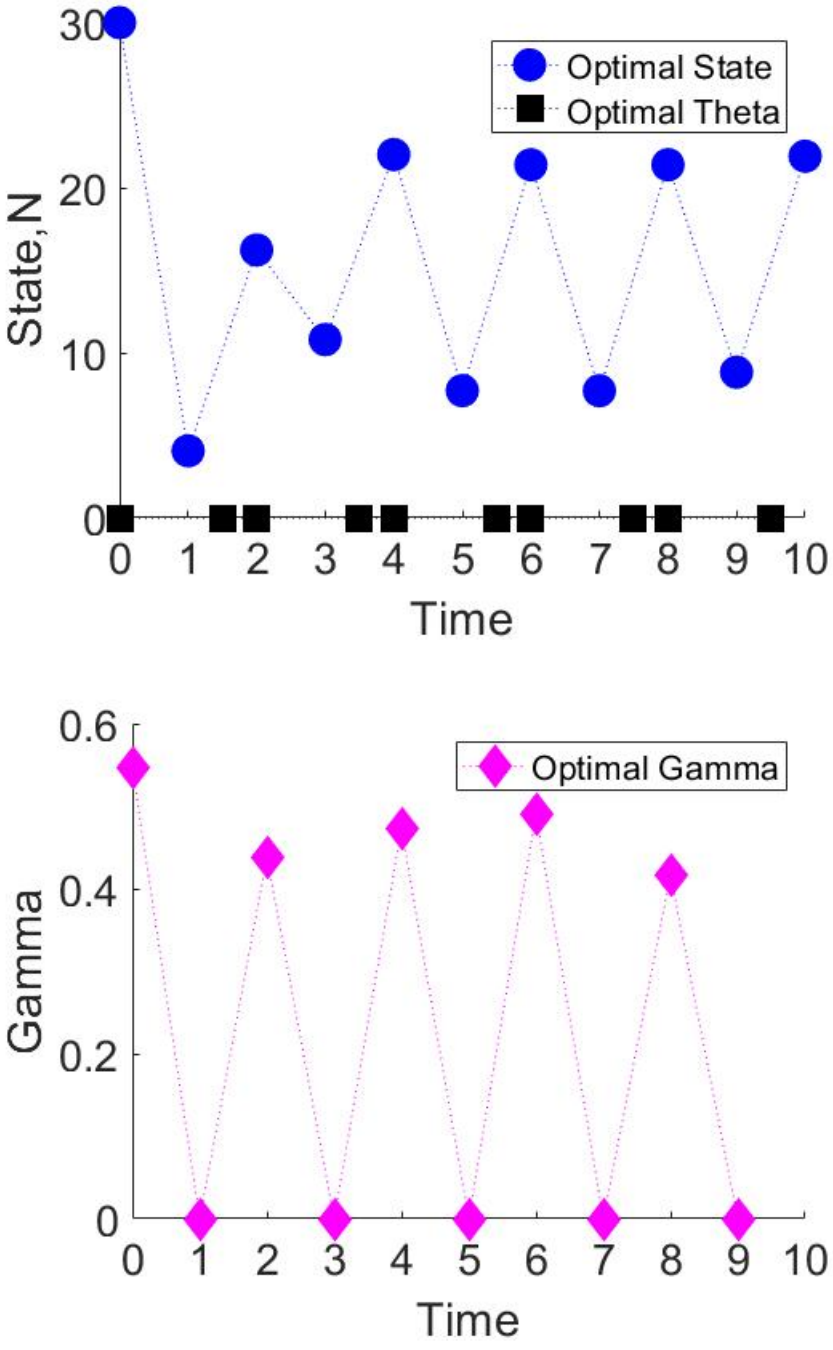

Figure 2.62: The graphs for optimal control in our second model of γ and θ above were generated with parameters as in Table 2.11 except with $\delta = 0.95$. The values of the objective functional are $J_5(\theta^*, \gamma^*) = 188.65$, $J_5(0, \gamma^*) = 188.55$ and $J_5(1, \gamma^*) = 148.25$.

Figure 2.62 shows optimal control and discounting of the second model and was generated with the same parameters as Figure 2.35 except with the discount factor of $\delta = 0.95$. The high-intensity final harvest seen in Figure 2.35 is absent in Figure 2.62 because of the discount factor. The objective functional values $J_5(\theta^*, \gamma^*) = 188.65$ and $J_5(0, \gamma^*) = 188.55$ differ by a mere 0.05%.

The graphs on the top half of Figure 2.63 were generated from the same parameters as those in Figure 2.62 except for $\delta = 0.9$ instead of $\delta = 0.95$. For the smaller value of δ, the first harvest is of higher intensity while the remaining harvests are of roughly the same intensity of those with larger δ. The objective functional values for the graphs on the top half of Figure 2.63 $J_5(\theta^*, \gamma^*) = 161.15$ and $J_5(0, \gamma^*) = 161.07$ differ by 0.05%. The graphs on the bottom half of Figure 2.63 were generated with the same parameters as those on the top half except for longer $T = 20$. With this longer value for T, the first harvest is of much higher intensity and there is another high intensity harvest at $t = 15$. The objective functional values for the bottom of Figure 2.63 $J_5(\theta^*, \gamma^*) = 208.28$ and $J_5(0, \gamma^*) = 208.16$ differ by .06%. Though the harvests on the bottom of Figure 2.63 were generally more high intensity than those on the top, because of the discount factor the value of J does not increase by much. Indeed, though the length of time doubles, the value $J_5(\theta^*, \gamma^*) = 208.28$ from the right is only 23% larger than the value $J_5(\theta^*, \gamma^*) = 161.15$ from the left.

The inclusion of a discount factor in the objective functional causes changes in the optimal controls, but those changes are difficult to predict.

2.7 Conclusions

We are interested in the order of events in models of harvest timing. We carefully built two mechanistic models with the order of events mortality-harvest-mortality-birth. Mortality was density dependent and continuous, while birth and harvest were both density independent and discrete in time. The census always took place directly after birth because we thought it more reasonable to notice births in a population and then trigger the census rather than to census somehow immediately before birth. We performed optimal control of the discrete models of harvest timing we developed, a novel application of the theory.

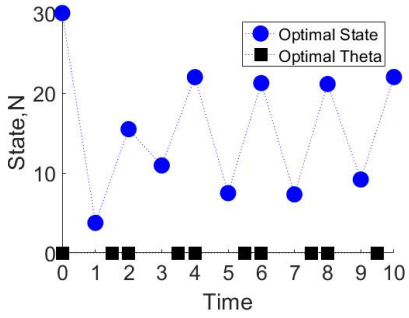

(a) $T = 10$

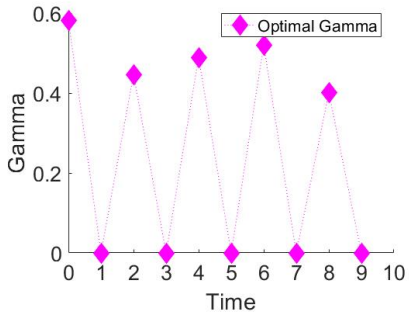

(b) $T = 10$

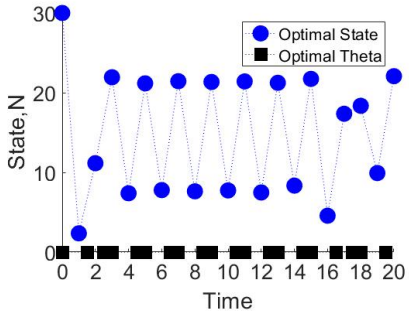

(c) $T = 20$

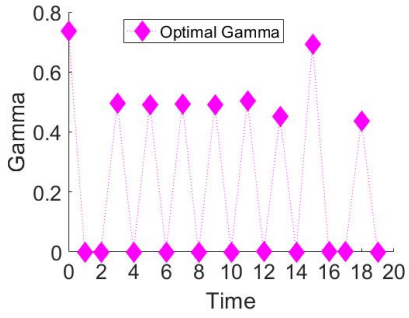

(d) $T = 20$

Figure 2.63: The parameters that generated the figures of optimal control and discounting of θ and γ of the second model above were from Table 2.11 except with $\delta = 0.9$. The objective functional values for the figures on the top were $J_5(\theta^*, \gamma^*) = 161.15$, $J_5(0, \gamma^*) = 161.07$ and $J_5(1, \gamma^*) = 125.47$, and for the figures on the bottom were $J_5(\theta^*, \gamma^*) = 208.28$, $J_5(0, \gamma^*) = 208.16$ and $J_5(1, \gamma^*) = 157.74$.

We compared our models with the Seno model, the only discrete time model of explicit within-season harvest timing in the literature. We found surprisingly little difference between our first mechanistic model and the corresponding Seno model. Though the Seno model always predicts larger next-generation size than our model, for large areas of parameter space they provide virtually identical time series. Despite this similarity in outputs, our model offers the benefit of known order of events and, critically, known yield. Our second mechanistic model was identical to one of the limit cases for the corresponding Seno model. However, the difference between our second model and Seno's corresponding model was nonetheless small over large areas of parameter space.

In general, whether controlling only harvest timing or both harvest timing and harvest intensity, mid-season harvest occurs when yield is low, intensity is low, or when cost associated with harvest timing is high. Low yield might result from low intensity harvesting, or from depletion of stock due to high intensity harvesting, or as an intermediate step (or two) in a cycle between a high intensity and high yield season.

When only controlling harvest intensity, we did not find any circumstances under which harvesting mid-season was preferable to harvesting at the beginning of the season. This is because all the terms in the objective functional are either maximized at $\theta \equiv 0$ or do not depend on θ at all. The lowest difference between the mid-season option and the beginning-of-season option came when yield was low due to low birth.

When exploring control of both harvest timing and intensity for our first model, we found fewer variations in our results than when exploring the second mechanistic model. In all of the situations explored in controlling both intensity and timing for our first mechanistic model, the final harvest had much higher intensity than intermediate harvests. This was due to the importance placed on yield, because even placing importance on stock conservation resulted in high intensity final harvest. When no importance was placed on stock conservation, the final harvest depleted the stock. We observed cycles in two cases, both with high cost placed on harvest timing (see Figures 2.30 and 2.32). We do not know an intuitive reason for these cycles.

For our second mechanistic model we observe a broader variety in results, including some interesting cycles. The prominence of cycles among these optimal control results likely is

related to our choice of a Ricker-type mortality term. Since the Ricker model is known to exhibit cycles, we expected that cycles would be a possibility. Indeed, for the baseline parameter cases, we observed cycles that were not present without optimal control (compare Figure 2.35 with Figure 2.34 and Figure 2.45 with Figure 2.44).

In many situations, control of harvest intensity seems to be much more important than control of harvest timing. Indeed, only with higher cost associated with harvest timing does $J_x(0, \gamma^*)$ differ significantly from $J_x(\theta^*, \gamma^*)$.

When time is increased, several types of things may happen. The pattern of the optimal controls might not change at all. The pattern might completely switch to a different one. The pattern may initially be the same, but then break down. A pattern may establish where before there was none. In general, over longer time periods the timing of harvest seems to be relatively more important, as seen in the increased relative difference between $J_4(0, \gamma^*)$ and $J_4(\theta^*, \gamma^*)$.

In future we plan to develop more mechanistic models and explore optimal control of both harvest timing and intensity for those models. We did some investigation of discounting without arriving at any conclusions and in future we will investigate discounting further. We plan to consider additionally investigating minimum viable population size. We will develop more mechanistic models using different types of processes for mortality, birth, or both. We will consider age-structured populations and spatially structured populations. In particular, we will explore models where the population is divided into two classes: Juveniles and Adults. We also plan to select a specific population for which we can access data, build a mechanistic model specifically designed to fit the ecology of that population, and perform optimal control.

Chapter 3

Contact tracing in Ebola

3.1 Introduction

In March 2014, the most deadly outbreak to date of Ebola virus disease (EVD), a hemorrhagic fever, began in Guinea and rapidly spread to Liberia, Nigeria, Senegal, and Sierra Leone [35]. In October 2014, the World Health Organization (WHO) Ebola Response Team estimated an overall case fatality rate of 70.8% and basic reproduction numbers ($\Re_0$) of 1.71 for Guinea, 1.83 for Libera and 1.38 for Sierra Leone [6]. Concern that Ebola might spread globally via airline travel led to recommendations for health assessments at airports in the affected countries [10]. A review and meta-analysis of 31 reports found that the main methods of spread were direct contact with an infected individual and contact with deceased loved ones during traditional funeral practices [11]. In the 2014-2016 outbreak in Sierra Leone, among individuals confirmed to have EVD, 47.9% reported that they had had contact with someone suspected of having EVD and 25.5% reported having attended a funeral [24]. These transmission pathways are further indicated as important by mathematical models [25] and by statistical models [77]. Ebola can survive on some surfaces for up to 192 hours unless they are properly disinfected [19]. This might be one of the reasons why so many health care workers became infected [73]. Ebola outbreaks most likely initiate due to contact between humans and fruit bats [31, 62]. Outcomes for individuals who contracted EVD during the outbreak varied based on location, time of infection, and whether the individual was hospitalized [36].

Contact tracing, sometimes called partner notification, is often used in the fight against HIV spread [20, 42, 43]. Contact tracing for Ebola is quite different, though, because it doesn't focus on sexual partners but rather on people who have been in some kind of close contact with the infected or deceased individual. The goal of contact tracing is to identify secondary infections and to isolate them in order to stop disease transmission. Contact tracing plays a vital role in controlling sexually transmitted diseases and emerging diseases [26, 46]. Throughout the outbreak, the Centers for Disease Control and Prevention's Morbidity and Mortality Weekly Report detailed the progress of the disease as well as some information about contact tracing efforts. "An Ebola contact was defined as a person who had a known exposure to a confirmed, probable, or suspected case. Contacts were actively monitored for 21 days after the date of last exposure" [15]. All contacts being traced were instructed to remain isolated from the general population. If a contact showed symptoms of EVD, they were moved to a suspected case isolation ward and tested. If the test was positive, that individual was moved to the confirmed case ward. If the test was negative the individual was sent home to be traced for another 21 days. Some individuals spread the disease to many more contacts than others, and these individuals are known as superspreaders [27]. In Liberia infected individuals from impoverished backgrounds reported more contacts on average than infected individuals from high SES backgrounds [29].

Many mathematical models of the 2014-2016 West African outbreak have been developed using various data sources. Using data from Ghana, Agusto et al. built a system of ordinary differential equations (ODEs) incorporating three control measures: educating the public of the danger posed by participating in traditional funeral practices, changing shift lengths for health care workers, and limiting visitation hours at hospitals [3]. Ajelli et al. produced an agent based model using data from Guinea [4]. They concluded that contact tracing in Guinea had a strong negative correlation with the time series of cases. Dénes and Gumel used a system of ODEs to model quarantine of suspected infectious individuals as a control for the West African epidemic and found that quarantine alone was insufficient to end the epidemic [21]. Ivorra et al. developed a compartmental ODE model of the spread of Ebola between countries [44]. One ODE model focused specifically on Montserrado, Liberia concluded that allocating many more hospital beds earlier in the epidemic and increased contact tracing

could have dramatically reduced the caseload [52]. Some patients with EVD exhibit different symptoms or severity of symptoms than others. Ponce et al. built a system of ODEs with separate compartments for severely ill patients to account for some of this variation [63]. They concluded that the most important control methods were contact tracing and isolation of individuals with EVD. Rachah and Torres developed two ODE models, an SIR model and an SEIR model, of EVD transmission and performed optimal control analysis of both models using educational campaigns, immunization, and isolation as controls [64]. Salem and Smith? developed an SEIR model with an additional compartment for infectious deceased and concluded that the best targets for interventional strategies are transmission probability and contact rate with infectious individuals [70]. Fang et al. developed a spatiotemporal Poisson model of transmission in Sierra Leone [30], and they found that population density and proximity to Ebola treatment centers were associated with Ebola transmission.

Browne et al. built two models using data from Sierra Leone and Guinea [13, 84]. In their SEIR model [13], they incorporated contact tracing by building separate compartments for Exposed individuals being traced and Infectious individuals being traced. Their model neglected spread within hospitals and spread from contact with deceased individuals. They found that increasing the fraction of cases reported and increasing the fraction of reported contacts that were traced could bring $\Re_0$ below 1. They also provided weekly point estimates for the effective reproduction number for Guinea and Sierra Leone. In this work, we will use a similar, but more mechanistic approach of counting persons being traced and accounting for the workload of the contact tracers.

Rivers et al. [67] built an SEIR model of the epidemic in Sierra Leone and Liberia while it was ongoing and before it had reached a peak. They concluded that improved contact tracing could have a large impact on number of cases but that even when combined with two other interventions contact tracing was insufficient to bring the epidemic to an end. The identified the duration of a traditional funeral in Sierra Leone as 4.5 days and the length of the incubation period as 10 days, values which we use in our model.

In Sierra Leone, "Initial case investigation and contact tracing were hindered by delayed reporting and under-reporting of symptomatic individuals from the community" [78]. Indeed, in some cases it was determined that individuals had lied when questioned about contacts and

funeral practices. According to personal communication from Michael Washington (Centers for Disease Control) [83], there were limitations on the number of contact tracing workers and the number of contacts per tracer per day. The number of contacts a contact tracer could trace per day was based on the area type. In an urban area a tracer could trace about 15 individuals per day, while in a rural area a tracer could trace 10 individuals per day. In January 2015 there were 1200 contact tracers in Western Area, Sierra Leone. According to [85], "It can take as many as ten staff to monitor the contacts of just a single case." In neighboring Liberia, "[S]everal challenges were encountered. These included difficulty locating contacts, difficulty with contacts completing 21 days of monitoring and unwillingness of symptomatic contacts to attend an Ebola Treatment Unit (ETU) be tested for Ebola among others" [86]. Other challenges faced by contact tracers in Liberia included contacts hiding from tracers, people failing to identify all contacts or lying about their own exposure, resistance to in-home isolation, and difficulties finding contact tracers. Many of the same problems were encountered in Sierra Leone. A study by Swanson et al. found that contact tracing in Liberia was performed for 26.7% of cases and only identified 3.6% of new cases [79], suggesting plenty of room for improvement. Chowell and Nishiura [17] illustrated the insights for disease management that can come from modeling connected with Ebola epidemiological data and discussed the need for understanding the effectiveness of contact tracing.

Olu et al. analyzed contact tracing interview data in the western area districts of Sierra Leone [61], and noted that "Challenges associated with effective contact tracing included lack of community trust, concealing of exposure information, political interference with recruitment of tracers, inadequate training of contact tracers, and incomplete EVD case and contact database." Contacts being traced were supposed to be provided with basic needs, such as food and water, but this often did not occur. Some contacts chose to disappear because of the stigma of being listed as a contact, with "The overall mean number of contacts per patient recorded in this outbreak (8.5 contacts per patient) falls short of what was obtained in similar settings." Olu et al. "identified provision of incorrect personal identity, lack of community trust in EVD prevention and control interventions (resulting in community resistance), and withholding of vital information on potential contacts and their health status as the challenges responsible for" the trend of missed contacts.

Our goal is to represent the contact tracing process carefully mechanistically to illustrate the management of this process. Our model uses a novel feature, which is explicitly counting the people being traced and connecting the total persons traced with the workload of contact tracer workers. We will focus our model on Sierra Leone, for which we have data from the Sierra Leone Ministry of Health [1, 2]. These data include cumulative confirmed cases and cumulative confirmed deaths as reported online during the outbreak in the daily situation report. We will design a system of ODEs explicitly incorporating contact tracing, fit this model to our data, and see what insights we might gain from this mechanistic approach. This work is in collaboration with Suzanne Lenhart (University of Tennessee), Christina Edholm (Scripps College), Benjamin Levy (Fitchburg State University), Michael Washington (Centers for Disease Control), Bradford R. Greening (Centers for Disease Control), Jane White (University of Bath, UK), Edward Lungu (Botswana International University of Science & Technology, Botswana), Obias Chimbola (Botswana International University of Science & Technology, Botswana), Moatlhodi Kgosimore (Botswana University of Agriculture and Natural Sciences, Botswana), and Faraimunashe Chirove (University of Johannesburg, South Africa), M. Helen Machingauta (Botswana International University of Science & Technology, Botswana).

3.2 Model

We begin as in Ebola models [13, 61, 67, 72, 84] using a system of ODEs, which follow an SEIR approach. In addition to the Susceptible, Exposed, Infected, and Recovered classes, Ebola models typically include dead bodies (D) as a class because they are a significant source of infection due to traditional funeral practices such as hugging and kissing the body of a deceased loved one. We also include a Hospitalized (H) class, in which individuals are assumed to be isolated and not contribute to infection, and if they die their bodies are assumed to be disposed of safely. We place no upper limit on the size of class H, which does not reflect the situation during the outbreak where insufficient beds and staffing were a major limiting factor in controlling the outbreak [57].

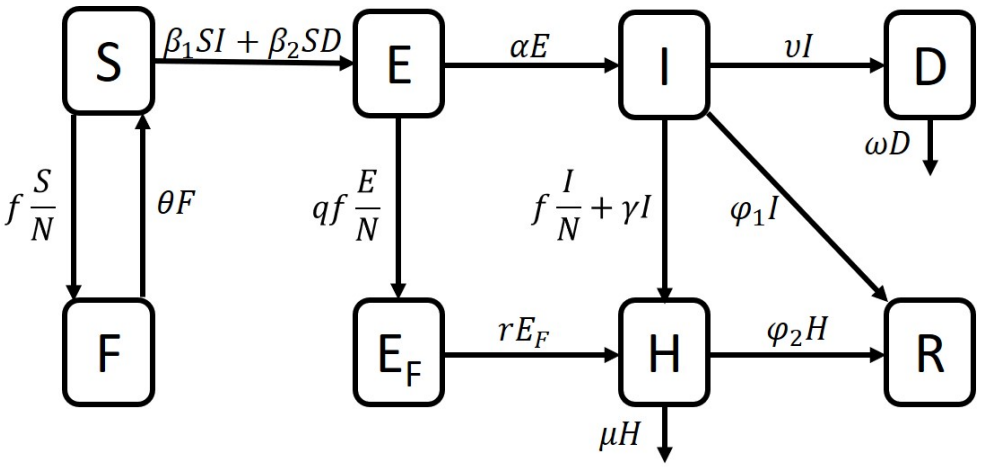

Figure 3.1: Flow diagram of our model

Our investigation of contact tracing begins with adding two new classes of individuals being traced. Since exposure is a hidden trait, individuals being traced are either susceptible or exposed. We created a class called F (for friends and family) of susceptible individuals who are being traced and a second class, E_F, for individuals being traced who are exposed. The coefficient f in Figure 3.1 is a function depending on E, F, and I which shows a transition into the F and E classes and contributes to the movement from I to H. Two events can lead to initiation of contact tracing: either a funeral is observed or an individual enters the hospital. The friends and family connected to the individuals involved in either of these two events will be contacted each day for 21 days by a contact tracer. We assume that individuals in the F class being traced will follow isolation guidelines to prevent them from becoming exposed. Individuals in E_F are moved to the hospital when they present symptoms. Also, we may consider contact tracers spend some effort on moving people from I to H, see the coefficient f on that term in the diagram in Figure 3.1. There is a limited number of contact tracers, and each contact tracer is able to trace a limited number of individuals at a time. To account for this, we place a threshold on the total number of contacts that can be traced at a time. Part of the work done by contact tracers is moving individuals to the hospital, and the remaining effort is dedicated to visiting contacts who haven't (yet) displayed any symptoms of Ebola. Our model with eight compartments is below.

$$S' = -\beta_1 SI - \beta_2 SD - f\frac{S}{N} + \theta F \tag{3.1}$$

$$F' = f\frac{S}{N} - \theta F \tag{3.2}$$

$$E' = \beta_1 SI + \beta_2 SD - qf\frac{E}{N} - \alpha E \tag{3.3}$$

$$E'_F = qf\frac{E}{N} - rE_F \tag{3.4}$$

$$I' = \alpha E - f\frac{I}{N} - \gamma I - \phi_1 I - \nu I \tag{3.5}$$

$$H' = rE_F + f\frac{I}{N} + \gamma I - \phi_2 H - \mu H \tag{3.6}$$

$$R' = \phi_1 I + \phi_2 H \tag{3.7}$$

$$D' = \nu I - \omega D \tag{3.8}$$

where $N = S + E + I$ and f is a function of F, E_F, and I which gives the rate of finding new contacts.

$$f = \begin{cases} \kappa_1 \gamma I + \kappa_2 \nu I & \text{if } F + E_F < 15 * 1200 * p \\ 0 & \text{else} \end{cases} \tag{3.9}$$

where $1 - p$ is the proportion of the total contact tracing effort available dedicated to hospitalizing individuals identified as symptomatic. Note that the two events (movement into H and funerals) can be seen in the function f with the rates γI and νI. In the cutoff for f, the number 15 is how many contacts on average one contact tracer can trace and the number 1200 is the number of contact tracers that were employed in the Western Area, Sierra Leone (containing the capital city of Freetown) during the 2014-2016 epidemic [83]. The units of f are persons per day. The units of each compartment are individuals. The units and interpretation of each parameter are listed in Table 3.1. Note that we do not account for births or for deaths from any other cause than Ebola.

People can move from Susceptible to Exposed by coming into contact with a member of the Infectious class (term $\beta_1 SI$) or by coming into contact with an infectious dead body (term $\beta_2 DS$). People who are being traced move from Susceptible to F or from Exposed to E_F by coming into contact with a person who has just been hospitalized or attending

Table 3.1: The parameters in our model with their interpretations and units.

Parameter	Interpretation	Units
β_1	transmission from interactions between I and S	per person per time
β_2	transmission from interactions between D and S	per person per time
θ	reciprocal of the number of days a person is traced	per time
α	reciprocal of the length of the exposed period	per time
r	rate of hospitalization for traced individuals	per time
γ	rate of hospitalization for untraced individuals	per time
ϕ_1	recovery rate for untreated	per time
ϕ_2	recovery rate for treated	per time
ν	death rate for untreated	per time
μ	death rate for treated	per time
ω	rate at which dead bodies become non-infectious	per time
κ_1	contacts recruited from hospitalization of one person	unitless
κ_2	contacts recruited from funeral of one person	unitless
q	contacts were more likely to have been exposed	unitless

a funeral for somebody who has just died of Ebola (term $f\frac{S}{N} = (\kappa_1\gamma I + \kappa_2\nu I)\frac{S}{N}$). This term is scaled by N because the persons moving in tracing are moved proportionally to the ratio of persons in their current class. For example, a person being traced from S moves to F at a rate proportional to $\frac{S}{N} = \frac{S}{S+E+I}$. A person is more likely to be in E_F while being traced than to be in S because of the contact they had with either an infected person or a dead body. To account for this, we multiply the term $f\frac{E}{N}$ by a number q. People who have completed their time being traced and haven't developed symptoms move back into S (term θF). Once a person has been in the Exposed class for an average of 10 days, they move to the Infectious class (term αE). A person in the class E_F is moved to the hospital once they develop symptoms (term rE_F). If somebody being traced shows symptoms the first time they are contacted, they are immediately moved to the hospital (term $f\frac{I}{N}$). Some Infectious people decide to go to the hospital on their own (term γI). Some Infectious people manage to survive Ebola and move to R (term $\phi_1 I$) but others die of the disease and we assume they are not safely buried and contribute to the class D (term νI). Some Hospitalized individuals will recover (term $\phi_2 H$) but others will die and be safely buried (term μH). We assume that the death and recovery rates for Hospitalized individuals are different from those who are

not hospitalized because they receive treatment. After some time has passed, an unsafely buried dead body is no longer able to infect people (with decay term ωD).

3.3 Stability analysis

We will derive the basic reproductive number $\Re_0$ using the Next Generation Method [22, 23, 81, 82]. Here we perform analysis of the two parts of f separately. First we assume that contact tracing has been turned off, which means the threshold has been reached. However, it would also make sense for contact tracing not to be started yet at the very beginning of an epidemic, because it takes some time to mobilize the contact tracers. Then we explore the case where contact tracing is turned on. This might happen at the beginning of an epidemic if contact tracers are mobilized in anticipation of an epidemic spreading from a nearby country.

3.3.1 Tracing level above cutoff

Now we will calculate $\Re_0$ when the threshold has been reached and no more contacts can be traced, $f = 0$. The system of equations becomes

$$
\begin{aligned}
S' &= -\beta_1 SI - \beta_2 SD + \theta F \\
F' &= -\theta F \\
E' &= \beta_1 SI + \beta_2 SD - \alpha E \\
E'_F &= -r E_F \\
I' &= \alpha E - \gamma I - \phi_1 I - \nu I \\
H' &= r E_F + \gamma I - \phi_2 H - \mu H \\
R' &= \phi_1 I + \phi_2 H \\
D' &= \nu I - \omega D
\end{aligned}
$$

where $N = S + E + I$.

To find the equilibria of the system above, we solve

$$0 = -\beta_1 SI - \beta_2 SD + \theta F \tag{3.10}$$

$$0 = -\theta F \tag{3.11}$$

$$0 = \beta_1 SI + \beta_2 SD - \alpha E \tag{3.12}$$

$$0 = -rE_F \tag{3.13}$$

$$0 = \alpha E - \gamma I - \phi_1 I - \nu I \tag{3.14}$$

$$0 = rE_F + \gamma I - \phi_2 H - \mu H \tag{3.15}$$

$$0 = \phi_1 I + \phi_2 H \tag{3.16}$$

$$0 = \nu I - \omega D. \tag{3.17}$$

First notice that equation (3.13) implies that $E_F = 0$ and equation (3.11) implies $F = 0$. Substituting $F = 0$ into equation (3.10) and adding equation (3.10) to equation (3.12) gives $E = 0$. Substituting $E = 0$ into equation (3.14) gives $I = 0$. Taking $I = 0$ and substituting into equations (3.16) and (3.17) gives $H = 0$ and $D = 0$. Since $E = I = 0$ and $N = S + E + I$, we conclude that $S = S^* = N(0)$. The disease free equilibrium of this system is $(S^*, 0, 0, 0, 0, 0, R^*, 0)$, where $S^* \geq 0$ and $R^* \geq 0$, where R^* is a constant. However for computation of $\Re_0$ we must assume a completely susceptible population, so we will assume $R^* = 0$.

We compute the Next Generation Matrix for this system. The diseased classes are E, E_F, I, H, and D, and the system for "infecteds" becomes

$$\begin{pmatrix} E \\ E_F \\ I \\ H \\ D \end{pmatrix}' = \mathscr{F} - \mathscr{V}$$

where

$$\mathscr{F} = \begin{pmatrix} \beta_1 SI + \beta_2 SD \\ 0 \\ 0 \\ 0 \\ 0 \end{pmatrix}, \quad \mathscr{V} = \begin{pmatrix} \alpha E \\ rE_F \\ (\phi_1 + \nu + \gamma)I - \alpha E \\ (\phi_2 + \mu)H - rE_F - \gamma I \\ \omega D - \nu I \end{pmatrix},$$

where $\mathscr{F}$ represents the new infections and $\mathscr{V}$ represents the other transitions.

Let's check to make sure we meet the assumptions required for the Next Generation Method as described on page 161 in [82].

1. There is no immigration into the diseased classes. There are no transitions in $\mathscr{V}$ when there are no individuals in the diseased classes.

2. $\mathscr{F} \geq 0$ when the numbers in all classes are non-negative.

3. Each row of $\mathscr{V}$ is non-positive when the corresponding compartment is empty. (Row 3 is negative with $I = 0$, for example.)

4. $\sum_{i=1}^{5} \mathscr{V}_i = \phi_1 I + (\phi_2 + \mu)H + \omega D \geq 0$ when all the classes are non-negative.

5. The disease free equilibrium (which is considered here) is asymptotically stable in the system without the equations from the diseased classes and $E = E_F = I = H = D = 0$. (Proof below.) Note that uniqueness is not required [5, 81].

Suppose we have any initial condition with $E = E_F = I = H = D = 0$, that is

$$(S(0), F(0), E(0), E_F(0), I(0), H(0), R(0), D(0)) = (S_0, F_0, 0, 0, 0, 0, R_0, 0) \tag{3.18}$$

for any non-negative S_0, F_0, R_0. Note that all inflows into compartments E, E_F, I, H, and D will be 0. Therefore these classes will not grow. The remaining three classes will be

represented by the ODEs

$$S' = \theta F$$
$$F' = -\theta F$$
$$R' = 0.$$

Therefore the system will asymptotically approach the equilibrium point $(S_0+F_0, 0, 0, 0, 0, 0, R_0, 0)$ and we take $R_0 = 0$ here.

Now that we have met the required assumptions, we can compute $\Re_0$ using the Next Generation Method. The Jacobian matrices corresponding to $\mathscr{F}$ and $\mathscr{V}$ are

$$F = \begin{pmatrix} 0 & 0 & \beta_1 S^* & 0 & \beta_2 S^* \\ 0 & 0 & 0 & 0 & 0 \\ 0 & 0 & 0 & 0 & 0 \\ 0 & 0 & 0 & 0 & 0 \\ 0 & 0 & 0 & 0 & 0 \end{pmatrix},$$

$$V = \begin{pmatrix} \alpha & 0 & 0 & 0 & 0 \\ 0 & r & 0 & 0 & 0 \\ -\alpha & 0 & \phi_1+\nu+\gamma & 0 & 0 \\ 0 & -r & -\gamma & \phi_2+\mu & 0 \\ 0 & 0 & -\nu & 0 & \omega \end{pmatrix}.$$

We can compute

$$V^{-1} = \begin{pmatrix} \frac{1}{\alpha} & 0 & 0 & 0 & 0 \\ 0 & \frac{1}{r} & 0 & 0 & 0 \\ \frac{1}{\phi_1+\nu+\gamma} & 0 & \frac{1}{\phi_1+\nu+\gamma} & 0 & 0 \\ \frac{\gamma}{(\phi_1+\nu+\gamma)(\phi_2+\mu)} & \frac{1}{\phi_2+\mu} & \frac{\gamma}{(\phi_1+\nu+\gamma)(\phi_2+\mu)} & \frac{1}{\phi_2+\mu} & 0 \\ \frac{\nu}{\omega(\phi_1+\nu+\gamma)} & 0 & \frac{\nu}{\omega(\phi_1+\nu+\gamma)} & 0 & \frac{1}{\omega} \end{pmatrix},$$

and

$$FV^{-1} = \begin{pmatrix} \frac{\beta_1 S^*}{\phi_1+\nu+\gamma} + \frac{\nu\beta_2 S^*}{\omega(\phi_1+\nu+\gamma)} & 0 & \frac{\beta_1 S^*}{\phi_1+\nu+\gamma} + \frac{\nu\beta_2 S^*}{\omega(\phi_1+\nu+\gamma)} & 0 & \frac{\beta_2 S^*}{\omega} \\ 0 & 0 & 0 & 0 & 0 \\ 0 & 0 & 0 & 0 & 0 \\ 0 & 0 & 0 & 0 & 0 \\ 0 & 0 & 0 & 0 & 0 \end{pmatrix}.$$

The spectral radius of this matrix is

$$\Re_0 = \frac{\beta_1 S^*}{\phi_1+\nu+\gamma} + \frac{\nu\beta_2 S^*}{\omega(\phi_1+\nu+\gamma)}. \tag{3.19}$$

The first term describes the number of new infections that we expect per individual from the I class, and the second term describes the number of new infections that we expect per body in the D class.

3.3.2 Tracing level below cutoff

We expect that near the disease free equilibrium, the number of infections will be small but nonzero. An alternate analysis of the DFE should come from nonzero f. With $f = \kappa_1\gamma I + \kappa_2\nu I$, the system of equations is

$$\begin{aligned} S' &= -\beta_1 SI - \beta_2 SD - (\kappa_1\gamma I + \kappa_2\nu I)\frac{S}{N} + \theta F \\ F' &= (\kappa_1\gamma I + \kappa_2\nu I)\frac{S}{N} - \theta F \\ E' &= \beta_1 SI + \beta_2 SD - q(\kappa_1\gamma I + \kappa_2\nu I)\frac{E}{N} - \alpha E \\ E'_F &= q(\kappa_1\gamma I + \kappa_2\nu I)\frac{E}{N} - rE_F \\ I' &= \alpha E - (\kappa_1\gamma I + \kappa_2\nu I)\frac{I}{N} - \gamma I - \phi_1 I - \nu I \\ H' &= rE_F + (\kappa_1\gamma I + \kappa_2\nu I)\frac{I}{N} + \gamma I - \phi_2 H - \mu H \\ R' &= \phi_1 I + \phi_2 H \end{aligned}$$

$$D' = \nu I - \omega D.$$

The equilibrium equations are

$$0 = -\beta_1 SI - \beta_2 SD - (\kappa_1 \gamma I + \kappa_2 \nu I)\frac{S}{N} + \theta F \tag{3.20}$$

$$0 = (\kappa_1 \gamma I + \kappa_2 \nu I)\frac{S}{N} - \theta F \tag{3.21}$$

$$0 = \beta_1 SI + \beta_2 SD - q(\kappa_1 \gamma I + \kappa_2 \nu I)\frac{E}{N} - \alpha E \tag{3.22}$$

$$0 = q(\kappa_1 \gamma I + \kappa_2 \nu I)\frac{E}{N} - rE_F \tag{3.23}$$

$$0 = \alpha E - (\kappa_1 \gamma I + \kappa_2 \nu I)\frac{I}{N} - \gamma I - \phi_1 I - \nu I \tag{3.24}$$

$$0 = rE_F + (\kappa_1 \gamma I + \kappa_2 \nu I)\frac{I}{N} + \gamma I - \phi_2 H - \mu H \tag{3.25}$$

$$0 = \phi_1 I + \phi_2 H \tag{3.26}$$

$$0 = \nu I - \omega D. \tag{3.27}$$

Now equation (3.26) implies

$$\phi_1 I = -\phi_2 H. \tag{3.28}$$

Giving $I = H = 0$. From equation (3.27), we get $D = 0$. Since $I = 0$, equation (3.21) gives $F = 0$ and equation (3.24) gives $E = 0$. Since $I = H = 0$, equation (3.25) gives $E_F = 0$. Since $E = I = 0$, we conclude that $S = S^* = N(0)$. We have the same DFE as above: $(S^*, 0, 0, 0, 0, 0, R^*, 0)$. But once again we take $R^* = 0$ for computation of the Next Generation Matrix. The diseased classes here are as above: E, E_F, I, H, and D. The corresponding $\mathscr{F}$ and $\mathscr{V}$ vectors are

$$\mathscr{F} = \begin{pmatrix} \beta_1 SI + \beta_2 SD \\ 0 \\ 0 \\ 0 \\ 0 \end{pmatrix}, \quad \mathscr{V} = \begin{pmatrix} \alpha E + q(\kappa_1 \gamma I + \kappa_2 \nu I)\frac{E}{S+I+E} \\ rE_F - q(\kappa_1 \gamma I + \kappa_2 \nu I)\frac{E}{S+I+E} \\ (\phi_1 + \nu + \gamma)I + (\kappa_1 \gamma I + \kappa_2 \nu I)\frac{I}{S+I+E} - \alpha E \\ (\phi_2 + \mu)H - rE_F - \gamma I - \frac{(\kappa_1 \gamma + \kappa_2 \nu)I^2}{S+I+E} \\ \omega D - \nu I \end{pmatrix}.$$

Once again we check the assumptions required to use the Next Generation Matrix method as described in [82].

1. There is no immigration into the diseased classes. There are no transitions in $\mathscr{V}$ when there are no individuals in the diseased classes.

2. $\mathscr{F} \geq 0$ when the numbers in all classes are non-negative.

3. Each row of $\mathscr{V}$ is non-positive when the corresponding compartment is empty. (For example, when $I = 0$ the third row is $-\alpha E$.)

4. $\sum_{i=1}^{5} \mathscr{V}_i = \phi_1 I + (\phi_2 + \mu)H + \omega D \geq 0$ when all the classes are non-negative.

5. The disease free system has an asymptotically stable equilibrium. (Proof same as in previous section.)

So we may compute

$$D\mathscr{F} = \begin{pmatrix} 0 & 0 & \beta_1 S & 0 & \beta_2 S \\ 0 & 0 & 0 & 0 & 0 \\ 0 & 0 & 0 & 0 & 0 \\ 0 & 0 & 0 & 0 & 0 \\ 0 & 0 & 0 & 0 & 0 \end{pmatrix},$$

$$D\mathscr{V} = \begin{pmatrix} \alpha + \frac{q(\kappa_1\gamma + \kappa_2\nu)I(S+I)}{(S+I+E)^2} & 0 & \frac{q(\kappa_1\gamma + \kappa_2\nu)E(S+E)}{(S+I+E)^2} & 0 & 0 \\ -\frac{q(\kappa_1\gamma + \kappa_2\nu)I(S+I)}{(S+I+E)^2} & r & -\frac{q(\kappa_1\gamma + \kappa_2\nu)E(S+E)}{(S+I+E)^2} & 0 & 0 \\ -\alpha - \frac{(\kappa_1\gamma + \kappa_2\nu)I^2}{(S+I+E)^2} & 0 & A & 0 & 0 \\ \frac{(\kappa_1\gamma + \kappa_2\nu)I^2}{(S+I+E)^2} & -r & B & \phi_2 + \mu & 0 \\ 0 & 0 & -\nu & 0 & \omega \end{pmatrix},$$

where

$$A = \phi_1 + \nu + \gamma + \frac{(\kappa_1\gamma + \kappa_2\nu)(2I(S+E) + I^2)}{(S+I+E)^2},$$
$$B = -\gamma - \frac{(\kappa_1\gamma + \kappa_2\nu)(2I(S+E) + I^2)}{(S+I+E)^2}.$$

When we evaluate $S = S^*$ and $E = I = 0$, we get the matrices F and V identical to those in the first section. Thus the basic reproductive number remains the same as equation (3.19). We may conclude that f does not influence $\Re_0$ in this model. The reason for this computationally is the products generated by the function f. When we take the derivative of $\frac{IS}{N}$ or $\frac{IE}{N}$ or $\frac{I^2}{N}$, there is always a remaining term which must then be evaluated as 0. For example,

$$\begin{aligned}\frac{\partial}{\partial S}\left(\frac{IS}{N}\right) &= \frac{\partial}{\partial S}\left(\frac{IS}{S+E+I}\right)\\ &= \frac{I(S+E+I) - IS(1)}{(S+E+I)^2}\\ &= \frac{I(E+I)}{(S+E+I)^2}.\end{aligned}$$

Thus, when this term is evaluated at $E^* = I^* = 0$, the whole term is 0. From a less computational and more biological perspective, the reason why f does not impact $\Re_0$ is that at the beginning of an epidemic contact tracing is not able to have much of an impact on the spread of the disease. Later in an epidemic, contact tracing becomes very important.

3.4 Parameter estimation

Our data are taken from the Sierra Leone Ministry of Health daily situation reports, published on their website during the epidemic. We accessed these old web sites via the Wayback Machine. Situation reports were available beginning at Day 77 with the final day being Day 504, but not every intermediate day had a report. There were 343 total reports available for us to use. Each report contained a table with cumulative suspected, probable, and confirmed cases and deaths. We chose to use confirmed cases and deaths for

our parameter estimation. The other information available on each report varied. Sometimes there was a table about contact tracing, a table with information about hospitalizations, a table with information about illness within health care workers, and sometimes other tables. There was one report we chose to exclude because it listed more confirmed deaths than subsequent reports, making our total number of data points 342.

We chose some parameters from the literature and estimated others using our data. We took the incubation period to be 10 days, meaning $\alpha = 0.1$ per day, and the decay rate for dead bodies to be $\omega = 1/4.5$ per day [67]. The number of days a contact was traced was $\frac{1}{\theta} = 21$ days, taken from multiple sources [15, 61, 72]. Our data indicated that the initial condition for the H class was $H(0) = 94$ individuals. We assumed the initial condition for the recovered class was $R(0) = 0$ individuals, and that the initial condition for S was roughly equivalent to the population of Sierra Leone at the time, $S(0) = 6,348,350$ people.

We estimated the following parameters:

- β_1: the rate of infection from contact between Susceptibles and Infecteds (per person per day)
- β_2: the rate of infection from contact between Susceptibles and Dead bodies (per person per day)
- γ: the rate of hospitalization for Infecteds (per day)
- κ_1: the number of contacts per hospitalized infected individual (unitless)
- κ_2: the number of contacts per funeral (unitless)
- r: the rate of hospitalization for traced individuals (per day)
- p: the proportion of tracing effort not devoted to hospitalization (unitless)
- ν: the death rate for untreated individuals (per day)
- μ: the death rate for treated individuals (per day)
- ϕ_1: the recovery rate for untreated individuals (per day)

- ϕ_2: the recovery rate for treated individuals (per day)
- $F(0)$: the initial number of Susceptibles being traced (individuals)
- $E(0)$: the initial number of Exposed (individuals)
- $E_F(0)$: the initial number of Exposed being traced (individuals)
- $I(0)$: the initial number of Infectious (individuals)
- $D(0)$: the initial number of Dead bodies (individuals).

Later the parameter q was added and taken to be 100 (unitless). Until the final attempt $q = 1$.

We estimated the above parameters using fmincon and multistart in MATLAB with ode45 as our solver. Parameter upper and lower bounds were based on ranges of parameters from the literature [61, 67] and from our data. We used papers [61, 67] for some ranges because they rely on data from Sierra Leone. For example, the upper bound for F_0 was taken as 2500 because our data indicated that in early days this was roughly the number of contacts being traced. To estimate our cumulative simulated cases, we summed over the entries into the H class, assuming that cases for people in the community were unconfirmed. To estimate our cumulative simulated deaths, we summed over the deaths from H and I together. The data to be compared with simulation results are cumulative confirmed cases and cumulative confirmed deaths. We minimized the following

$$J = \sum_{i=77}^{504} \frac{(\text{Cases}_{Estimated}(i) - \text{Cases}_{Data}(i))^2}{(\text{Cases}_{Data}(i))^2} + \frac{(\text{Deaths}_{Estimated}(i) - \text{Deaths}_{Data}(i))^2}{(\text{Deaths}_{Data}(i))^2}. \quad (3.29)$$

Our data began at day 77 and ended at day 504 with 342 total data points each for cases and deaths. Note that this does not include every day between day 77 and day 504. The missing data are for days when the Ministry of Health situation report was unavailable. The data from one day, when cumulative deaths were higher than for following days, were excluded. You can see that some days do not have data by the gaps in the red dots in our figures on the following pages.

We tried several ways of fitting the data. First, we estimated all the parameters listed above, holding them all constant throughout the epidemic. This resulted in poor simulations of the data. The J values were too high (about 0.20) and the simulated epidemic curves did not flatten at the end, indicating the epidemic would have kept going. Second, we chose five parameters that seemed to vary during the epidemic according to the literature and allowed those five parameters to switch from one value to a second value in the middle of the epidemic. This resulted in a much better simulations of the data (with J values of about 0.09), but some of the compartments were still unrealistic. We wanted not only to approximate the data well but to also have realistic curves for each of the compartments in our model. Third we tried running the code for more starting points in multistart. This resulted in an even better simulation of the data and gave use reasonable curves for each of the compartments as well. However, some of the compartments showed corners in their graphs where the five parameters changed discontinuously. Next, we changed the parameters to vary continuously. This resulted in a less tight match between our simulations and the data, but more realistic curves for the compartments. However, the value we had estimated for r was far too small. In order to achieve a good simulation of the data with reasonable compartments, we modified the model by inserting the parameter q. Then we reestimated the paramters using the varying approach for five of the parameters. This resulted in good simulations of the data with reasonable compartments. The details of each of these steps are described below, with accompanying figures.

3.4.1 First attempt: all parameters constant

We began by estimating all parameters listed above as fixed for the duration of the epidemic. This yielded disappointing results, since our simulated curves for cumulative cases and cumulative deaths continued increasing strongly even after the data had flattened out. One example of such a problematic fit is shown in Figure 3.2 and has a J value of 0.1963. In this figure you can also see the data point we later excluded. This data point is the one which has more confirmed deaths than in following days. We were, however, able to find good estimates for a handful of parameters, which are listed in Table 3.2. These parameters

Table 3.2: Parameter values from our first attempt which we kept for the second attempt.

Parameter	Value
β_2 early	$6.53e^{-7}$
μ	0.013
ϕ_1	0.016
ϕ_2	0.021

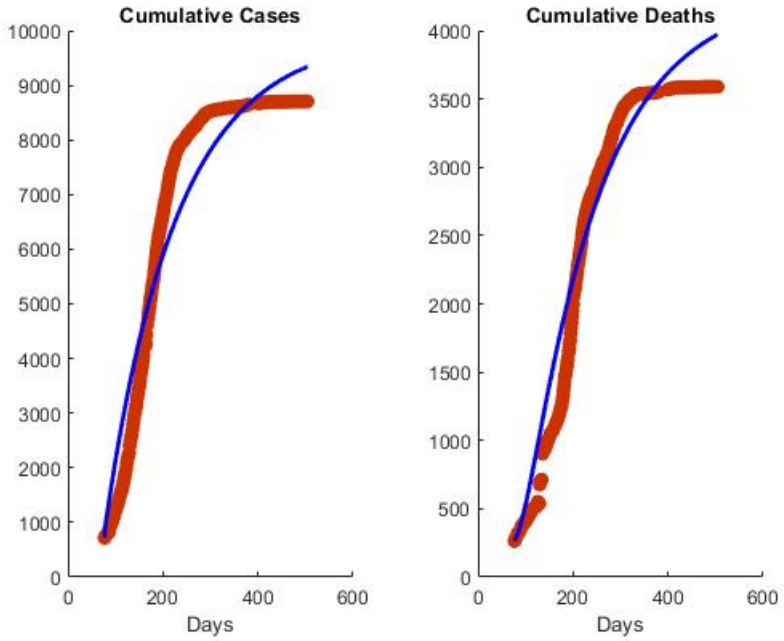

Figure 3.2: First attempt match to the data of cumulative cases and cumulative deaths with all parameters constant. The value of J is 0.1963.

had similar values for all of the best runs, so we kept these parameter values from this first method and left the rest to be fitted by our second approach.

3.4.2 Second attempt: allowing five parameters to have two values

In order to achieve a simulated fit of the data which would include a flattening of the cumulative cases and cumulative deaths curves, rather than simulations which indicated the epidemic wouldn't have ended, we decided to allow some parameters (specifically $\beta_1, \beta_2, \gamma, \kappa_1$, and κ_2) to vary over the course of the epidemic. We chose these parameters because we knew

that people's behavior changed during the epidemic. The literature supports our decision to allow $\beta_1, \beta_2, \gamma, \kappa_1$ and κ_2 to change over the course of the epidemic. Senga et al. [72] analyzed data on probable and confirmed cases of EVD and their contacts in Kenema district, Sierra Leone taken from the national database. They found that the number of contacts per case increased over time. The low number of contacts per case reported early in the epidemic was much lower than those reported in other countries, which they concluded meant that the contact listings were incomplete. Olu et al. found that during the months of June 2014 to November 2014 the average number of contacts per case was 9 and that during the months of December 2014 to May 2015 the average number of contacts per case increased to 16 [61]. Lokuge et al. reported that later in the epidemic people were more likely to come to the hospital of their own volition, less likely to report funeral contact, and that contact tracing increased in efficacy [57]. These findings from the literature indicate it is reasonable to conclude that values for $\beta_1, \beta_2, \gamma, \kappa_1$ and κ_2 changed during the course of the epidemic due to changes in behavior and level of education in the population about EVD.

At first, we varied these five parameters discontinuously. For each of those five parameters, we estimated one value for days 77 through 175 and another value for days 176 through 504. All other parameters were estimated on days 77 through 175 of the data and we used those same values for days 176 through 504. With this parameter fitting scheme, we achieved a much better match of our simulations to the data. We chose to change the parameters at day 175 because the flattening of the data curves occurred after day 175.

Figure 3.3 shows in blue the curves for our estimated cumulative cases and cumulative deaths and in red dots shows the data. Figure 3.4 shows the estimated dynamics of classes F and E_F on top and the sum of both on bottom and then Figure 3.5 shows estimated dynamics of classes S, E, I, H, R and D. Note that the flow back into S occurs not from waning immunity but from contacts completing their tracing period. Classes E, E_F, I and D show a lack of differentiability at the switch from one parameter set to the other. The parameter values associated with these plots are listed in Table 3.3. The values estimated by multistart with fmincon for $E_F(0)$ and for $I(0)$ were unrealistic because they caused a large drop at the very beginning, so we gradually changed these parameters until the initial values fit better with the curves for those two classes.

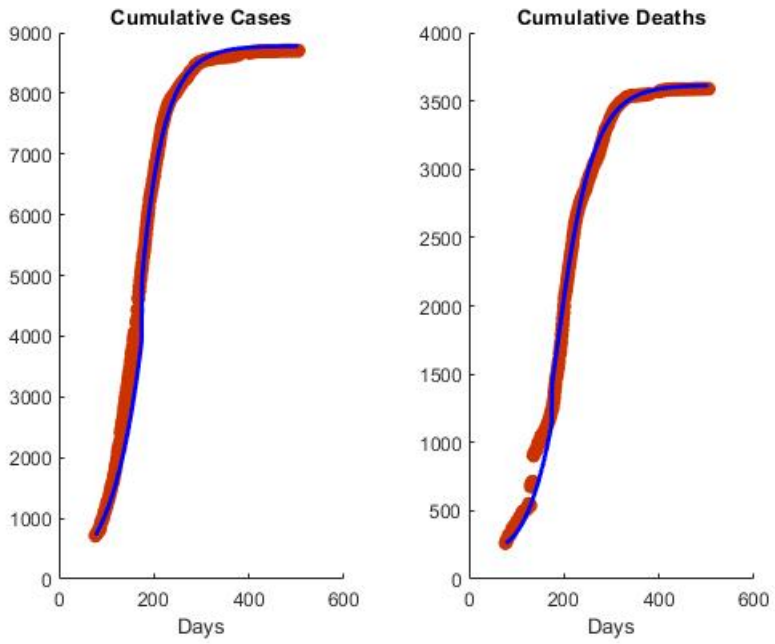

Figure 3.3: In this second attempt, the value of the objective was 0.0944. These simulations were generated using the parameters in Table 3.3.

Our simulations in Figure 3.3 match the data much more closely than those achieved in the previous estimation scheme shown in Figure 3.2. In particular, J has improved from 0.1963 to 0.944, an improvement of 52%. However, our simulations underestimate the cumulative number of cases between about days 100 and 200 and overestimate the cumulative number of cases from about day 300 onward. Our simulations also underestimate cumulative deaths data from about the beginning to day 175 and then overestimate the cumulative deaths data from about day 175 to day 200 and again from about day 250 to day 300.

The plateau of contacts being traced in Figure 3.4 between about days 180 and 250 aligns with reports that the contact tracing system was overwhelmed as the number of contacts needing tracing dramatically increased. The number of contacts being traced at this maximum, approximately $16,000$, roughly matches the higher values of contacts being traced reported in the Ministry of Health situation reports. However, E_F is unrealistically close to 0 throughout the epidemic. This does not match the success of contact tracing shown in the literature [61]. In Figures 3.4 and 3.5, note that the peaks in E, E_F, I, and D occur at the time of the switch, day 175 but that the peak in hospitalized individuals occurs

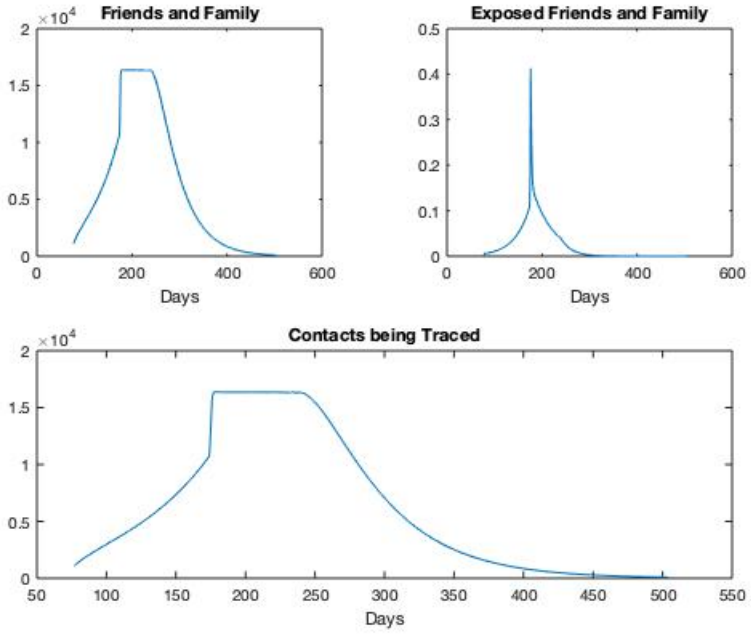

Figure 3.4: From the second attempt, simulated dynamics of Class F in the upper left, class E_F in the upper right, and their sum on the bottom. These classes correspond to the parameters from Table 3.3 and the data fits from Figure 3.3. Note that the size of class E_F is unrealistically small.

closer to day 200. The delay in the peak of H matches expectations that the peak in E would occur earlier, and then as people who had been exposed earlier developed symptoms and came to the hospital, this would cause a later peak in H.

The values of the parameters listed in Table 3.3 are not the only set of parameters that give a good fit for our data. Indeed, these are not the best choice because they cause such a low size for the E_F class, as you can see in Figure 3.4. This low size is not reflective of the success contact tracing achieved in locating exposed individuals during the outbreak.

3.4.3 Third attempt: more runs

We ran our code again with the same bounds and a larger number of multistart points (500 increased from 100) and found a set of parameters which produced an even better match between our simulations and the data and also had a more reasonable class E_F. These results are in Figures 3.6, 3.7, and 3.8. The parameters for these simulations are in Table 3.4.

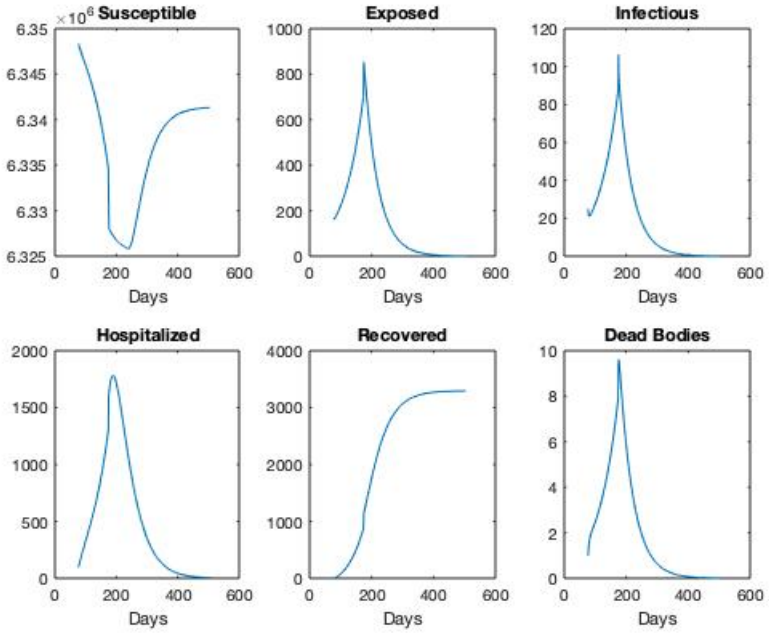

Figure 3.5: From the second attempt, the simulated graphs above correspond to the parameters from Table 3.3 and the data fits from Figure 3.3. Note that the scales are all different.

Table 3.3: In the second attempt, values for estimated parameters corresponding with Figures 3.3,3.4, and 3.5.

Parameter	Value	Parameter	Value
β_1 early	$8.77e^{-8}$	r	0.67
β_1 late	$1.10e^{-7}$	p	0.91
β_2 early	$6.53e^{-7}$	ν	0.021
β_2 late	$1.01e^{-8}$	μ	0.013
γ early	0.75	ϕ_1	0.016
γ late	0.89	ϕ_2	0.021
κ_1 early	10	$F(0)$	1087
κ_1 late	36.90	$E(0)$	160
κ_2 early	11.82	$E_F(0)$	0
κ_2 late	35.61	$I(0)$	20
		$D(0)$	1

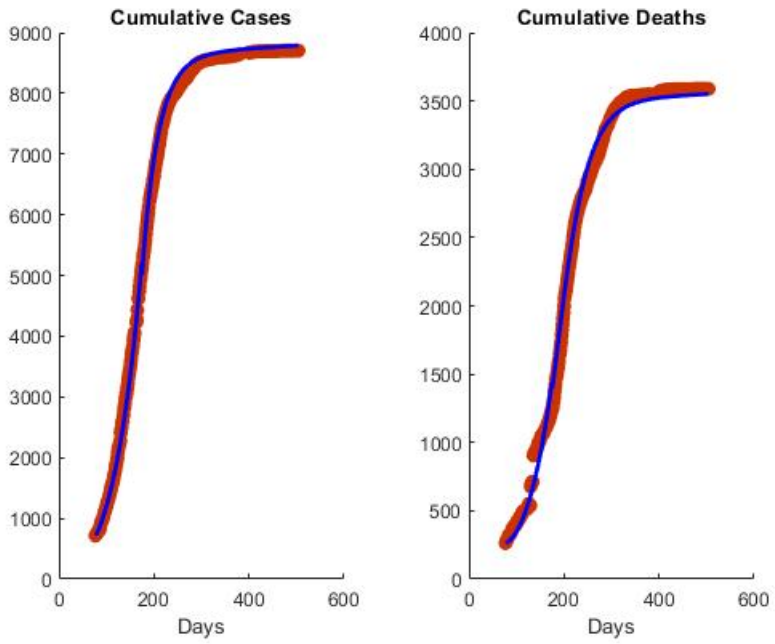

Figure 3.6: Simulations and corresponding data from the third attempt. The value of the objective for this was $J = 0.0502$. This simulation was generated using the parameters from Table 3.4.

In Figure 3.6, the blue estimation curve is much closer to the red data than in Figure 3.3. In particular, J improved from 0.0944 to 0.0502, an improvement of 47%. However, starting sometime after day 200, our simulation overestimates cumulative case data and underestimates cumulative death data.

Figure 3.7 contains a much more realistic curve for E_F than does Figure 3.4. Here we can see that though the number of contacts who were exposed is a small proportion of the overall number of contacts being traced, it still represents a large number of people. Stopping those people from spreading the disease further would definitely help end the epidemic. In Figure 3.8 we see that E, I and D still have corners at the transition between the early and late values for the five parameters being varied.

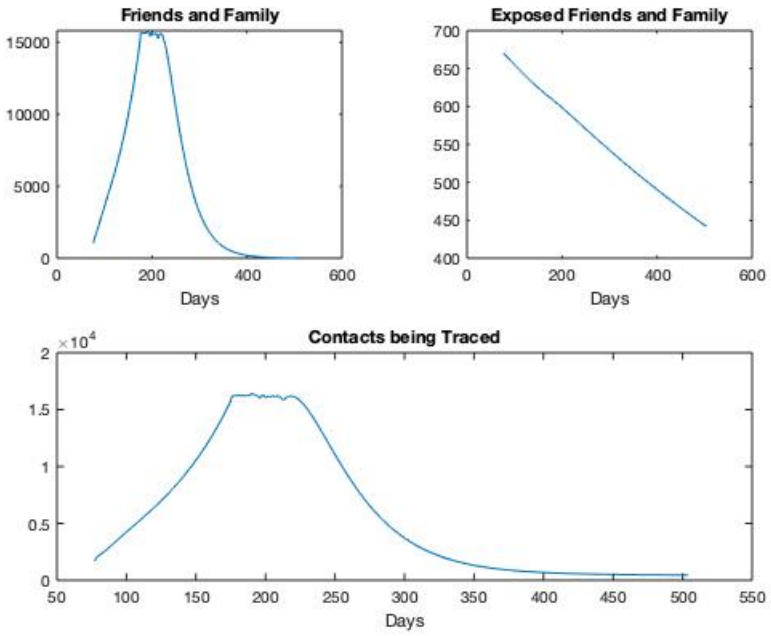

Figure 3.7: From the third attempt, dynamics of class F in the upper left, class E_F in the upper right, and their sum on the bottom. These classes correspond to the parameters from Table 3.4 and the data simulations from Figure 3.6.

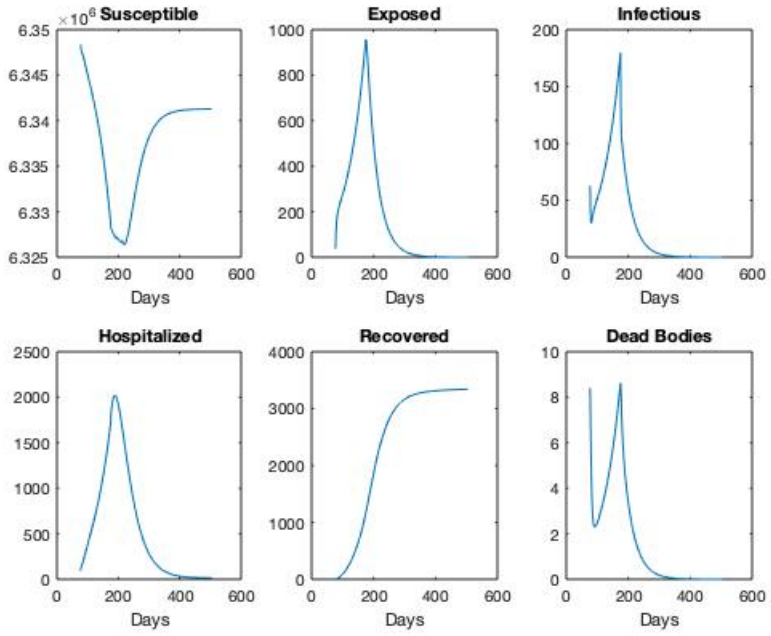

Figure 3.8: From the third attempt, the graphs above correspond to the parameters from Table 3.4 and the data simulations from Figure 3.6. Note that the scales are all different.

Table 3.4: From the third attempt, values for estimated parameters corresponding with Figures 3.6, 3.7, and 3.8, with five parameters having early and late values.

Parameter	Value	Parameter	Value
β_1 early	$6.68e^{-8}$	r	0.001
β_1 late	$3.94e^{-8}$	p	0.90
β_2 early	$6.53e^{-7}$	ν	0.011
β_2 late	$9.95e^{-7}$	μ	0.013
γ early	0.49	ϕ_1	0.016
γ late	0.89	ϕ_2	0.021
κ_1 early	10	$F(0)$	1031
κ_1 late	24.95	$E(0)$	37
κ_2 early	45.8	$E_F(0)$	670
κ_2 late	25.89	$I(0)$	63
		$D(0)$	8

3.4.4 Fourth attempt: smoothing the transition between five parameters

The dynamics of the classes E, I, and D in Figure 3.8 show sharp corners at the transition between parameter sets. To ameliorate this, we smoothed the transition using piecewise functions such as the one below for each of the parameters.

$$\beta_1(t) = \begin{cases} 6.68e^{-8} & t < 160 \\ 6.68e^{-8}(1 - \frac{t-160}{30}) + 3.94e^{-8}\left(\frac{t-160}{30}\right) & 160 \leq t \leq 190 \\ 3.94e^{-8} & t > 190. \end{cases} \tag{3.30}$$

The resulting simulations with data comparisons and classes are found in Figures 3.9, 3.10, and 3.11. Chowell et al. [16] built a system of ODEs representing Ebola outbreaks in Congo and Uganda and used a smooth transition between two transmission rates due to control interventions (like education and contact tracing followed by quarantine).

As a result of the smoothed transitions for the 5 varying parameters, and changing the initial conditions for $E(0) = 100$ and $I(0) = 20$, the value for J improved slightly from 0.0502 to 0.492.

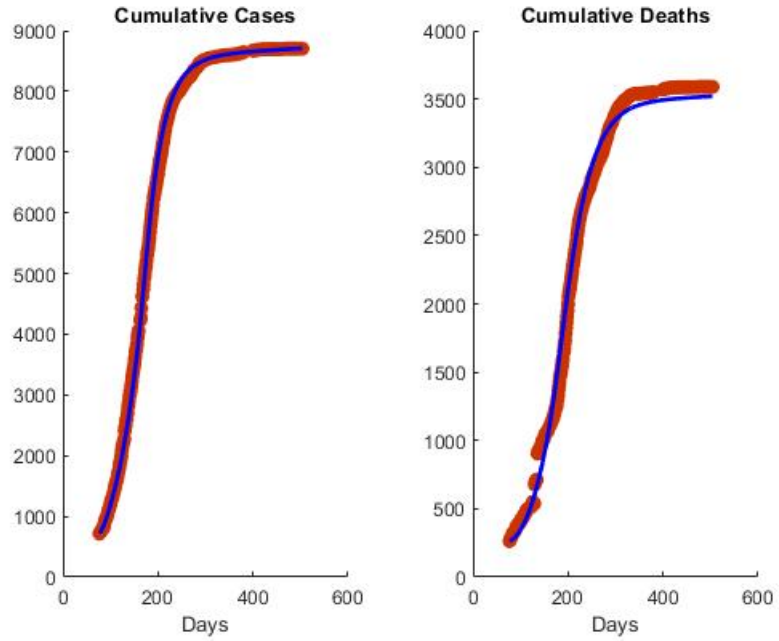

Figure 3.9: From the fourth attempt, simulation results with data using smoothed transitions in the 5 varying parameters. The value of the objective for this simulation was $J = 0.0492$. Note the later days in the simulation are an underestimate of the cumulative deaths data.

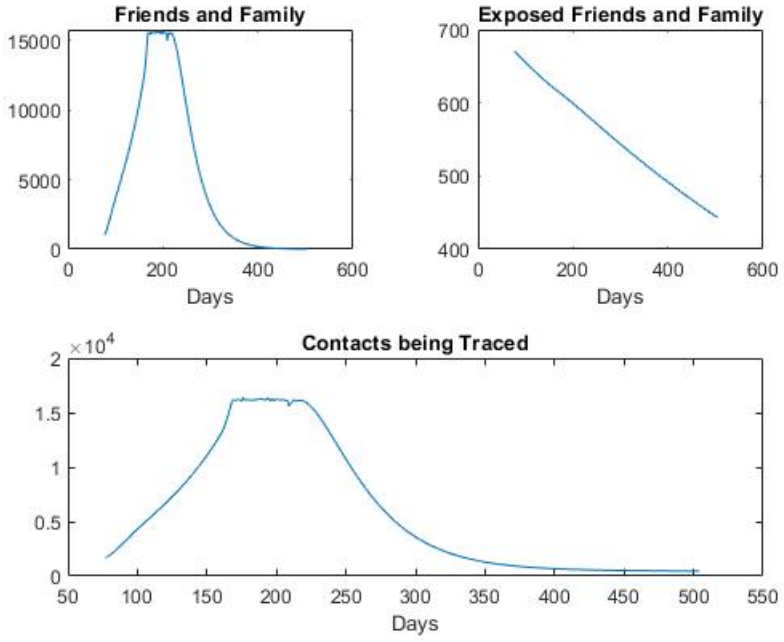

Figure 3.10: From the fourth attempt, dynamics of class F in the upper left, class E_F in the upper right, and their sum on the bottom. These classes correspond to the parameters from Table 3.4 and the data fits from Figure 3.9.

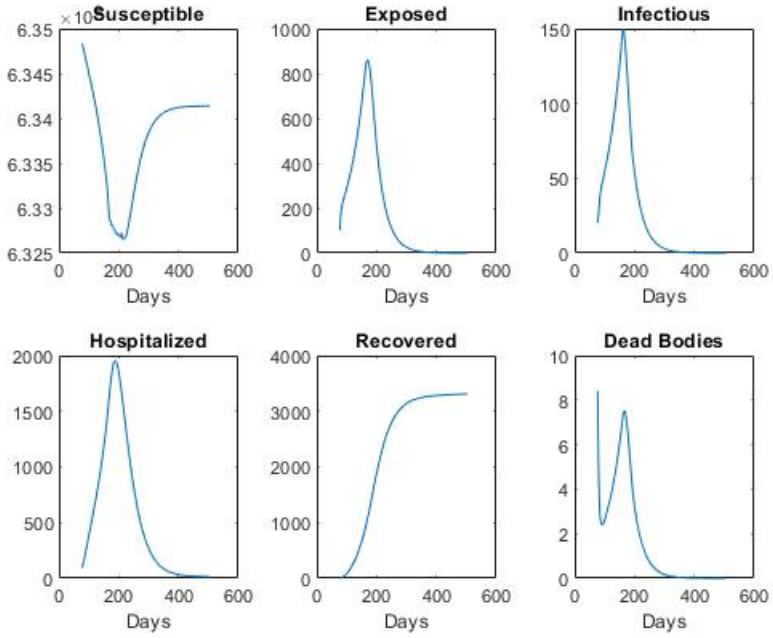

Figure 3.11: From the fourth attempt, the graphs above correspond to the parameters from Table 3.4 and the data fits from Figure 3.9. Note that the scales are all different.

Figure 3.10 is not very different from Figure 3.7, despite the change to continuously varying the five parameters. In Figure 3.11 we see the peaks of E, I and D are much smoother than those from Figure 3.8. Note that in Figure 3.11 we again see the peak in H delayed from the peaks in E, I and D.

3.4.5 Final attempt: more realistic transition from E_F to H

Though we were satisfied with how the fourth attempt simulations matched the data, there was a problem with the parameter bounds for r, the transition rate from E_F to H. Once we began to interpret our parameter values, this became quite clear. With the value of $r = 0.001$ from Table 3.4, this would mean that a person would spend an average of 1000 days in E_F before transitioning to H. In other words, they would take 1000 days to develop symptoms, and would be traced for 1000 days before being taken to the hospital. Contacts were only followed for 21 days, so this is impossible. To build a more realistic lower bound for r to use in multistart, we used 0.04, which is approximately $\frac{1}{21}$.

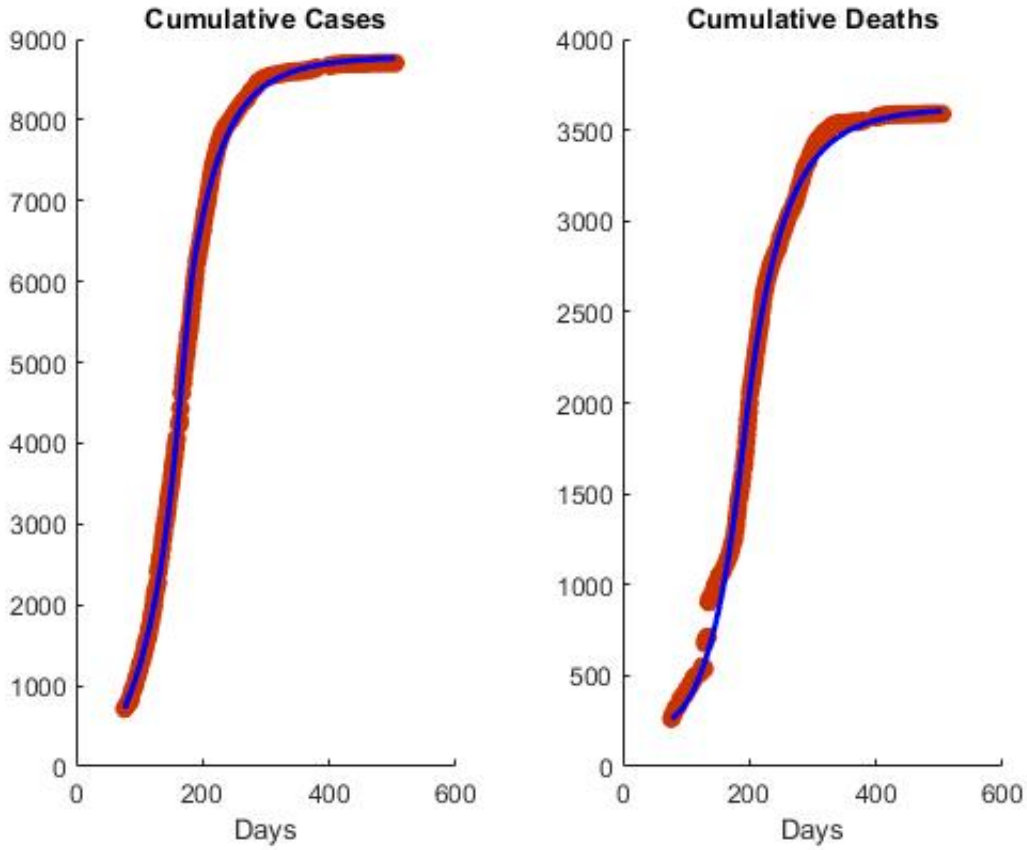

Figure 3.12: For the final attempt, simulation results with smoothed transitions in the 5 varying parameters and data. The value of the objective for this simulation was $J = 0.0426$.

However, with higher values for r we were unable to generate reasonable sizes for compartment E_F. We decided to modify the model by adding a multiplier, q, in front of the $f\frac{E}{N}$ term. We tried several values and found that a value of $q = 100$ generated reasonable sizes for compartment E_F. This multiplier indicates that people who were being traced had had contact with somebody who was infectious or with a dead body, so they were more likely to have been exposed to Ebola than a member of the population who hadn't had such contact. These changes resulted in the simulations shown in Figures 3.12, 3.13, and 3.14 which were generated using the parameters found in Table 3.5.

In Figure 3.12 the value of the objective for this simulation was $J = 0.0426$.

Figure 3.13 shows how many cases total were identified as part of the contact tracing effort. Near the end of the outbreak this number reaches about 1100, which represents more

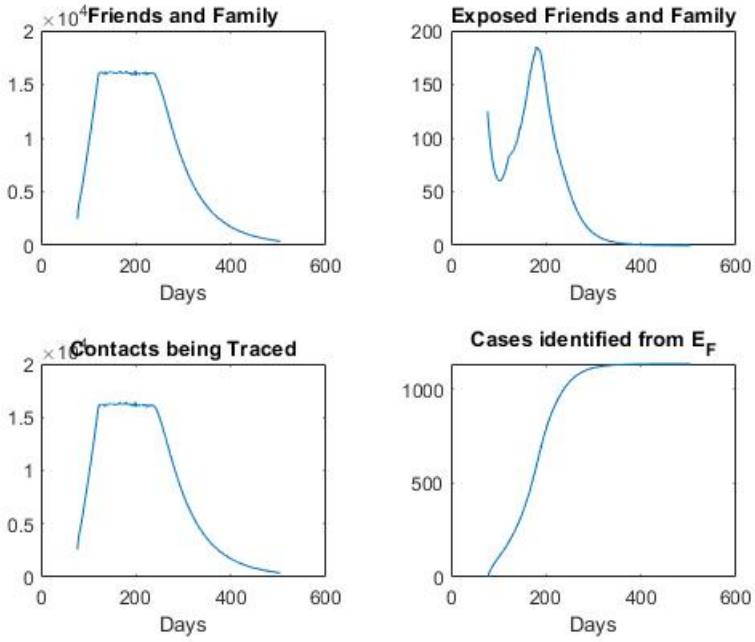

Figure 3.13: For the final attempt, the dynamics of class F in the upper left, class E_F in the upper right, their sum on the bottom left, and the integral of those leaving E_F to be hospitalized on the bottom right. These classes correspond to the parameters from Table 3.5 and the data simulations from Figure 3.12.

than a tenth of all confirmed cases. This demonstrates the importance of successful contact tracing. The peak of contact tracing numbers corresponds to the slowing of the increase in cumulative cases, around day 200. This indicates that contact tracing efforts contributed to ending the epidemic.

In Figure 3.14, the peak in E occurs at day 164, the peak in H about two weeks later on day 176, the peak in I about two weeks after that on day 192, and then the peak in D on day 197. It is not surprising that the peak in E precedes the other peaks, but it is surprising that the peak in D is the last peak to occur. This indicates that there may have been unsafely buried bodies later in the epidemic, but that fewer people were catching Ebola from funeral interactions despite this increase in funerals.

In Table 3.5, there is no difference between β_1 early and β_1 late. However, β_2 changes from an early value of $1 * 10^{-6}$ to a much lower later value of $1 * 10^{-7}$. These parameter values indicate that while the rate of transmission from interactions between S and I remained

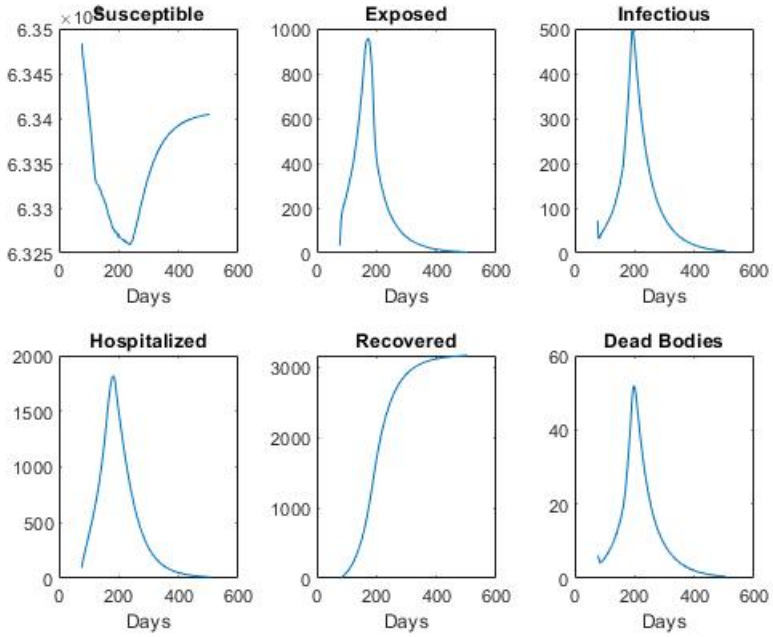

Figure 3.14: For the final attempt, the graphs above correspond to the parameters from Table 3.5 and the data simulations from Figure 3.12. Note that the scales are all different.

Table 3.5: For the final attempt, values for estimated parameters corresponding with Figures 3.12, 3.13, and 3.14, with five parameters having early and late values.

Parameter	Value	Parameter	Value
β_1 early	$1e^{-9}$	r	0.056
β_1 late	$1e^{-9}$	p	0.90
β_2 early	$1e^{-6}$	ν	0.024
β_2 late	$1e^{-7}$	μ	0.010
γ early	0.23	ϕ_1	0.020
γ late	0.062	ϕ_2	0.028
κ_1 early	29.7	$F(0)$	2451
κ_1 late	44.9	$E(0)$	32
κ_2 early	44.6	$E_F(0)$	125
κ_2 late	16.6	$I(0)$	72
		$D(0)$	6

about the same throughout the epidemic, the rate of transmission from D to S decreased dramatically as people became more educated about Ebola. Oddly, $\gamma = 0.23$ decreases to a later value of $\gamma = 0.062$, which does not agree with accounts from the literature that people were more likely to come to the hospital once they developed symptoms later in the epidemic than they were earlier in the epidemic. The value of $\kappa_1 = 29.7$ early increases to $\kappa_1 = 44.9$ late, corresponding to reports from the literature that people were more likely to report more complete lists of contacts later in the epidemic. However, $\kappa_2 = 44.6$ early decreased to $\kappa_2 = 16.6$ late, adding to the conclusion that people were less likely to attend traditional funerals later in the epidemic. The changes in these parameters during the outbreak might be caused by a combination of factors including educating the public about Ebola [51], increases in available beds at Ebola Treatment Centers, and more effective implementation of contact tracing.

The value of $r = 0.056$ means that contacts who were infected took an average of 18 days to show symptoms. This value for r is probably still unrealistically small, as it should likely be closer to $\alpha = 0.1$. The parameter ν was slightly larger than μ, since those who were treated had slightly lower chance of dying from Ebola. Similarly, ϕ_2 was larger than ϕ_1 because those who were treated were more likely to recover from the disease.

3.5 Importance of contact tracing

Figure 3.15 shows potential trajectories for epidemics with different numbers of contact tracer workers available, either more or fewer than were actually available during the epidemic. We varied the number of these workers from 0 to 2000, and note that 1200 is the corresponding number in our model. Without contact tracing at all, the highest blue curve, there would have been thousands more cases and deaths. Even a much smaller work force than existed would have made a dramatic improvement on the trajectory of the epidemic from what would have happened without contact tracing. Once the number of contact tracers reaches about 1000, each increase in the number of workers has much less dramatic effects. More tracers still would have been better, but the difference in trajectories is much less dramatic than the difference between 0 tracers and 200 tracers.

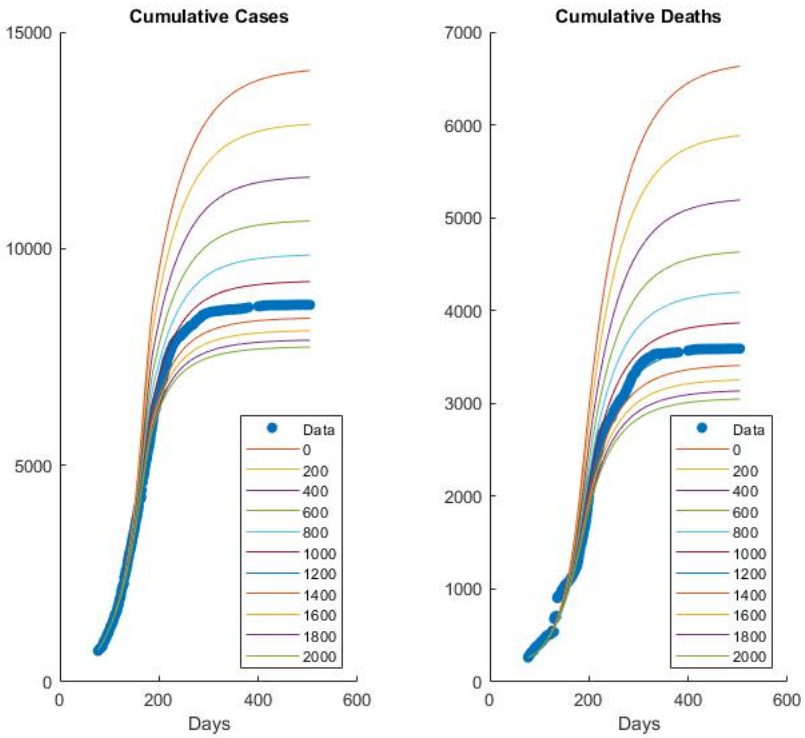

Figure 3.15: Effect of varying the number of contact tracers available from 0 to 2000, with 1200 as the corresponding number in our model.

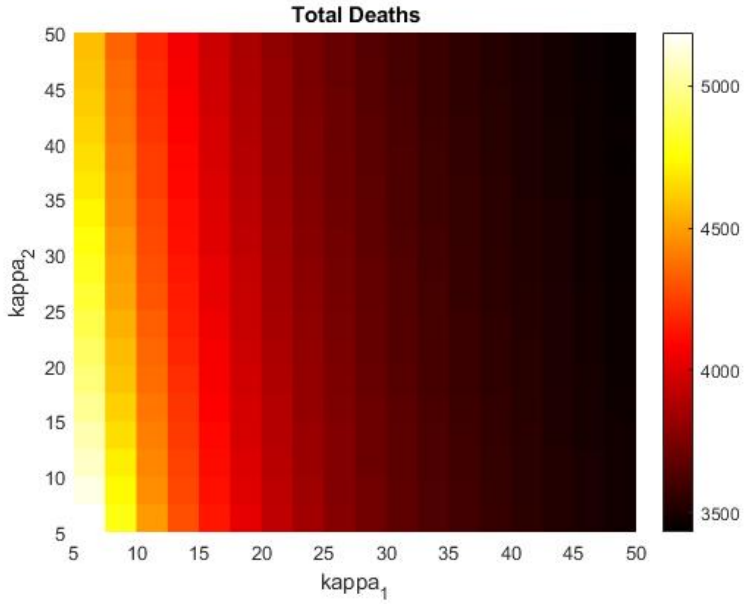

Figure 3.16: Effect of varying contact tracing parameters κ_1 and κ_2 on the total number of deaths by day 504 of the epidemic.

The number of person traced from each hospitalization (κ_1) and the number from each funeral (κ_2), were estimated as $\kappa_1 = 29.7$ early, $\kappa_1 = 44.9$ late, $\kappa_2 = 44.6$ early, and $\kappa_2 = 16.6$ late in our model. We vary those numbers from 5 to 50 to see the effect on the epidemic. If we hold each of the contact tracing parameters κ_1 and κ_2 constant at the values in Figure 3.16, the heat map shows the total number of deaths by day 504 of the outbreak. Increasing each of the two parameters reduces the total number of deaths, but κ_1 has a much more dramatic effect than κ_2. This seems to indicate that more deaths resulted from people having contact with infected individuals than resulted from people having contact with dead bodies.

3.6 Conclusions

Better understanding of the mechanisms of contact tracing is important for disease management. Our model is novel in its inclusion of explicit contact tracing of both Susceptible and Exposed individuals as well as including the limitation on the number of total contact tracers available for the work. We counted the total number of people being traced and tracked the length of time they were being traced. Li et al. analyzed 37 compartmental models of Ebola [53] and they identified models which explicitly included classes of hospitalized individuals and of funerals as more useful to management decisions, because they explicitly included targeted interventions. For this reason, we explicitly included contact tracing in our model, including the logistical limitations resulting from limited numbers of contact tracers, because contact tracing is another targeted intervention.

We found that better matching of the simulations with the data was possible when we allowed five parameters to change over the course of the epidemic: $\beta_1, \beta_2, \gamma, \kappa_1$ and κ_2. These parameters are the per capita rate of transmission from the Infectious compartment to the Susceptible compartment, the per capita rate of transmission from the Dead body compartment to the Susceptible compartment, the rate of transition from the Infectious compartment to the Hospital compartment, the number of contacts per person generated from a hospitalized case, and the number of contacts per person generated from a funeral. These parameters changed during the outbreak because more hospitals were available as the outbreak went on, people became more educated about the disease, and contact tracing

became more effective. This work illustrates the value of changing parameters due to known behavior changes.

Early in the epidemic people were less likely to report as many contacts as they did later in the epidemic, as demonstrated by the increase from $\kappa_1 = 10.16$ early to $\kappa_1 = 25.87$ late. Later in the epidemic people were less likely to attend traditional funerals, as seen in the decrease from $\kappa_2 = 50.00$ early to $\kappa_2 = 21.71$ late. The transmission parameter β_1 remained unchanged, while β_2 decreased from $1e^{-6}$ early to $1.02e^{-7}$ late.

There was a period when the contact tracing infrastructure was overwhelmed by cases, as seen in the plateaus in Figures 3.14. More contact tracers available to work would have prevented this plateau, but the number of contact tracers available was sufficient to prevent many more cases and deaths from occurring. More contact tracers could also ..., as seen in Figure **??**. Increasing either κ_1 or κ_2 would have decreased the number of deaths that occurred, but κ_1 had a stronger effect than κ_2. Overall this work makes a strong contribution to understanding the effects of contact tracing and changes in behavior on disease management.

In future we plan to further explore the role of contact tracing in epidemics. We plan to build a model with a more realistic form to the function f which represents how contact tracing capacity grows in response to an epidemic. We will also explore the role contact tracing plays in outbreaks of other diseases, including diseases with a latent period such as CoViD-19. The mechanisms of contact tracing proceedures for other disease might be quite different and require the development of disease-specific models.

Bibliography

[1] (2015). Ebola situation report, Ministry of Health and Sanitation, Sierra Leone. web.archive.org/web/20150314233800. 4, 127

[2] (2016). Ebola situation report, Ministry of Health and Sanitation, Sierra Leone. web.archive.org/web/20160509014636. 4, 127

[3] Agusto, F. B., Teboh-Ewungkem, M. I., and Gumel, A. B. (2015). Mathematical assessment of the effect of traditional beliefs and customs on the transmission dynamics of the 2014 Ebola outbreaks. *BMC Medicine*, 13(1):96. 124

[4] Ajelli, M., Merler, S., Fumanelli, L., Pastore y Piontti, A., Dean, N. E., Longini, I. M., Halloran, M. E., and Vespignani, A. (2016). Spatiotemporal dynamics of the Ebola epidemic in Guinea and implications for vaccination and disease elimination: A computational modeling analysis. *BMC Medicine*, 14(1):1–11. 124

[5] Arino, J., Bowman, C., Gumel, A., and Portet, S. (2007). Effect of pathogen-resistant vectors on the transmission dynamics of a vector-borne disease. *Journal of Biological Dynamics*, 1(4):320–346. 133

[6] Aylward, B., Barboza, P., Bawo, L., Bertherat, E., Bilivogui, P., Blake, I., Brennan, R., Briand, S., Chakauya, J. M., Chitala, K., Conteh, R. M., Cori, A., Croisier, A., Dangou, J. M., Diallo, B., Donnelly, C. A., Dye, C., Eckmanns, T., Ferguson, N. M., Formenty, P., Fuhrer, C., Fukuda, K., Garske, T., Gasasira, A., Gbanyan, S., Graaff, P., Heleze, E., Jambai, A., Jombart, T., Kasolo, F., Kadiobo, A. M., Keita, S., Kertesz, D., Koné, M., Lane, C., Markoff, J., Massaquoi, M., Mills, H., Mulba, J. M., Musa, E., Myhre, J., Nasidi, A., Nilles, E., Nouvellet, P., Nshimirimana, D., Nuttall, I., Nyenswah, T., Olu, O., Pendergast, S., Perea, W., Polonsky, J., Riley, S., Ronveaux, O., Sakoba, K., Krishnan, R. S. G., Senga, M., Shuaib, F., Van Kerkhove, M. D., Vaz, R., Kannangarage, N. W., and Yoti, Z. (2014). Ebola virus disease in West Africa - The first 9 months of the epidemic and forward projections. *New England Journal of Medicine*, 371(16):1481–1495. 123

[7] Beverton, R. J. and Holt, S. J. (2012). *On the dynamics of exploited fish populations*, volume 11. Springer Science & Business Media. 3, 7

[8] Blomberg, E. J. (2015). The influence of harvest timing on greater sage-grouse survival: A cautionary perspective. *Journal of Wildlife Management*, 79(5):695–703. 20

[9] Bodine, E. N., Gross, L. J., and Lenhart, S. (2012). Order of events matter: comparing discrete models for optimal control of species augmentation. *Journal of Biological Dynamics*, 6(sup2):31–49. PMID: 22882021. 1, 2, 22

[10] Bogoch, I. I., Creatore, M. I., Cetron, M. S., Brownstein, J. S., Pesik, N., Miniota, J., Tam, T., Hu, W., Nicolucci, A., Ahmed, S., Yoon, J. W., Berry, I., Hay, S. I., Anema, A., Tatem, A. J., MacFadden, D., German, M., and Khan, K. (2015). Assessment of the potential for international dissemination of Ebola virus via commercial air travel during the 2014 west African outbreak. *The Lancet*, 385(9962):29–35. 123

[11] Brainard, J., Hooper, L., Pond, K., Edmunds, K., and Hunter, P. R. (2016). Risk factors for transmission of Ebola or Marburg virus disease: A systematic review and meta-analysis. *International Journal of Epidemiology*, 45(1):102–116. 123

[12] Braverman, E. and Mamdani, R. (2008). Continuous versus pulse harvesting for population models in constant and variable environment. *Journal of Mathematical Biology*, 57(3):413–434. 20

[13] Browne, C., Gulbudak, H., and Webb, G. (2015). Modeling contact tracing in outbreaks with application to Ebola. *Journal of Theoretical Biology*, 384:33–49. 125, 127

[14] Cannon, M., Cullum, C., and Polak, E. (1970). *Theory of Optimal Control and Mathematical Programming*. McGraw Hill: New York. 22

[15] CDC (2014). Increases in Heroin Overdose Deaths — 28 States, 2010 to 2012. 63(39):849–854. 124, 139

[16] Chowell, G., Hengartner, N. W., Castillo-Chavez, C., Fenimore, P. W., and Hyman, J. M. (2004). The basic reproductive number of Ebola and the effects of public health measures: The cases of Congo and Uganda. *Journal of Theoretical Biology*, 229(1):119–126. 149

[17] Chowell, G. and Nishiura, H. (2014). Transmission dynamics and control of Ebola virus disease (EVD): A review. *BMC Medicine*, 12(1). 126

[18] Cid, B., Hilker, F. M., and Liz, E. (2014). Harvest timing and its population dynamic consequences in a discrete single-species model. *Mathematical Biosciences*, 248(1):78–87. 20

[19] Cook, B. W. M., Cutts, T. A., Nikiforuk, A. M., Poliquin, P. G., Court, D. A., Strong, J. E., and Theriault, S. S. (2015). Evaluating environmental persistence and disinfection of the Ebola virus Makona variant. *Viruses*, 7(4):1975–1986. 123

[20] De Arazoza, H. and Lounes, R. (2002). A non-linear model for a sexually transmitted disease with contact tracing. *IMA Journal of Mathematics Applied in Medicine and Biology*, 19(3):221–234. 124

[21] Dénes, A. and Gumel, A. B. (2019). Modeling the impact of quarantine during an outbreak of Ebola virus disease. *Infectious Disease Modelling*, 4:12–27. 124

[22] Diekmann, O. (2000). *Mathematical epidemiology of infectious diseases : model building, analysis, and interpretation*. Wiley series in mathematical and computational biology. John Wiley, Chichester. 131

[23] Diekmann, O., Heesterbeek, H., and Britton, T. (2012). *Mathematical tools for understanding infectious disease dynamics*, volume 7. Princeton University Press. 131

[24] Dietz, P. M., Jambai, A., Paweska, J. T., Yoti, Z., and Ksaizek, T. G. (2015). Epidemiology and risk factors for ebola virus disease in Sierra Leone - 23 May 2014 to 31 January 2015. *Clinical Infectious Diseases*, 61(11):1648–1654. 123

[25] Drake, J. M., Bakach, I., Just, M. R., O'Regan, S. M., Gambhir, M., and Chun-Hai, I. F. (2015). Transmission models of historical ebola outbreaks. *Emerging Infectious Diseases*, 21(8):1447–1450. 123

[26] Eames, K. T. and Keeling, M. J. (2003). Contact tracing and disease control. *Proceedings of the Royal Society B: Biological Sciences*, 270(1533):2565–2571. 124

[27] Edholm, C. J., Emerenini, B. O., Murillo, A. L., Saucedo, O., Shakiba, N., Wang, X., Allen, L. J. S., and Peace, A. (2018). Searching for superspreaders: Identifying epidemic patterns associated with superspreading events in stochastic models. In Radunskaya, A., Segal, R., and Shtylla, B., editors, *Understanding Complex Biological Systems with Mathematics*, pages 1–29. Springer International Publishing, Cham. 124

[28] Eskola, H. and Geritz, S. (2007). On the mechanistic derivation of various discrete-time population models. *Bulletin of Mathematical Biology*, 69:329–346. 8, 22

[29] Fallah, M. P., Skrip, L. A., Gertler, S., Yamin, D., and Galvani, A. P. (2015). Quantifying Poverty as a Driver of Ebola Transmission. *PLoS Neglected Tropical Diseases*, 9(12):1–10. 124

[30] Fang, L. Q., Yang, Y., Jiang, J. F., Yao, H. W., Kargbo, D., Li, X. L., Jiang, B. G., Kargbo, B., Tong, Y. G., Wang, Y. W., Liu, K., Kamara, A., Dafae, F., Kanu, A., Jiang, R. R., Sun, Y., Sun, R. X., Chen, W. J., Ma, M. J., Dean, N. E., Thomas, H., Longini, I. M., Halloran, M. E., and Cao, W. C. (2016). Transmission dynamics of Ebola virus disease and intervention effectiveness in Sierra Leone. *Proceedings of the National Academy of Sciences of the United States of America*, 113(16):4488–4493. 125

[31] Fauci, A. S. (2014). Ebola–underscoring the global disparities in health care resources. *The New England Journal of Medicine*, 371(12):1084–6. 123

[32] Franco, D., Logemann, H., Perán, J., and Segura, J. (2017). Dynamics of the discrete Seno population model : Combined effects of harvest timing and intensity on population stability. 48:885–898. 18

[33] Franco, D., Perán, J., and Segura, J. (2018). Effect of harvest timing on the dynamics of the Ricker–Seno model. *Mathematical Biosciences*, 306(June):180–185. 80

[34] Franco, D. and Ruiz-Herrera, A. (2015). To connect or not to connect isolated patches. *Journal of Theoretical Biology*, 370:72–80. 21

[35] Frieden, T. R., Damon, I., Bell, B. P., Kenyon, T., and Nichol, S. (2014). Ebola 2014–New Challenges, New Global Response and Responsibility. *The New England Journal of Medicine*, 371(13):1177–1180. 123

[36] Garske, T., Cori, A., Ariyarajah, A., Blake, I. M., Dorigatti, I., Eckmanns, T., Fraser, C., Hinsley, W., Jombart, T., Mills, H. L., Nedjati-Gilani, G., Newton, E., Nouvellet, P., Perkins, D., Riley, S., Schumacher, D., Shah, A., Van Kerkhove, M. D., Dye, C., Ferguson, N. M., and Donnelly, C. A. (2017). Heterogeneities in the case fatality ratio in the west African Ebola outbreak 2013–2016. *Philosophical Transactions of the Royal Society B: Biological Sciences*, 372(1721). 123

[37] Guiver, C., Edholm, C., Jin, Y., Mueller, M., Powell, J., Rebarber, R., Tenhumberg, B., and Townley, S. (2016). Simple adaptive control for positive linear systems with applications to pest management. *SIAM Journal on Applied Mathematics*, 76(1):238–275. 20

[38] Gyllenberg, M. (1997). Continuous versus discrete single species population models with adjustable reproductive strategies. *Bulletin of Mathematical Biology*, 59(4):679–705. 26

[39] Hilker, F. M. and Liz, E. (2013). Harvesting, census timing and "hidden" hydra effects. *Ecological Complexity*, 14:95–107. 20

[40] Holling, C. S. (1959a). The components of predation as revealed by a study of small-mammal predation of the european pine sawfly. *The Canadian Entomologist*, 91(5):293–320. 8

[41] Holling, C. S. (1959b). Some characteristics of simple types of predation and parasitism. *The Canadian Entomologist*, 91(7):385–398. 8

[42] Hsieh, Y. H., Wang, Y. S., de Arazoza, H., and Lounes, R. (2010). Modeling secondary level of HIV contact tracing: Its impact on HIV intervention in Cuba. *BMC Infectious Diseases*, 10. 124

[43] Hyman, J. M., Li, J., and Stanley, E. A. (2003). Modeling the impact of random screening and contact tracing in reducing the spread of HIV. *Mathematical Biosciences*, 181(1):17–54. 124

[44] Ivorra, B., Ngom, D., and Ramos, Á. M. (2014). Be-CoDiS: A mathematical model to predict the risk of human diseases spread between countries. Validation and application to the 2014-15 Ebola Virus Disease epidemic. *Bulletin of Mathematical Biology*, 77(9):1–30. 124

[45] Jonzen, N. and Lundberg, P. (1999). Temporally structured density-dependence and population management. *Annales Zoologici Fennici*, 36(1):39–44. 20

[46] Klinkenberg, D., Fraser, C., and Heesterbeek, H. (2006). The effectiveness of contact tracing in emerging epidemics. *PLoS ONE*, 1(1):1–7. 124

[47] Kokko, H. and Lindström, J. (1998). Seasonal density dependence, timing of mortality, and sustainable harvesting. *Ecological Modelling*, 110:293–304. 20, 21, 76

[48] Kot, M. (2001). *Elements of Mathematical Ecology*. Cambridge University Press, Cambridge. 9

[49] Kot, M. and Schaffer, W. M. (1984). The Effects of Seasonality on Discrete Models of Population-Growth. *Theoretical Population Biology*, 26(3):340–360. 20

[50] Lenhart, S. and Workman, J. T. (2007). *Optimal control applied to biological models*. CRC press. 41

[51] Levy, B., Edholm, C., Gaoue, O., Kaondera-Shava, R., Kgosimore, M., Lenhart, S., Lephodisa, B., Lungu, E., Marijani, T., and Nyabadza, F. (2017). Modeling the role of public health education in Ebola virus disease outbreaks in Sudan. *Infectious Disease Modelling*, 2(3):323–340. 155

[52] Lewnard, J. A., Ndeffo Mbah, M. L., Alfaro-Murillo, J. A., Altice, F. L., Bawo, L., Nyenswah, T. G., and Galvani, A. P. (2014). Dynamics and control of Ebola virus

transmission in Montserrado, Liberia: A mathematical modelling analysis. *The Lancet Infectious Diseases*, 14(12):1189–1195. 125

[53] Li, S. L., Bjørnstad, O. N., Ferrari, M. J., Mummah, R., Runge, M. C., Fonnesbeck, C. J., Tildesley, M. J., Probert, W. J., and Shea, K. (2017). Essential information: Uncertainty and optimal control of Ebola outbreaks. *Proceedings of the National Academy of Sciences of the United States of America*, 114(22):5659–5664. 157

[54] Liz, E. (2017a). Effects of strength and timing of harvest on seasonal population models: stability switches and catastrophic shifts. *Theoretical Ecology*, 10:235–244. 20

[55] Liz, E. (2017b). Effects of strength and timing of harvest on seasonal population models: stability switches and catastrophic shifts. *Theoretical Ecology*, 10(2):235–244. 20

[56] Loe, L. E., Rivrud, I. M., Meisingset, E. L., Bøe, S., Hamnes, M., Veiberg, V., and Mysterud, A. (2016). Timing of the hunting season as a tool to redistribute harvest of migratory deer across the landscape. *European Journal of Wildlife Research*, 62(3):315–323. 21

[57] Lokuge, K., Caleo, G., Greig, J., Duncombe, J., McWilliam, N., Squire, J., Lamin, M., Veltus, E., Wolz, A., Kobinger, G., de la Vega, M. A., Gbabai, O., Nabieu, S., Lamin, M., Kremer, R., Danis, K., Banks, E., and Glass, K. (2016). Successful Control of Ebola Virus Disease: Analysis of Service Based Data from Rural Sierra Leone. *PLoS Neglected Tropical Diseases*, 10(3):1–12. 127, 143

[58] Lundberg, P. and Lundberg, S. (2013). Population dynamics with sequential density-dependencies. *Oikos*, 75(2):174–181. 20

[59] May, R. M. and Oster, G. F. (1976). Bifurcations and dynamic complexity in simple ecological models. *The American Naturalist*, 110(974):573–599. 13

[60] Michaelis, L. and Menten, M. (1913). Die kinetik der invertinwirkung. *Biochem Z.*, 49:333–369. 8

[61] Olu, O. O., Lamunu, M., Nanyunja, M., Dafae, F., Samba, T., Sempiira, N., Kuti-George, F., Abebe, F. Z., Sensasi, B., Chimbaru, A., Ganda, L., Gausi, K., Gilroy, S., and Mugume, J. (2016). Contact Tracing during an Outbreak of Ebola Virus Disease in the Western Area Districts of Sierra Leone: Lessons for Future Ebola Outbreak Response. *Frontiers in Public Health*, 4(June):1–9. 126, 127, 139, 140, 143, 144

[62] Pigott, D. M., Golding, N., Mylne, A., Huang, Z., Henry, A. J., Weiss, D. J., Brady, O. J., Kraemer, M. U., Smith, D. L., Moyes, C. L., Bhatt, S., Gething, P. W., Horby, P. W., Bogoch, I. I., Brownstein, J. S., Mekaru, S. R., Tatem, A. J., Khan, K., and Hay, S. I. (2014). Mapping the zoonotic niche of Ebola virus disease in Africa. *eLife*, 3:e04395. 123

[63] Ponce, J., Zheng, Y., Lin, G., and Feng, Z. (2019). Assessing the effects of modeling the spectrum of clinical symptoms on the dynamics and control of Ebola. *Journal of Theoretical Biology*, 467:111–122. 125

[64] Rachah, A. and Torres, D. F. (2017). Predicting and controlling the ebola infection. *Mathematical Methods in the Applied Sciences*, 40(17):6155–6164. 125

[65] Ratikainen, I. I., Gill, J. A., Gunnarsson, T. G., Sutherland, W. J., and Kokko, H. (2008). When density dependence is not instantaneous: Theoretical developments and management implications. *Ecology Letters*, 11(2):184–198. 20

[66] Ricker, W. E. (1954). Stock and Recruitment. *Journal of the Fisheries Research Board of Canada*, 11(5):559–623. 3, 10

[67] Rivers, C. M., Lofgren, E. T., Marathe, M., Eubank, S., and Lewis, B. L. (2014). Modeling the impact of interventions on an epidemic of Ebola in Sierra Leone and Liberia. *PLoS Currents*, pages 1–12. 125, 127, 139, 140

[68] Rodriguez, D. J. (1988). Models of growth with density regulation in more than one life stage. *Theoretical Population Biology*, 34:93–117. 21

[69] Royden, H. and Fitzpatrick, P. (2010). *Real Analysis*. Prentice Hall, Boston, fourth edition. 34

[70] Salem, D. and Smith, R. (2016). A mathematical model of ebola virus disease: Using sensitivity analysis to determine effective intervention targets. *Simulation Series*, 48(9):16–23. 125

[71] Segura, J., Hilker, F. M., and Franco, D. (2017). Population control methods in extinction and outbreak scenarios. *PloS ONE*, 12:e0170837. 20

[72] Senga, M., Koi, A., Moses, L., Wauquier, N., Barboza, P., Fernandez-Garcia, M. D., Engedashet, E., Kuti-George, F., Mitiku, A. D., Vandi, M., Kargbo, D., Formenty, P., Hugonnet, S., Bertherat, E., and Lane, C. (2017). Contact tracing performance during the ebola virus disease outbreak in kenema district, Sierra Leone. *Philosophical Transactions of the Royal Society B: Biological Sciences*, 372(1721). 127, 139, 143

[73] Senga, M., Pringle, K., Ramsay, A., Brett-Major, D. M., Fowler, R. A., French, I., Vandi, M., Sellu, J., Pratt, C., Saidu, J., Shindo, N., and Bausch, D. G. (2016). Factors underlying Ebola virus infection among health workers, Kenema, Sierra Leone, 2014-2015. *Clinical Infectious Diseases*, 63(4):454–459. 123

[74] Seno, H. (2008). A paradox in discrete single species population dynamics with harvesting/thinning. *Mathematical Biosciences*, 214(1-2):63–69. 3, 21

[75] Seno, H. (2010). Native intra- and inter-specific reactions may cause the paradox of pest control with harvesting. *Journal of Biological Dynamics*, 4(3):235–247. 21

[76] Sethi, S. P. (2019). *Optimal Control Theory*. Springer International Publishing, Boston, third edition. 22, 40, 41

[77] Skrip, L. A., Fallah, M. P., Gaffney, S. G., Yaari, R., Yamin, D., Huppert, A., Bawo, L., Nyenswah, T., and Galvani, A. P. (2017). Characterizing risk of Ebola transmission based on frequency and type of case–contact exposures. *Philosophical Transactions of the Royal Society B: Biological Sciences*, 372(1721). 123

[78] Stehling-Ariza, T., Rosewell, A., Moiba, S. A., Yorpie, B. B., Ndomaina, K. D., Jimissa, K. S., Leidman, E., Rijken, D. J., Basler, C., Wood, J., and Manso, D. (2016). The

impact of active surveillance and health education on an Ebola virus disease cluster - Kono District, Sierra Leone, 2014-2015. *BMC Infectious Diseases*, 16(1):1–7. 125

[79] Swanson, K. C., Altare, C., Wesseh, C. S., Nyenswah, T., Ahmed, T., Eyal, N., Hamblion, E. L., Lessler, J., Peters, D. H., and Altmann, M. (2018). Contact tracing performance during the Ebola epidemic in Liberia, 2014-2015. *PLoS Neglected Tropical Diseases*, 12(9):2014–2015. 126

[80] Tang, S. and Chen, L. (2004). The effect of seasonal harvesting on stage-structured population models. *Journal of Mathematical Biology*, 48(4):357–374. 21

[81] van den Driessche, P. and Watmough, J. (2002). Reproduction numbers and sub-threshold endemic equilibria for compartmental models of disease transmission. *Mathematical Biosciences*, 180(1-2):29–48. 131, 133

[82] van den Driessche, P. and Watmough, J. (2008). Further notes on the basic reproduction number. *Lecture Notes in Mathematics*, 1945:159–178. 131, 133, 137

[83] Washington, M. (2017). personal communication. 126, 129

[84] Webb, G., Browne, C., Huo, X., Seydi, O., Seydi, M., and Magal, P. (2015). A model of the 2014 ebola epidemic in West Africa with contact tracing. *PLoS Currents*, 7:1–8. 125, 127

[85] Whitty, C. J. M. (2014). Tough choices to reduce Ebola transmission. *Nature*, 515:192–194. 126

[86] Wolfe, C. M., Hamblion, E. L., Schulte, J., Williams, P., Koryon, A., Enders, J., Sanor, V., Wapoe, Y., Kwayon, D., Blackley, D. J., Laney, A. S., Weston, E. J., Dokubo, E. K., Davies-Wayne, G., Wendland, A., Daw, V. T., Badini, M., Clement, P., Mahmoud, N., Williams, D., Gasasira, A., Nyenswah, T. G., and Fallah, M. (2017). Ebola virus disease contact tracing activities, lessons learned and best practices during the Duport Road outbreak in Monrovia, Liberia, November 2015. *PLoS Neglected Tropical Diseases*, 11(6):1–16. 126

[87] Xu, C., Boyce, M. S., and Daley, D. J. (2005). Harvesting in seasonal environments. *Journal of Mathematical Biology*, 50(6):663–682. 20

[88] Zhong, P. and Lenhart, S. (2013). Study on the order of events in optimal control of a harvesting problem modeled by integrodifference equations. *Evolution Equations and Control Theory*, 2(4):749–769. 20

Appendices

A Estimates of difference between Seno model and our first mechanistic model

We discovered numerically that the difference in time series for the Seno model and for our first mechanistic model are very small for any reasonable choice of parameters. In this appendix we attempt to estimate that difference algebraically without much success.

First, we examine the absolute difference between Seno's model and our model. We attempt to estimate an upper bound on the RHS of Seno's model (2.35) minus the RHS of our model (2.15) (from (2.37) we know this quantity is positive)

$$\theta_t \frac{(1-\gamma)bN_t}{1+\beta N_t} + (1-\theta_t)\frac{(1-\gamma)bN_t}{1+\beta(1-\gamma)N_t} - \frac{(1-\gamma)bN_t}{1+\beta N_t\left(1-\gamma(1-\theta_t)\right)}. \tag{31}$$

Let's get a common denominator of

$$\left(1+\beta N_t\right)\left(1+\beta(1-\gamma)N_t\right)\left(1+\beta N_t\left(1-\gamma(1-\theta_t)\right)\right). \tag{32}$$

Factoring out the common term in the numerator, $(1-\gamma)bN_t$, the numerator of the first term will give

$$\begin{aligned}
&\theta_t\left(1+\beta(1-\gamma)N_t\right)\left(1+\beta N_t\left(1-\gamma(1-\theta_t)\right)\right)\\
=&\theta_t\left(1+\beta N_t-\beta\gamma N_t\right)\left(1+\beta N_t-\beta\gamma N_t+\beta\gamma\theta_t N_t\right)\\
=&\theta_t\left(1+2\beta N_t-2\beta\gamma N_t+\beta^2N_t^2-2\beta^2\gamma N_t^2+\beta^2\gamma^2N_t^2+\beta\gamma\theta_tN_t+\beta^2\gamma\theta_tN_t^2-\beta^2\gamma^2\theta_tN_t^2\right)\\
=&\theta_t+2\beta\theta_tN_t-2\beta\gamma\theta_tN_t+\beta^2\theta_tN_t^2-2\beta^2\gamma\theta_tN_t^2+\beta^2\gamma^2\theta_tN_t^2\\
&+\beta\gamma\theta_t^2N_t+\beta^2\gamma\theta_t^2N_t^2-\beta^2\gamma^2\theta_t^2N_t^2.
\end{aligned} \tag{33}$$

Similarly, for the second term,

$$\begin{aligned}
&(1-\theta_t)\,(1+\beta N_t)\,(1+\beta N_t-\beta\gamma N_t+\beta\gamma\theta_t N_t)\\
=&(1-\theta_t)\left(1+2\beta N_t+\beta^2 N_t^2-\beta\gamma N_t-\beta^2\gamma N_t^2+\beta\gamma\theta_t N_t+\beta^2\gamma\theta_t N_t^2\right)\\
=&1+2\beta N_t+\beta^2 N_t^2-\beta\gamma N_t-\beta^2\gamma N_t^2+2\beta\gamma\theta_t N_t+2\beta^2\gamma\theta_t N_t^2-\theta_t\\
&-2\beta\theta_t N_t-\beta^2\theta_t N_t^2-\beta\gamma\theta_t^2 N_t-\beta^2\gamma\theta_t^2 N_t^2. \qquad (34)
\end{aligned}$$

And for the third term:

$$\begin{aligned}
&-1\,(1+\beta N_t)\,(1+\beta N_t-\beta\gamma N_t)\\
=&-1\left(1+2\beta N_t+\beta^2 N_t^2-\beta\gamma N_t-\beta^2\gamma N_t^2\right)\\
=&-1-2\beta N_t-\beta^2 N_t^2+\beta\gamma N_t+\beta^2\gamma N_t. \qquad (35)
\end{aligned}$$

Note that terms in (35) cancel with the first 5 terms of (34). Also, the remaining terms of (34) cancel with terms in (33) leaving only the 6^{th} and final term of (33). So adding the terms in (33), (34), and (35) yields

$$\begin{aligned}
&\beta^2\gamma^2\theta_t N_t^2-\beta^2\gamma^2\theta_t^2 N_t^2\\
=&\beta^2\gamma^2\theta_t N_t^2\,(1-\theta_t)\,. \qquad (36)
\end{aligned}$$

So, multiplying the terms in (36) by the common term $(1-\gamma)bN_t$ and dividing by the terms in (32) gives us a single fraction

$$\frac{(1-\gamma)b\beta^2\gamma^2\theta_t\,(1-\theta_t)\,N_t^3}{(1+\beta N_t)\,(1+\beta(1-\gamma)N_t)\,(1+\beta N_t\,(1-\gamma(1-\theta_t)))} \qquad (37)$$

which is equal to the difference in (31). Therefore (31) is less than or equal to

$$(1-\gamma)b\beta^2\gamma^2\theta_t\,(1-\theta_t)\,N_t^3. \qquad (38)$$

Let

$$u=(1-\gamma)\gamma^2.$$

Then

$$u' = 2\gamma - 3\gamma^2$$

and

$$u'' = 2 - 6\gamma.$$

So setting $u' = 0$ yields two critical points: $\gamma = 0$ and $\gamma = \frac{2}{3}$. Since $u''(0) > 0$, $\gamma = 0$ is a local minimum. But $u''(\frac{2}{3}) < 0$ so this is a local maximum. Which implies $\gamma = \frac{2}{3}$ is a maximum of u on the interval $\gamma \in [0, 1]$. Therefore

$$(1 - \gamma)\gamma^2 \leq \left(1 - \frac{2}{3}\right)\frac{2^2}{3^2} = \frac{2^2}{3^3}. \tag{39}$$

Similarly, let

$$v = (1 - \theta_t)\theta_t.$$

Then

$$v' = 1 - 2\theta_t$$

and

$$v'' = -2.$$

Setting $v' = 0$ yields $\theta_t = \frac{1}{2}$. Since $v'' < 0$, this is the global maximum of θ_t. So we have

$$(1 - \theta_t)\theta_t \leq \frac{1}{2^2}. \tag{40}$$

Since our population is undergoing harvest and has no hydra effect, N_t is bounded above by the without-harvest equilibrium. (A hydra effect occurs when harvesting results in higher population levels than would occur in the absence of harvesting.) Without harvest, we have the Beverton-Holt equation

$$N_{t+1} = \frac{bN_t}{1 + \beta N_t}$$

which has equilibrium $N^* = \frac{b-1}{\beta}$. So, as long as $N_0 \leq \frac{b-1}{\beta}$,

$$N_t \leq \frac{b - 1}{\beta} \tag{41}$$

for all t. Using inequalities (39), (40), and (41), as long as $N_0 \leq \frac{b-1}{\beta}$, we have the expression in (38) less than or equal to

$$\begin{aligned}&\frac{2^2}{3^3} b\beta^2 \frac{1}{2^2} \frac{(b-1)^3}{\beta^3}\\ =&\frac{b(b-1)^3}{27\beta}.\end{aligned} \tag{42}$$

This bound is not helpful, so we attempt an alternative approach. For this alternative approach we will use (2.20), which is

$$\frac{1}{1+\beta N_t} \leq \frac{1}{1+\beta\left(1-\gamma(1-\theta_t)\right)N_t} \leq \frac{1}{1+\beta(1-\gamma)N_t} \tag{43}$$

We then estimate the expression (37) (coming from the difference (31)) using (43) to see that (31) is less than or equal to

$$\begin{aligned}&\frac{(1-\gamma)\gamma^2 b\beta^2(1-\theta)\theta N_t^3}{(1+\beta(1-\gamma)N_t)^3}\\ <&\frac{(1-\gamma)\gamma^2 b\beta^2(1-\theta)\theta N_t^3}{\beta^3(1-\gamma)^3 N_t^3}\\ =&\frac{\gamma^2 b(1-\theta)\theta}{\beta(1-\gamma)^2}\\ \leq&\frac{b}{4\beta(1-\gamma)^2}\end{aligned} \tag{44}$$

so long as $N_t \neq 0$, $\gamma \neq 1$.

As another approach to estimating the difference (31), we might apply (43) initially to get

$$\begin{aligned}&\theta_t \frac{(1-\gamma)bN_t}{1+\beta N_t} + (1-\theta_t)\frac{(1-\gamma)bN_t}{1+\beta(1-\gamma)N_t} - \frac{(1-\gamma)bN_t}{1+\beta N_t\left(1-\gamma(1-\theta_t)\right)}\\ \leq&\frac{\theta_t(1-\gamma)bN_t}{1+\beta(1-\gamma)N_t} + \frac{(1-\theta_t)(1-\gamma)bN_t}{1+\beta(1-\gamma)N_t} - \frac{(1-\gamma)bN_t}{1+\beta(1-\gamma(1-\theta_t))N_t}\\ =&\frac{(1-\gamma)bN_t}{1+\beta(1-\gamma)N_t} - \frac{(1-\gamma)bN_t}{1+\beta(1-\gamma(1-\theta_t))N_t}.\end{aligned} \tag{45}$$

Combining the fractions in (45) and then using (43) yields

$$\begin{aligned}
&(1-\gamma)bN_t\left(\frac{1+\beta(1-\gamma(1-\theta_t))N_t-(1+\beta(1-\gamma)N_t)}{(1+\beta(1-\gamma)N_t)\,(1+\beta(1-\gamma(1-\theta_t))N_t)}\right)\\
=&(1-\gamma)bN_t\left(\frac{1+\beta N_t-\beta\gamma N_t+\beta\gamma\theta_t N_t-1-\beta N_t+\beta\gamma N_t}{(1+\beta(1-\gamma)N_t)\,(1+\beta(1-\gamma(1-\theta_t))N_t)}\right)\\
=&\frac{(1-\gamma)b\beta\gamma\theta_t N_t^2}{(1+\beta(1-\gamma)N_t)\,(1+\beta(1-\gamma(1-\theta_t))N_t)}\\
\leq&\frac{(1-\gamma)\gamma b\beta\theta_t N_t^2}{(1+\beta(1-\gamma)N_t)^2}.
\end{aligned}$$

This can be estimated in two ways, since both

$$\frac{1}{(1+\beta(1-\gamma)N_t)^2}<\frac{1}{\beta^2(1-\gamma)^2N_t^2} \tag{46}$$

so long as $N_t\neq 0$ and $\gamma\neq 1$ and

$$\frac{1}{(1+\beta(1-\gamma)N_t)^2}\leq 1. \tag{47}$$

The first estimate gives the difference in (45) being less than

$$\begin{aligned}
&\frac{(1-\gamma)\gamma b\beta\theta_t N_t^2}{\beta^2(1-\gamma)^2N_t^2}\\
\leq&\frac{b}{(1-\gamma)\beta}.
\end{aligned} \tag{48}$$

The second estimate together with inequality (41) gives our difference coming from (45) less than or equal to

$$\begin{aligned}
&(1-\gamma)\gamma b\beta\theta_t N_t^2\\
\leq&\frac{1}{4}b\beta\left(\frac{b-1}{\beta}\right)^2\\
=&\frac{b(b-1)^2}{4\beta}.
\end{aligned} \tag{49}$$

These estimates are summarized in Table 6. Since the function $\frac{1}{1-\gamma}$ on the domain $\gamma\in[0,1]$ has the range $[1,\infty)$, as does the function $\frac{1}{(1-\gamma)^2}$, the bottom two estimates might

Table 6: We obtained the upper estimates above for the difference of the RHS of Seno's and the RHS of our first mechanistic model (31), which require the listed assumptions.

Estimate	Assumptions
$\frac{b}{(1-\gamma)\beta}$	$N_t \neq 0$ and $\gamma \neq 1$
$\frac{b}{4(1-\gamma)^2\beta}$	$N_t \neq 0$ and $\gamma \neq 1$
$\frac{b(b-1)^2}{4\beta}$	$N_0 \leq \frac{b-1}{\beta}$
$\frac{b(b-1)^3}{27\beta}$	$N_0 \leq \frac{b-1}{\beta}$

be preferred. However none of these estimates imply that the difference between the RHS of Seno and the RHS of our first mechanistic model (31) is very small for large parts of parameter space. For this reason we did numerical estimates of the difference (31).

In order for the population to be stable enough to harvest, we expect $b > \beta$. We have explored several ways of estimating the difference (31) and they each result in some kind of ratio between b and β. This might seem to imply that for some combinations of b and β, (2.15) and (2.35) aren't close together. But though the difference between the two models might get larger for $b \gg \beta$, our simulations indicate that the relative distance between the two models does not get large. To explore this, we'll take (31) and divide it by the RHS of the smaller of the two models (2.15), to stay conservative in our estimate. Note that both expressions (31) and (2.15) are nonnegative, so we have

$$\begin{aligned}
&\frac{\theta_t \frac{(1-\gamma)bN_t}{1+\beta N_t} + (1-\theta_t)\frac{(1-\gamma)bN_t}{1+\beta(1-\gamma)N_t} - \frac{(1-\gamma)bN_t}{1+\beta N_t(1-\gamma(1-\theta_t))}}{\frac{b(1-\gamma)N_t}{1+\beta N_t(1-\gamma(1-\theta_t))}} \\
&= \left(\theta_t \frac{(1-\gamma)bN_t}{1+\beta N_t} + (1-\theta_t)\frac{(1-\gamma)bN_t}{1+\beta(1-\gamma)N_t} - \frac{(1-\gamma)bN_t}{1+\beta N_t\left(1-\gamma(1-\theta_t)\right)}\right) \\
&\quad * \frac{1+\beta N_t\left(1-\gamma(1-\theta_t)\right)}{b(1-\gamma)N_t} \\
&= \frac{\theta_t\left(1+\beta N_t\left(1-\gamma(1-\theta_t)\right)\right)}{1+\beta N_t} + \frac{(1-\theta_t)\left(1+\beta N_t\left(1-\gamma(1-\theta_t)\right)\right)}{1+\beta(1-\gamma)N_t} - 1.
\end{aligned} \tag{50}$$

We observed earlier that

$$\frac{1}{1+\beta N_t} \leq \frac{1}{1+\beta(1-\gamma)N_t}$$

and

$$1 + \beta\left(1 - \gamma(1 - \theta_t)\right) N_t \leq 1 + \beta N_t.$$

So the expression in (50) is less than or equal to

$$\begin{aligned}
&\frac{\theta_t\left(1+\beta N_t\right)}{1+\beta N_t} + \frac{\left(1-\theta_t\right)\left(1+\beta N_t\right)}{1+\beta(1-\gamma)N_t} - 1 \\
\leq &\frac{\theta_t\left(1+\beta N_t\right)}{1+\beta(1-\gamma)N_t} + \frac{\left(1-\theta_t\right)\left(1+\beta N_t\right)}{1+\beta(1-\gamma)N_t} - 1 \\
= &\frac{1+\beta N_t}{1+\beta(1-\gamma)N_t} - 1 \\
= &\frac{1}{1+\beta(1-\gamma)N_t} + \frac{\beta N_t}{1+\beta(1-\gamma)N_t} - 1 \\
\leq &\frac{1}{1} + \frac{\beta N_t}{\beta(1-\gamma)N_t} - 1 \\
= &\frac{1}{1-\gamma}
\end{aligned} \tag{51}$$

so long as $N_t \neq 0$ and $\gamma \neq 1$. This bound is not helpful, since on the domain $\gamma \in [0, 1]$ it has range $[1, \infty)$. We need to explore some other estimates of (50). Starting from a term in the middle of the inequalities above, we have (50) less than or equal to

$$\begin{aligned}
&\frac{1+\beta N_t}{1+\beta(1-\gamma)N_t} - 1 \\
= &\frac{1+\beta N_t - 1 - \beta N_t + \beta\gamma N_t}{1+\beta(1-\gamma)N_t} \\
= &\frac{\beta\gamma N_t}{1+\beta(1-\gamma)N_t} \qquad (52) \\
\leq &\beta\gamma N_t \\
\leq &\frac{\beta\gamma(b-1)}{\beta} \\
= &\gamma(b-1) \qquad (53)
\end{aligned}$$

assuming that $N_0 \leq \frac{b-1}{\beta}$. Alternatively, the expression in (52) is less than or equal to

$$\begin{aligned} &\frac{\beta\gamma N_t}{\beta(1-\gamma)N_t} \\ =&\frac{\gamma}{1-\gamma} \end{aligned} \tag{54}$$

assuming that $\gamma \neq 1$ and $N_t \neq 0$. However, for the domain $\gamma \in [0,1]$ the quotient (54) has range $[0,\infty)$.

Starting over from expression (50) and combining the terms into one fraction with a common denominator, we get

$$\begin{aligned} &\frac{\theta_t\left(1+\beta N_t\left(1-\gamma(1-\theta_t)\right)\right)}{1+\beta N_t} + \frac{(1-\theta_t)\left(1+\beta N_t\left(1-\gamma(1-\theta_t)\right)\right)}{1+\beta(1-\gamma)N_t} - 1 \\ &= \frac{\beta^2\gamma^2\theta_t(1-\theta_t)N_t^2}{\left(1+\beta N_t\right)\left(1+\beta(1-\gamma)N_t\right)}. \end{aligned} \tag{55}$$

Using (43), we see that the quotient (55) is less than or equal to

$$\begin{aligned} &\frac{\beta^2\gamma^2\theta_t(1-\theta_t)N_t^2}{\left(1+\beta(1-\gamma)N_t\right)^2} \qquad (56) \\ \leq&\frac{\beta^2\gamma^2\theta_t(1-\theta_t)N_t^2}{\beta^2(1-\gamma)^2N_t^2} \\ =&\frac{\gamma^2\theta(1-\theta)}{(1-\gamma)^2} \\ \leq&\frac{\gamma^2}{(1-\gamma)^2}. \qquad (57) \end{aligned}$$

This estimate is also useless since for $\gamma \in [0,1]$ its range is $[0,\infty)$. For low values of γ it will be small, but for values of γ approaching 1 it will be huge.

These estimates are summarized in Table 7. These estimates are for the RHS of Seno minus the RHS of our first mechanistic model divided by the RHS of our first mechanistic model. The estimates in Table 6 were for the absolute difference between the RHS of Seno and the RHS of our first mechanistic model, without division. Neither approach yielded estimates that reflect how small the differences between Seno and our first mechanistic model actually

Table 7: We obtained the relative estimates above for expression (50), which is the RHS of Seno minus the RHS of our first mechanistic model divided by the RHS of our first mechanistic model. The estimates require the listed assumptions.

Estimate	Assumptions
$\frac{1}{1-\gamma}$	$N_t \neq 0$ and $\gamma \neq 1$
$\frac{\gamma}{1-\gamma}$	$N_t \neq 0$ and $\gamma \neq 1$
$\left(\frac{\gamma}{1-\gamma}\right)^2$	$N_t \neq 0$ and $\gamma \neq 1$
$\gamma(b-1)$	$N_0 \leq \frac{b-1}{\beta}$

are in large portions of parameter space, as shown by our numerical investigation. We did not obtain better estimates by dividing the difference (31) by (2.35) instead of (2.15).

B Data from the Sierra Leone Ministry of Health situation reports

Date	Day	Cumulative Cases	Cumulative Deaths
12-Aug-14	77	717	264
13-Aug-14	78	733	273
14-Aug-14	79	747	280
15-Aug-14	80	757	287
16-Aug-14	81	775	297
17-Aug-14	82	778	305
18-Aug-14	83	783	312
19-Aug-14	84	804	320
20-Aug-14	85	813	322
21-Aug-14	86	823	329
22-Aug-14	87	881	333
23-Aug-14	88	904	336
24-Aug-14	89	935	341
25-Aug-14	90	955	355
26-Aug-14	91	961	363
27-Aug-14	92	988	372
28-Aug-14	93	1018	377
29-Aug-14	94	1033	383
30-Aug-14	95	1077	387
31-Aug-14	96	1106	388
1-Sep-14	97	1115	396
2-Sep-14	98	1146	399
3-Sep-14	99	1174	404
5-Sep-14	101	1234	413
6-Sep-14	102	1276	426
7-Sep-14	103	1287	428
8-Sep-14	104	1305	433
9-Sep-14	105	1341	436
10-Sep-14	106	1367	445
11-Sep-14	107	1401	450
12-Sep-14	108	1432	459
13-Sep-14	109	1464	463
14-Sep-14	110	1513	468
15-Sep-14	111	1542	474
16-Sep-14	112	1571	483
17-Sep-14	113	1585	489
18-Sep-14	114	1618	495
19-Sep-14	115	1640	497

20-Sep-14	116	1696	501
21-Sep-14	117	1745	502
22-Sep-14	118	1775	506
23-Sep-14	119	1816	509
24-Sep-14	120	1885	509
25-Sep-14	121	1920	513
26-Sep-14	122	1944	513
27-Sep-14	123	2000	518
28-Sep-14	124	2090	522
29-Sep-14	125	2155	527
30-Sep-14	126	2184	550
1-Oct-14	127	2212	532
3-Oct-14	129	2276	538
4-Oct-14	130	2411	678
5-Oct-14	131	2459	699
6-Oct-14	132	2504	703
7-Oct-14	133	2585	708
8-Oct-14	134	2593	713
10-Oct-14	136	2698	904
11-Oct-14	137	2792	921
12-Oct-14	138	2849	926
13-Oct-14	139	2894	931
14-Oct-14	140	2977	932
15-Oct-14	141	3003	943
16-Oct-14	142	3058	947
17-Oct-14	143	3097	954
18-Oct-14	144	3154	973
19-Oct-14	145	3223	986
20-Oct-14	146	3295	997
21-Oct-14	147	3345	1001
22-Oct-14	148	3389	1008
23-Oct-14	149	3449	1012
24-Oct-14	150	3490	1026
25-Oct-14	151	3560	1037
26-Oct-14	152	3622	1044
27-Oct-14	153	3713	1049
28-Oct-14	154	3760	1057
30-Oct-14	156	3841	1064
31-Oct-14	157	3936	1070

1-Nov-14	158	3996	1077
2-Nov-14	159	4057	1085
6-Nov-14	163	4232	1114
7-Nov-14	164	4277	1126
8-Nov-14	165	4433	1133
10-Nov-14	167	4617	1149
12-Nov-14	169	4744	1169
13-Nov-14	170	4828	1180
14-Nov-14	171	4913	1196
15-Nov-14	172	4967	1206
16-Nov-14	173	5056	1223
17-Nov-14	174	5109	1233
18-Nov-14	175	5152	1240
19-Nov-14	176	5210	1249
20-Nov-14	177	5304	1282
21-Nov-14	178	5355	1303
22-Nov-14	179	5402	1333
23-Nov-14	180	5441	1364
24-Nov-14	181	5524	1397
25-Nov-14	182	5595	1429
26-Nov-14	183	5683	1464
27-Nov-14	184	5767	1481
28-Nov-14	185	5831	1496
29-Nov-14	186	5906	1522
30-Nov-14	187	5978	1549
1-Dec-14	188	6039	1575
2-Dec-14	189	6132	1601
4-Dec-14	191	6238	1648
5-Dec-14	192	6292	1669
6-Dec-14	193	6317	1708
7-Dec-14	194	6375	1734
8-Dec-14	195	6420	1786
9-Dec-14	196	6457	1823
10-Dec-14	197	6497	1865
11-Dec-14	198	6557	1910
12-Dec-14	199	6592	1952
13-Dec-14	200	6638	1999
14-Dec-14	201	6702	2051
15-Dec-14	202	6757	2076

16-Dec-14	203	6808	2095
17-Dec-14	204	6856	2111
18-Dec-14	205	6903	2136
19-Dec-14	206	6932	2163
20-Dec-14	207	6975	2190
21-Dec-14	208	7017	2216
22-Dec-14	209	7075	2235
23-Dec-14	210	7130	2273
24-Dec-14	211	7160	2289
25-Dec-14	212	7220	2319
26-Dec-14	213	7275	2345
27-Dec-14	214	7326	2366
28-Dec-14	215	7354	2392
29-Dec-14	216	7419	2410
30-Dec-14	217	7458	2435
31-Dec-14	218	7476	2461
1-Jan-15	219	7505	2501
2-Jan-15	220	7542	2524
3-Jan-15	221	7572	2550
4-Jan-15	222	7606	2578
5-Jan-15	223	7641	2607
6-Jan-15	224	7665	2612
7-Jan-15	225	7696	2630
8-Jan-15	226	7718	2650
9-Jan-15	227	7749	2663
10-Jan-15	228	7777	2684
11-Jan-15	229	7797	2697
12-Jan-15	230	7816	2702
13-Jan-15	231	7839	2718
14-Jan-15	232	7855	2732
15-Jan-15	233	7861	2742
16-Jan-15	234	7885	2760
17-Jan-15	235	7897	2767
18-Jan-15	236	7917	2780
19-Jan-15	237	7923	2788
20-Jan-15	238	7935	2794
21-Jan-15	239	7944	2802
22-Jan-15	240	7958	2814
23-Jan-15	241	7966	2822

24-Jan-15	242	7977	2830
25-Jan-15	243	7982	2834
26-Jan-15	244	7991	2842
27-Jan-15	245	8003	2851
28-Jan-15	246	8015	2859
29-Jan-15	247	8033	2873
31-Jan-15	249	8056	2909
1-Feb-15	250	8073	2911
2-Feb-15	251	8077	2921
3-Feb-15	252	8098	2936
4-Feb-15	253	8111	2949
5-Feb-15	254	8117	2950
6-Feb-15	255	8124	2959
7-Feb-15	256	8136	2971
8-Feb-15	257	8149	2978
10-Feb-15	259	8169	2998
11-Feb-15	260	8183	3009
12-Feb-15	261	8193	3018
13-Feb-15	262	8208	3030
14-Feb-15	263	8213	3036
15-Feb-15	264	8226	3043
16-Feb-15	265	8230	3050
17-Feb-15	266	8237	3058
18-Feb-15	267	8239	3063
19-Feb-15	268	8244	3066
20-Feb-15	269	8260	3079
21-Feb-15	270	8275	3088
22-Feb-15	271	8289	3095
23-Feb-15	272	8301	3103
24-Feb-15	273	8308	3113
25-Feb-15	274	8320	3124
27-Feb-15	276	8349	3151
28-Feb-15	277	8353	3164
1-Mar-15	278	8370	3180
2-Mar-15	279	8374	3188
3-Mar-15	280	8383	3199
4-Mar-15	281	8389	3210
5-Mar-15	282	8398	3222
7-Mar-15	284	8416	3245

8-Mar-15	285	8428	3263
9-Mar-15	286	8444	3279
10-Mar-15	287	8463	3289
11-Mar-15	288	8469	3297
12-Mar-15	289	8472	3303
13-Mar-15	290	8476	3312
15-Mar-15	292	8487	3325
16-Mar-15	293	8501	3327
17-Mar-15	294	8502	3336
19-Mar-15	296	8508	3360
20-Mar-15	297	8515	3370
21-Mar-15	298	8518	3376
22-Mar-15	299	8520	3381
23-Mar-15	300	8528	3393
24-Mar-15	301	8529	3398
25-Mar-15	302	8532	3407
26-Mar-15	303	8535	3413
27-Mar-15	304	8539	3421
29-Mar-15	306	8545	3433
31-Mar-15	308	8547	3444
1-Apr-15	309	8549	3448
2-Apr-15	310	8549	3454
3-Apr-15	311	8551	3459
4-Apr-15	312	8555	3461
5-Apr-15	313	8555	3466
6-Apr-15	314	8558	3472
7-Apr-15	315	8558	3475
8-Apr-15	316	8559	3476
9-Apr-15	317	8560	3481
10-Apr-15	318	8560	3488
11-Apr-15	319	8561	3490
12-Apr-15	320	8563	3491
13-Apr-15	321	8565	3496
14-Apr-15	322	8566	3499
15-Apr-15	323	8569	3499
16-Apr-15	324	8571	3503
17-Apr-15	325	8572	3506
18-Apr-15	326	8573	3508
19-Apr-15	327	8573	3511

20-Apr-15	328	8580	3516
21-Apr-15	329	8581	3519
22-Apr-15	330	8584	3520
23-Apr-15	331	8585	3526
24-Apr-15	332	8585	3526
25-Apr-15	333	8585	3529
26-Apr-15	334	8586	3533
27-Apr-15	335	8587	3534
29-Apr-15	337	8590	3535
30-Apr-15	338	8591	3535
2-May-15	340	8592	3536
3-May-15	341	8595	3537
4-May-15	342	8597	3538
5-May-15	343	8597	3538
6-May-15	344	8597	3538
7-May-15	345	8597	3538
8-May-15	346	8597	3538
9-May-15	347	8597	3538
10-May-15	348	8597	3538
12-May-15	350	8597	3538
13-May-15	351	8598	3538
15-May-15	353	8601	3539
17-May-15	355	8605	3541
18-May-15	356	8606	3541
19-May-15	357	8607	3541
20-May-15	358	8608	3541
21-May-15	359	8608	3542
22-May-15	360	8608	3542
23-May-15	361	8608	3542
24-May-15	362	8608	3542
25-May-15	363	8608	3543
26-May-15	364	8611	3545
27-May-15	365	8614	3545
28-May-15	366	8616	3545
29-May-15	367	8617	3545
30-May-15	368	8618	3545
31-May-15	369	8619	3546
1-Jun-15	370	8620	3546
2-Jun-15	371	8623	3546

3-Jun-15	372	8624	3546
4-Jun-15	373	8626	3546
5-Jun-15	374	8628	3547
6-Jun-15	375	8630	3547
8-Jun-15	377	8636	3549
11-Jun-15	380	8647	3551
1-Jul-15	400	8671	3569
3-Jul-15	402	8672	3572
4-Jul-15	403	8673	3574
5-Jul-15	404	8674	3574
6-Jul-15	405	8674	3574
7-Jul-15	406	8675	3575
9-Jul-15	408	8679	3575
10-Jul-15	409	8686	3578
11-Jul-15	410	8687	3580
12-Jul-15	411	8688	3581
13-Jul-15	412	8688	3582
15-Jul-15	414	8690	3582
16-Jul-15	415	8690	3582
17-Jul-15	416	8691	3582
18-Jul-15	417	8692	3583
19-Jul-15	418	8692	3583
20-Jul-15	419	8694	3583
21-Jul-15	420	8694	3583
23-Jul-15	422	8694	3583
24-Jul-15	423	8695	3584
25-Jul-15	424	8695	3585
27-Jul-15	426	8695	3585
29-Jul-15	428	8695	3585
31-Jul-15	430	8694	3585
1-Aug-15	431	8695	3585
2-Aug-15	432	8695	3585
3-Aug-15	433	8695	3585
4-Aug-15	434	8696	3585
5-Aug-15	435	8696	3585
7-Aug-15	437	8697	3585
9-Aug-15	439	8697	3585
11-Aug-15	441	8697	3585
12-Aug-15	442	8697	3586

13-Aug-15	443	8697	3586
14-Aug-15	444	8697	3586
15-Aug-15	445	8697	3586
16-Aug-15	446	8697	3586
17-Aug-15	447	8697	3586
18-Aug-15	448	8697	3586
19-Aug-15	449	8697	3586
20-Aug-15	450	8697	3586
23-Aug-15	453	8697	3586
24-Aug-15	454	8697	3586
25-Aug-15	455	8697	3586
26-Aug-15	456	8697	3586
27-Aug-15	457	8697	3586
31-Aug-15	461	8698	3587
2-Sep-15	463	8698	3587
3-Sep-15	464	8698	3587
7-Sep-15	468	8702	3587
12-Sep-15	473	8703	3587
13-Sep-15	474	8704	3587
16-Sep-15	477	8704	3589
17-Sep-15	478	8704	3589
19-Sep-15	480	8704	3589
20-Sep-15	481	8704	3589
21-Sep-15	482	8704	3589
25-Sep-15	486	8704	3589
26-Sep-15	487	8704	3589
29-Sep-15	490	8704	3589
4-Oct-15	495	8704	3589
5-Oct-15	496	8704	3589
6-Oct-15	497	8704	3589
13-Oct-15	504	8704	3589

Vita

Danielle Burton was born in DeQueen, Arkansas on August 22, 1986. They moved with their parents, Pamela and Larry Burton, and their brother, Jeremy Burton to Michigan in 1995. They graduated with a BA in English Literature from Andrews University in 2008 and an MS in Mathematics and Science with emphases on Math and Biology from Andrews University in 2013. Shandelle Henson was their research mentor during their master's studies and they co-authored a paper with Dr. Henson in 2014.

Danielle moved to Knoxville, TN in the fall of 2013 to pursue their PhD in Mathematics at the University of Tennessee. They were supported for two years by a Program for Excellence and Equity in Research (PEER) fellowship, for one year by a National Institute for Mathematical and Biological Synthesis research assistantship, and for four years by a teaching assistantship from the Department of Mathematics. They graduated with their PhD in Mathematics in August 2020.

They will begin a position as a Van Vleck Assistant Professor at the University of Wisconsin, Madison in fall 2020.